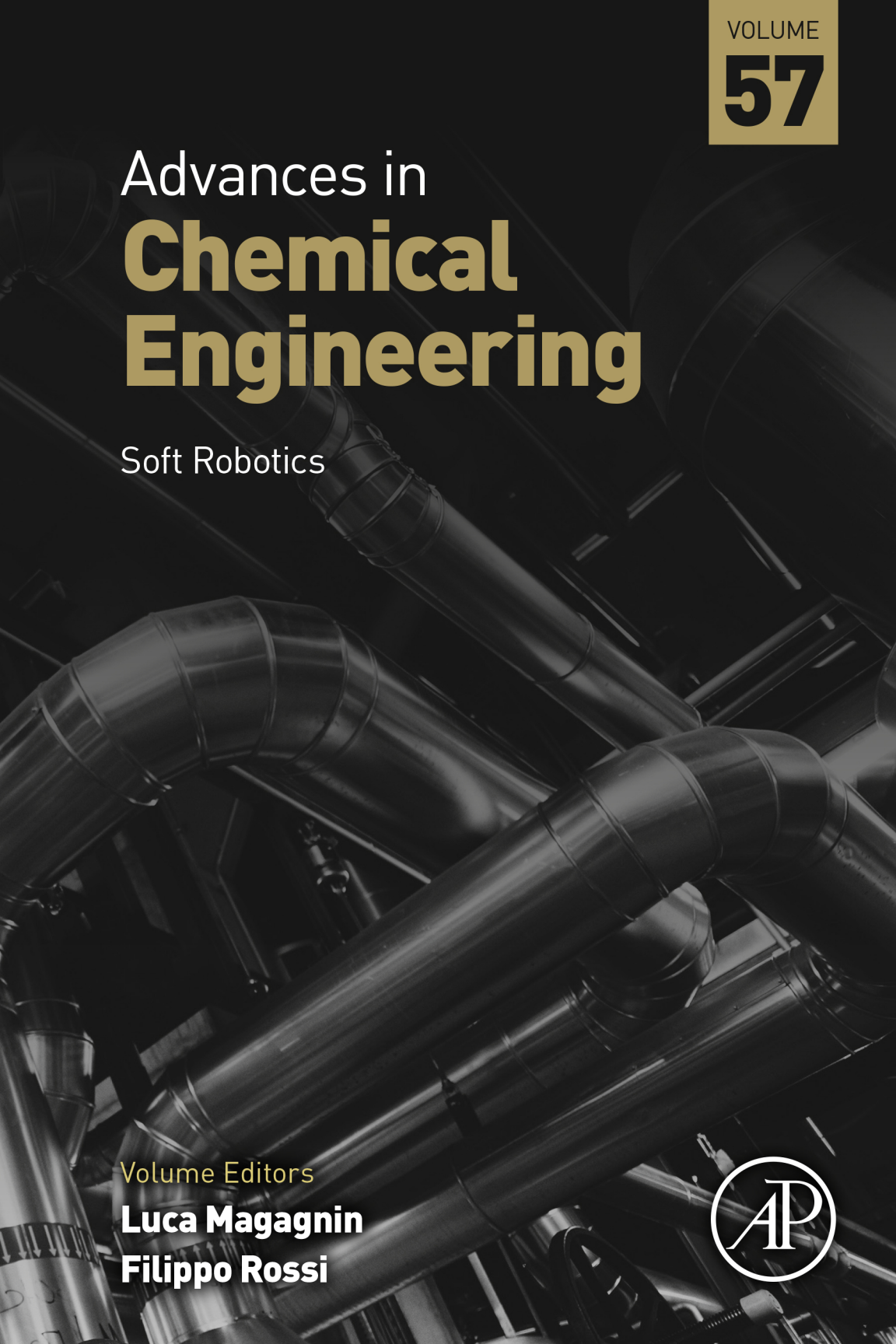
VOLUME
57
Advances in
Chemical
Engineering
Soft Robotics
Volume Editors
Luca Magagnin
Filippo Rossi

VOLUME FIFTY SEVEN

ADVANCES IN
CHEMICAL ENGINEERING

Soft Robotics

ADVANCES IN CHEMICAL ENGINEERING

Serial Editor

DAVIDE MOSCATELLI
Department of Chemistry,
Materials and Chemical Engineering "Giulio Natta"
Politecnico di Milano, Milano, Italy

VOLUME FIFTY SEVEN

ADVANCES IN CHEMICAL ENGINEERING

Soft Robotics

Edited by

LUCA MAGAGNIN
Department of Chemistry,
Materials and Chemical Engineering "Giulio Natta,"
Polytechnic of Milan, Milan, Italy

FILIPPO ROSSI
Department of Chemistry,
Materials and Chemical Engineering "Giulio Natta"
of Politecnico di Milano in Milan, Italy

ACADEMIC PRESS
An imprint of Elsevier

Academic Press is an imprint of Elsevier
50 Hampshire Street, 5th Floor, Cambridge, MA 02139, United States
525 B Street, Suite 1650, San Diego, CA 92101, United States
The Boulevard, Langford Lane, Kidlington, Oxford OX5 1GB, United Kingdom
125 London Wall, London, EC2Y 5AS, United Kingdom

First edition 2021

Notices

Knowledge and best practice in this field are constantly changing. As new research and experience broaden our understanding, changes in research methods, professional practices, or medical treatment may become necessary.

Practitioners and researchers must always rely on their own experience and knowledge in evaluating and using any information, methods, compounds, or experiments described herein. In using such information or methods they should be mindful of their own safety and the safety of others, including parties for whom they have a professional responsibility.

To the fullest extent of the law, neither the Publisher nor the authors, contributors, or editors, assume any liability for any injury and/or damage to persons or property as a matter of products liability, negligence or otherwise, or from any use or operation of any methods, products, instructions, or ideas contained in the material herein.

ISBN: 978-0-12-820646-1
ISSN: 0065-2377

Publisher: Zoe Kruze
Acquisitions Editor: Sam Mahfoudh
Developmental Editor: Federico Paulo S. Mendoza
Production Project Manager: Denny Mansingh
Cover Designer: Greg Harris

Typeset by SPi Global, India

Contents

Contributors *vii*
Introduction *ix*

1. Soft microrobotics **1**
Roberto Bernasconi, Salvador Pané, and Luca Magagnin

1. Introduction 2
2. Robotics at the microscale 4
3. Materials for soft microrobots 6
4. Manufacturing techniques for soft microrobots 13
5. Actuation strategies for soft microrobots 18
6. Applications of soft microrobots 25
7. Hard-soft hybrid microrobots 28
8. Biohybrid soft microrobots 31
9. Conclusions 32
References 33

2. Advances in printing technologies for soft robotics devices applications **45**
Martina Aurora Costa Angeli, Manuela Ciocca, Luisa Petti, and Paolo Lugli

1. Introduction 46
2. Printing technologies for soft robotics 47
3. Printable materials and substrates for soft robotics 60
4. Examples of printed devices for soft robotics 75
5. Conclusions and outlook 81
References 82

3. Metal-organic frameworks (MOFs) for sensing **91**
Alessandro Sacchetti, Arianna Rossetti, and Javier Martí-Rujas

1. Definition of MOF 92
2. Sensing of gases, vapors and VOC 99
3. MOFs for sensing of biomolecules 109
4. Conclusions 118
References 118

4. Hydrogels for sensing applications **123**
Fabio Pizzetti and Giuseppe Perale

1. Introduction 124

2. Physical, chemical and biosensors 125
3. Hydrogels 126
4. Physicochemical sensing mechanism 129
5. Biochemical sensing mechanism 138
6. Hydrogel-based sensors for biomedical applications 145
7. Conclusions 150
References 150

5. Integrated microsystems for bridging multiscale elements 157
Koki Yoshida and Hiroaki Onoe

1. Introduction 158
2. Nano-scale function of hydrogels 158
3. Fabrication of hydrogel 161
4. Multi-scale function of hydrogels with functional materials 173
5. Integrated soft robots by bridging multiscale elements 181
6. Discussion 186
7. Conclusion 190
References 191

6. Smart sensors for volatile organic compounds (VOCs) and their possible application as end of service life indicator (ESLI) for respirator cartridges 197
Filippo Pinelli and Marco Miceli

1. Introduction 198
2. Smart sensors 200
3. Conclusions 228
References 228

7. Additive manufacturing of biomaterials 233
Miranda Torre, Sara M. Giannitelli, Emanuele Mauri, Marcella Trombetta, and Alberto Rainer

1. Introduction 234
2. Tissue engineering 234
3. Drug delivery 235
4. 3D printing 236
5. Biomedical applications 247
6. Conclusions 254
References 255

Conclusions 261
Index 263

Contributors

Roberto Bernasconi
Department of Chemistry, Materials and Chemical Engineering "Giulio Natta," Polytechnic of Milan, Milan, Italy

Manuela Ciocca
Free University of Bolzano-Bozen, Bolzano, Italy

Martina Aurora Costa Angeli
Free University of Bolzano-Bozen, Bolzano, Italy

Sara M. Giannitelli
Department of Engineering, Università Campus Bio-Medico di Roma, Rome, Italy

Paolo Lugli
Free University of Bolzano-Bozen, Bolzano, Italy

Luca Magagnin
Department of Chemistry, Materials and Chemical Engineering "Giulio Natta," Polytechnic of Milan, Milan, Italy

Javier Martí-Rujas
Department of Chemistry, Materials and Chemical Engineering G. Natta, Politecnico di Milano, Milano, Italy

Emanuele Mauri
Department of Engineering, Università Campus Bio-Medico di Roma, Rome, Italy

Marco Miceli
BLS Headquarters, Cormano, Milan, Italy

Hiroaki Onoe
Keio University, Kanagawa, Japan

Salvador Pané
Multi-Scale Robotics Laboratory, Institute of Robotics and Intelligent Systems, ETH Zurich, Zurich, Switzerland

Giuseppe Perale
Faculty of Biomedical Sciences, University of Southern Switzerland (USI), Lugano, Switzerland; Ludwig Boltzmann Institute for Experimental and Clinical Traumatology, Vienna, Austria

Luisa Petti
Free University of Bolzano-Bozen, Bolzano, Italy

Filippo Pinelli
Department of Chemistry, Materials and Chemical Engineering "Giulio Natta", Politecnico di Milano, Milan, Italy

Fabio Pizzetti
Department of Chemistry, Materials and Chemical Engineering "Giulio Natta", Politecnico di Milano, Milano, Italy

Alberto Rainer
Department of Engineering, Università Campus Bio-Medico di Roma, Rome; Institute of Nanotechnology (NANOTEC), National Research Council, Lecce, Italy

Arianna Rossetti
Department of Chemistry, Materials and Chemical Engineering G. Natta, Politecnico di Milano, Milano, Italy

Alessandro Sacchetti
Department of Chemistry, Materials and Chemical Engineering G. Natta, Politecnico di Milano, Milano, Italy

Miranda Torre
Department of Engineering, Università Campus Bio-Medico di Roma, Rome, Italy

Marcella Trombetta
Department of Engineering, Università Campus Bio-Medico di Roma, Rome, Italy

Koki Yoshida
Keio University, Kanagawa, Japan

Introduction

Soft robotics is the specific subfield of robotics dealing with constructing robots from highly compliant materials, similar to those found in living organisms. Soft robotics draws heavily from the way in which living organisms move and adapt to their surroundings. In contrast to robots built from rigid materials, soft robots allow for increased flexibility and adaptability for accomplishing tasks, as well as improved safety when working around humans. These characteristics allow for its potential use in the fields of medicine and manufacturing. To perceive the pervasiveness of soft robotics in research, a simple search in the Web of Science database as late as April 2021 for the keyword "soft robotics" resulted in over 6.6k entries, with a boost started in the early 2010s and still gaining increasing interest (Fig. 1).

The aim of this book is to provide a comprehensive overview on the broad field of soft robotics and how chemical engineering can be involved. The reader will be primed on the fundamentals of soft robotics and will be walked through the most salient applications of soft robotics in the different industrial and research fields. Importantly, the book will also pose emphasis on the open challenges and issues related to the implementation of soft robotics in large-scale products.

The book has been divided into seven chapters.

The first chapter deals with main principles of soft robotics and in particular soft microrobotics. Dr. Bernasconi (Chapter 1) describes the novel functionalities and actuation strategies that have been implemented in the last years. This chapter describes materials, fabrication techniques, actuation strategies, and applications of microrobots fabricated employing soft matter, focusing on some peculiar types of materials like biological entities and hard-soft hybrids.

Dr. Costa Angeli (Chapter 2) gives an overview on the printing technologies and printable materials that could be used in soft robotics. Strong attention is also devoted to the main challenges that should be solved to open the use of these technologies in industry.

Prof. Sacchetti (Chapter 3) provides further insights on metal organic frameworks (MOFs) in this field. The coordination between the metal centers and the organic scaffolds gives rise to complex assemblies which can develop into coordination polymers from one- to three-dimensional structures. In this chapter, the application of MOFs for the sensing of chemical species will be briefly illustrated. The interaction of the MOF with

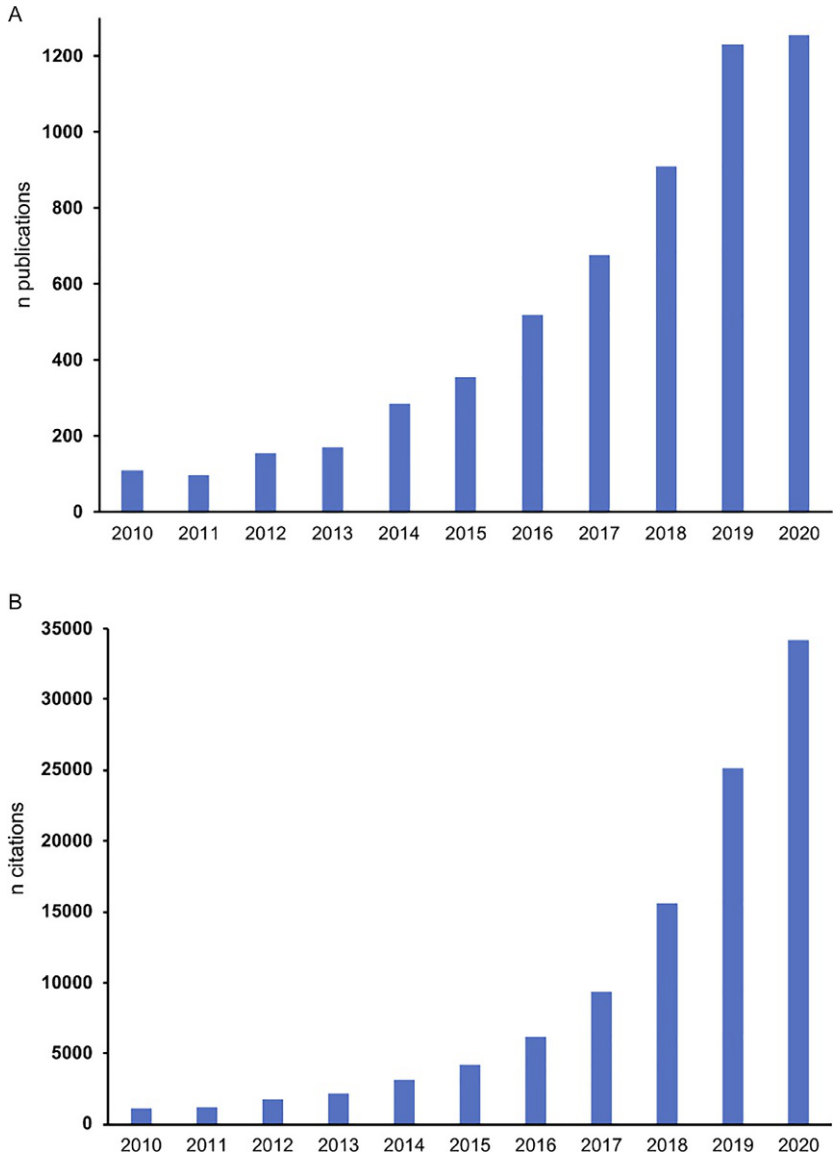

Fig. 1 Trend of publications and citations in the field of soft robotics. *Data source: WoS, April 2021.*

the guest often results in a modification of the MOF crystalline structure, which eventually produces a change in the physical properties of the materials. These variations can be exploited to detect the presence of a specific guest.

Another category of devices that seem to be extremely promising in sensing applications is represented by hydrogels, a three-dimensional structure made up from crosslinked polymers showing a hydrophilic behavior, biocompatible, and able to swell in the presence of a thermodynamic compatible solvent.

Prof. Perale (Chapter 4) discusses the advantages reached in the last years for hydrogel-based sensors both physicochemical sensors and biosensors.

Hydrogel flexibility is another key characteristic that make these materials extremely promising for soft robotics applications. Indeed polymer chains of the hydrogel have a nanoscale function of swelling and contracting in response to external stimuli. In particular, Prof. Onoe (Chapter 5) provides a detailed understanding of hydrogels and the recent development of novel fabrication and integration of hydrogel with functional materials such as magnetic nanoparticles, Pt catalytic, graphene, photonic colloidal crystal, and living cells.

In parallel with academic research studies also industrial applications of soft-based sensors are gaining high success. In this context, gas sensors and volatile organic compound sensors are for sure very interesting devices, thanks to the wide range of applications in which they can be employed. Dr. Pinelli (Chapter 6) gives an overview of the latest developed sensing materials that can be employed for volatile organic compound detection, focusing first of all on their synthesis and features and then going deeper in their engineering applications.

Finally, Prof. Rainer (Chapter 7) focuses the attention on the possibility to manufacture personalized biomedical devices (from metals to hydrogels) using additive manufacturing, where the donor shortage for organ transplantations and the lack of fully effective systems for drug administration still represent a major issue.

We hope you will enjoy reading this book.

The Editors

This page intentionally left blank

CHAPTER ONE

Soft microrobotics

Roberto Bernasconi[a,*], Salvador Pané[b], and Luca Magagnin[a]
[a]Department of Chemistry, Materials and Chemical Engineering "Giulio Natta," Polytechnic of Milan, Milan, Italy
[b]Multi-Scale Robotics Laboratory, Institute of Robotics and Intelligent Systems, ETH Zurich, Zurich, Switzerland
*Corresponding author: e-mail address: roberto.bernasconi@polimi.it

Contents

1. Introduction 2
2. Robotics at the microscale 4
3. Materials for soft microrobots 6
   3.1 Stimuli-responsive smart materials 8
   3.2 Synthetic and natural hydrogels 9
   3.3 Conductive polymers 11
   3.4 Self-assembled materials 12
   3.5 Materials for the future of soft microbotics 13
4. Manufacturing techniques for soft microrobots 13
   4.1 3D printing 15
   4.2 Laser micromachining and lithography 16
   4.3 Natural templating 17
   4.4 Other techniques 17
5. Actuation strategies for soft microrobots 18
   5.1 Chemical actuation 20
   5.2 Magnetic actuation 21
   5.3 Other actuation strategies 23
   5.4 Advanced actuation routes 23
6. Applications of soft microrobots 25
   6.1 Drug delivery 25
   6.2 Cell delivery 25
   6.3 Microsurgery applications 27
   6.4 Microdevices imaging and guidance 28
7. Hard-soft hybrid microrobots 28
8. Biohybrid soft microrobots 31
9. Conclusions 32
References 33

Abstract

In the last few decades, the highly multisciplinary field of microrobotics has seen important developments. Among the most significant landmarks in the field is the introduction of soft materials in the microfabrication of untethered devices. Novel functionalities

Advances in Chemical Engineering, Volume 57
ISSN 0065-2377
https://doi.org/10.1016/bs.ache.2021.04.001

and actuation strategies have been implemented thanks to the use of soft and smart materials. In this context, it is useful to take stock of the current situation of soft microrobotics to provide a complete overview of the field. The present chapter describes materials, fabrication techniques, actuation strategies and applications of microrobots fabricated of soft materials. Finally, we also focus on some peculiar types of materials such as biological structures and hard-soft hybrids.

1. Introduction

The last few decades have seen the emergence of soft robotics, an innovative field in mechatronics that is largely inspired by biological structures and makes use of so-called soft materials (Dong, 2019; Hassan et al., 2011). These are substances (e.g., liquids, polymers, foams, gels, biological structures, etc.) that can be easily deformed by mechanical, chemical or thermal stress. Soft robotics capitalizes on these materials in the realization of highly functional devices, radically changing the conventional approach followed so far. Soft, highly deformable and adaptive structures present significant advantages over conventional hard robotic components: they are characterized by a high usage flexibility, display a higher affinity with biological structures, they allow gentle manipulation of fragile materials, their cost and weight are considerably reduced, and their biocompatibility (and resorbability) characteristics are typically good. Moreover, soft materials present a high potential for the manufacturing of untethered soft machines and can be integrated with stretchable electronics and sensors (Boyraz et al., 2018; Schmitt and Haeufle, 2015). The best evidence of the potential of soft robotics and the interest from the scientific community are the large number of reviews that have been published in the last few years (Kim et al., 2013a; Lee et al., 2017; Majidi, 2014) as well as the release of a dedicated journal (Soft Robotics (SoRo), 2021).

The advantages and features of macroscopic soft structures can also be transferred to the microscale, giving rise to the novel concept of soft microrobotics (Hu et al., 2018a; Medina-Sánchez et al., 2018). By employing a wide variety of materials (metals, polymers or ceramics), researchers have fabricated remotely actuated devices using lithography (Tung et al., 2014), nanotemplating (Li et al., 2014), sputtering deposition (Huang et al., 2009), electrodeposition (Zeeshan et al., 2014), 3D printing (Bernasconi et al., 2018, 2019a; Qiu et al., 2015) or combinations of these techniques (Kim et al., 2013b, 2016a). The swimming capabilities of motile microstructures

in fluidic environments has already been accomplished using a number of different propulsion strategies, which are based on various energy sources (chemical reactions (Paxton et al., 2004), magnetism (Chautems et al., 2017; Sitti and Wiersma, 2020), electromagnetic radiation (Sitti and Wiersma, 2020), ultrasound (Aghakhani et al., 2020), or combinations thereof. Following the original concept, micrometric-sized untethered devices can be remotely controlled and guided to perform specific medical (Choi et al., 2020; Jang et al., 2019) or environmental (Maric et al., 2020) tasks. In medical applications, microrobots can be guided in-vivo in the human body to perform a profusion of different tasks, including cell delivery (Erkoc et al., 2019), drug release (Luo et al., 2018), diagnosis (Nelson et al., 2010) and micromanipulation (Kim et al., 2016b). In addition to the established functionalities typical of rigid microrobots, the introduction of soft materials could potentially create microrobots, inspired by living microorganisms, that simulate biological systems to an even higher degree. This would result in soft micromachines with superior biocompatibility, higher flexibility and motility, and enhanced adaptability. Although the production and actuation of untethered machines at the microscale presents significant challenges, most have been addressed through various approaches. It is important to emphasize the relative abundance of soft microrobotics literature, with many significant publications being released every year. This is indicative of the importance of the topic in perspective and shows the potential for significant developments in the coming years.

With this in mind, the aim of this chapter is to provide a review of the current state of soft microrobotics, with a general overview of existing manufacturing approaches, actuation methodologies and applications, based primarily on literature examples and the support of some key reviews. Robotics, soft robotics and consequently, soft microrobotics, are all multidisciplinary branches of engineering, combining disciplines such as materials science, biology, chemistry, electronics and physics. The materials and techniques employed for the manufacturing of soft microrobots will be described in this chapter, as well as the most interesting applications for such microsystems. The differences between rigid and soft microrobots and the manufacturing techniques of macro and micro soft machines will also be discussed. In general, certain manufacturing techniques and actuation approaches can also be used for soft microrobots, but with some important distinctions. The final part of this chapter focuses on two additional soft robotics topics: rigid-soft hybrid microdevices and biohybrid microrobots.

2. Robotics at the microscale

Robotic devices that work at the microscale are subject to completely different physical interactions with the surrounding environment when compared to their macroscopic counterparts (Abbott et al., 2007; Nelson et al., 2008; Qiu et al., 2014). The general laws of physics are obviously the same, but their relative influence on the final behavior of the device is significantly different (Chaillet and Régnier, 2013). Micromachines typically operate in what is known as a low Reynolds number (*Re*) regime, defined by Eq. (1)

$$Re = \frac{\rho v L}{\mu} \ll 1 \tag{1}$$

where ρ is the density of the fluid, v is the speed of the device, L is its characteristic length and μ is the dynamic viscosity. From a physical point of view, *Re* represents the ratio between inertial (F_i) and viscous (F_v) forces acting on the system (Eq. (2)

$$Re = \frac{F_i}{F_v} \tag{2}$$

Consequently, when $Re \ll 1$, viscous forces dominate over inertial forces, e.g., volume-related forces tend to become negligible with respect to surface-related forces. Under these conditions, the fluid dynamics of the system is characterized by instantaneous and time-reversible flows. E. M. Purcell, who studied motion at low *Re* in 1977 (Purcell, 1977), noticed that the high reversibility of the flows created around objects swimming at the microscale makes reciprocal motion impossible (based on a sequence of moves that are identical when reversed). Such motion would invariably result in a zero net displacement (provided the fluid is incompressible and Newtonian). Consequently, movement at a low *Re* generally involves nonreciprocal actuation to be effective. These considerations were stated by the Purcell's "scallop theorem."

At the microscale, non-inertial interactions such as electrostatic and van der Waals interactions tend to dominate. The latter are of particular interest, since their relative importance with respect to other forces increases as the size of the object decreases (Abbott et al., 2007). The van der Waals attraction between a sphere with radius r and an infinite plane can be described by Eq. (3)

$$F_{VDW} = \frac{H\, r}{8\, \pi\, x^2} \tag{3}$$

where x is the distance between the sphere and the plane, r is the radius of the sphere and H is the Hamaker constant. If the distance between the sphere-plane and the radius of the sphere x are equal, it is evident that the force decreases with x^{-1}. Consequently, its relative importance becomes dominant when x is very small. Similar considerations can be made for electrostatic interactions, which are governed by the Coulomb's law (Eq. 4)

$$F_C = k_e \frac{q_1\, q_2}{x^2} \tag{4}$$

where q_1 and q_2 are the two charged particles, k_e is Coulomb's constant and x is the distance between the particles. In this case, the force decreases with x^{-2}. In addition to interactive interactions, the surface tension and viscous drag strongly influence the motion of micrometric devices moving at many body lengths per second. In general, all these interactions strongly depend on the surface of the device rather than its volume and are of particular interest in the downscaling process from macro to micro robotics (Abbott et al., 2009; Chaillet and Régnier, 2013).

Since the emergence of life on Earth, biological microorganisms have swum with flagella and cilia that can efficiently address the problem of low *Re* propulsion in viscous fluids. It is therefore not surprising that researchers took inspiration from living microorganisms for the design of artificial microrobots (Palagi and Fischer, 2018; Peyer et al., 2013). For example, one of the most represented class of microdevices in literature is artificial bacterial flagella (ABFs), which mimic the shape of helical flagella of bacteria (Zhang et al., 2009a, b). ABFs are generally controlled wirelessly using a low-strength rotating magnetic field, which allows high control over their direction and speed (Zhang et al., 2010). ABFs are particularly useful to describe and contextualize the challenges connected to downscaling robots to the micrometric world, and a myriad of shapes and approaches have been proposed for bioinspired microrobots. ABFs can move in low *Re* environments due to their chirality, which lends itself to the scallop theorem thanks to their non-reciprocal rotatory propulsion. Furthermore, the corkscrewing motion obtained from their actuation is particularly efficient and can achieve an actuation speeds of many body lengths per second. Their behavior can be described by a propulsion matrix (Eq. 5)

$$\begin{bmatrix} f \\ \tau \end{bmatrix} = \begin{bmatrix} a & b \\ b & c \end{bmatrix} \begin{bmatrix} v \\ \omega \end{bmatrix} \tag{5}$$

where v is the forward velocity, ω is the angular velocity, τ is the applied torque and f is the applied force. The most interesting point of this matrix is the well-defined and linear relationship between the force and torque applied on the device, and its translational and rotational speeds, as well as the inter-relationship between speed of rotation and linear displacement. It suggests that the translational speed of the devices can be controlled by adjusting their rotation speed. In fact, ABFs present a linear dependence between the rotation frequency of the magnetic field applied and their linear speed. This constitutes one of the most relevant examples of fine actuation control at the microscale employing architectures derived from the natural world.

3. Materials for soft microrobots

The greatest difference between conventional and soft microrobotics resides in the typology of the materials employed. As the name suggests, soft microrobotics capitalizes on the use of the so-called soft materials (Fig. 1). In their commentary on soft robotics, Sitti and Alici (Alici, 2018; Sitti, 2018) identify some fundamental characteristics for suitable materials. The first and most significant, which is common to all applications, is the capability to withstand large elastic deformation. This enables the use of locomotion strategies that would be impossible to obtain using rigid materials, and permits physical adaptability to the external environment. Quantitatively, adapted materials should have an elastic modulus not higher than 1000 MPa and should be highly stretchable (strain not lower than 10% and possibly even higher than 100%). In addition to this fundamental characteristic, Alici (2018) further specifies that materials for soft microrobotics should not only allow for large deformations, but also have a programmable behavior. Ideally, soft robots should combine multiple functions (actuation, manipulation, sensing, drug release, etc.) in a single continuum body. It is therefore essential to employ smart materials, with programmable compliance and functionalities activated by external stimuli. Furthermore, soft materials should be biocompatible and easily integrable with living tissues, and they should also be inexpensive and easily implementable in a large variety of fabrication techniques. These fundamental requirements can be satisfied by a great variety of hydrogels and polymeric materials, some of which are often

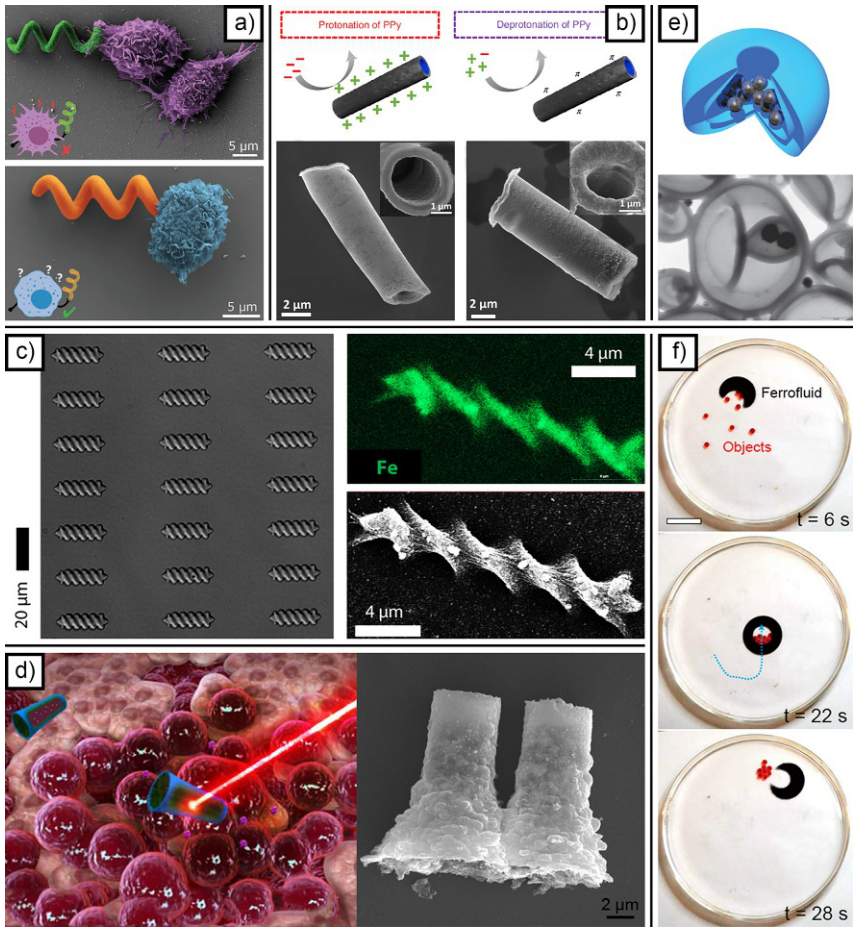

Fig. 1 SEM image of macrophage interacting with a control robot and with a 3D printed zwitterionic microrobot made of ionic methacrylates (A); programmable polypyrrole-based microrobots incorporated with a Pt catalytic layer and superparamagnetic iron oxide nanoparticles (B); 3D fabrication of microswimmers starting from gelatin/magnetite and using two-photon polymerization (C); biodegradable, self-propelled bovine serum albumin/poly-L-lysine multilayer rockets for light triggered release (D); platinum-loaded stomatocytes with autonomous movement (E); magnetically actuated soft robots based on ferrofluids (F). *Panel (A) reprinted with permission from Cabanach P, Pena-Francesch A, Sheehan D, et al: Zwitterionic 3D-printed non-immunogenic stealth microrobots,* Adv Mater *32 (42):1–11, 2020. https://doi.org/10.1002/adma.202003013; Panel (B) reprinted with permission from Dekanovsky L, Khezri B, Rottnerova Z, et al: Chemically programmable microrobots weaving a web from hormones,* Nat Mach Intell *2(11):711–718, 2020. https://doi.org/10.1038/s42256-020-00248-0; Panel (C) reprinted with permission from Ceylan H, Yasa IC, Yasa Oet al: 3D-printed biodegradable microswimmer for theranostic cargo delivery and release,* ACS Nano *13(3):3353–3362, 2019. https://doi.org/10.1021/acsnano.8b09233; Panel (D) reprinted with permission from Wu Z, Lin X, Zou X, et al: Biodegradable protein-based rockets for drug transportation and light-triggered release,* ACS Appl Mater Interfaces *7(1):250–255, 2015. https://doi.org/10.1021/am507680u; Panel (E) reprinted with permission from Wilson DA, Nolte RJM, Van Hest JCM: Autonomous movement of platinum-loaded stomatocytes,* Nat Chem *4(4):268–274, 2012. https://doi.org/10.1038/nchem.1281; Panel (F) reprinted with permission from Fan X, Dong X, Karacakol AC, et al: Reconfigurable multifunctional ferrofluid droplet robots,* Proc Natl Acad Sci U S A *117(45):27916–27926, 2020a https://doi.org/10.1073/pnas.2016388117.*

stimuli-responsive, including artificial and natural hydrogels, conductive polymers and a significant number of nanocomposites. The latter are of interest due to their ability to combine many functionalities in the same material, enabling the production of multifunctional soft robotic systems.

3.1 Stimuli-responsive smart materials

One of the most attractive properties of soft materials is the option to program the response of the material when subject to a particular stimulus (Theato et al., 2013) or stimuli (Cao and Wang, 2016; Fu et al., 2018). This introduces the possibility to change the shape of the device upon exposure to a controlled stimulus. This property can be used to induce the motion of the microrobots or to introduce novel functionality (such as gripping ability, triggered drug release or cell delivery) (Soto et al., 2021). Many different types of stimuli have been used to trigger a response in suitable materials, such as pH, temperature, magnetic fields, electrochemical, light, ultrasound or biological agents (Cao and Wang, 2016). The induced response can vary from a mechanical action (as with shape-memory polymers), to a change in permeability (Stuart et al., 2010; Wei et al., 2017), a variation in electrical properties or a color modification (Gao et al., 2019).

In general, the ability of a polymeric material to change its properties in response to an external stimulus can be controlled at the molecular level by introducing suitable functional groups, or by controlling the architecture of the molecular backbone. Temperature sensitive materials, for example, are usually built starting from an alkylic polymeric chain where specific groups are grafted. Such groups are characterized by hydrophobic and hydrophilic moieties and a variation in the external temperature can alter their interaction, thereby favoring molecular rearrangement (Almeida et al., 2012). Materials such as poly[tri(ethylene glycol) methyl ether acrylate] (PTEGMA) or poly(*N*-isopropylacrylamide) (PNIPAM) fall into this category. Interactions between different groups in the same molecule can also be further controlled by synthesizing block copolymers (Jochum and Theato, 2013), which can be used to control a color or transparency variation in the final material. Light-sensitive smart materials are mainly based on the presence of chromophores in the molecular backbone. Light driven shape-changing polymers can be created through the incorporation of light sensitive groups or molecules into the polymer (Stoychev et al., 2019). For example, many materials reported in literature contain an azobenzene moiety, attached directly to the polymeric chain or introduced via block copolymerization (Jochum and Theato, 2013; Stoychev et al., 2019). In some cases, such azobenzene

derivatives present liquid crystal properties (Kim and Jeong, 2019; Mehta et al., 2020) that can be exploited in specifically tailored microactuators (Pilz Da Cunha et al., 2020a). pH-sensitive polymers are invariably characterized by the presence of acidic or alkaline groups on the polymeric chain (Cao and Wang, 2016; Kocak et al., 2017). These moieties, which include, for example, carboxylic acids or tertiary ammines (Ahn et al., 2008; Cao and Wang, 2016), respond to variations in the pH of the external environment. Specifically, such ionic groups are counter-balanced by oppositely charged ions that can diffuse in and out of the polymer structure, thus varying the mechanical properties of the material or its permeability (Ahn et al., 2008). In other instances, pH variations can change the affinity between different groups present in the same molecule (introduced, for example, via block polymerization) (Ahn et al., 2008). Electrochemically responsive soft materials usually contain redox groups that are sensitive to the application of an electric field (Zhang et al., 2017), for example, disulfide bridges (Huo et al., 2014), nitroxide groups (Cao and Wang, 2016) or ferrocene derivatives (Peng et al., 2014). One of the most interesting characteristics of redox responsive materials is that the redox sensitive species can also be separated from the polymeric chain. For example, a metallic inorganic ion in a polymer solution will undergo oxidation/reduction between different valence states. An example of this is Cu^{2+}, which can be mixed with hydrogels and reduced to Cu^{+} as the hydrogel undergoes changes in mechanical properties due to an alteration in the crosslinking degree (Harris et al., 2013).

The final important characteristic of stimuli-responsive smart materials is their ideal integrability with 3D printing technologies, which gives origin to the 4D printing approach (Kuang et al., 2019). In this case, the fourth dimension for 3D printing is time, as the use of stimuli responsive materials introduces a time dependent behavior induced by the external stimulus applied. Smart materials can be either directly printed using extrusion based technologies (like fused deposition modelling) or, by implementing suitable materials with photo-initiators, they can be printed via photoinduced polymerization (Shafranek et al., 2019; Suriano et al., 2019). 4D printing can also be easily scaled down to the microscale (Spiegel et al., 2020).

3.2 Synthetic and natural hydrogels

Hydrogels are among the most common materials used for the construction of soft microrobotic systems. These materials fulfill the majority of the requirements previously discussed: they can withstand large deformations, their chemistry can be easily modified to introduce programmable behaviors,

they are inexpensive and display optimal biocompatibility characteristics (Lee et al., 2020). Consequently, a wealth of examples for hydrogel-based microrobots is available in literature.

This class of materials includes water swellable polymers obtained by chemical synthesis or by extraction from natural sources. One of the most utilized synthetic hydrogels is poly(ethylene glycol) diacrylate (PEGDA), which is used, for example, by Hu et al. (2012) for the realization of disc-shaped microrobots optothermally actuated by laser-induced bubbles. Also Fusco et al. (2015) employed PEGDA for the realization of shape switching microdevices for drug delivery. Some stimuli responsive polymers are actually hydrogels. One of the most widely used synthetic hydrogel in soft microrobots fabrication is PNIPA, which has interesting thermosensitive properties (Irie, 1993). In particular, it can reduce its size in response to a temperature increase. Tabatabaei employed PNIPA (Tabatabaei et al., 2011) to manufacture shrinkable microdevices suitable for medical intervention in the vascular network. In addition to chemical synthesis, nature is another important source of soft hydrogels for possible application in soft microrobotics. An important example is alginate, which was used by Ali et al. to produce rolling microbeads that could potentially be used for tissue engineering or pharmaceutical research (Ali et al., 2016). Palagi et al. fabricated magnetically propelled microrobots by pouring droplets of alginate into calcium chloride (Palagi et al., 2011). Mair et al. synthesized magnetic alginate capsules usable as tumbling robots for manipulation and drug delivery (Mair et al., 2019). Chitosan can also be used for microdevice production, as demonstrated by Go et al. with their multifunctional biodegradable devices (Go et al., 2020).

In many cases, two or more hydrogels are blended to tailor their mechanical or functional properties. For example, Kim et al. blended gelatin and poly vinyl alcohol (PVA) (Kim, 2019) to improve the thermal stability of gelatin while maintaining its biocompatibility. Lee et al. blended alginate and PNIPA (Lee et al., 2018) to create soft microrobots for controlled drug delivery. In this case, alginate was used to address drug release and PNIPA to tune the release. Some microrobot designs are based on multilayers of different hydrogels: Chen et al. designed double-layer drug-loaded microrobots (Chen et al., 2020), with an outer layer of alginate hydrogel and an inner layer of chitosan microspheres, and Kim et al. created a bilayered microrobot (Kim et al., 2020a), containing a gelatin/PVA therapeutic layer and a PEGDA/magnetite actuation layer. In most cases, hydrogels are used in the form of composites to combine different functionalities and

in particular to allow magnetic movement. Due to their non-magnetic nature, hydrogels have to be combined with magnetic materials, in most cases magnetite nanoparticles. This is the approach followed in virtually all the examples cited so far (Ali et al., 2016; Chen et al., 2020; Go et al., 2020; Kim, 2019; Kim et al., 2020a; Lee et al., 2018; Mair et al., 2019; Palagi et al., 2011; Tabatabaei et al., 2011). Similarly, Li et al. used NdFeB nanoparticles (Li et al., 2018) to impart magnetic properties in their polymeric microrobots. Another important advantage of hydrogels is the possibility for functionalization after polymerization in order to link molecules, with a cleavable bond, to specific points of the polymeric backbone (Mauri et al., 2017). Bond cleavability can be governed by many different stimuli able to break chemical bonds, like pH (Mauri et al., 2017) or light (Wang et al., 2020). This strategy is of great interest for drug delivery applications, in which the release can be triggered to take place only when desired inside human body (Bernasconi et al., 2021). A specific mention must be given to 3D printable hydrogels—to make a hydrogel 3D printable with stereolithography (SLA) or two-photon lithography (2PL), its monomeric form is used (which must have suitable reactive groups) and it is activated with a photoinitiator. Reports on the use of many different monomers are available in literature: ionic methacrylates (Cabanach et al., 2020), modified gelatins (Ceylan et al., 2019) and PEGDA (Park et al., 2019).

3.3 Conductive polymers

Conductive polymers represent an interesting class of materials for the potential development of soft microrobots. In addition to biocompatibility and deformability, their ability to conduct electricity introduces important attributes over other polymeric materials. For example, they can be electropolymerized (Patois et al., 2011) and consequently nanostructured via templating techniques (Bernasconi et al., 2019b). These attributes have already been utilized for the fabrication of microrobots (Bernasconi et al., 2020; Zeeshan et al., 2014). Moreover, some conductive polymers present a redox behavior accompanied by a volume variation, which can be used to build microactuators (Yan et al., 2017).

A notable example of such actuators was provided by Benouhiba et al., who used polypyrrole (PPy) to build soft millimeter-sized robots (Benouhiba et al., 2019). Tyagi et al. electropolymerized PPy on gold and passive gel to build microactuators for soft microrobots (Tyagi et al., 2020a). The redox behavior of PPy can also be exploited to alter the affinity

of the microrobot for specific molecules. Dekanovsky et al. built programmable polypyrrole-based microrobots (Dekanovsky et al., 2020): as the pH of the environment changed, the surface affinity of PPy toward hormonal pollutants improved, thus allowing efficient sorting and collection. Other conductive polymers also can be used in addition to PPy: polyaniline (PANI) and poly(3,4-ethylenedioxythiophene) (PEDOT) constitute notable examples. Their ability to withstand electropolymerization allowed Gao et al. to electroform chemically propelled tubular microdevices (Gao et al., 2012).

3.4 Self-assembled materials

Another class of materials that is interesting for soft microrobotics are self-assembled supramolecular structures. These self-organizing assemblies are typically composed of elongated molecules that have two distinct ends with opposite behaviors, hydrophobic and hydrophilic, which self-assemble using intermolecular electric interactions. A notable example of self-assembled structures can be found in nature, where cell membranes are comprised of a self-organized double layer of phospholipids (Coskun and Simons, 2011).

From the soft microrobotics point of view, an interesting example of self-assembled microdevices are stomatocytes. These are synthetic polymersomes with an introflexed bowl-shaped structure (Kim et al., 2010a). Stomatocytes are normally self-assembled starting from block copolymers, whose behavior can be tuned by manipulating the phase behavior of one of the two monomers (Kim et al., 2010a) or their magnetic susceptibility (Van Rhee et al., 2014). Furthermore, stomatocytes have the ability to trap nanoparticles (Van Rhee et al., 2014), allowing Pt or magnetite nanoparticle loading for chemical (Wilson et al., 2012) or magnetic (Zhang et al., 2020) actuation. Tu et al. built stomatocytes using two block copolymers, poly(ethylene glycol)-b-poly (ε-caprolactone) (PEG-b-PCL) and poly(ethylene glycol)-b-polystyrene (PEG-b-PS) (Tu et al., 2017a), they loaded the devices with Pt nanoparticles for use in controlled doxorubicin delivery. Another interesting approach is the one followed by Mathesh et al., who introduced pH sensitivity in their stomatocytes (Mathesh et al., 2020) to build biocompatible $CaCO_3$-loaded devices that could move in slightly acidic environments and deliver doxorubicin. Ph sensitivity was also introduced by Tu et al., who rendered their stomatocytes sensitive to pH variations by introducing a disulfide bridge between the hydrophilic poly(ethylene glycol) block and the hydrophobic polystyrene block (Tu et al., 2017b). By doing this, the devices released their drugs and self-destroyed for resorption.

3.5 Materials for the future of soft microbotics

Even if not yet completely implemented in fully working microdevices, some advanced materials currently under development show considerable potential for soft microrobots fabrication. They present unique behaviors, specific actuation patterns and properties that makes them unclassifiable under the previously discussed categories. A notable example is stimuli-responsive polymeric liquid crystals (White and Broer, 2015). With respect to common stimuli-response polymers, these are able to self-organize and form parts with homogeneous composition but with a spatial variation of the mechanical properties. Liquid crystals show a marked tendency to self-organize in stacks and piles, whose orientation can be controlled by applying rubbing, magnetic fields and light. Another class of relevant materials is DNA hydrogels, which are fabricated via gelation of DNA building blocks (Jahanban-Esfahlan et al., 2019). These materials share many advantages with other hydrogels, but also present specific characteristics: they gelate under physiological conditions, and drugs can be encapsulated in them during the gelation process. Significantly, they have already been used to fabricate microspheres for protein delivery (Kim et al., 2016c). Moreover, magnetic actuability of DNA hydrogels via blending with magnetic nanoparticles has already been demonstrated (Ma et al., 2017). Moving to extremely low elastic moduli, ferrofluids may also find potential applications in the production of soft robots (Fan et al., 2020a, b). Fan et al. demonstrated magnetic actuation and object manipulation at the millimeter scale with a magnetite based ferrofluid.

4. Manufacturing techniques for soft microrobots

The discussion on the materials employed for soft microrobots would be incomplete without considering the manufacturing techniques, as in many cases, materials are specifically tailored for the technique employed or vice versa (Fig. 2). Rigid microrobot manufacturing relies on a wide selection of manufacturing techniques or combinations of these techniques, making it one of the most multidisciplinary fields in current research. In the case of soft-robotics, some techniques are limited by the characteristics of the materials employed. For example, electrodeposition of metals shows limited applicability, due to the high elastic modulus of the materials deposited. In contrast, some techniques, e.g., 3D printing, adapt well to the production of soft microrobots.

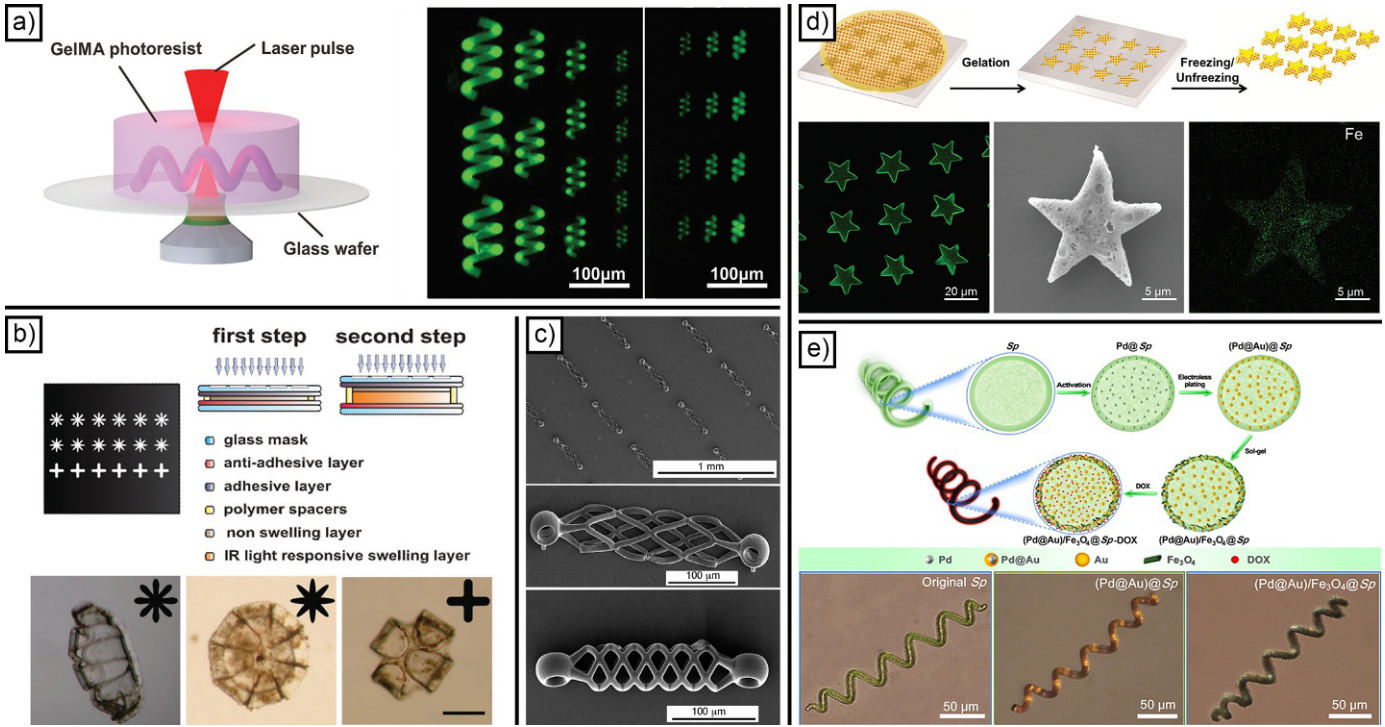

Fig. 2 See figure legend on opposite page.

4.1 3D printing

One of the most interesting technologies employed in soft microrobotics manufacturing is 3D printing (Gibson et al., 2014; Li and Pumera, 2021). The main advantages include low cost, low material wastage, superior design freedom and high customizability of printed parts. In light of these advantages, 3D printing has already been extensively implemented in standard soft robotics applications (Gul et al., 2018; Wallin et al., 2018). Although the term "3D printing" indicates a substantial variety of manufacturing technologies (Gibson et al., 2014), the only two techniques widely employed for microfabrication are micro stereolithography (μ-SLA) and two-photon lithography (2PL) (Fassi and Shipley, 2017). Both technologies are based on the selective polymerization of a photocurable monomer by means of a laser. In the case of μ-SLA, the laser works in the UV range, while for 2PL the laser works in the IR range. This disparity is linked to the different starting mechanisms followed by the initiators employed in the two technologies. In μ-SLA, the photoinitiator absorbs a single high-energy photon to start the polymerization. In 2PL, the photoinitiator absorbs two low-energy photons before giving origin to the reactive radical that starts the reaction. As a consequence, 2PL is significantly more precise than μ-SLA, since the density of light required for the double absorption process is reached in a smaller area around the focus of the laser beam (Piqué, 2020). In addition, μ-SLA

Fig. 2 2PL 3D printed helical microswimmers made of photocrosslinkable hydrogel gelatin methacryloyl (A); lithography fabricated microrobotic platform for on-demand release of microbeads (B); indirectly 3D printed soft robotic microstructures (C); star-shaped microswimmers obtained from the gelation of a PVA/alginate/magnetic nanoparticles inside a micromold (D); biotemplate fabricated microrobots based on *Spirulina* for targeted delivery (E). *Panel (A) reprinted with permission from Wang X, Qin XH, Hu C, et al: 3D printed enzymatically biodegradable soft helical microswimmers,* Adv Funct Mater *28(45):1–8, 2018. https://doi.org/10.1002/adfm.201804107; Panel (B) reprinted with permission from Fusc, S, Saka, MS, Kennedy S, et al: An integrated microrobotic platform for on-demand. Targeted therapeutic interventions,* Adv Mater *26(6):952–957, 2014. https://doi.org/10.1002/adma.201304098; Panel (C) reprinted with permission from de Marco C, Alcântara CCJ, Kim Set al: Indirect 3D and 4D printing of soft robotic microstructures,* Adv Mater Technol *4(9):1–7, 2019. https://doi.org/10.1002/admt.201900332; Panel (D) reprinted with permission from Hu N, Wang L, Zhai Wet al: Magnetically actuated rolling of star-shaped hydrogel microswimmer,* Macromol Chem Phys *219(5):1–6, 2018b. https://doi.org/10.1002/macp.201700540; Panel (E) reprinted with permission from Wang X, Cai J, Sun L, et al: Facile fabrication of magnetic microrobots based on spirulina templates for targeted delivery and synergistic chemo-photothermal therapy,* ACS Appl Mater Interfaces *11(5):4745–4756, 2019. https://doi.org/10.1021/acsami.8b15586.*

operates layer-by-layer, while 2PL does not (hence its classification as Direct Write technology). Both technologies can, in principle, also achieve multi-material deposition (Alcântara et al., 2020; Soreni-Harari et al., 2020), thereby expanding the potential for combining more than a single functionality in the same device.

As mentioned, 2PL is promising due to its small printable feature size, Wang et al. (2018) and Dong et al. (2020) demonstrated the potential of 2PL for soft microrobot fabrication by printing ABFs for cell delivery, using a gelatin modified to make it photocurable. Cabanach et al. also used 2PL for ABFs microfabrication (Cabanach et al., 2020). Giltinan et al. manufactured composite PETA ABFs loaded with hard magnetic FePt nanoparticles (Giltinan et al., 2021) using 2PL. μ-SLA can, in principle, also be used for soft robotic fabrication (Ge et al., 2020).

Another interesting 3D printing technique, although to a lesser extent than μ-SLA and 2PL, is microscale continuous optical printing (μCOP), which offers high fabrication speeds, improved feature resolution and high throughput. Zhu et al employed this technology to produce PEGDA-based microfish able to achieve chemically-induced swimming (Zhu et al., 2015). Extrusion techniques like syringe-based printing (Tyagi et al., 2020b) can also be used for soft microrobots production, however this technique lacks the resolution required to produce microdevices. A notable example was provided by Son et al., who produced soft microgrippers via syringe based bioprinting (Son et al., 2020). However, these microgrippers had a dimension of more than one centimeter, with finer features of a few millimeters. Despite their relatively large dimensions, the grippers successfully demonstrated magnetic guidance and ultrasound mediated actuation. Soft microrobots can be also fabricated using indirect 3D printing. This technique, which falls into the categories of both 3D printing and micromolding, was developed by de Marco et al. (2019), who used 2PL to 3D print a micromold, which served as the negative shape of the microrobot. The cavity was then filled with a hydrogel and the resist was stripped to form soft robotic microstructures.

4.2 Laser micromachining and lithography

Soft microrobotic systems can also be manufactured with more traditional manufacturing techniques like laser machining or lithography. These techniques show considerable advantages in terms of throughput and miniaturization, but have significant disadvantages in terms of tri-dimensionality and customizability.

Kim et al. used laser micromachining to manufacture biodegradable drug-encapsulating microrobots based on poly(lactic-co-glycolic acid) (PLGA) (Kim et al., 2018). Gao et al. employed the same technique to produce magnetically actuated flowerlike soft platforms for micromanipulation (Gao et al., 2016). Fusco et al. and Li et al. provided two notable examples of lithography-fabricated devices. The former fabricated drug-releasing microrobots actuated by temperature variations (Fusco et al., 2014), while the latter built pH-responsive microdevices for drug delivery (Li et al., 2016a). In both cases, two hydrogel layers characterized by different swelling behaviors were patterned via lithography.

4.3 Natural templating

As already mentioned, nature is a major source of inspiration for microrobot shapes and functionalities. It even provides natural templates that can be employed to manufacture artificial soft microrobots, such as monocellular entities, either eucariotic or procariotic. An important example was provided by Magdanz et al., who built magnetically controllable microdevices using electrostatic self-assembly of non-motile sperm cells and magnetic nanoparticles (Magdanz et al., 2020). The result, called "IRONsperm," was found to be biocompatible and able to carry drugs for localized delivery applications.

Following a similar approach, Wang et al. coated monocellular algae of the genus Spirulina with magnetic nanoparticles to impart magnetic motility (Wang et al., 2019). Such algae, as their name suggests, are characterized by a spiral shape that surprisingly resembles the morphology of synthetic ABFs. For this reason, they are a natural choice for the realization of soft biomimetic ABFs. Wang et al. applied core-shell-structured Pd@Au nanoparticles, magnetite nanoparticles and doxorubicin on the surface of the Spirulina cells to obtain microrobots characterized by magnetic actuability and a synergistic chemo-photothermal therapeutic efficacy.

4.4 Other techniques

Some additional techniques for soft microrobot fabrication are micromolding and electrodeposition. Micromolding can be used to manufacture micrometric sized devices with a variety of materials. It uses molds that are fabricated via other patterning techniques like lithography. When working at the microscale however, this technology presents additional difficulties as opposed to standard macromolding, for example, mold release can be

challenging. Hu et al. cleverly overcame this obstacle by applying periodical freezing/unfreezing cycles to expand and contract the molded material and induce the release form the micromold (Hu et al., 2018b). Thanks to this approach, they were able to fabricate micrometric star-shaped PVA/alginate hydrogel microswimmers for drug release. Electrodeposition is routinely employed in the fabrication of metallic microrobots. For soft microrobots, its importance as a fabrication technique is considerably diminished. However, it can be used to manufacture devices based on conducting polymers or hydrogels. Hu et al employed a two-step electrodeposition of CoNi and alginate hydrogel to manufacture hydrogel pillars with defined structures (Hu et al., 2016). Gao et al. used electrodeposition for the production of their chemically actuated microtubules based on the conducting polymers PPy, PANI and PEDOT (Gao et al., 2012).

Worthy of mention in this review is also self-assembly. Groups of particles at the microscale often interact between themselves as a consequence of local interactions (electrostatic, chemical, etc.). As a result of this phenomenon, they often tend to self-organize in specific structures. This feature can be tailored and exploited to produce desired structures at the microscale. Self-assembling materials, which were discussed in Section 3.4, exhibit exactly this behavior and can be used to manufacture structures like stomatocytes. In addition to specifically tailored materials however, a great variety of materials exhibit self-assembly behavior that can be exploited for soft microrobotics fabrication. Magnetic nanoparticles, for example, tend to self-organize and attach to surfaces, allowing the functionalization of biotemplates (Magdanz et al., 2020; Wang et al., 2019). Self-assembly is, in some cases, not limited to single molecules or nanometric objects, but can also be observed in larger structures. Indeed, it can also be used to assemble at the microscale, as demonstrated by Hamed et al. (2018) and Wang et al. (2017).

5. Actuation strategies for soft microrobots

The propulsion of soft robots have an advantage over their rigid counterparts, as the presence of highly deformable regions in the device can allow for additional degrees of freedom, providing innovative actuation strategies (Fig. 3). Some of these strategies can emulate natural actuation, again evoking the similarity between artificial soft materials and natural tissues.

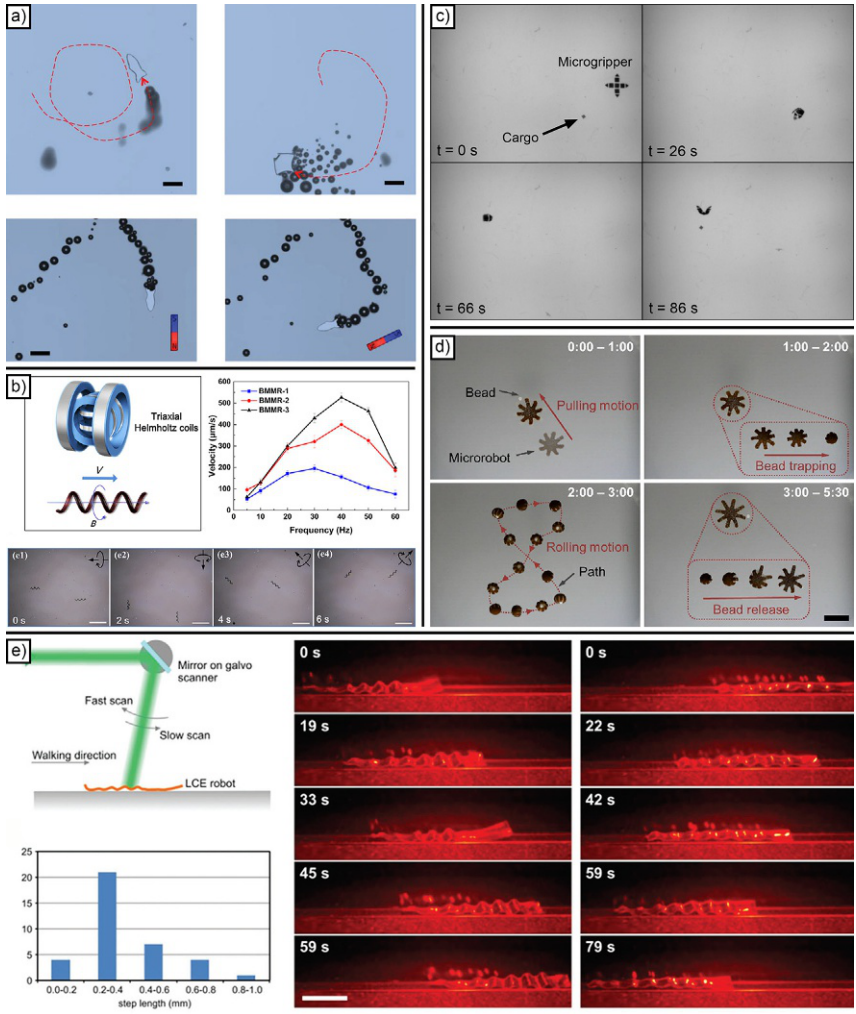

Fig. 3 Chemical propulsion of microfish and a micro manta ray in a of 10% wt. hydrogen peroxide solution (A); magnetic actuation of biotemplate fabricated microrobots based on *Spirulina* (B); tetherless mobile microgripper capable of performing fast repeatable grasping motions (C); thermo-electromagnetically actuated microdevice for targeted transport of microbeads (D); caterpillar light driven actuation of a microrobot (E). *Panel (A) reprinted with permission from Zhu W, Li J, Leong YJ, et al: 3D-printed artificial microfish,* Adv Mater *27(30):4411–4417, 2015. https://doi.org/10.1002/adma.201501372; Panel (B) reprinted with permission from Wang X, Cai J, Sun L, et al: Facile fabrication of magnetic microrobots based on spirulina templates for targeted delivery and synergistic chemo-photothermal therapy,* ACS Appl Mater Interfaces *11(5): 4745–4756, 2019. https://doi.org/10.1021/acsami.8b15586; Panel (C) reprinted with permission from Zhang J, Diller E: Tetherless mobile micrograsping using a magnetic elastic composite material,* Smart Mater Struct *25(11):1–8, 2016. https://doi.org/10.1088/0964-1726/25/11/11LT03; Panel (D) reprinted with permission from Go G, Du Nguyen V, Jin Z, et al: A thermo-electromagnetically actuated microrobot for the targeted transport of therapeutic agents,* Int J Control Autom Syst *16(3):1341–1354, 2018. https://doi.org/10.1007/s12555-017-0060-z; Panel (E) reprinted with permission from Rogóż M, Zeng H, Xuan C, et al: Light-driven soft robot mimics caterpillar locomotion in natural scale,* Adv Opt Mater *4 (11):1689–1694, 2016. https://doi.org/10.1002/adom.201600503.*

To fully comprehend this discussion, a definition of some basic soft robotics actuation concepts is required. First, the term "actuation" is generic and simply indicates making a machine start to work. Indeed, microrobots are actuated at different levels: in general, they are characterized by long-range motion (they should move on a scale much larger than their dimensions to reach the target region), and by short-range actuation (when they reach the target zone, they must accomplish the task for which they are designed). The first, called "propulsion" or "long-range actuation," is simply a mechanical actuation in which the device acts as a transducer to convert an external source of power into motion. These power sources can be magnetic fields, ultrasound, chemical fuels or light. The second, termed "localized actuation" or "short-range actuation," is the performance of the function of the microrobot upon reaching the target zone. While the propulsion is, by definition, a mechanical action, localized actuation may also rely on non-mechanical variations in the chemical or physical state of the soft material of the device. These may induce, for example, drug release or a variation in the surface properties of the materials. Localized actuation can be triggered by the same external stimuli employed for propulsion or by others that cannot be used for propulsion (pH variations, electromagnetic radiation, thermal gradients, etc.). In general, both propulsion and localized actuation require energy. This can be provided from outside the environment in which the device is moving, or is generated directly on the device using fuel present in the environment. In the first case, the device is externally powered, in the second case, it is self-powered.

5.1 Chemical actuation

The most notable example of self-powered propulsion is chemical actuation (Safdar et al., 2018). The devices that base their motion on this approach, which are properly called self-propelled micromotors (Terzopoulou et al., 2020) rather than microrobots due to their limited wireless controllability (Chen et al., 2018), convert chemical species present in the environment into motion through a chemical reaction. The most classic example is the degradation of hydrogen peroxide into water and oxygen (Safdar et al., 2018). The presence on the device of a bimetallic structure translates into an anodic region and a cathodic region, where hydrogen peroxide oxidizes at the anodic segment and reduces at the cathodic segment. The device, in this condition, moves due to a self-electrophoresis mechanism (Puigmartí-Luis et al., 2020). Indeed, the presence of the two reactions described builds

up an electron flux inside the device and a diffusion of protons from the anode to the cathode. Such protons diffusion is at the base of the movement. Chemically actuated micromotors can also move exploiting other mechanisms, like direct chemical degradation or self-diffusiophoresis (Puigmartí-Luis et al., 2020). Hydrogen peroxide is of course incompatible with in-vivo use, and indeed finding a suitable fuel in the actuation environment constitutes one of the most important limitations of chemical actuation. However, other species characterized by a redox behavior can be used (Safdar et al., 2018) (e.g., glucose, urea, etc.). The introduction of a catalytic functionality in soft devices is a major challenge, as opposed to rigid devices, where layers of metals such as Pt or Au can be easily integrated. In soft robots, the catalytic material can be applied by depositing metallic nanoparticles, for example. Li et al. used poly(allylamine hydrochloride) and poly(styrene sulfonic acid) in combination with Pt nanoparticles to impart the catalytic behavior required for hydrogen peroxide propulsion (Si et al., 2019). In this way, they were able to build catalytic microrockets. A similar approach was followed by Wu et al. by employing chitosan and alginate (Wu et al., 2013a). Huang et al. discussed the effect of device geometry on the propulsion of catalytic polymeric microrockets (Huang et al., 2017). Wu et al. demonstrated the possibility to regulate the motion speed of chemically propelled micromotors by using infrared light (Wu et al., 2014a). Specifically, they observed that polymeric microrockets remain motionless at low peroxide concentration, however infrared illumination led to a photothermal effect that rapidly triggered motion. Chemical propulsion can be combined with localized actuation to perform specific tasks. Wu et al., for example, built biodegradable poly-L-lysine hydrochloride/bovine serum albumin multilayered microtubes (Wu et al., 2015). These were loaded with doxorubicin, which was released on demand by shining a near infrared laser beam on the devices.

5.2 Magnetic actuation

The most investigated propulsion technique for externally powered devices is based on the controlled application of magnetic fields (Ebrahimi et al., 2020). Indeed, many of the examples previously discussed in the materials section are based on magnetic propulsion, which has important advantages over chemical or other types of propulsion as there is no need for "fuel" in the actuation environment. Additionally, magnetic fields do not significantly interact with living tissues in a wide range of conditions, and high precision

actuation can be achieved. Through magnetic actuation, both forces and torques can be easily applied (Eqs. 6 and 7)

$$\vec{F} = \int_V \left(\vec{M}\bullet\nabla\right)\vec{B}\,dV = V\left(\vec{M}\bullet\nabla\right)\vec{B} \tag{6}$$

$$\vec{T} = \int_V \vec{M}\times\vec{B}\,dV = V\,\vec{M}\times\vec{B} \tag{7}$$

where V is the volume of magnetic material, B is the applied external magnetic field and M is the magnetization of the material. As suggested in Eqs. (6) and (7), magnetic actuation requires the presence of a magnetically responsive material inside the device. Usually, ferro-, ferrimagnetic and superparamagnetic materials are commonly used for the realization of magnetic microrobotic structures, as they exhibit large magnetization. Yet, several investigations have also demonstrated manipulation of paramagnetic and diamagnetic devices (Chen et al., 2017). In the case of rigid microdevices, the problem is usually addressed by depositing metallic or oxide layers on the surface or manufacturing fully bodied metallic architectures. However, this is a challenge for soft robotics, since ferromagnetic materials are usually characterized by a high elastic modulus. A solution consists of blending the soft material with magnetic nanoparticles (Kim, 2019). Magnetic actuation of soft microrobots can be carried out by employing magnetic fields gradients, which exert a force on the devices in accordance with Eq. (6). For example, Wei et al. propelled their degradable polymeric microrobots for the controlled delivery of stem cells by applying gradients in the order of few T/m (Wei et al., 2020). In addition, rotating magnetic fields can also be efficiently employed for controlled locomotion, thereby exploiting the torque exerted on the devices (Eq. 7). ABFs base their actuation on the application of a few mT rotating fields (Zhang et al., 2009a). In contrast, oscillating fields can be employed to impart distinctive motion like the bipedal actuation proposed by (He et al. (2020), the sperm-like actuation obtained by (Khalil et al., 2014) or the orbiting two-tailed actuation by Khalil et al. (2020) By carefully designing the material and the device, more than one magnetic actuation strategy can be implemented on the same device, as demonstrated by Hu et al. with their multimodal microrobots (Hu et al., 2018c). In some cases, the magnetic properties of the material can be programmed to introduce an anisotropy, thus generating special magnetic actuation paths. Indeed, a magnetically anisotropic material tends to align its magnetic

moment with its easy axis, which can be programmed in advance. A prototypical example of this approach was proposed by (Kim et al. (2011), who built a snake-like actuator composed of different sections (each section containing an easy axis programmed along a specific direction). By applying an external field, they achieved a controlled snake-like movement (Xu et al., 2019) and (Huang et al., 2018) proposed other examples of programmed anisotropy.

5.3 Other actuation strategies

To a lesser extent, acoustic propulsion is also employed for the locomotion of soft microrobots. For example, ultrasound can be used to obtain a reproducible motion via the generation of microbubbles. Ahmed et al. carved a microcavity in their microdevice that was able to produce microbubbles via ultrasound stimulation (Ahmed et al., 2017). Although chemical and magnetic propulsion are routinely employed for both rigid and soft microdevices, some actuation strategies are exclusively used in the world of soft microrobots. These include methods based on the presence of a specifically tailored stimuli responsive material, e.g., light and temperature. Light induced motion is cited in many examples in literature (Nocentini et al., 2018) and is typical of devices containing polymers modified with chromophores that can be employed to induce motion via photomechanical non-reciprocal actuation (Lahikainen et al., 2020; Palagi et al., 2019; Zeng et al., 2018). Pilz da Cunha et al proposed a millimetric robot based on this principle (Pilz da Cunha et al., 2020b). Furthermore, by employing structured light, biomimetic swimming (Palagi et al., 2016) and caterpillar-like locomotion (Rogóż et al., 2016) can be achieved. Propulsion can also be achieved by applying alternative heating and cooling cycles to heat-sensitive microdevices, for example, Mourran et al. actuated helical microdevices via plasmonic heating (Mourran et al., 2017) by inducing two non-reciprocal shape variations, the first obtained during heating and the second during cooling.

5.4 Advanced actuation routes

Melting propulsion and photosynthetic propulsion are two advanced methods of actuation. The first is based on a light-controlled travelling-wave approach, which allows a soft microrobot to propel itself through a solid hydrogel (Palagi et al., 2017). The latter takes inspiration from nature,

generating O_2 bubbles from visible light. In this way, controlled propulsion can be achieved by varying the exposure of the device to light (Mathesh and Wilson, 2020).

Another possibility, which is exclusive to soft robotics, is the exploitation of stimuli responsive materials (Deng et al., 2017; Jeon et al., 2017; Stoychev et al., 2013) to change the shape of the devices during motion (Wu et al., 2013b). By doing this, reconfigurable microrobots that can change their actuation mechanism or actively control motion can be obtained, allowing high environmental adaptability and novel locomotion strategies. Shape-morphing devices are characterized by an intrinsic reprogrammability, which results in a superior flexibility in production and usage. Magdanz et al. built chemically propelled microrobots that can fold and unfold (Magdanz et al., 2014), when folded in a tubular shape, the devices move and when unfolded, they stop. This allows good control over their motion. Xie et al. adopted an analogous strategy with magnetic actuation, obtaining reconfigurable magnetic microrobot swarms (Xie et al., 2019). Huang et al. exploited magnetic anisotropy to produce devices with programmable morphology (Huang et al., 2016). Further examples of shape-morphing magnetic soft machines have been provided by (Alapan et al., 2020).

It is with short-range actuation, however, that soft robotics exhibit the greatest advantages over rigid robotics thanks to the use of stimuli responsive materials. Generally, after reaching the target site via chemical, magnetic or light propulsion, soft microrobots can perform localized actuation to carry out their function. By introducing shape-changing functionalities, a variety of different actuation patterns can be obtained. With a temperature sensitive material, long-range magnetic locomotion can be combined with short range mechanical actuation to release therapeutic agents (Go et al., 2018; Malachowski et al., 2014) or capture living cells (Breger et al., 2015). Other triggers can also be employed to mechanically actuate soft microrobots, such as changes in pH (Fernandes and Gracias, 2012; Yoon et al., 2014), magnetisation (Zhang and Diller, 2016), or light. Lee et al. employed a near-infrared stimulus to change the permeability of magnetically propelled hydrogel coated devices for drug delivery (Lee et al., 2018). Light can also be used to change the device morphology, enabling the capture of small objects (Wani et al., 2017). The final method of short-range actuation is obtained by electrochemical stimuli, which can be used to deform hydrogel layers in magnetically guided devices (Kim et al., 2020b).

6. Applications of soft microrobots

The advantages of soft microrobots have been exploited in a large variety of applications, mainly biomedical (Field et al., 2019), which range from already well-established uses typical also of rigid devices (like drug and cell delivery or localized surgery), to exclusive applications (like soft micro-gripping). The unique properties of soft robots (controllable permeability, stimuli responsiveness, shape variations, high biocompatibility and resorbability) demonstrate significant potential for many applications (Fig. 4).

6.1 Drug delivery

The intrinsic permeability to small molecules and the biocompatibility of many soft materials, such as hydrogels (Hoare and Kohane, 2008; Narayanaswamy and Torchilin, 2019) or chitosan (Peers et al., 2020), are ideal properties for drug delivery applications. Furthermore, the ability of controlled release from the hydrogel by means of heat, light, magnetic (Liao and Huang, 2020) or chemical (Rizwan et al., 2017) stimuli provides another significant advantage over conventional microrobots. Furthermore, the redox behavior of some conducting polymers can be employed to control or enhance drug release (Shah et al., 2018). In addition to the examples reported in the previous sections, some supplementary cases can be cited. Park et al. built microrobots based on PEGDA and pentaerythritol triacrylate (PETA) and containing magnetic Fe_3O_4 nanoparticles (Park et al., 2019). They employed these devices in actively controlled drug delivery and hyperthermia therapy. Peters et al. 3D printed biodegradable magnetic composite microswimmers able to release drugs (Peters et al., 2016). Darmawan et al. developed a self-folding microrobot for ultrasound-triggered drug release: devices were guided towards a target zone, where non-covalently bonded anti-cancer drugs were released via ultrasonic stimulation (Darmawan et al., 2020). The stomatocytes described in the materials section can also be applied to controlled drug delivery (Schmidt et al., 2020). Indeed, their naturally hollow structure is ideal to allocate nanoparticles or molecular drugs (Tu et al., 2017a, b).

6.2 Cell delivery

The superior biocompatibility of many soft materials and their intrinsic conformity to biological tissues can be used for cell delivery in a wide variety of in-vivo situations. For example, in the previously cited work of (Dong et al.,

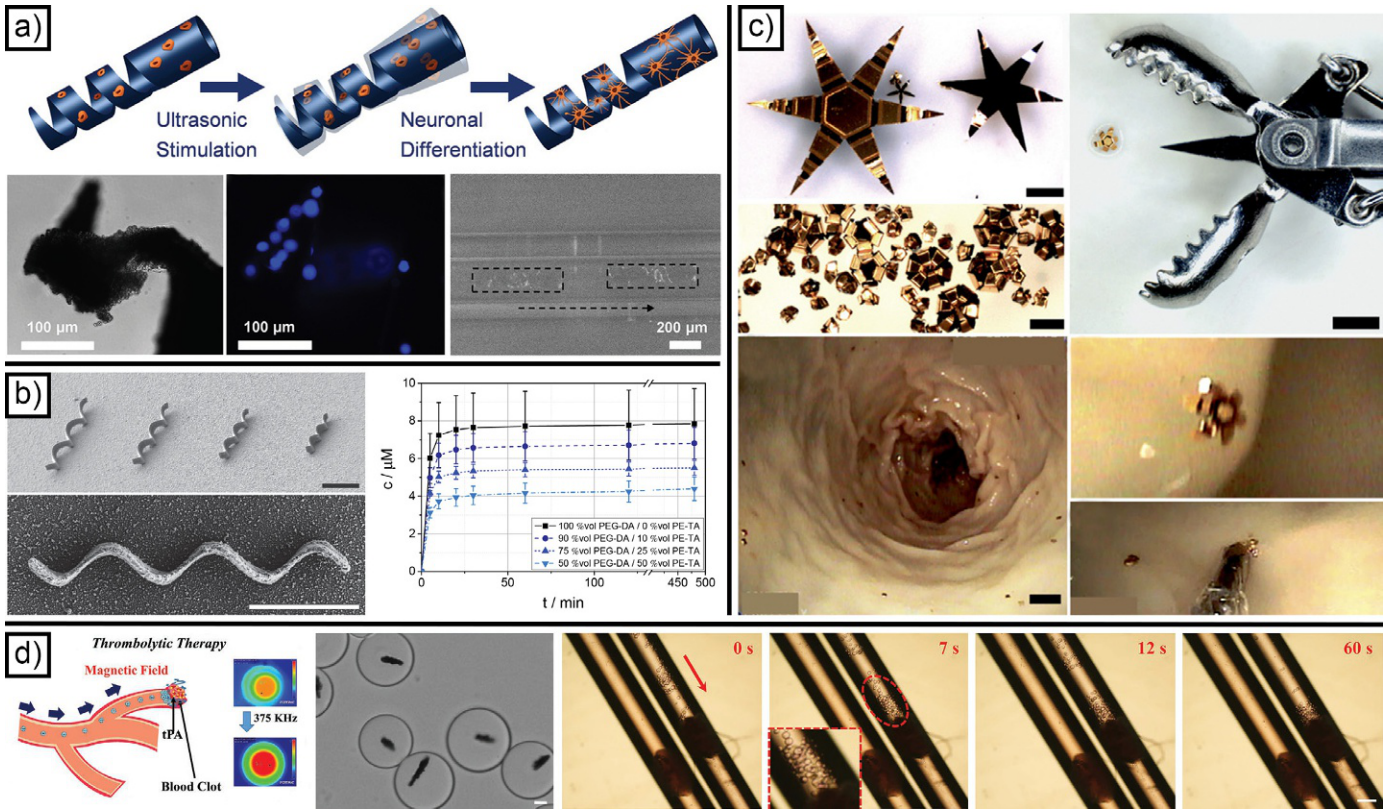

Fig. 4 See figure legend on opposite page.

2020), neuron-like cells were actively transported using 3D printed soft microswimmers. A similar approach was followed by (Chen et al., 2019). In some cases, when the material employed is totally resorbable, devices can be left inside the body, thus allowing scaffolding applications (TirgarBahnamiri and Bagheri-Khoulenjani, 2017). As already discussed, the shape reconfigurability of many soft materials can be used to build microgrippers for in-vivo tissue sampling. Indeed, even if the trend of modern medicine is moving toward non-invasive diagnosis methodologies, tissue biopsy coupled with histopathologic examination is still required for a large number of pathologies. Consequently, microgrippers able to selectively collect tissue samples and extract them from the body are highly desirable. Gultepe et al. described this approach in their papers on diagnostic thermally enabled microgrippers (Gultepe et al., 2013a, b). Jin et al. also described multi-fingered grippers for single cell biopsies (Jin et al., 2020).

6.3 Microsurgery applications

Soft microrobots also can be employed to carry out localized microsurgery tasks. For example, they can operate inside blood vessels, as cited in the work of Tabatabaei et al. (2011), who built shrinkable hydrogel-based microrobots able to navigate the vascular system. Another example of application is hyperthermia therapy, which can be carried out using microdevices such as those produced by Park et al. (2019). The devices described by Xie et al. can be used to perform ultra-minimally invasive thrombolysis (Xie et al., 2020).

Fig. 4 Untethered devices able to transport neurons in a targeted and precise way, while creating an electrically stimulated microenvironment to favor their differentiation (A); biodegradable helical microswimmers for targeted drug delivery (B); microgrippers for controlled in-vivo tissue sampling (C); soft microrobots with collective behavior for microvascular thrombolysis (D). *Panel (A) reprinted with permission from Chen XZ, Liu JH, Dong M, et al: Magnetically driven piezoelectric soft microswimmers for neuron-like cell delivery and neuronal differentiation,* Mater Horizons *6(7):1512–1516, 2019. https://doi.org/10.1039/c9mh00279k; Panel (B) reprinted with permission from Peters C, Hoop M, Pané S, et al: Degradable magnetic composites for minimally invasive interventions: device fabrication, targeted drug delivery, and cytotoxicity tests,* Adv Mater *28(3):533–538, 2016; Panel (C) reprinted with permission from Gultepe E, Yamanaka S, Laflin KE, et al: Biologic tissue sampling with untethered microgrippers,* Gastroenterology *144(4):691–693, 2013a. https://doi.org/10.1053/j.gastro.2013.01.066; Panel (D) reprinted with permission from Xie M, Zhang W, Fan C, et al: Bioinspired soft microrobots with precise magneto-collective control for microvascular thrombolysis,* Adv Mater *32(26):1–11, 2020. https://doi.org/10.1002/adma.202000366.*

Finally, soft microrobots can be efficiently employed to drive a guidewire through blood vessels (Jeon et al., 2019).

6.4 Microdevices imaging and guidance

To complete the discussion on soft microrobots applications, we should mention the imaging and guidance for in-vivo applications. Real time guidance of microrobots is strongly application-related and has always been a major concern throughout the development of microrobotics. For rigid microrobots, the movement of the devices inside the human body can be tracked and guided via both closed-loop and open-loop approaches using ionizing radiation, ultrasound, magnetic feedback or light (Aziz et al., 2020; Pane et al., 2021; Wu et al., 2019). Guidance for soft microrobots presents additional problems, for example, the low mean atomic weights results in poor contrast with biological tissues for radio imaging techniques. High resolution tracking and imaging can be improved with the inclusion of radioactive compounds. Iacovacci et al. added pertechnetate to thermoresponsive magnetic microrobots and tracked their motion inside a mouse via tomography imaging (Iacovacci et al., 2019). Overall, in-vivo microrobot guidance is still in the early stages and is one of the most critical topics in microrobotics.

7. Hard-soft hybrid microrobots

In some cases, the movement and functionalities of a microrobot can be accomplished by integrating both rigid and soft sections into the body of the microdevice. This technology is known as hard-soft hybrid microrobots (Fig. 5).

The presence of soft sections (made of hydrogels or conductive polymers) alternated with hard metallic components enables specific actuation strategies based on selective bending and rotation depending on the different flexibilities (Pak et al., 2011). This principle has been demonstrated in many examples in literature. For example, Yoshizumi et al. connected two gold/platinum micromotors (able to provide chemical propulsion) with a polymeric joint made of poly(allylamine hydrochloride) (PAH) and poly(acrylic acid) (PAA) (Yoshizumi and Suzuki, 2017). By doing this, they were able to introduce a rotatory component to the motion of their devices in addition to the translational motion induced by the chemical propulsion, giving a higher control over the movement of the device. Mirkovic et al. employed a similar approach to manufacture metallic nanorods with

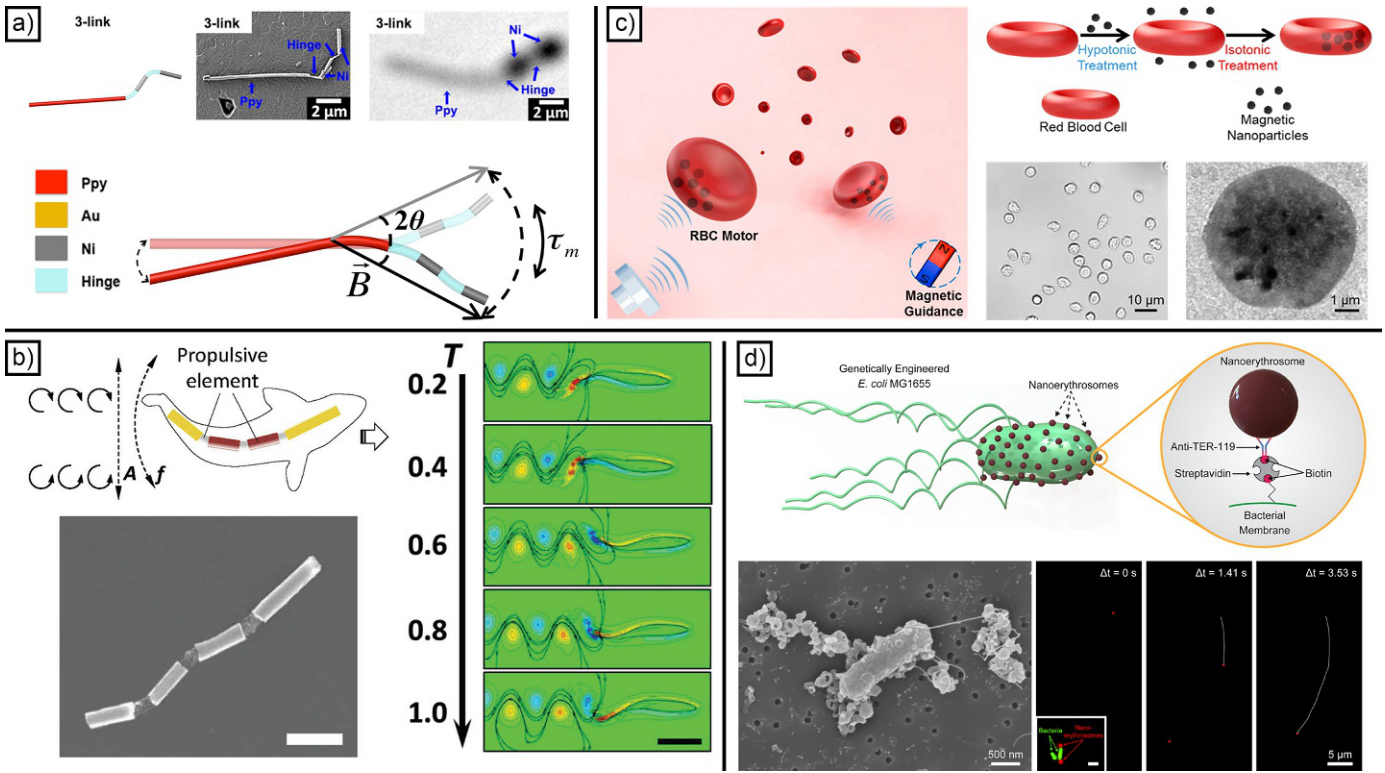

Fig. 5 See figure legend on next page.

polyelectrolyte hinges (Mirkovic et al., 2007). Further rotational degrees of freedom can be introduced by using multiple hinges along the nanorods. Li et al. first tested double hinged (Li et al., 2017) and then multiple hinged (Li et al., 2016b) microswimmers. In the latter, by introducing three hinges, they were able to build microswimmers that mimic the caudal fin propulsion mechanism displayed by fish. The devices developed by Li et al. also constitute examples of magnetically actuated flexible microswimmers, as does those of Jang et al., who created triple linked devices using PPy, polyallylamine chloride (PAH) plus polystyrenesulfonate (PSS) and nickel (Jang et al., 2015). In another example, miniaturized grippers were constructed using hinges that employed biopolymer triggers (gelatin and carboxymethylcellulose) and metallic elements (Ni, Au and Cr) (Bassik et al., 2010). The selective enzymatic degradation of the biopolymer employed triggered the closing of the grippers, while nickel enabled magnetic motion. Soft materials combined with hard materials can maximize the advantages of both categories. For example, Bernasconi et al. applied a pH sensitive hydrogel to a 3D printed wet metallized structure (Bernasconi et al., 2021) and was thus able to combine the high magnetic properties typical of ferromagnetic alloys with the shape customizability typical of 3D printing, and the drug releasing properties of hydrogels (in this case triggered by pH). Finally, Ahmed et al. demonstrated the feasibility of acoustic actuation on hard-soft hybrid devices (Ahmed et al., 2016). They fabricated microswimmers composed of a rigid bimetallic head (Ni/Au) and a flexible tail (polypyrrole). By exploiting the different oscillations acoustically generated inside the tail and the head, the authors were able to propel the devices.

Fig. 5 Hinged hard-soft microswimmers with ondulatory motion (A); multilinked artificial nanofish (B); biohybrid erythrocytes-based functional micromotors (C); biohybrid bacterial microswimmers functionalized with red blood cell membrane nanoliposomes (D). *Panel (A) reprinted with permission from Jang B, Gutman E, Stucki N, et al: Undulatory locomotion of magnetic multilink nanoswimmers,* Nano Lett *15(7):4829–4833, 2015. https://doi.org/10.1021/acs.nanolett.5b01981; Panel (B) reprinted with permission fromLi T, Li J, Zhang H, et al: Magnetically propelled fish-like nanoswimmers,* Small *12(44):6098–6105, 2016b. https://doi.org/10.1002/smll.201601846; Panel (C) reprinted with permission from Wu Z, Li T, Li J, et al: Turning erythrocytes into functional micromotors,* ACS Nano *8(12):12041–12048, 2014b. https://doi.org/10.1021/nn506200x; Panel (D) reprinted with permission from Buss N, Yasa O, Alapan Y, et al: Nanoerythrosome-functionalized biohybrid microswimmers,* APL Bioeng *4(2):026103, 2020. https://doi.org/10.1063/1.5130670.*

8. Biohybrid soft microrobots

Recently, the use of a particular form of soft matter, biological entities, for the propulsion or functionalization of synthetic microrobots is being explored, giving rise to a novel class of soft microdevices known as biohybrid microrobots (Bastos-Arrieta et al., 2018; Feinberg, 2015; Hosseinidoust et al., 2016; Martel, 2012; Ricotti et al., 2017; Sun et al., 2020) (Fig. 5). Indeed, living cells constitute a natural choice for the propulsion of microrobots, since they are naturally adapted for low *Re* actuation (Edwards et al., 2014; Ng et al., 2018). Biological entities are propelled by highly efficient molecular motors (e.g., myocytes), which transform chemical energy into motion. This approach must not be confused with natural templating, where the biological entity is simply employed as a mold to obtain the desired microdevice and does not take part in the actuation.

The first logical choice to realize biohybrid devices is the use of microorganisms like bacteria (Leaman et al., 2019) or protozoan (Alapan et al., 2019). These are usually connected to a cargo by means of emulsion synthesis (Singh et al., 2017), optically mediated assembly (Barroso et al., 2015) or chemical/electrostatic bonding. The latter is probably the most important technique to bind microorganisms to a cargo, since it enables easy and reproducible linking of organisms to inorganic entities (potentially also with patterning (Singh and Sitti, 2016)). For example, Kojima et al. propelled liposomes by attaching them to bacteria via antibody bonding (Kojima et al., 2013). Akolpoglu produced biohybrid microalgae for cargo delivery tasks by electrostatically depositing magnetite nanoparticles on a single-cell green alga (Akolpoglu et al., 2020). Soto et al. fed rotifers with magnetic nanoparticles to create self-propelling microcleaners (Soto et al., 2019). The last two examples are significant as an important factor in biohybrid devices: their control. Biological entities are highly performant in low Re propulsion, but they are also intrinsically difficult to control: the solution is to combine magnetic nanoparticles with the biological entities employed (Carlsen et al., 2014). Other notable examples of microorganisms controlled in this way include spores (Yang et al., 2020), macrophages (Han et al., 2016), erythrocytes (Wu et al., 2014b) and bioengineered bacteria (Buss et al., 2020). A class of microorganisms that is of particular interest for the realization of magnetic microdevices is magnetotactic bacteria. These biological entities are naturally sensitive to the presence of magnetic fields and this characteristic can be used for their guidance. In this

context, Taherkhani et al. loaded drug releasing liposomes, linking them via amine bonding, onto the surface of *Magnetococcus marinus* bacteria (Taherkhani et al., 2014). Another methodology is to guide microorganisms by chemical variation of the environment in which the device swims (also known as chemotaxis): by applying chemical gradients, microorganisms can be propelled in the desired direction (Zhuang and Sitti, 2016).

In addition to bacteria and protozoan, animal cells also can be employed for the realization of biohybrid entities. The most obvious choice, in this case, are muscular cells, which convert chemical energy into mechanical energy. Chan et al. 3D printed a hydrogel in the form of cantilever structures. They then seeded the structures with contractile cardiomyocytes to convert the cantilevers into microwalkers able to carry a cargo (Chan et al., 2012). Kim et al. also proposed a similar approach (Kim et al., 2010b). Nawroth et al. built a jellyfish-like entity by combining a patterned elastomer with engineered muscular fibers (Nawroth et al., 2012). Park et al. followed a similar approach but added a supplementary layer to allow phototactic guidance (Park et al., 2016). The last example worth mentioning is the use of spermatozoa to create microdevices. Although these cells belong to animals, they exhibit bacterial-like behavior in their swimming motion. The resulting devices, colloquially called Spermbots, can be employed for artificial fertilization as well as for drug delivery (Singh et al., 2020; Williams et al., 2014).

9. Conclusions

The current chapter summarizes many examples of functional micromachines built using exclusively soft matter or combinations of hard and soft materials. It also discloses possible applications of programmable materials, which constitute probably the most important advantage of soft materials usage. The examples cited strongly support the potentialities of soft materials in overcoming the limitations of rigid microrobots. They demonstrate that it is possible to achieve complex and dexterous actuation paths by simply introducing large deformable parts inside the device. Obviously, this requires using specific materials and fabrication technologies, which have been extensively treated in the present chapter. As demonstrated in the last part of the treatise, bio inspiration and biohybridization further expanded the possibilities for microrobots design and actuation. In front of all these considerations, the most important idea suggested by the chapter is that the future of microrobotics, and most importantly real applications, will be realistically dominated by highly adaptable and smart devices. Soft

materials have all the potentialities to fulfill these tasks, making them an essential choice for the microrobotics of tomorrow.

References

Abbott JJ, Nagy Z, Beyeler F, Nelson BJ: Robotics in the small, part I: microbotics, *IEEE Robot Autom Mag* 14(2):92–103, 2007. https://doi.org/10.1109/mra.2007.380641.

Abbott JJ, Peyer KE, Lagomarsino MC, et al.: How should microrobots swim? *Int J Rob Res* 28(11–12):1434–1447, 2009. https://doi.org/10.1177/0278364909341658.

Aghakhani A, Yasa O, Wrede P, Sitti M: Acoustically powered surface-slipping mobile microrobots, *Proc Natl Acad Sci U S A* 117(7):3469–3477, 2020. https://doi.org/10.1073/pnas.1920099117.

Ahmed D, Baasch T, Jang B, Pane S, Dual J, Nelson BJ: Artificial swimmers propelled by acoustically activated flagella, *Nano Lett* 16(8):4968–4974, 2016. https://doi.org/10.1021/acs.nanolett.6b01601.

Ahmed D, Dillinger C, Hong A, Nelson BJ: Artificial acousto-magnetic soft microswimmers, *Adv Mater Technol* 2(7):1–5, 2017. https://doi.org/10.1002/admt.201700050.

Ahn S, Kasi RM, Kim S, Zhou Y: *Stimuli-Responsive Polymer Gels*, 2008, pp 1151–1157. https://doi.org/10.1039/b714376a.

Akolpoglu MB, Dogan NO, Bozuyuk U, Ceylan H, Kizilel S, Sitti M: High-Yield Production of biohybrid microalgae for on-demand cargo delivery, *Adv Sci* 7(16):1–10, 2020. https://doi.org/10.1002/advs.202001256.

Alapan Y, Yasa O, Yigit B, Yasa IC, Erkoc P, Sitti M: Microrobotics and Microorganisms: biohybrid autonomous cellular robots, *Annu Rev Control Robot Auton Syst* 2(1):205–230, 2019. https://doi.org/10.1146/annurev-control-053018-023803.

Alapan Y, Karacakol AC, Guzelhan SN, Isik I, Sitti M: Reprogrammable shape morphing of magnetic soft machines, *Sci Adv* 6(38), 2020. https://doi.org/10.1126/sciadv.abc6414.

Alcântara CCJ, Landers FC, Kim S, et al.: Mechanically interlocked 3D multi-material micromachines, *Nat Commun* 11(1), 2020. https://doi.org/10.1038/s41467-020-19725-6.

Ali J, Cheang UK, Liu Y, et al.: Fabrication and magnetic control of alginate-based rolling microrobots, *AIP Adv* 6(12), 2016. https://doi.org/10.1063/1.4971277.

Alici G: Softer is harder: what differentiates soft robotics from hard robotics? *MRS Adv* 3 (28):1557–1568, 2018. https://doi.org/10.1557/adv.2018.159.

Almeida H, Amaral MH, Lobão P: Temperature and PH stimuli-responsive polymers and their applications in controlled and selfregulated drug delivery, *J Appl Pharm Sci* 2 (6):01–10, 2012. https://doi.org/10.7324/JAPS.2012.2609.

Aziz A, Pane S, Iacovacci V, et al.: Medical imaging of microrobots: toward in vivo applications, *ACS Nano* 14(9):10865–10893, 2020. https://doi.org/10.1021/acsnano.0c05530.

Barroso Á, Landwerth S, Woerdemann M, et al.: Optical assembly of bio-hybrid micro-robots, *Biomed Microdevices* 17(2):1–8, 2015. https://doi.org/10.1007/s10544-015-9933-1.

Bassik N, Brafman A, Zarafshar AM, et al.: Enzymatically triggered actuation of miniaturized tools, *J Am Chem Soc* 132(46):16314–16317, 2010. https://doi.org/10.1021/ja106218s.

Bastos-Arrieta J, Revilla-Guarinos A, Uspal WE, Simmchen J: Bacterial biohybrid microswimmers, *Front Robot AI* 5(AUG):1–16, 2018. https://doi.org/10.3389/frobt.2018.00097.

Benouhiba A, Rougeot P, Ouisse M, Clévy C, Andreff N, Rabenorosoa K: Toward conductive polymer-based soft milli-robots for vacuum applications, *Front Robot AI* 6 (November):1–12, 2019. https://doi.org/10.3389/frobt.2019.00122.

Bernasconi R, Cuneo F, Carrara E, et al.: Hard-magnetic cell microscaffolds from electroless coated 3D printed architectures, *Mater Horizons* 5(4):699–707, 2018. https://doi.org/10.1039/c8mh00206a.

Bernasconi R, Carrara E, Hoop M, et al.: Magnetically navigable 3D printed multifunctional microdevices for environmental applications, *Addit Manuf* 28:127–135, 2019a.
Bernasconi R, Favara N, Turri S, Magagnin L: Electrodeposited nanoporous polypyrrole layers for controlled drug release, *J Electrochem Soc* 166(10):G122, 2019b.
Bernasconi R, Favara N, Fouladvari N, et al.: Nanostructured polypyrrole layers implementation on magnetically navigable 3d printed microdevices for targeted gastrointestinal drug delivery, *Multifunct Mater*, 2020.
Bernasconi R, Mauri E, Rossetti A, et al.: 3D integration of PH-cleavable drug-hydrogel conjugates on magnetically driven smart microtransporters, *Mater Des* 197, 2021. https://doi.org/10.1016/j.matdes.2020.109212.
Boyraz P, Runge G, Raatz A: An overview of novel actuators for soft robotics, *High-Throughput* 7(3):1–21, 2018. https://doi.org/10.3390/act7030048.
Breger JC, Yoon C, Xiao R, et al.: Self-folding thermo-magnetically responsive soft microgrippers, *ACS Appl Mater Interfaces* 7(5):3398–3405, 2015. https://doi.org/10.1021/am508621s.
Buss N, Yasa O, Alapan Y, Akolpoglu MB, Sitti M: Nanoerythrosome-functionalized biohybrid microswimmers, *APL Bioeng* 4(2), 2020, 026103. https://doi.org/10.1063/1.5130670.
Cabanach P, Pena-Francesch A, Sheehan D, et al.: Zwitterionic 3D-printed non-immunogenic stealth microrobots, *Adv Mater* 32(42):1–11, 2020. https://doi.org/10.1002/adma.202003013.
Cao ZQ, Wang GJ: Multi-stimuli-responsive polymer materials: particles, films, and bulk gels, *Chem Rec*:1398–1435, 2016. https://doi.org/10.1002/tcr.201500281.
Carlsen RW, Edwards MR, Zhuang J, Pacoret C, Sitti M: Magnetic steering control of multi-cellular bio-hybrid microswimmers, *Lab Chip* 14(19):3850–3859, 2014. https://doi.org/10.1039/c4lc00707g.
Ceylan H, Yasa IC, Yasa O, Tabak AF, Giltinan J, Sitti M: 3D-printed biodegradable microswimmer for theranostic cargo delivery and release, *ACS Nano* 13(3):3353–3362, 2019. https://doi.org/10.1021/acsnano.8b09233.
Chaillet N, Régnier S: *Microrobotics for Micromanipulation*, 2013 https://doi.org/10.1002/9781118622810.
Chan V, Park K, Collens MB, Kong H, Saif TA, Bashir R: Development of miniaturized walking biological machines, *Sci Rep* 2, 2012. https://doi.org/10.1038/srep00857.
Chautems C, Zeydan B, Charreyron S, Chatzipirpiridis G, Pané S, Nelson BJ: Magnetically powered microrobots: a medical revolution underway? *Eur J Cardiothorac Surg* 51(3):405–407, 2017. https://doi.org/10.1093/ejcts/ezw432.
Chen X-Z, Hoop M, Mushtaq F, et al.: Recent developments in magnetically driven micro-and nanorobots, *Appl Mater Today* 9:37–48, 2017.
Chen X, Jang B, Ahmed D, et al.: Small-scale Machines Driven by External Power Sources, *Adv Mater* 30(15):1705061, 2018.
Chen XZ, Liu JH, Dong M, et al.: Magnetically driven piezoelectric soft microswimmers for neuron-like cell delivery and neuronal differentiation, *Mater Horizons* 6(7):1512–1516, 2019. https://doi.org/10.1039/c9mh00279k.
Chen W, Sun M, Fan X, Xie H: Magnetic/PH-sensitive double-layer microrobots for drug delivery and sustained release, *Appl Mater Today* 19:100583, 2020. https://doi.org/10.1016/j.apmt.2020.100583.
Choi J, Hwang J, Kim Jy, Choi H: Recent progress in magnetically actuated microrobots for targeted delivery of therapeutic agents, *Adv Healthc Mater* 10:1–24, 2020. https://doi.org/10.1002/adhm.202001596.
Coskun Ü, Simons K: Cell membranes: the lipid perspective, *Structure* 19(11):1543–1548, 2011. https://doi.org/10.1016/j.str.2011.10.010.

Darmawan BA, Lee SB, Du Nguyen V, et al.: Self-folded microrobot for active drug delivery and rapid ultrasound-triggered drug release, *Sens Actuators B* 324(August):128752, 2020. https://doi.org/10.1016/j.snb.2020.128752.

de Marco C, Alcântara CCJ, Kim S, et al.: Indirect 3D and 4D printing of soft robotic microstructures, *Adv Mater Technol* 4(9):1–7, 2019. https://doi.org/10.1002/admt.201900332.

Dekanovsky L, Khezri B, Rottnerova Z, Novotny F, Plutnar J, Pumera M: Chemically programmable microrobots weaving a web from hormones, *Nat Mach Intell* 2(11):711–718, 2020. https://doi.org/10.1038/s42256-020-00248-0.

Deng H, Dong Y, Su JW, et al.: Bioinspired programmable polymer gel controlled by swellable guest medium, *ACS Appl Mater Interfaces* 9(36):30900–30908, 2017. https://doi.org/10.1021/acsami.7b07837.

Dong X: *Smart and Functional Soft Materials; BoD–Books on Demand*, 2019.

Dong M, Wang X, Chen XZ, et al.: 3D-printed soft magnetoelectric microswimmers for delivery and differentiation of neuron-like cells, *Adv Funct Mater* 30(17):1–7, 2020. https://doi.org/10.1002/adfm.201910323.

Ebrahimi N, Bi C, Cappelleri DJ, et al.: Magnetic actuation methods in bio/soft robotics, *Adv Funct Mater* 2005137:1–40, 2020. https://doi.org/10.1002/adfm.202005137.

Edwards MR, Carlsen RW, Zhuang J, Sitti M: Swimming characterization of serratia marcescens for bio-hybrid micro-robotics, *J Micro-Bio Robot* 9(3–4):47–60, 2014. https://doi.org/10.1007/s12213-014-0072-1.

Erkoc P, Yasa IC, Ceylan H, Yasa O, Alapan Y, Sitti M: Mobile microrobots for active therapeutic delivery, *Adv Ther* 2(1):1800064, 2019. https://doi.org/10.1002/adtp.201800064.

Fan X, Dong X, Karacakol AC, Xie H, Sitti M: Reconfigurable multifunctional ferrofluid droplet robots, *Proc Natl Acad Sci U S A* 117(45):27916–27926, 2020a. https://doi.org/10.1073/pnas.2016388117.

Fan X, Sun M, Sun L, Xie H: Ferrofluid droplets as liquid microrobots with multiple deformabilities, *Adv Funct Mater* 30(24):1–12, 2020b. https://doi.org/10.1002/adfm.202000138.

Fassi I, Shipley D: Micro-manufacturing technologies and their applications, *Springer Tracts Mech Eng* 10:973–978, 2017.

Feinberg AW: Biological soft robotics, *Annu Rev Biomed Eng* 17:243–265, 2015. https://doi.org/10.1146/annurev-bioeng-071114-040632.

Fernandes R, Gracias DH: Self-folding polymeric containers for encapsulation and delivery of drugs, *Adv Drug Deliv Rev* 64(14):1579–1589, 2012. https://doi.org/10.1016/j.addr.2012.02.012.

Field RD, Anandakumaran PN, Sia SK: Soft medical microrobots: design components and system integration, *Appl Phys Rev* 6(4), 2019. https://doi.org/10.1063/1.5124007.

Fu X, Hosta-Rigau L, Chandrawati R, Cui J: Multi-stimuli-responsive polymer particles, films, and hydrogels for drug delivery, *Chem* 4(9):2084–2107, 2018. https://doi.org/10.1016/j.chempr.2018.07.002.

Fusco S, Sakar MS, Kennedy S, et al.: An integrated microrobotic platform for on-demand. Targeted therapeutic interventions, *Adv Mater* 26(6):952–957, 2014. https://doi.org/10.1002/adma.201304098.

Fusco S, Huang H-W, Peyer KE, et al.: Shape-switching microrobots for medical applications: the influence of shape in drug delivery and locomotion, *ACS Appl Mater Interfaces* 7(12):6803–6811, 2015.

Gao W, Sattayasamitsathit S, Uygun A, Pei A, Ponedal A, Wang J: Polymer-based tubular microbots: role of composition and preparation, *Nanoscale* 4(7):2447–2453, 2012. https://doi.org/10.1039/c2nr30138e.

Gao W, Wang L, Wang X, Liu H: Magnetic driving flowerlike soft platform: biomimetic fabrication and external regulation, *ACS Appl Mater Interfaces* 8(22):14182–14189, 2016. https://doi.org/10.1021/acsami.6b03218.

Gao S, Tang G, Hua D, et al.: Stimuli-responsive bio-based polymeric systems and their applications, *J Mater Chem B* 7(5):709–729, 2019. https://doi.org/10.1039/c8tb02491j.

Ge Q, Li Z, Wang Z, et al.: Projection micro stereolithography based 3D printing and its applications, *Int J Extrem Manuf* 2(2), 2020. https://doi.org/10.1088/2631-7990/ab8d9a.

Gibson I, Rosen DW, Stucker B: Additive manufacturing technologies, *Springer* 17, 2014.

Giltinan J, Sridhar V, Bozuyuk U, Sheehan D, Sitti M: 3D microprinting of iron platinum nanoparticle-based magnetic mobile microrobots, *Adv Intell Syst* 3(1):2000204, 2021. https://doi.org/10.1002/aisy.202000204.

Go G, Du Nguyen V, Jin Z, Park JO, Park S: A thermo-electromagnetically actuated microrobot for the targeted transport of therapeutic agents, *Int J Control Autom Syst* 16(3): 1341–1354, 2018. https://doi.org/10.1007/s12555-017-0060-z.

Go G, Yoo A, Song HW, et al.: Multifunctional biodegradable microrobot with programmable morphology for biomedical applications, *ACS Nano*, 2020. https://doi.org/10.1021/acsnano.0c07954.

Gul JZ, Sajid M, Rehman MM, et al.: 3D printing for soft robotics–a review, *Sci Technol Adv Mater* 19(1):243–262, 2018. https://doi.org/10.1080/14686996.2018.1431862.

Gultepe E, Yamanaka S, Laflin KE, et al.: Biologic tissue sampling with untethered microgrippers, *Gastroenterology* 144(4):691–693, 2013a. https://doi.org/10.1053/j.gastro.2013.01.066.

Gultepe E, Randhawa JS, Kadam S, et al.: Biopsy with thermally-responsive untethered microtools, *Adv Mater* 25(4):514–519, 2013b. https://doi.org/10.1002/adma.201203348.

Hamed Y, Tawakol M, El Zahar L, Klingner A, Abdennadher S, Khalil ISM: Realization of a soft microrobot with multiple flexible flagella, *Proc IEEE RAS EMBS Int Conf Biomed Robot Biomechatronics* 2018(Augus):61–66, 2018. https://doi.org/10.1109/BIOROB.2018.8488008.

Han J, Zhen J, Du Nguyen V, et al.: Hybrid-actuating macrophage-based microrobots for active cancer therapy, *Sci Rep* 6(June):1–10, 2016. https://doi.org/10.1038/srep28717.

Harris RD, Auletta JT, Motlagh SAM, et al.: Chemical and electrochemical manipulation of mechanical properties in stimuli-responsive copper-cross-linked hydrogels, *ACS Macro Lett* 2(12):1095–1099, 2013. https://doi.org/10.1021/mz4004997.

Hassan P, Verma G, Ganguly R: Soft Materials-properties and applications, In *Functional materials: preparation, processing and applications*, London, UK, 2011, Elsevier, p 1.

He Y, Dong S, Wang L, Rong W, Sun L: Bipedal microwalkers actuated by oscillating magnetic fields, *Soft Matter* 16(34):7927–7934, 2020. https://doi.org/10.1039/d0sm01228a.

Hoare TR, Kohane DS: Hydrogels in drug delivery: progress and challenges, *Polymer (Guildf)* 49(8):1993–2007, 2008.

Hosseinidoust Z, Mostaghaci B, Yasa O, Park BW, Singh AV, Sitti M: Bioengineered and biohybrid bacteria-based systems for drug delivery, *Adv Drug Deliv Rev* 106:27–44, 2016. https://doi.org/10.1016/j.addr.2016.09.007.

Hu W, Ishii KS, Fan Q, Ohta AT: Hydrogel microrobots actuated by optically generated vapour bubbles, *Lab Chip* 12(19):3821–3826, 2012. https://doi.org/10.1039/c2lc40483d.

Hu C, Riederer K, Klemmer M, Pane S, Nelson BJ: Electrosynthesis of magnetoresponsive microrobot for targeted drug delivery using calcium alginate, *Proc Annu Int Conf IEEE Eng Med Biol Soc EMBS* 2016(Octob):2111–2114, 2016. https://doi.org/10.1109/EMBC.2016.7591145.

Hu C, Pané S, Nelson BJ: Soft micro- and nanorobotics, *Annu Rev Control Robot Auton Syst* 1 (1):53–75, 2018a. https://doi.org/10.1146/annurev-control-060117-104947.

Hu N, Wang L, Zhai W, et al.: Magnetically actuated rolling of star-shaped hydrogel microswimmer, *Macromol Chem Phys* 219(5):1–6, 2018b. https://doi.org/10.1002/macp.201700540.

Hu W, Lum GZ, Mastrangeli M, Sitti M: Small-scale soft-bodied robot with multimodal locomotion, *Nature* 554(7690):81–85, 2018c. https://doi.org/10.1038/nature25443.

Huang G, Mei Y, Thurmer DJ, Coric E, Schmidt OG: Rolled-up transparent microtubes as two-dimensionally confined culture scaffolds of individual yeast cells, *Lab Chip* 9 (2):263–268, 2009. https://doi.org/10.1039/b810419k.

Huang HW, Sakar MS, Petruska AJ, Pané S, Nelson BJ: Soft micromachines with programmable motility and morphology, *Nat Commun* 7:1–10, 2016. https://doi.org/10.1038/ncomms12263.

Huang HW, Chao Q, Sakar MS, Nelson BJ: Optimization of tail geometry for the propulsion of soft microrobots, *IEEE Robot Autom Lett* 2(2):727–732, 2017. https://doi.org/10.1109/LRA.2017.2651167.

Huang HW, Huang TY, Charilaou M, et al.: Investigation of magnetotaxis of reconfigurable micro-origami swimmers with competitive and cooperative anisotropy, *Adv Funct Mater* 28(36):1–9, 2018. https://doi.org/10.1002/adfm.201802110.

Huo M, Yuan J, Tao L, Wei Y: Redox-responsive polymers for drug delivery: from molecular design to applications, *Polym Chem* 5(5):1519–1528, 2014. https://doi.org/10.1039/c3py01192e.

Iacovacci V, Blanc A, Huang H, et al.: High-resolution SPECT imaging of stimuli-responsive soft microrobots, *Small* 15(34):1–7, 2019. https://doi.org/10.1002/smll.201900709.

Irie M: Photo- and chemical-induced phase transitions, In *Responsive Gels Vol. Transitions II*, 110, 1993, pp 49–65.

Jahanban-Esfahlan A, Seidi K, Jaymand M, et al.: Dynamic DNA nanostructures in biomedicine: beauty utility and limits, *J Control Release* 315(October):166–185, 2019. https://doi.org/10.1016/j.jconrel.2019.10.003.

Jang B, Gutman E, Stucki N, et al.: Undulatory locomotion of magnetic multilink nanoswimmers, *Nano Lett* 15(7):4829–4833, 2015. https://doi.org/10.1021/acs.nanolett.5b01981.

Jang D, Jeong J, Song H, Chung SK: Targeted drug delivery technology using untethered microrobots: a review, *J Micromech Microeng* 29(5):53002, 2019.

Jeon SJ, Hauser AW, Hayward RC: Shape-morphing materials from stimuli-responsive hydrogel hybrids, *Acc Chem Res* 50(2):161–169, 2017. https://doi.org/10.1021/acs.accounts.6b00570.

Jeon S, Hoshiar AK, Kim K, et al.: A magnetically controlled soft microrobot steering a guidewire in a three-dimensional phantom vascular network, *Soft Robot* 6(1):54–68, 2019. https://doi.org/10.1089/soro.2018.0019.

Jin Q, Yang Y, Jackson JA, Yoon C, Gracias DH: Untethered single cell grippers for active biopsy, *Nano Lett* 20(7):5383–5390, 2020. https://doi.org/10.1021/acs.nanolett.0c01729.

Jochum FD, Theato P: Temperature- and light-responsive smart polymer materials, *Chem Soc Rev* 42(17):7468–7483, 2013. https://doi.org/10.1039/c2cs35191a.

Khalil ISM, Dijkslag HC, Abelmann L, Misra S: MagnetoSperm: a microrobot that navigates using weak magnetic fields, *Appl Phys Lett* 104(22), 2014. https://doi.org/10.1063/1.4880035.

Khalil ISM, Klingner A, Hamed Y, Hassan YS, Misra S: Controlled noncontact manipulation of nonmagnetic untethered microbeads orbiting two-tailed soft microrobot, *IEEE Trans Robot* 36(4):1320–1332, 2020. https://doi.org/10.1109/TRO.2020.2990768.

Kim D, Lee H, Kwon Sh, Choi H, Park S: Magnetic nano-particles retrievable biodegradable hydrogel microrobot, *Sens Actuators B* 289(March):65–77, 2019. https://doi.org/10.1016/j.snb.2019.03.030.

Kim DY, Jeong KU: Light responsive liquid crystal soft matters: structures, properties, and applications, *Liq Cryst Today* 28(2):34–45, 2019. https://doi.org/10.1080/1358314X.2019.1653588.

Kim KT, Zhu J, Meeuwissen SA, et al.: Polymersome stomatocytes: controlled shape transformation in polymer vesicles, *J Am Chem Soc* 132(36):12522–12524, 2010a. https://doi.org/10.1021/ja104154t.

Kim J, Yoon E-S, Park S: Biohybrid walking microrobot with self-assembled cardiomyocytes, *Climbing Walk Robot*, 2010b. https://doi.org/10.5772/8820.

Kim J, Chung SE, Choi SE, Lee H, Kim J, Kwon S: Programming magnetic anisotropy in polymeric microactuators, *Nat Mater* 10(10):747–752, 2011. https://doi.org/10.1038/nmat3090.

Kim S, Laschi C, Trimmer B: Soft robotics: a bioinspired evolution in robotics, *Trends Biotechnol* 31(5):287–294, 2013a. https://doi.org/10.1016/j.tibtech.2013.03.002.

Kim S, Qiu F, Kim S, et al.: Fabrication and characterization of magnetic microrobots for three-dimensional cell culture and targeted transportation, *Adv Mater* 25(41):5863–5868, 2013b. https://doi.org/10.1002/adma.201301484.

Kim S, Lee S, Lee J, Nelson BJ, Zhang L, Choi H: Fabrication and manipulation of ciliary microrobots with non-reciprocal magnetic actuation, *Sci Rep* 6(July):1–9, 2016a. https://doi.org/10.1038/srep30713.

Kim H, Ali J, Cheang UK, Jeong J, Kim JS, Kim MJ: Micro manipulation using magnetic microrobots, *J Bionic Eng* 13(4):515–524, 2016b. https://doi.org/10.1016/S1672-6529(16)60324-4.

Kim T, Park S, Lee M, Baek S, Lee JB, Park N: DNA hydrogel microspheres and their potential applications for protein delivery and live cell monitoring, *Biomicrofluidics* 10(3), 2016c. https://doi.org/10.1063/1.4953046.

Kim Jy, Jeon S, Lee J, et al.: A simple and rapid fabrication method for biodegradable drug-encapsulating microrobots using laser micromachining, and characterization thereof, *Sens Actuators B* 266:276–287, 2018. https://doi.org/10.1016/j.snb.2018.03.033.

Kim DI, Lee H, Kwon SH, Sung YJ, Song WK, Park S: Bilayer hydrogel sheet-type intraocular microrobot for drug delivery and magnetic nanoparticles retrieval, *Adv Healthc Mater* 9(13):1–13, 2020a. https://doi.org/10.1002/adhm.202000118.

Kim D, Song S, Jang S, et al.: Untethered gripper-type hydrogel millirobot actuated by electric field and magnetic field, *Smart Mater Struct* 29(8):85024, 2020b.

Kocak G, Tuncer C, Bütün V: PH-responsive polymers, *Polym Chem* 8(1):144–176, 2017. https://doi.org/10.1039/c6py01872f.

Kojima M, Zhang Z, Nakajima M, Ooe K, Fukuda T: Construction and evaluation of bacteria-driven liposome, *Sens Actuators B* 183:395–400, 2013. https://doi.org/10.1016/j.snb.2013.03.127.

Kuang X, Roach DJ, Wu J, et al.: Advances in 4D printing: materials and applications, *Adv Funct Mater* 29(2):1–23, 2019. https://doi.org/10.1002/adfm.201805290.

Lahikainen M, Zeng H, Priimagi A: Design principles for non-reciprocal photomechanical actuation, *Soft Matter* 16(25):5951–5958, 2020. https://doi.org/10.1039/d0sm00624f.

Leaman EJ, Geuther BQ, Behkam B: *Hybrid Centralized / Decentralized Control of a Network of Bacteria-Based Bio-Hybrid Microrobots*, 2019, pp 1–12.

Lee C, Kim M, Kim YJ, et al.: Soft Robot Review, *Int J Control Autom Syst* 15(1):3–15, 2017.

Lee H, Choi H, Lee M, Park S: Preliminary study on alginate/NIPAM hydrogel-based soft microrobot for controlled drug delivery using electromagnetic actuation and near-infrared stimulus, *Biomed Microdevices* 20(4), 2018. https://doi.org/10.1007/s10544-018-0344-y.

Lee Y, Song WJ, Sun JY: Hydrogel soft robotics, *Mater Today Phys* 15:100258, 2020. https://doi.org/10.1016/j.mtphys.2020.100258.

Li J, Pumera M: 3D printing of functional microrobots, *Chem Soc Rev*, 2021.

Li J, Sattayasamitsathit S, Dong R, et al.: Template electrosynthesis of tailored-made helical nanoswimmers, *Nanoscale* 6(16):9415–9420, 2014. https://doi.org/10.1039/c3nr04760a.

Li H, Go G, Ko SY, Park J-O, Park S: Magnetic actuated ph-responsive hydrogel-based soft micro-robot for targeted drug delivery, *Smart Mater Struct* 25(2):27001, 2016a.

Li T, Li J, Zhang H, et al.: Magnetically propelled fish-like nanoswimmers, *Small* 12(44):6098–6105, 2016b. https://doi.org/10.1002/smll.201601846.

Li T, Li J, Morozov KI, et al.: Highly efficient freestyle magnetic nanoswimmer, *Nano Lett* 17(8):5092–5098, 2017. https://doi.org/10.1021/acs.nanolett.7b02383.

Li H, Chen J, Zhang J, Zhang J, Zhao G, Wang L: Photopatternable magnetic hollowbots by Nd-Fe-B nanocomposite for potential targeted drug delivery applications, *Micromachines* 9(4), 2018. https://doi.org/10.3390/mi9040182.

Liao J, Huang H: Review on magnetic natural polymer constructed hydrogels as vehicles for drug delivery, *Biomacromolecules* 21(7):2574–2594, 2020. https://doi.org/10.1021/acs.biomac.0c00566.

Luo M, Feng Y, Wang T, Guan J: Micro-/nanorobots at work in active drug delivery, *Adv Funct Mater* 28(25):1706100, 2018.

Ma X, Yang Z, Wang Y, et al.: Remote controlling dna hydrogel by magnetic field, *ACS Appl Mater Interfaces* 9(3):1995–2000, 2017. https://doi.org/10.1021/acsami.6b12327.

Magdanz V, Stoychev G, Ionov L, Sanchez S, Schmidt OG: Stimuli-responsive microjets with reconfigurable shape, *Angew Chemie* 126(10):2711–2715, 2014. https://doi.org/10.1002/ange.201308610.

Magdanz V, Khalil ISM, Simmchen J, et al.: IRONSperm: sperm-templated soft magnetic microrobots, *Sci Adv* 6(28):1–16, 2020. https://doi.org/10.1126/sciadv.aba5855.

Mair LO, Chowdhury S, Paredes-Juarez GA, et al.: Magnetically aligned nanorods in alginate capsules (MANiACs): soft matter tumbling robots for manipulation and drug delivery, *Micromachines* 10(4), 2019. https://doi.org/10.3390/mi10040230.

Majidi C: Soft robotics: a perspective—current Trends and prospects for the future, *Soft Robot* 1(1):5–11, 2014. https://doi.org/10.1089/soro.2013.0001.

Malachowski K, Breger J, Kwag HR, et al.: Stimuli-responsive theragrippers for chemo-mechanical controlled release, *Angew Chemie—Int Ed* 53(31):8045–8049, 2014. https://doi.org/10.1002/anie.201311047.

Maric T, Nasir MZM, Rosli NF, et al.: Microrobots derived from variety plant pollen grains for efficient environmental clean up and as an anti-cancer drug carrier, *Adv Funct Mater* 30(19):1–13, 2020. https://doi.org/10.1002/adfm.202000112.

Martel S: Bacterial microsystems and microrobots, *Biomed Microdevices* 14(6):1033–1045, 2012. https://doi.org/10.1007/s10544-012-9696-x.

Mathesh M, Wilson DA: Photosynthesis drives the motion of bio-nanomotors, *Adv Intell Syst* 2(5):2000028, 2020. https://doi.org/10.1002/aisy.202000028.

Mathesh M, Sun J, Van Der Sandt F, Wilson DA: Supramolecular nanomotors with "ph taxis" for active drug delivery in the tumor microenvironment, *Nanoscale* 12(44):22495–22501, 2020. https://doi.org/10.1039/d0nr04415f.

Mauri E, Papa S, Masi M, Veglianese P, Rossi F: Novel functionalization strategies to improve drug delivery from polymers, *Expert Opin Drug Deliv* 14(11):1305–1313, 2017.

Medina-Sánchez M, Magdanz V, Guix M, Fomin VM, Schmidt OG: Swimming microrobots: soft, reconfigurable, and smart, *Adv Funct Mater* 28(25):1–27, 2018. https://doi.org/10.1002/adfm.201707228.

Mehta K, Peeketi AR, Liu L, Broer D, Onck P, Annabattula RK: Design and applications of light responsive liquid crystal polymer thin films, *Appl Phys Rev* 7(4), 2020. https://doi.org/10.1063/5.0014619.

Mirkovic T, Foo ML, Arsenault AC, Fournier-Bidoz S, Zacharia NS, Ozin GA: Hinged nanorods made using a chemical approach to flexible nanostructures, *Nat Nanotechnol* 2(9):565–569, 2007. https://doi.org/10.1038/nnano.2007.250.

Mourran A, Zhang H, Vinokur R, Möller M: Soft microrobots employing nonequilibrium actuation via plasmonic heating, *Adv Mater* 29(2), 2017. https://doi.org/10.1002/adma.201604825.

Narayanaswamy R, Torchilin VP: Hydrogels and their applications in targeted drug delivery, *Molecules* 24(3), 2019. https://doi.org/10.3390/molecules24030603.

Nawroth JC, Lee H, Feinberg AW, et al.: A tissue-engineered jellyfish with biomimetic propulsion, *Nat Biotechnol* 30(8):792–797, 2012. https://doi.org/10.1038/nbt.2269.

Nelson BJ, Dong L, Arai F: Micro/nanorobots, In *Springer Handbook of Robotics*, 2008, Springer New York, pp 411–450.

Nelson BJ, Kaliakatsos IK, Abbott JJ: Microrobots for minimally invasive medicine, *Annu Rev Biomed Eng* 12(1):55–85, 2010. https://doi.org/10.1146/annurev-bioeng-010510-103409.

Ng WM, Teng XJ, Guo C, et al.: Motion control of biohybrid microbots under low Reynolds number environment: magnetotaxis, *Chem Eng Process—Process Intensif* 2019 (141):107530, 2018. https://doi.org/10.1016/j.cep.2019.107530.

Nocentini S, Parmeggiani C, Martella D, Wiersma DS: Optically driven soft micro robotics, *Adv Opt Mater* 6(14):1–17, 2018. https://doi.org/10.1002/adom.201800207.

Pak OS, Gao W, Wang J, Lauga E: High-speed propulsion of flexible nanowire motors: theory and experiments, *Soft Matter* 7(18):8169–8181, 2011. https://doi.org/10.1039/c1sm05503h.

Palagi S, Fischer P: Bioinspired microrobots, *Nat Rev Mater* 3(6):113, 2018.

Palagi S, Pensabene V, Beccai L, Mazzolai B, Menciassi A, Dario P: Design and development of a soft magnetically-propelled swimming microrobot, *Proc—IEEE Int Conf Robot Autom*:5109–5114, 2011. https://doi.org/10.1109/ICRA.2011.5980109.

Palagi S, Mark AG, Reigh SY, et al.: Structured light enables biomimetic swimming and versatile locomotion of photoresponsive soft microrobots, *Nat Mater* 15(6):647–653, 2016. https://doi.org/10.1038/nmat4569.

Palagi S, Mark AG, Melde K, et al.: Locomotion of light-driven soft microrobots through a hydrogel via local melting, *Int Conf Manip Autom Robot Small Scales, MARSS 2017—Proc*:1–5, 2017. https://doi.org/10.1109/MARSS.2017.8001916.

Palagi S, Singh DP, Fischer P: Light-controlled micromotors and soft microrobots, *Adv Opt Mater* 7(16):1900370, 2019.

Pane S, Iacovacci V, Sinibaldi E, Menciassi A: Real-time imaging and tracking of microrobots in tissues using ultrasound phase analysis, *Appl Phys Lett* 118(1):14102, 2021.

Park SJ, Gazzola M, Park KS, et al.: Phototactic guidance of a tissue-engineered soft-robotic ray, *Science* 353(6295):158–162, 2016. https://doi.org/10.1126/science.aaf4292.

Park J, Jin C, Lee S, Kim J, Choi H: Magnetically actuated degradable microrobots for actively controlled drug release and hyperthermia therapy, *Adv Healthc Mater* 8(16):1900213, 2019.

Patois T, Lakard B, Monney S, Roizard X, Fievet P: Characterization of the surface properties of polypyrrole films: influence of electrodeposition parameters, *Synth Met* 161(21–22):2498–2505, 2011. https://doi.org/10.1016/j.synthmet.2011.10.003.

Paxton WF, Kistler KC, Olmeda CC, et al.: Catalytic nanomotors: autonomous movement of striped nanorods, *J AmChem Soc* 126(41):13424–13431, 2004. https://doi.org/10.1021/ja047697z.

Peers S, Montembault A, Ladavière C: Chitosan hydrogels for sustained drug delivery, *J Control Release* 326:150–163, 2020. https://doi.org/10.1016/j.jconrel.2020.06.012.

Peng L, Feng A, Huo M, Yuan J: Ferrocene-based supramolecular structures and their applications in electrochemical responsive systems, *Chem Commun* 50(86):13005–13014, 2014. https://doi.org/10.1039/c4cc05192k.

Peters C, Hoop M, Pané S, Nelson BJ, Hierold C: Degradable magnetic composites for minimally invasive interventions: device fabrication, targeted drug delivery, and cytotoxicity tests, *Adv Mater* 28(3):533–538, 2016.

Peyer KE, Zhang L, Nelson BJ: Bio-inspired magnetic swimming microrobots for biomedical applications, *Nanoscale* 5(4):1259–1272, 2013. https://doi.org/10.1039/c2nr32554c.

Pilz Da Cunha M, Debije MG, Schenning APHJ: Bioinspired light-driven soft robots based on liquid crystal polymers, *Chem Soc Rev* 49(18):6568–6578, 2020a. https://doi.org/10.1039/d0cs00363h.

Pilz da Cunha M, Ambergen S, Debije MG, Homburg EFGA, den Toonder JMJ, Schenning APHJ: A soft transporter robot fueled by light, *Adv Sci* 7(5):1–7, 2020b. https://doi.org/10.1002/advs.201902842.

Piqué A: Laser-based microadditive manufacturing technologies, In *Three-Dimensional Microfabrication Using Two-Photon Polymerization*, 2020, Elsevier, pp 1–23.

Puigmartí-Luis J, Pellicer E, Jang B, et al.: Magnetically and chemically propelled nanowire-based swimmers, *Magn Nano- Microwires*:777–799, 2020. https://doi.org/10.1016/b978-0-08-102832-2.00026-8.

Purcell EM: Life at low reynolds number, *Am J Physiol* 45(1):3–11, 1977. https://doi.org/10.1119/1.10903.

Qiu T, Lee TC, Mark AG, et al.: Swimming by reciprocal motion at low Reynolds number, *Nat Commun* 5(May):1–8, 2014. https://doi.org/10.1038/ncomms6119.

Qiu F, Fujita S, Mhanna R, Zhang L, Simona BR, Nelson BJ: Magnetic helical microswimmers functionalized with lipoplexes for targeted gene delivery, *Adv Funct Mater* 25(11):1666–1671, 2015.

Ricotti L, Trimmer B, Feinberg AW, et al.: Biohybrid actuators for robotics: a review of devices actuated by living cells, *Sci Robot* 2(12):1–18, 2017. https://doi.org/10.1126/scirobotics.aaq0495.

Rizwan M, Yahya R, Hassan A, et al.: PH sensitive hydrogels in drug delivery: brief history, properties, swelling, and release mechanism, material selection and applications, *Polymers (Basel)* 9(4), 2017. https://doi.org/10.3390/polym9040137.

Rogóż M, Zeng H, Xuan C, Wiersma DS, Wasylczyk P: Light-driven soft robot mimics caterpillar locomotion in natural scale, *Adv Opt Mater* 4(11):1689–1694, 2016. https://doi.org/10.1002/adom.201600503.

Safdar M, Khan SU, Jänis J: Progress toward catalytic micro- and nanomotors for biomedical and environmental applications, *Adv Mater* 30(24):1–27, 2018. https://doi.org/10.1002/adma.201703660.

Schmidt CK, Medina-Sánchez M, Edmondson RJ, Schmidt OG: Engineering microrobots for targeted cancer therapies from a medical perspective, *Nat Commun* 11(1):1–18, 2020. https://doi.org/10.1038/s41467-020-19322-7.

Schmitt S, Haeufle D: *Mechanics and thermodynamics of biological muscle-a simple model approach*, 2015 https://doi.org/10.1007/978-3-662-44506-8_10.

Shafranek RT, Millik SC, Smith PT, Lee CU, Boydston AJ, Nelson A: Stimuli-responsive materials in additive manufacturing, *Prog Polym Sci* 93:36–67, 2019. https://doi.org/10.1016/j.progpolymsci.2019.03.002.

Shah SAA, Firlak M, Berrow SR, et al.: Electrochemically enhanced drug delivery using polypyrrole films, *Materials (Basel)* 11(7):1–16, 2018. https://doi.org/10.3390/ma11071123.

Si T, Zou X, Wu Z, et al.: A bubble-dragged catalytic polymer microrocket, *Chem—An Asian J* 14(14):2460–2464, 2019. https://doi.org/10.1002/asia.201900277.

Singh AV, Sitti M: Patterned and specific attachment of bacteria on biohybrid bacteria-driven microswimmers, *Adv Healthc Mater* 5(18):2325–2331, 2016. https://doi.org/10.1002/adhm.201600155.

Singh AV, Hosseinidoust Z, Park BW, Yasa O, Sitti M: Microemulsion-based soft bacteria-driven microswimmers for active cargo delivery, *ACS Nano* 11(10):9759–9769, 2017. https://doi.org/10.1021/acsnano.7b02082.

Singh AV, Ansari MHD, Mahajan M, et al.: Sperm cell driven microrobots-emerging opportunities and challenges for biologically inspired robotic design, *Micromachines* 11(4), 2020. https://doi.org/10.3390/MI11040448.

Sitti M: Miniature soft robots—road to the clinic, *Nat Rev Mater* 3(6):74–75, 2018. https://doi.org/10.1038/s41578-018-0001-3.
Sitti M, Wiersma DS: Pros and cons: magnetic versus optical microrobots, *Adv Mater* 32(20), 2020. https://doi.org/10.1002/adma.201906766.
Soft Robotics (SoRo) 2021. https://home.liebertpub.com/publications/soft-robotics/616/overview (Accessed Feb 6, 2021).
Son H, Byun E, Yoon YJ, Nam J, Song SH, Yoon C: Untethered actuation of hybrid hydrogel gripper via ultrasound, *ACS Macro Lett*:1766–1772, 2020. https://doi.org/10.1021/acsmacrolett.0c00702.
Soreni-Harari M, St. Pierre R, McCue C, Moreno K, Bergbreiter S: Multimaterial 3D printing for microrobotic mechanisms, *Soft Robot* 7(1):59–67, 2020. https://doi.org/10.1089/soro.2018.0147.
Soto F, Lopez-Ramirez MA, Jeerapan I, et al.: Rotibot: use of Rotifers as self-propelling biohybrid microcleaners, *Adv Funct Mater* 29(22):1–8, 2019. https://doi.org/10.1002/adfm.201900658.
Soto F, Karshalev E, Zhang F, Esteban Fernandez de Avila B, Nourhani A, Wang J: Smart materials for microrobots, *Chem Rev*, 2021.
Spiegel CA, Hippler M, Münchinger A, et al.: 4D printing at the microscale, *Adv Funct Mater* 30(26), 2020. https://doi.org/10.1002/adfm.201907615.
Stoychev G, Turcaud S, Dunlop JWC, Ionov L: Hierarchical multi-step folding of polymer bilayers, *Adv Funct Mater* 23(18):2295–2300, 2013. https://doi.org/10.1002/adfm.201203245.
Stoychev G, Kirillova A, Ionov L: Light-responsive shape-changing polymers, *Adv Opt Mater* 7(16):1–30, 2019. https://doi.org/10.1002/adom.201900067.
Stuart MAC, Huck WTS, Genzer J, et al.: Emerging applications of stimuli-responsive polymer materials, *Nat Mater* 9(2):101–113, 2010. https://doi.org/10.1038/nmat2614.
Sun L, Yu Y, Chen Z, et al.: Biohybrid robotics with living cell actuation, *Chem Soc Rev* 49(12):4043–4069, 2020. https://doi.org/10.1039/d0cs00120a.
Suriano R, Bernasconi R, Magagnin L, Levi M: 4D printing of smart stimuli-responsive polymers, *J Electrochem Soc* 166(9):B3274–B3281, 2019. https://doi.org/10.1149/2.0411909jes.
Tabatabaei SN, Lapointe J, Martel S: Shrinkable hydrogel-based magnetic microrobots for interventions in the vascular network, *Adv Robot* 25(8):1049–1067, 2011. https://doi.org/10.1163/016918611X568648.
Taherkhani S, Mohammadi M, Daoud J, Martel S, Tabrizian M: Covalent binding of nanoliposomes to the surface of magnetotactic bacteria for the synthesis of self-propelled therapeutic agents, *ACS Nano* 8(5):5049–5060, 2014. https://doi.org/10.1021/nn5011304.
Terzopoulou A, Nicholas JD, Chen XZ, Nelson BJ, Pane S, Puigmartí-Luis J: Metal–organic frameworks in motion, *Chem Rev* 120(20):11175–11193, 2020. https://doi.org/10.1021/acs.chemrev.0c00535.
Theato P, Sumerlin BS, O'reilly RK, Epp TH: Stimuli responsive materials, *Chem Soc Rev* 42(17):7055–7056, 2013. https://doi.org/10.1039/c3cs90057f.
TirgarBahnamiri P, Bagheri-Khoulenjani S: Biodegradable microrobots for targeting cell delivery, *Med Hypotheses* 102:56–60, 2017. https://doi.org/10.1016/j.mehy.2017.02.015.
Tu Y, Peng F, André AAM, Men Y, Srinivas M, Wilson DA: Biodegradable hybrid stomatocyte nanomotors for drug delivery, *ACS Nano* 11(2):1957–1963, 2017a. https://doi.org/10.1021/acsnano.6b08079.
Tu Y, Peng F, White PB, Wilson DA: Redox-sensitive stomatocyte nanomotors: destruction and drug release in the presence of glutathione, *Angew Chemie—Int Ed* 56(26):7620–7624, 2017b. https://doi.org/10.1002/anie.201703276.
Tung HW, Maffioli M, Frutiger DR, Sivaraman KM, Pané S, Nelson BJ: Polymer-based wireless resonant magnetic microrobots, *IEEE Trans Robot* 30(1):26–32, 2014. https://doi.org/10.1109/TRO.2013.2288514.

Tyagi M, Spinks GM, Jager EWH: 3D printing microactuators for soft microrobots, *Soft Robot* 00(00):1–9, 2020a. https://doi.org/10.1089/soro.2019.0129.
Tyagi M, Spinks GM, Jager EWH: Fully 3D printed soft microactuators for soft microrobotics, *Smart Mater Struct* 29(8), 2020b. https://doi.org/10.1088/1361-665X/ab9f48.
Van Rhee PG, Rikken RSM, Abdelmohsen LKEA, et al.: Polymersome magneto-valves for reversible capture and release of nanoparticles, *Nat Commun* 5:1–8, 2014. https://doi.org/10.1038/ncomms6010.
Wallin TJ, Pikul J, Shepherd RF: 3D printing of soft robotic systems, *Nat Rev Mater* 3 (6):84–100, 2018. https://doi.org/10.1038/s41578-018-0002-2.
Wang W, Giltinan J, Zakharchenko S, Sitti M: Dynamic and programmable self-assembly of micro-rafts at the air-water interface, *Sci Adv* 3(5):1–10, 2017. https://doi.org/10.1126/sciadv.1602522.
Wang X, Qin XH, Hu C, et al.: 3D printed enzymatically biodegradable soft helical microswimmers, *Adv Funct Mater* 28(45):1–8, 2018. https://doi.org/10.1002/adfm.201804107.
Wang X, Cai J, Sun L, et al.: Facile fabrication of magnetic microrobots based on spirulina templates for targeted delivery and synergistic chemo-photothermal therapy, *ACS Appl Mater Interfaces* 11(5):4745–4756, 2019. https://doi.org/10.1021/acsami.8b15586.
Wang C, Liu C, Wei Q, et al.: S,S-Tetrazine-based hydrogels with visible light cleavable properties for on-demand anticancer drug delivery, *Research* 2020:1–11, 2020. https://doi.org/10.34133/2020/6563091.
Wani OM, Zeng H, Priimagi A: A light-driven artificial flytrap, *Nat Commun* 8(May):1–7, 2017. https://doi.org/10.1038/ncomms15546.
Wei M, Gao Y, Li X, Serpe MJ: Stimuli-responsive polymers and their applications, *Polym Chem* 8(1):127–143, 2017. https://doi.org/10.1039/c6py01585a.
Wei T, Liu J, Li D, et al.: Development of magnet-driven and image-guided degradable microrobots for the precise delivery of engineered stem cells for cancer therapy, *Small* 16(41):1–13, 2020. https://doi.org/10.1002/smll.201906908.
White TJ, Broer DJ: Programmable and adaptive mechanics with liquid crystal polymer networks and elastomers, *Nat Mater* 14(11):1087–1098, 2015. https://doi.org/10.1038/nmat4433.
Williams BJ, Anand SV, Rajagopalan J, Saif MTA: A self-propelled biohybrid swimmer at low Reynolds number, *Nat Commun* 5:1–8, 2014. https://doi.org/10.1038/ncomms4081.
Wilson DA, Nolte RJM, Van Hest JCM: Autonomous movement of platinum-loaded stomatocytes, *Nat Chem* 4(4):268–274, 2012. https://doi.org/10.1038/nchem.1281.
Wu Z, Wu Y, He W, Lin X, Sun J, He Q: Self-propelled polymer-based multilayer nanorockets for transportation and drug release, *Angew Chem Int Ed* 52(27):7000–7003, 2013a.
Wu ZL, Moshe M, Greener J, et al.: Three-dimensional shape transformations of hydrogel sheets induced by small-scale modulation of internal stresses, *Nat Commun* 4:1–7, 2013b. https://doi.org/10.1038/ncomms2549.
Wu Z, Lin X, Wu Y, Si T, Sun J, He Q: Near-infrared light-triggered on/off motion of polymer multilayer rockets, *ACS Nano* 8(6):6097–6105, 2014a. https://doi.org/10.1021/nn501407r.
Wu Z, Li T, Li J, et al.: Turning erythrocytes into functional micromotors, *ACS Nano* 8 (12):12041–12048, 2014b. https://doi.org/10.1021/nn506200x.
Wu Z, Lin X, Zou X, Sun J, He Q: Biodegradable protein-based rockets for drug transportation and light-triggered release, *ACS Appl Mater Interfaces* 7(1):250–255, 2015. https://doi.org/10.1021/am507680u.
Wu Z, Li L, Yang Y, et al.: A microrobotic system guided by photoacoustic computed tomography for targeted navigation in intestines in vivo, *Sci Robot* 4(32), 2019.
Xie H, Sun M, Fan X, et al.: Reconfigurable magnetic microrobot swarm: multimode transformation, locomotion, and manipulation, *Sci Robot* 4(28):1–15, 2019. https://doi.org/10.1126/scirobotics.aav8006.

Xie M, Zhang W, Fan C, et al.: Bioinspired soft microrobots with precise magneto-collective control for microvascular thrombolysis, *Adv Mater* 32(26):1–11, 2020. https://doi.org/10.1002/adma.202000366.

Xu T, Zhang J, Salehizadeh M, Onaizah O, Diller E: Millimeter-scale flexible robots with programmable three-dimensional magnetization and motions, *Sci Robot* 4(29), 2019. https://doi.org/10.1126/scirobotics.aav4494.

Yan B, Wu Y, Guo L: Recent advances on polypyrrole electroactuators, *Polymers (Basel)* 9 (9):1–20, 2017. https://doi.org/10.3390/polym9090446.

Yang L, Zhang Y, Wang Q, Chan KF, Zhang L: Automated control of magnetic spore-based microrobot using fluorescence imaging for targeted delivery with cellular resolution, *IEEE Trans Autom Sci Eng* 17(1):490–501, 2020. https://doi.org/10.1109/TASE.2019.2937232.

Yoon C, Xiao R, Park J, Cha J, Nguyen TD, Gracias DH: Functional stimuli responsive hydrogel devices by self-folding, *Smart Mater Struct* 23(9), 2014. https://doi.org/10.1088/0964-1726/23/9/094008.

Yoshizumi Y, Suzuki H: Self-propelled metal-polymer hybrid micromachines with bending and rotational motions, *ACS Appl Mater Interfaces* 9(25):21355–21361, 2017. https://doi.org/10.1021/acsami.7b03656.

Zeeshan MA, Grisch R, Pellicer E, et al.: Hybrid helical magnetic microrobots obtained by 3D template-assisted electrodeposition, *Small* 10(7):1284–1288, 2014. https://doi.org/10.1002/smll.201302856.

Zeng H, Wasylczyk P, Wiersma DS, Priimagi A: Light robots: bridging the gap between microrobotics and photomechanics in soft materials, *Adv Mater* 30(24):1–9, 2018. https://doi.org/10.1002/adma.201703554.

Zhang J, Diller E: Tetherless mobile micrograsping using a magnetic elastic composite material, *Smart Mater Struct* 25(11):1–8, 2016. https://doi.org/10.1088/0964-1726/25/11/11LT03.

Zhang L, Abbott JJ, Dong L, Kratochvil BE, Bell D, Nelson BJ: Artificial bacterial flagella: fabrication and magnetic control, *Appl Phys Lett* 94(6):2007–2010, 2009a. https://doi.org/10.1063/1.3079655.

Zhang L, Abbott JJ, Dong L, et al.: Characterizing the swimming properties of artificial bacterial flagella, *Nano Lett* 9(10):3663–3667, 2009b. https://doi.org/10.1021/nl901869j.

Zhang L, Peyer KE, Nelson BJ: Artificial bacterial flagella for micromanipulation, *Lab Chip* 10(17):2203–2215, 2010. https://doi.org/10.1039/c004450b.

Zhang X, Han L, Liu M, et al.: Recent Progress and Advances in redox-responsive polymers as controlled delivery nanoplatforms, *Mater Chem Fron* 1(5):807–822, 2017. https://doi.org/10.1039/c6qm00135a.

Zhang P, Wu G, Zhao C, Zhou L, Wang X, Wei S: Magnetic stomatocyte-like nanomotor as photosensitizer carrier for photodynamic therapy based cancer treatment, *Colloids Surf B Biointerfaces* 194:111204, 2020. https://doi.org/10.1016/j.colsurfb.2020.111204.

Zhu W, Li J, Leong YJ, et al.: 3D-printed artificial microfish, *Adv Mater* 27(30):4411–4417, 2015. https://doi.org/10.1002/adma.201501372.

Zhuang J, Sitti M: Chemotaxis of bio-hybrid multiple bacteria-driven microswimmers, *Sci Rep* 6(August):1–10, 2016. https://doi.org/10.1038/srep32135.

CHAPTER TWO

Advances in printing technologies for soft robotics devices applications

Martina Aurora Costa Angeli*, Manuela Ciocca, Luisa Petti, and Paolo Lugli
Free University of Bolzano-Bozen, Bolzano, Italy
*Corresponding author: e-mail address: martinaaurora.costaangeli@unibz.it

Contents

1. Introduction 46
2. Printing technologies for soft robotics 47
   2.1 Screen printing 47
   2.2 Inkjet printing 56
3. Printable materials and substrates for soft robotics 60
   3.1 Screen printable substrates 60
   3.2 Inkjet printable substrates 62
   3.3 Screen printable inks 64
   3.4 Inkjet printable inks 71
4. Examples of printed devices for soft robotics 75
   4.1 Example: Stretchable screen printed nanocomposite sensors for feedback–loop control of a soft earthworm robot 75
   4.2 Example: Inkjet printed conductive gold electrodes for e-skin for soft robotics 79
5. Conclusions and outlook 81
References 82

Abstract

Soft robots, made of deformable and stretchable materials, have been exploited and investigated as promising technologies for a wide range of applications, from human assistance to rehabilitation. In this context, the possibility to integrate conformable, flexible and stretchable sensors able to detect external stimuli allows a further increase of the potentiality of soft robotics. The realization of soft, flexible, and stretchable electronic circuits and sensors is mainly enabled by the low-cost prototyping possibilities offered by the printing techniques, especially screen and inkjet printing. Simplified processing steps, reduced material wastage, low fabrication cost, high throughput, as well as the ability to dispose of different small patterns over larger areas while being able to pattern

Advances in Chemical Engineering, Volume 57
ISSN 0065-2377
https://doi.org/10.1016/bs.ache.2021.05.001

a wide range of materials on diverse flexible and soft substrates, are some of the advantages that have made screen and inkjet printing techniques very attractive also in this field.

1. Introduction

In the past few years, research in the soft robotics sector has seen substantial developments with soft robots rapidly allowing the carrying out of typical robotic tasks, as well as introducing new ways of supporting humans (Wang et al., 2018). The increasing demand for soft robots in numerous emerging applications including aerospace (Hu et al., 2018), human-machine interface and interaction (Barmpakos and Kaltsas, 2021), rehabilitation and wearable robots (Yan et al., 2020), as well as locomotion for therapeutics (Zhu et al., 2021) and prosthetics (Kaur et al., 2021), generated a great interest in the development of specialized and efficient technologies to fabricate conformable electronic components (Galloway et al., 2016; Marchese et al., 2014; Park et al., 2014). Indeed, these soft machines need soft and conformable bending actuators, stretchable circuits, deformable sensors, and strain or curvature sensors that allow them to perceive both the encumbrance of their body (proprioception) and the external environment (exteroception). Initially, commercially available sensors were embedded into soft robots to realize sensorized soft machines (Gerboni et al., 2017). However, this rather traditional approach is considered not ideal due to the sensor design which cannot be adapted to the robot design and softness. Flexible and stretchable electrical circuits and sensors fabricated using customized manufacturing techniques instead allow overcoming such limitation (Amjadi et al., 2016). In this context, printing techniques, such as inkjet printing and screen printing, are especially promising low-cost prototyping solutions to realize soft, flexible, and stretchable electronic circuits and sensors for soft robotics applications. Simplified processing steps, reduced material wastage, low fabrication cost, high throughput, and the ability to dispose of several small patterns over large areas while being able to pattern a wide range of materials on flexible and soft substrates, are some of the advantages that have made inkjet and screen printing techniques very attractive also in this field. Indeed, in the recent literature, several examples of inkjet and screen printed electronic components and devices employed in soft machines can be found. Electronic skins (e-skins) which can replicate the human somatosensory system (Guinovart et al., 2013; Zhao et al., 2020), conformable strain sensors with large stretchability and high

sensitivity (Goldoni et al., 2020; Tetsu et al., 2017), flexible temperature sensors (Vuorinen et al., 2016), actuator and sensors (Ta et al., 2019; Yeo et al., 2016), are just some of the available examples of particularly suitable printed components for soft robots.

In this chapter, we present recent advances in screen and inkjet printing techniques used for soft robotic applications. First, a description of the main technical features and parameters that need to be understood to successfully use screen and inkjet printers is given. Then the properties of the employed materials, inks and substrates, are examined. Finally, a short comparison between the two techniques, highlighting their advantages and disadvantages and recent applications in the field of soft robotics is provided.

2. Printing technologies for soft robotics

2.1 Screen printing

Routes of screen printing are generally credited to China around AD 960. It is a rather ancient art form that nowadays is used both as an artistic medium and in commercial applications, recently (in the last 30 years) turning out to be the most used technique to manufacture printed electronics (Market-Reports, 2020; Suresh et al., 2021). While the theory of this technique has not changed significantly over the years, the increasing interest in low-cost, flexible, and smarter products as well as the exploitation of new materials, paved the way to an extensive employment of this technique with new applications, goals, and aims. In fact, the main drivers of this increased interest and changed scope are linked to the major advantages of this technique, namely low-cost, simplicity, high speed, as well as suitability to fabricate deformable devices over large areas, which place this method among the best additive manufacturing techniques (Chang et al., 2012). Among the various advantages, the possibility to realize flexible, stretchable, and comfortable devices directly on soft, bendable and stretchable polymer substrates and/or textile has played a major role in the spread of this technique. For soft robotic applications, in particular, the ability to directly deposit a wide range of materials (conductive, semiconductive, and insulating) characterized by an intrinsic softness on deformable substrates to realize stretchable devices is a key aspect.

In fact, screen printing has become an extremely popular technique to realize stretchable electronic active devices (Zabihipour et al., 2020), stretchable interconnects (Cahn et al., 2020), bendable displays (Li et al., 2020), pressure sensors (Yang et al., 2018), stretchable batteries (Kumar et al., 2017) (as shown in Fig. 1B), wearable sensors (Liao et al., 2018),

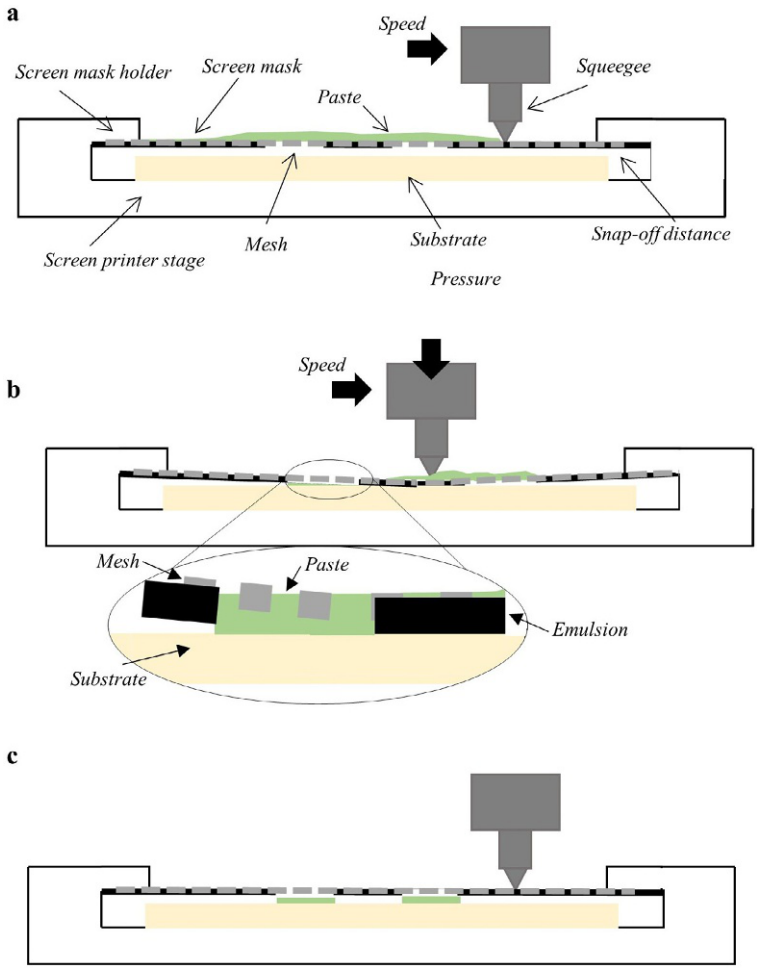

Fig. 1 Schematic of a screen printing process and representation of the printer components. A screen printer consists of a screen mask, made of a mesh coated with a photoemulsion that reproduces the pattern that it would be printed. The squeegee that performs the printing process (called printing stroke), the substrate that is held to the screen printer stage, and the paste. During printing, the first printing step is the (A) flooding, in which the squeegee, which is barely in contact with the mesh, spreads the paste over the mesh. (B) Then the printing stroke is performed: the squeegee travels across the screen with a defined speed and pressure and presses the paste through the screen mask openings onto the substrate. (C) Finally, due to the snap-off distance, the screen lifts off from the substrate after the squeegee passed and the paste remains on the substrate at the open areas of the screen and forms a replica of the desired pattern.

epidermal electronics (Zhao et al., 2020), strain sensors (Wang et al., 2020a), deformable biosensors (Abellán-Llobregat et al., 2017), soft sensors and actuators (Yeo et al., 2016). As a consequence, such variety of applications make flexible printed electronic devices appealing to a broad range of industries capturing an extensive part of the global market. Indeed, besides its considerable use in research, screen printing is currently one of the most employed processes in the production lines of printed electronics whereas many screen printed commercial devices, such as force sensors ("FlexiForce", 2021) electrochemical sensors ("Metrohm", 2021), and solar cells ("infinityPV", 2021) are already available on the market.

Screen printing is a contact-based printing technique that offers the ability to accurately deposit thick films of paste through a simple and fast process over a large surface area. Like in any other contact printing approach, in screen printing the ink is transferred to the substrate by physical contact through the use of a so-called screen mask. The thickness of the printed track can range from one to several hundreds of micrometers, (Merilampi et al., 2009). In particular, an area up to 80 cm x 60 cm can easily be printed in few minutes with a throughput of up to a thousand copies per hour (Khan et al., 2015). Screen printing may be also performed using a flatbed or rotary (roll-to-roll, R2R) process, with the latter being a fully continuous process allowing high speed production (100 m/min) compared to the flatbed (35 m/min) approach. While a higher throughput can be achieved with a rotatory process, the setup is more expensive and characterized by a higher ink waste (Huttunen et al., 2019; Søndergaard et al., 2013). This is why rotatory methods are preferred at the industrial scale, whereas flatbed setups are mostly used for small laboratory systems and in general in research. Here, we will focus on flatbed systems, referring to it generally screen printing system, however with small modifications the given principles and discussions suit also the R2R method.

As highlighted in Fig. 1, screen printing comprises five main core components:

- The screen mask, which is made of a metallic or wooden frame that holds a mesh on which the desired print pattern is reproduced (the photochemical emulsion).
- The mesh, which is the key element of a screen mask, it is a metallic or polymeric net, made of interlaced weaving threads, that leaves small openings through which the paste is pushed.
- The photochemical emulsion blocks all openings in the mesh that are not needed for the reproduction of the pattern. Therefore, the paste pressed

on the screen mask passes through the portions of the mesh that are not covered by the emulsion, replicating the design on the substrate.
- The screen mask holder, a metallic or wooden structure that holds the screen mask above the substrate at a fixed distance.
- The squeegee, which performs the primary function of transferring the paste to the substrate. It is used to create the dynamic pressure which forces the paste through the apertures on the screen mask onto the substrate. It consists of a rubber piece (hardness ranging from 65 to 85 shore) mounted to a wooden or metallic holder (the squeegee holder) with a defined angle of about 45° to 75° that is usually used to press the sharp edge of the rubber onto the screen mask (Faddoul et al., 2012; Kołodziej et al., 2020).
- The screen printer stage (substrate holder), on which the substrate is fixed by vacuum, glue, or by simple tape. A mechanically stable fixture of the substrate, which holds the substrate in place and withstands high shear and normal forces, is a fundamental aspect to guarantee high quality print.
- The substrate, which can vary from classical rigid printed circuit boards (PCBs), silicon wafers, glass, ceramic to flexible and soft polymers, as well as textiles.
- The paste, which is typically a viscous liquid or semi-liquid material (500–50,000 cPa) with a non-Newtonian shear-thinning thixotropic behavior (Khan et al., 2015). A wide range of conductive, semiconductive, and dielectric functional materials screen printable pastes exists. The formulation of the paste is simple if compared to the ink used for other printing techniques, and usually, it is typically made of conductive functional polymers or nanomaterials dispersed in a polymeric matrix.

Screen printing can be performed either by hand or using a semi or fully automated system. In a fully automated machine, the substrate is loaded by an automatic system, while in a semi-automatic system the substrate is taken off and fed in manually using a mechanized squeegee. On the other side, in a hand system, the printing procedure itself is completely done by a human. In all cases, the printing process involves few and simple steps. A schematic of the printing process is shown in Fig. 1. The screen mask is placed on a screen mask holder while the substrate, which has to be perfectly flat, is placed over the screen printer stage. The substrate is not in contact with the mesh: a small space (typically of few millimeters) between the mesh and the underneath substrate, called snap-off distance, is set (Potts et al., 2020b). This distance prevents the screen from being in direct contact

with the substrate avoiding smearing or mesh marks on the deposited paste. This value is usually set as a function of the print area and the mesh tension (Abbott, 2008).

Usually, the printing process involves first the flooding of the paste over the opening areas of the screen mask. During this step, the paste is spread over the screen mask using a squeegee, which is barely in contact with the screen mask to avoid the paste dripping beneath the mesh (Fig. 1A). Then, the printing process (called printing stroke) is performed (Fig. 1B). During this step, the squeegee applies the necessary pressure to locally force the mesh in contact with the substrate and simultaneously push the paste through the openings of the emulsion to form the desired pattern on the substrate. Due to the snap-off distance, the screen lifts off from the substrate slowly after the squeegee passed and releases the paste from the mesh. After the release, the paste remains on the substrate at the open areas of the screen and forms a replica of the desired pattern (Fig. 1C). The rheological properties of the paste are tuned in order to avoid the ink flooding out of the printed design and in the meanwhile leave a wet-track with a flat and uniform cross-section. Then, the solvent starts to evaporate at room temperature, and the wet-track needs a post-treatment by heat or UV or laser to anneal or cross-link the binder of the paste.

A similar technique, which however does not use a mesh, is stencil printing. In this case, a metallic or polymeric stencil, made from a thin sheet ($\sim$100 μm) of stainless steel, with laser-cut, etched, or milled free openings is used to shape the paste over the substrate. Contrary to screen printing, the stencil is in contact with the substrate (without any snap-off distance). Compared to screen printing, the stencil method is an easier and cheaper method (the stencil is cheaper and also polymeric stencil can be used), characterized by thicker wet-deposit, with the thickness ruled by the stencil thickness itself. Since a mesh is not used, as in the screen printer, stabilization gutters are required, which may lead to unwanted broken strokes in lines and thus limited types of designs that can be printed (Larmagnac et al., 2014). However, stencil printing is a widely used method because it enables the employment of cheap polymeric stencils, thus funding application especially as a fast-prototyping technique (Yokus et al., 2016).

As with every printing technique, the output quality of the printed pattern is the result of the choice and the combination of the characteristics of the components of the screen printer employed, such as the screen mask and the mesh type, the squeegee, the printing settings (the printing speed, the snap-off distance, and the squeegee pressure), and the properties of the

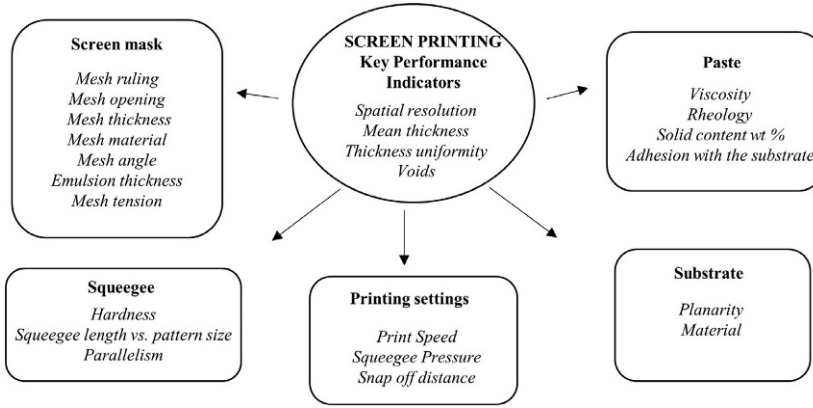

Fig. 2 The screen printing key performance indicators (KPI) include the minimum spatial resolution of the printed structure, its thickness, and uniformity, as well as the possible presence of voids or defects in the printed pattern. The output quality of the printed pattern is the result of the choice and the combination of different aspects characteristics of the components of the screen printer employed, such as the screen mask and the mesh type, the squeegee, the printing settings (the printing speed, the snap-off distance, and the squeegee pressure), and the properties of the materials used, such as the paste viscosity and the planarity of the substrate.

materials used, such as the paste viscosity and surface tension of the substrate, that will be detailed explained in the below paragraphs (Ney et al., 2019; Pan et al., 1999).

The detailed variables that influence print quality are summarized in Fig. 2. The screen printing key performance indicators (KPI) include the minimum spatial resolution of the printed structure, its thickness and uniformity, as well as the possible presence of voids or defects in the printed pattern. Not all the above-listed characteristics play the same role in pursuing a specific printing quality and moreover, the screen printing KPI are not only limited to the printing process itself but should include also the demands or nature of the final printed product, such as its conductivity, the deformability, the sensing properties. Thus, in the following paragraphs, we will critically examine the most important aspects that should be considered in the screen printing process for the specific realization of soft devices sensors, actuators in soft robot applications.

In screen printing technique, the screen mask is the most important element, which allows the selective deposition of the conductive paste on the substrate through a stencil. The screen mask not only defines the design to be patterned but it affects the outcome quality and resolution, as well as the final

thickness of the printed structures. Thus, choosing the correct screen mask is fundamental to guarantee high print quality. A screen printing mask is constituted by a metallic or wooden frame that carries a tightly stretched mesh on which a photochemical emulsion reproduces the desired pattern. The screen printing mesh should be flexible so that the squeegee can conform to the substrate and then recover the initial condition after the printing stroke. The mesh is made of metallic, stainless steel, or polymeric, polyester, weaving monofilament threads, as shown in the schematic representation of Fig. 3.

Due to its low cost, polyester is the most used material, however, stainless steel is recommended for high-precision printing because of its low flexibility and capability to use thinner threads, leading thereby to a finer mesh. The screen mesh should be selected based on criteria directly related to the ink paste and the application, indeed it is well known that the mesh has a greatest effect on the print quality and resolution, as well as thickness of the printed pattern, because the mesh interacts to alter the available volume of material transfer (Abbott, 2008). The most important features of a screen printing

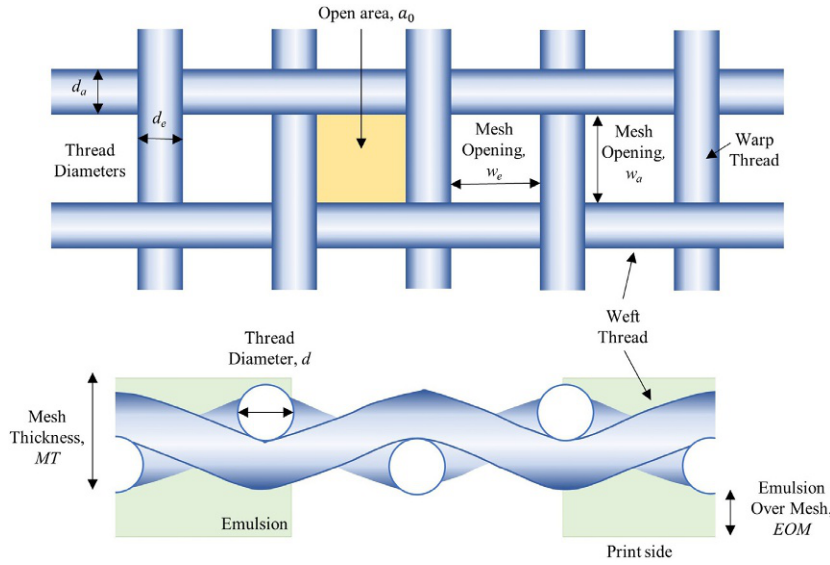

Fig. 3 Schematic top view (top panel) and side view (bottom panel) of a screen mesh with the most important characteristics: the thread diameters of wefts (d_e) and warps (d_a) direction, the mesh opening in wefts (w_e) and warp (w_a) directions, the open area (a_0), and the mesh thickness (MT), which can be roughly estimated as the double of the thread diameter, the opening area, and the thickness of the emulsion over mesh (EOM).

mask are the mesh ruling, the thread diameter, the opening area, the mesh thickness and the mesh angle. Among all, the mesh ruling (n) and the thread diameter (d) are the most used parameters to identify the mask type. The mesh ruling is the number of threads per centimeter or per inch. The finer is the mesh, the higher is the ruling. A typical value of fine mesh ruling is 120 threads/cm. Finer meshes are more suitable for printing fine structures (line width lower than 500 μm) and coarser meshes are used for thicker layers. Indeed, using a coarse mesh ruling leads to a higher volume of printed paste because it is characterized by a higher mesh opening, which defines the distance between the warp or weft threads. The thread diameters (d) may vary between wefts (d_e) and warps (d_a) and the real values may be different from the nominal ones due to the applied mesh tension that compresses the fibers, especially for polymeric materials. The mesh ruling and the diameters of the wires are used to calculate another common parameter, the open area (a_0), which is the ratio of opened area to the overall area of one mesh unit and can be calculated by the Eq. (1).

$$a_0 = \frac{d_e \bullet d_a}{(d_a + w_a) \bullet (d_e + w_e)} \tag{1}$$

where w_a and w_e are the mesh opening width in warps and weft direction, respectively. The greater a_0 is, the better the resolution of the screen mesh is. Indeed, for a larger a_0, a higher quantity of paste can pass through the mesh limiting the formation of the mesh markers on the wet deposited structure (Ney et al., 2019). In order to maximize a_0, it is possible to reduce the wired diameters employing stainless steel mesh (Jewell et al., 2015). The thickness of the wet film (t) is dictated by the mesh thickness (MT), which can be roughly estimated as the double of the thread diameter, the opening area, and the thickness of the emulsion over mesh (EOM), as described by the Eq. (2).

$$t = (MT \bullet a_0) + EOM \tag{2}$$

It is worth highlighting that only a fraction (70%) of the theoretic volume is really deposited due to the adhesive forces on the interfaces of the paste with the threads and the emulsion (Kapur et al., 2013). Since EOM affects screen thickness, it also influences resolution capability. Indeed, the smallest feature size of the design must be larger than the overall thickness of the emulsion-coated screen. The smallest feature size dictates also the selection of the mesh type, indeed the sum of the opening width and wire diameter (w+d) should be at least half of the smallest feature size (Ney et al., 2019).

However, it must be considered that the opening width should be at least three to five times larger than the size of the largest particle of the screen paste (usually of few micrometers) to avoid clogging. Finally, the mesh angle parameter refers to the alignment between the mesh and the stencil design. Common angles for printing fine lines are 30° and 22° (Clement et al., 2019; Tepner et al., 2020).

The effect of mesh type on the print quality was found to be relatively consistent for a wide range of inks (especially silver and carbon-based): finer meshes lead to reduced film thickness and improved definition. However, the printing parameters, such as squeegee pressure, snap-off distance, and print speed have not demonstrated consistent trends and have been shown to vary with the rheology of the paste (Phillips et al., 2017; Potts et al., 2020a;). Thus, it is difficult to draw general conclusions on these parameters. Although in the next paragraphs we will try to give a general overview of the parameters, the best advice still remains to always experimentally evaluate the quality output of the specific printing systems, screen mask, and paste that are you using.

Concerning the printing pressure, it should be minimized to guarantee the squeegee of the paste through the mesh openings. Indeed, high pressure can damage the mask or cause printing defects such as streaking, increased dot gain, as well as deformations at the squeegee tip. In general, the impact of the printing pressure does not significantly affect the print quality. In fact, it should be selected first regarding the tension and flexibility of the screen (it should be enough to put in contact the mesh with the substrate) and in function of the paste rheology. This is mainly linked to the fact that a screen printable paste is a non-Newtonian material characterized by a shear-thinning behavior, which means that the viscosity decreases with the increase of the shear rate, as explained in Section 3.3. Thus a greater pressure reduces the viscosity of the paste, improving the ability to flow through the mesh (Faddoul et al., 2013).

The snap-off distance is the space left between the mesh and the substrate, which generally ranges from 0.5 to 2 mm. As for the printing pressure, the research suggests that the effect of snap-off distance depends on their interaction with the paste rheology. Indeed, some authors found that increasing the snap-off non-linearly affects the printing topology, while choosing a medium snap-off distance (around 1.5 mm) will lead to the best printing quality (Kun et al., 2007). On the other hand, other researchers found that the snap-off distance had no significant effects on the print quality of fine lines (Pan et al., 1999). Overall, the discussed considerations show

that it is quite difficult to draw a conclusion and that the snap-off distance should be selected in function of the ink, mesh, and the screen-printed system used. Indeed, this parameter can not be adjusted in manual screen printers.

In the last years, the research effort was focused on printing smaller structures by increasing the process speed in order to enhance the throughput rates. This trend suggests that the study of the effect of printing speed on the quality of the printed fine structure is becoming important. In this context, high print speeds can reduce the viscosity of the paste, which displays the inherent elasticity of the paste. Thus, also in this case, the print speed effect depends on the paste rheology as demonstrated by Tepner et al. (2020) and Potts et al. (2020b), who showed that there is a correlation between printing speed and spreading of the deposited paste.

2.2 Inkjet printing

Inkjet printing has seen fast evolving improvements since the 1970s when it was first commercialized. It is a digital printing process allowing to print a digital-based image directly to a variety of substrates by getting small droplets of ink in rapid succession (Derby, 2010). The first inkjet printer was developed to print text and images, then it became common as home-office printer and in textile industries. Differently from screen printer, inkjet printing is a mask-less non-contact deposition technique that nowadays is widely used especially for prototyping and manufacturing components and circuits for human-oriented technologies and soft robotics. The process is suited for a rapid mass-production of numerous samples by providing excellent design flexibility and precise control in materials deposition. This technology provides minimal materials usage and waste production by enabling contactless, mask-free and digital patterning (Yan et al., 2020). Moreover, inkjet printing can reach a resolution of 20–30 μm, turning to be the best among the other printing techniques as concern the spatial resolution (Liu et al., 2019). Although current micro-nano fabrication techniques (i.e., lithographical techniques) can achieve resolutions in the nanometer range (Jung et al., 2020) and can reach high levels of pattern accuracy, the simplicity, arbitrary geometries, low cost, and flexibility of inkjet printing make it highly attractive for the fabrication of soft-miniaturized, multifunctional devices and components for soft robotics. The printing process involves the storage of the ink in a cartridge and the ejection of an exact amount of material through the nozzles. A basic ink-jet system consists of three critical parts (Figs. 4 and 5):

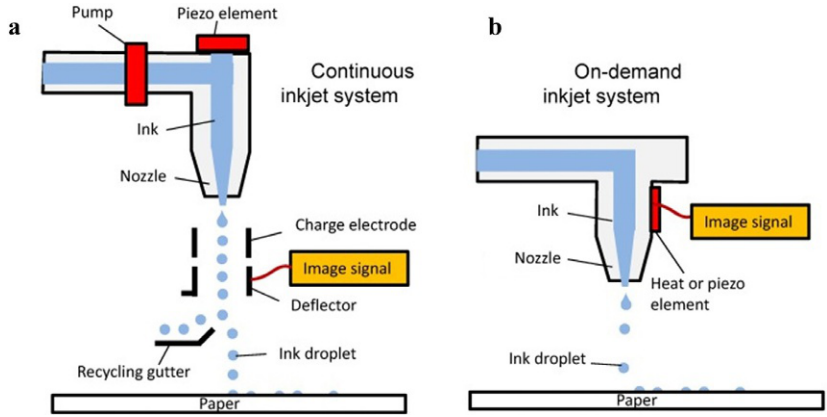

Fig. 4 Schematics showing continuous (A) and drop on demand (B) inkjet printing modes (Lau and Shrestha, 2017).

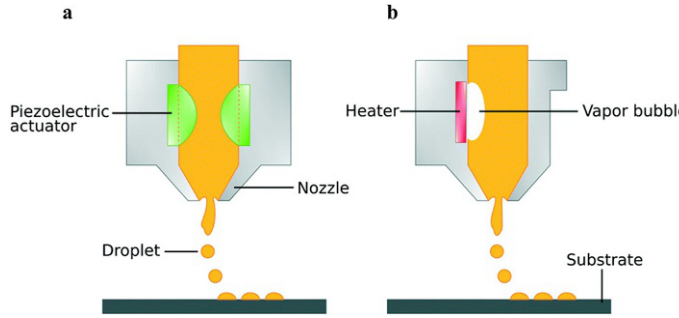

Fig. 5 Schematic illustration of drop-on-demand (DOD) inkjet printing process: (A) piezoelectric DOD mode and (B) thermal DOD mode (Maleki and Bertola, 2020), Published by The Royal Society of Chemistry.

- A nozzle to dispense controlled volumes of liquid from a reservoir where the ink is stored,
- A system to move the print-head or the substrate,
- A computer to digitally coordinate droplet ejection and the movement of the print-head.

Several inkjet methods exist and operate mainly in two modes: continuous or drop-on-demand (DOD) mode (Lau and Shrestha, 2017) (Fig. 4). In continuous mode, the ink is pumped through a nozzle to form a liquid jet and a continuous stream of ink is dispensed. The ink that is not needed for the print job is collected and recirculated back to the reservoir (recycling gutter).

It is mainly used for high-speed graphical applications such as textile printing and labeling. With DOD printing mode, the ink is dispensed only when needed. The DOD method has a smaller drop size and higher placement accuracy compared to the continuous mode. Continuous inkjet printing is an older technology with respect to DOD printing mode, which is the most used nowadays.

The two most used inkjet systems are thermal and piezoelectric (Maleki and Bertola, 2020) (Fig. 5). In the former, a thermally induced bubble is used to create a pressure wave and to eject droplets, whereas in the latter a piezoelectric crystal is used to deform the printing channel and to expel liquid droplets. In both systems, an acoustic pulse ejects ink, in form of droplets, from a reservoir through a nozzle in order to print a specific pattern. The desired layouts can be printed directly from a software-generated design drawn via a standard vector (e.g., Inkscape) or raster (e.g., GIMP) graphics software. Thus, complex shapes with feature resolution in the micron ranges can be printed (Ciocca et al., 2020; Costa Angeli et al., 2019).

In a thermal inkjet printer, a vapor bubble that ejects an ink droplet is formed by local heating at a temperature around 300 °C. Water is usually utilized as a solvent and may therefore impose restrictions on the number of ink-materials, especially polymers, that cannot be printed using this technique (De Gans et al., 2004), even though non-aqueous thermal inks are available in the market. Piezoelectric inkjet printing has the advantage of control the temperature of the jetting nozzles. Piezoelectric inkjet printing can eject a small droplet of only a few pico-liters (Li et al., 2018).

Piezoelectric DOD printing is the main inkjet printing technology used for engineering-laboratories. The voltage-driven deformations of the piezoelectric membrane wall of the nozzles chamber generate a waveform that can be optimized for each ink and accordingly for the intended printing job.

To obtain stable droplet formation and good printing results, some crucial parameters need to be carefully settled accordingly to the final project needs (Bernasconi et al., 2019).

- Waveform: it is the voltage to apply to each jet nozzle to eject the droplets. It determines the size and the velocity of the inkjet droplet (Sridhar et al., 2011). The waveform consists in different segments that must be adjusted to the specific used fluid (ink). A commonly used bipolar waveform is shown in Fig. 6.
- Cartridge temperature: it is useful to set the appropriate temperature of the cartridge according to the used ink. For example, when the used

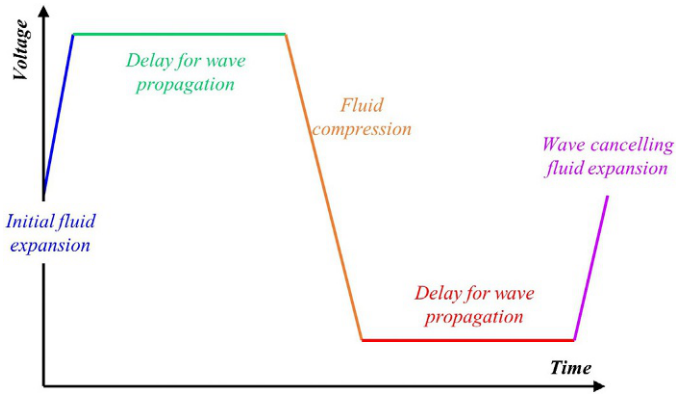

Fig. 6 Example of the commonly used bipolar waveform with a brief description of the significance of each segment of the waveform.

ink is too viscous to be jetted, raising the temperature will lead to a lower viscosity and get to the desired jetting performance.

- Platen temperature, which is also important to set at the optimum value on the platen (where the substrate is placed) to generate optimum printing quality (Riheen et al., 2019). Indeed, by modifying the substrate temperature, it is possible to change the dynamic of the solvent evaporation and thus modifying the profile of the printed patterns.
- Print height: it sets the distance of the printhead above the substrate during printing. Setting the right print height and taking into account the substrate thickness, is important to avoid hitting the substrate during printing.
- Drop spacing, which is the spacing between drops to form a pattern feature. The drop spacing affects the resolution of the inkjet printed pattern.

Overall, this printing technique allows controlled-easy and fast deposition of functional fluids on specific areas of theoretically any substrate including plastic, glass, ceramics, and silicon, as well as flexible substrates from membranes, gels, and paper. Moreover, three-dimensional structures can be fabricated by combining multiple inkjet printable components and depositing layers on top of the other. In this way, the 2D-printing technique can be expanded as 3D printing method (Kaur et al., 2021). Nowadays the technology has been widely extended and the ink can now also comprise living cells for application in novel biosensors and tissue engineering. Some brands of inkjet printers used for research and development are Dimatix from Fujifilm USA and Omnijet from Unijet Korea.

3. Printable materials and substrates for soft robotics

Soft robots are mainly composed of soft and light-weight materials such as elastomers, fluids and gels, which allow obtaining lightweight, flexible, and conformable devices able on one side to perform multimodal movements and on the other side to easily conform to the human body. Therefore, the selection of the materials, substrates, and inks, is a crucial step in the realization of printed electrical devices suitable for soft robotics. Moreover, these printed devices besides being mechanically compliant need to maintain conductive pathways under severe mechanical deformations, while surviving in a wide range of different environments. Meeting these conditions requires good knowledge of innovations in materials science, but also good know-how of the requirements of the employed printing techniques. Indeed, the different printing methods require specific and different ink properties for precise resolution and performance—both mechanical and electrical. Thus, it is crucial to have a good knowledge of the materials (and their properties) that can be used for screen and inkjet printing techniques to fabricate electronic devices and sensors for soft robotic applications. This is way in the following paragraphs, some important properties of inks/pastes and substrates employed in inkjet and screen printing technologies will be discussed.

3.1 Screen printable substrates

Screen printing technology has allowed to explore new routes for materials processing and to develop low-cost electronic systems on non-planar deformable surfaces, which otherwise are difficult to realize with conventional wafer-based fabrication techniques, by establishing at the same time a close double link between the development of this printing technique and the realization of soft devices (White et al., 2017). Indeed, screen printing technology can be used to deposit several materials on different substrates, such as PCB, silicon wafer, glass but also on paper, textile, thermoplastic polymers, as poly (ethylene terephthalate) (PET), polyimide (PI), and thermoplastic polyurethane (TPU) and elastomeric rubbers, such as Poly(dimethylsiloxane) (PDMS) and Ecoflex. As shown in Table 1 (Vaicekauskaite et al., 2020), these substrates have different characteristics in terms of thickness, surface roughness, working temperature and particularly Young's modulus, which allows distinguishing between three substrate types: rigid, flexible, and stretchable (Fig. 7).

Table 1 Comparison of printable substrates.

	Classification	Thickness (μm)	Elastic Modulus (MPa)	Stretchability	Working temperature (°C)
Silicon wafer	Rigid	200–1500	150 10^3	–	Up to 1200
Glass		–	–	–	Up to 800
PI	Flexible	10–125	2.5 10^3	2%	Up to 400
PET		13–175	2–4 10^3	4%	Up to 150
Paper		25–500	0.5–3.5 10^3	–	Up to 200
TPU	Stretchable	100–500	2	60%	Up to 130
PDMS		100–5000	1	100%	Up to 120
Ecoflex		100–5000	0.5	300%	Up to 120

Values are taken from Qi D, Zhang K, Tian G, Jiang B, & Huang Y: Stretchable electronics based on PDMS substrates, Adv Mater 33:1–25, 2020b https://doi.org/10.1002/adma.202003155. 2,003,155, Suresh RR, Lakshmanakumar M, Arockia Jayalatha JBB, Rajan KS, Sethuraman S, Krishnan UM, & Rayappan JBB: Fabrication of screen-printed electrodes: opportunities and challenges, J Mater Sci 56:8951–9006, 2021 https://doi.org/10.1007/s10853-020-05499-1, Vaicekauskaite J, Mazurek P, Vudayagiri S, & Skov AL: Mapping the mechanical and electrical properties of commercial silicone elastomer formulations for stretchable transducers, J Mater Chem C 8:1273–1279, 2020 https://doi.org/10.1039/c9tc05072h.

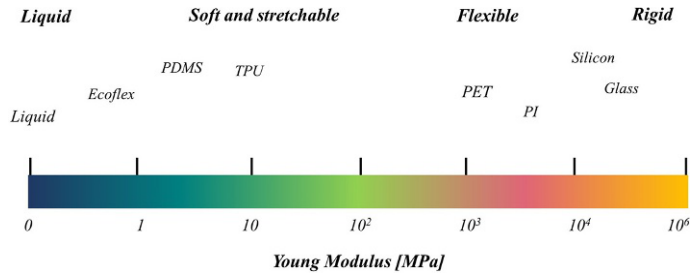

Fig. 7 Soft screen printable substrates characterized by a wide range Young's modulus. The materials substrate from stretchable elastomers, flexible polymers, and rigid silicon wafer.

The first ones are characterized by a high elastic modulus in the range of 50–1000 GPa, whereas flexible materials have a low bending stiffness that allows them to conform to irregularly curved surfaces, however, they possess a low elastic range, around 4% strain, above which plastic deformation occurs. Only stretchable polymers, such as TPU, rubber PDMS and Ecoflex are characterized by a low Young's modulus (<10 MPa) and a high linear elastic

regime (up to 300%) that allows being repetitively and reversibly stretched without failure or plastic deformation up to 100,000 times (Qi et al., 2020b; Wagner and Bauer, 2012). It is the employment of the latter material that is providing grounds for low-cost high-speed manufacturing of devices, sensors and actuators for applications requiring a high degree of deformability such as soft robotics (White et al., 2017), wearable sensors (Marra et al., 2021) and electronic skin (Zhu et al., 2020). In this context, screen printing stands out for the ability to easily deposit functional inks, particularly on stretchable substrates. This capability is closely linked to two aspects of screen printing; the first one is that contrary to other printing techniques, such as inkjet and gravure printing, the surface wettability has a limited influence on the print quality of screen printing. Indeed, the above-mentioned stretchable substrates are characterized by low surface wettability, and so they are commonly addressed as hydrophobic substrates. The surface wettability is the measurement of the surface energy, which influences mutual interaction between the deposited paste and the substrate so also its adhesion. Therefore, the surface wettability is a fundamental parameter that has to perfectly tune for non-contact printing techniques, limiting their employment on hydrophobic and inert substrates (Costa Angeli et al., 2019), as explained in Section 3.2. Whereas screen printing, as contact technique, proved to be highly compatible with stretchable low-energy surface substrates. The second reason is that the screen printing technique can print intrinsic stretchable functional conductive composites made by the same polymers used for the substrate, such as PDMS, Ecoflex and TPUs allowing to induce a strict chemical affinity between ink and substrate. Moreover, this aspect allows also to deposit intrinsic stretchable conductive and functional materials that enable the realization of reliable soft devices. Furthermore, screen printing technique is robust in terms of its ability to print on flat surfaces with the surface texture and wettability not having any influence on the printing quality (as profited by direct printing on textiles). However, due to the usage of flat screens, printing activities on not planar devices proved to be problematic (Suresh et al., 2021), contrary to other techniques, as spray coating and 3D printing, in which is possible to deposit conductive material directly on the device or integrating it during the device manufacturing (Falco et al., 2016).

3.2 Inkjet printable substrates

Commonly used inkjet printable substrates for soft robotics applications are soft printable materials. PET and polyethylene naphthalate (PEN) are two common polymeric substrates used for inkjet printing of soft and/or flexible

electronic devices (Riheen et al., 2019). PI substrates are also ideal for the inkjet deposition due to the thermal stability also at high temperature, and low surface roughness (Fang and Tentzeris, 2018). Paper substrates are also useful for the emerging field of "paper mechatronics" which merges printed robotics and paper electronics (Shigemune et al., 2016) with a special focus on the "green electronics" fulfilling the environmental sustainability. As it will be discussed in Section 3.4, surface tension is one of the crucial parameters to take into account for good printing results. Table 2 lists the surface tensions of some commonly used solvents and substrates in inkjet printing technology (Hu et al., 2018).

Substrate treatments to control wettability and surface tension and consequently hydrophilicity/hydrophobicity according to the final device needs are crucial to achieve good printing results. These treatments include: chemical surface functionalization, oxygen plasma, and UV/ozone exposure.

The spreading of ink over the substrate surface is defined by wetting, which can be explained by Young's equation (Eq. 3):

$$\gamma_{s-v} = \gamma_{s-i} + \gamma_{i-v} \cos\theta \tag{3}$$

where γ_{s-v}, γ_{s-i} and γ_{i-v} are the interfacial tensions between the solid surface (s), the vapor (v) and the ink (i), and θ is the formed contact angle. A small contact angle, $\theta < 90°$ suggests a good wetting, while a large contact angle, $\theta > 90°$ indicates a poor wetting. Therefore, substrates with high surface energies (i.e., copper) are easy to wet, while plastics substrates with low surface energy (i.e., polytetrafluoroethylene—PTFE) are difficult to wet. A poor wetting leads to a discontinuous inkjet deposition. Within the print industry, it is generally considered that if the surface tension of the ink is

Table 2 Surface tensions (at 20 °C) of common solvents and substrates.

Solvent	Surface tension ($mN\,m^{-1}$)	Substrate	Surface tension ($mN\,m^{-1}$)
Water	72	Copper	1000
Glycerol	64	Kapton	50
Ethylene glycol	48	PET	48
Epoxy resin	43	Polyamide	46
Chlorobenzene	34	Polyurethane	40
IPA	23	Polyimide	40
Ethanol	22	PTFE	18

7–10 mN m^{-1} lower than the surface energy of the substrate, appropriate wetting can be achieved (Hu et al., 2018). Once the desired layout is inkjet printed on the surface, additional treatments are needed to obtain a functional material. This may involve drying, curing, and sintering steps (Cano-Raya et al., 2019). Whatever process is used, it must be compatible with all the materials used in the device structure.

3.3 Screen printable inks

One of the major advantages of screen printing, especially if compared to other printing techniques such as inkjet printing, is the capability to deposit a wide range of materials, from conductive to semiconductive and dielectric, most of which characterized by an intrinsic softness and stretchability up to 200% strain (He et al., 2017), which a key aspect in the development of devices for soft robotics. Indeed, the usual approach to integrate sensors and actuators into soft robots is to fabricate devices that are themselves flexible and stretchable. The stretchability is the main figure of merit of stretchable electronics and refers to the maximum percentage of strain, usually uniaxial tensile strain, that the materials/devices can sustain without compromising their integrity in terms of conductivity and functionality (Plovie et al., 2018). In this context, an ideal paste for the realization of screen printed devices for soft robotics should be (i) printable, (ii) characterized by adequate electrical conductivity and corresponding sensing properties where needed (e.g., temperature, mechanical, chemical, optical) and should have (iii) a good mechanical and electrical reliability, i.e., maintaining the performance under the needed working condition, e.g., under strain. The co-existence of all these aspects at the same time is at the same time extremely crucial and challenging. In the last years, many efforts have been made to formulate ever more high-performing screen printable inks exploiting new functional organic/inorganic materials and nanomaterials (Qi et al., 2020a; Wu, 2019). In the effort to formulate new inks, the first aspect that should be considered is printability. A printable ink is a material that can be easily and homogeneously deposited to the substrate with a fine resolution (up to 30 μm) without leaving defects and voids, thus ensuring good print quality. Over the years, the researchers showed that there is a strict correlation between the print quality and the specifications of the screen mesh, as discussed in Section 2.1, as well as of ink rheology (Tepner et al., 2020). Thus, in approaching the use of the screen printer, a deep understanding of the composition and rheology of a screen printable paste is fundamental to select the most adequate paste and ensure the print quality for the deposition of homogenous ad reliable structures.

A perfect screen printable ink should be a viscous non-Newtonian' material, with thixotropic shear thinning property (Yüce et al., 2018). The typical viscosity [Pas] (μ) of a screen printable materials is between 0.5 and 50 Pas (Kim et al., 2017).

The viscosity is the measure of the internal resistance of a liquid to flow and it is defined by the Newton's law (Eq. 4):

$$\tau = \mu \bullet \frac{du}{dy} \tag{4}$$

where τ is the sear stress [Pa s] and $^{du}/_{dy}$ is the shear rate [s^{-1}], i.e., the derivative of the fluid speed u, in the direction perpendicular to the plates, as shown in Fig. 8A (Wilson, 2017). In Newtonian fluids, the viscosity is a constant value that depends only on temperature and pressure, whereas for shear-thinning non-Newtonian' fluids the viscosity decreases with the increase of the shear rate, as shown in Fig. 8B (*left*). Screen printable pastes are also characterized by a thixotropic behavior, which means that the viscosity change is time-dependent. The decrease of viscosity, when the fluid is submitted to shearing stress, is not immediate but it continuously decreases and when the flow is decreased or arrested the viscosity returns slowly to its original value (Mewis and Wagner, 2009). The major consequence of this rheological behavior is that the paste viscosity changes during the printing process because it is subjected to three different share rates, as shown in Fig. 8B (*right*). Initially, after the flooding, the ink is at rest or characterized by a low shear rate ($0.1\,s^{-1}$) consequently, it shows a relatively high viscosity (1000 Pa s); whereas in the second step, during the print stroke, the squeegee applies a high shear rate (up to be $200\,s^{-1}$), which induces a sharp viscosity reduction causing the paste to flow through the mesh. Finally, the paste progressively regains its initial viscosity, while the screen lifts off from the substrate and the shear rate comes back to the initial value ($0.1\,s^{-1}$) (Liang et al., 2016; Tian et al., 2019). This last viscosity recovery is a fundamental aspect of screen printable materials that allows the left behind structures to maintain their geometry, limiting the spreading on the substrate. However, the viscosity recovery should not occur too quickly because it is necessary to give enough time for the film to leveling and filling the irregularities and voids. So, the paste must have appropriate thixotropic behavior. For instance, Fig. 8B shows the thixotropic behavior of three different silver nano-dendrites (AgND) conductive pastes, with the viscosityof the Ag ND Ink-55 wt% quickly recovering to its original value after the reduction of the shear rate, which is not beneficial to ink leveling, resulting in a

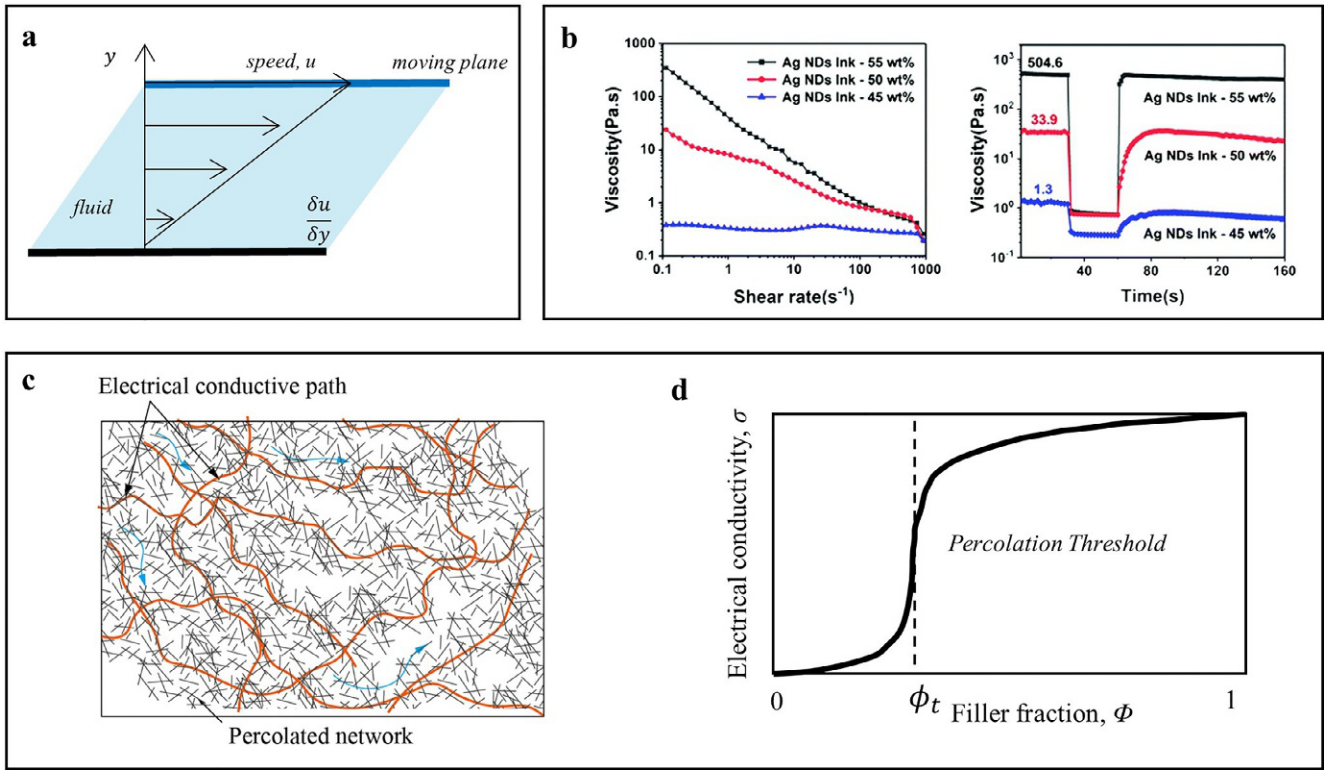

Fig. 8 See figure legend on opposite page.

not-homogenous print (Tian et al., 2019). Only the above described rheological behavior ensures good printability because the paste flows only when sheared by the squeegee and it does not spread out the edges or slump once printed especially for narrow lines. The viscosity is the simplest and most used rheological parameter for the characterization of screen printable pastes. However, due to the complex rheological properties of screen printing inks, which are also related to the printing parameters, such as printing speed, squeegee pressure, mesh type, and a lack of understanding of the physical mechanism by which the ink is transferred, it is difficult to draw a precise correlation between the viscosity and the print quality (Alias and Mohd, 2012). As a rule of thumb, we can infer that pastes characterized by higher viscosity usually lead to thicker and narrower tracks. With a limited spreading after printing, however, they are usually characterized by a quick viscosity recovery that leads to a not-completed leveling. Contrary, lower viscosity has a better ink leveling but higher ink lumping (Faddoul et al., 2012; Phillips et al., 2017). Independently from the viscosity, the most important aspect is that a good screen printable paste should have a proper shear-thinning thixotropic behavior. A more insight description of the rheology of screen printing pastes can be found in Potts et al., Tepner et al., and Tian et al. manuscripts (Potts et al., 2020a; Tepner et al., 2020; Tian et al., 2019).

The formulation of screen printable pastes is not only related to their rheological behavior, but also their functional, electrical, and mechanical properties. Indeed, as before stated an ink for the realization of sensor/actuators for soft robotics should be printable but also stretchable, thus characterized by adequate sensing/electrical conductive properties that can be maintained also during mechanical loading. In order to understand this aspect, it is

Fig. 8 (A) Schematic of a planar Couette flow, in which u is the velocity of the moving plane, and the velocity gradient (du/dy) is the shear velocity (B) The relationships between viscosity and the shear rate for a shear-thinning thixotropic silver nanodendrites (AgNDs) conductive ink. Thixotropic behavior of the AgNDs conductive ink. (C) Schematic diagram of the theory of a percolated network and the current pathways through the matrix (Dang et al., 2017). (D) Percolative theory: electrical conductivity, σ, of conductive composites as a function of filler fraction, Φ. *Panel B reproduced from Tian B, Yao W, Zeng P, Li X, Wang H, Liu L, Feng Y, Luo C, & Wu W: All-printed, low-cost, tunable sensing range strain sensors based on Ag nanodendrite conductive inks for wearable electronics, J Mater Chem C 7:809–818, 2019 https://doi.org/10.1039/c8tc04753g with permission from The Royal Society of Chemistry; Panel C from Dang W, Vinciguerra V, Lorenzelli L, & Dahiya R: Printable stretchable interconnects. Flex Print Electron 2: 2017 https://doi.org/10.1088/2058-8585/aa5ab2.*

necessary to better clarify which are the standard components of a conductive screen printable paste. The pastes are usually a mixture of three parts: the functional fillers/material, the binder, and the solvents/additives.

- The fillers

The screen printable conductive pastes are mostly made by composites of metal/carbon-based nanomaterials or organic conductive polymers blended in a polymeric matrix. The fillers are the functional components of the ink that provide the characteristics required for the specific application. Depending to the application, the fillers can be metallic, organic, ceramic or a mixture. Different types of conductive metallic nanomaterials, such as silver (Ag), copper (Cu), platinum (Pt) and gold (Au), are employed. Among them, the most common to realize highly conductive ink is Ag, particularly in the shape of nanoflakes (AgFKs) and nanowires (AgNWs). AgFKs are 2D nanomaterials characterized by an average dimension between 5 and 10 μm. Their large dimensions and planar structure provide a large contact area if compared to other nanomaterials, such as silver nanoparticles (AgNPs), thus ensuring better conductive properties. Instead, the AgNWs are classified as 1D nanomaterial because characterized by a large aspect ratio (the ratio between the longest size L and the shortest size D of the particle, L/D). Nanowires are commonly used for stretchable conductors (Liang et al., 2016) and heaters (He et al., 2017).

Besides metallic solutions, the carbon-based inks are also broadly employed to realize cheaper, higher resistive conductors (Quinsaat et al., 2019) or sensing materials for strain (Giffney et al., 2017; Lugoda et al., 2021) or temperature (Wu et al., 2019) sensors. Traditional carbon-based nanomaterials are carbon nanotubes (CNTs), carbon blacks (CB), and graphene. The first is a 1D nanomaterial characterized by an aspect ratio between 100 and 1000, high surface area to volume ratio enabling the possible use in a plethora of applications. CB is a 0D nanomaterial made of sub-micron particles with a roughly spherical shape. CB are typically cheaper compare to CNTs, whereas graphene is a 2D material, characterized by high electrician (10^4–10^5 S/m) and thermal conductivity ($\sim 3000\,\mathrm{W\,m^{-1}\,K^{-1}}$) (Fang et al., 2020; Stankovich et al., 2006).

The electrical conductivity of both metallic and carbon-based nanocomposite is ruled by the percolation theory (Eq. 5), which is represented and outstanding properties as sensing materials (Dang et al., 2017).

$$\sigma \approx \sigma_0 \bullet (\varphi - \varphi_t)^a \tag{5}$$

where σ is the electrical conductivity of the composite, σ_0 is the conductivity of the filler, φ is the weight percentage (concentration) of the filler, a is the

critical exponent, and φ_t is the percolation threshold. As shown in Fig. 8C the current passes through the matrix following pathways that are created by the contact between the filler (in the Fig. 8C 1D filler is shown). Increasing the filler concentration, φ, the numbers of possible pathways increase with a consequent increase of the composite conductance that follows a percolation power law. This process stops when the percolation threshold is reached, at which with the further addition of fillers a conductive network is generated and the electrical conductivity of composite further increases gradually, until leveling off at a constant. Reaching the percolation threshold is important for conductive material to build a continuous and stable electrical current (Fig. 8D). Several parameters affect the value of the percolation threshold such as the material, the morphology, and the dimensions of the fillers. For instance, 1D nanomaterials such as AgNWs and CNTs, due to their high aspect ratio can form a percolation network at lower loading density, if compared to 0D materials. This is an important aspect in the realization of stretchable conductors, indeed there is a trade-off between the mechanical and the electrical properties of a stretchable composite. It is possible to lower the resistance by increasing the conductive filler fraction, however, at the same time, the material stiffness increases and its stretchability reduces. This issue can be solved using 1D nanomaterials, or also a mixture of different shapes of nanomaterials (Vo et al., 2020), conducting polymer blends with nanomaterials (Yu et al., 2019) and through the selection of the proper binder (Kim et al., 2017). Thus, such composites are simultaneously conductive and stretchable when the nanofillers form percolating pathways. The mechanism underlining the stretchability of this composite is that their networks can accommodate a certain amount of tensile strain by the matrix deformation, while still maintaining a good percolating pathway for electrical conduction. It is worth highlight that the filler fraction composite has also an effect on the rheological properties of the ink and particularly increasing the filler increases its viscosity and it can change the overall rheological properties with an effect of the print quality (Qi et al., 2020a).

Intrinsically conductive polymers are also widely employed as filler materials to realize conductive and functional screen printable soft devices. Some examples of common conductive polymers are polyaniline (PANI), polypyrrole (PPy), and poly(3,4-ethylenedioxythiophene) (PEDOT:PSS) (Bandodkar et al., 2015; Gosselin et al., 2017). They are also known as conjugated polymers, and they can be prepared with a broad range of conductivities from 10^{-10} to 1000 S/cm (Weng et al., 2010). They are low-cost (if compared to metal nanomaterials), show good environmental stability and

biocompatibility, however, they have poor mechanical properties (with a stretchability up to 10% strain) (Lipomi et al., 2012). Fortunately, the stretchability and printability of conductive polymers can be improved by incorporating elastomeric materials such as TPU and PDMS (Roh et al., 2015), or surfactants such as Zonyl and Triton X-100 (Sinha et al., 2017; Yoon and Khang, 2016). Conducting polymers are employed for many applications including strain sensors (Cruz et al., 2017), temperature sensors (Wang et al., 2020a,b), electrochemical sensors (Bandodkar et al., 2015), semiconductive materials for active devices (Matsui et al., 2019), flexible photodetectors (Falco et al., 2014), and soft electrodes (Shi et al., 2019). An insight description can be found in the papers of Grancarić et al. (2018), Weng et al. (2010).

- Polymer binders

The polymeric binder has the role to bind together the fillers and bind them to the substrate. The polymeric binder plays an important role in both the rheological and mechanical properties of the paste ensuring the thixotropic shear-thinning behavior and simultaneously the flexibility or stretchability of the ink. The most used stretchable binders are PDMS, Ecoflex, fluorine rubber, polyurethane, isoprene block *co*-polymers (Kim et al., 2017). The proper selection of the polymer is also a function of the application and the filler types because it also functions as a dispersive agent. A good nanomaterials dispersion and dispersion stability are fundamental to minimize the possibility of stress concentrations and increase the composite stretchability and electrical conductibility.

- Solvents/Additives

The solvent is the carrier for the filler when mixed with the polymeric matrix. The solvent selection depends on the dispersibility of the filler and the affinity with the polymeric binder. The most common are organic solvents such as isopropyl alcohol, acetone, toluene, ethanol. The mixture of the binder and solvent promotes wetting of the fillers, dispersion stability, but also allows for adjustment of the rheological behavior of the ink more suitable for screen printing. Apart from solvents, additives are also included to adjust the wetting rheological adhesion and the mechanical properties of the ink for the specific applications.

For all types of screen printed inks, after the deposition on the substrate, a post-printing process, that is usually called annealing or curing is necessary. This is typically made using heat or UV light to anneal or cross-link the binder of the paste. This post-printing process is fundamental to first allow the complete evaporation of the solvents in the ink and then to ensure a

mechanical continuum of the deposited material. This is also necessary for conductive inks, usually made of composite or conductive nanomaterials and polymeric matrixes, to achieve high electrical conductivity. Indeed, during the annealing, the evaporation of the reaming solvent and the decomposition of the dispersing agent leads to the formation of a compact and close nanomaterials network, with a consequent increase of the structural conductivity. The most used annealing method is the thermal one that is achieved by heating the entire printed devices. However, the employment of the typical soft and stretchable substrates used in soft robotics (such as PDMS) that possess low glass-transition temperature limits the curing temperature up to a maximum of 120 °C. This temperature is far below the sintering temperature of metallic nanomaterials (e.g., 900 °C for silver) restricting the highest electrical conductivity achievable (Barras et al., 2017). Thus, over the last year other annealing methods were exploited, such as UV curable smart materials (Mendes-Felipe et al., 2019) or chemical treatments (Kang et al., 2017) and laser method (Li et al., 2019), which are able to perform a local nanowelding.

3.4 Inkjet printable inks

Diverse inkjet printable inks for different applications are present on the market or can be prepared in a research laboratory. The most crucial aspect for inkjet printing technology is the ink formulation and its physical and rheological properties. Indeed, the composition of the ink defines its physical properties (e.g., viscosity, surface tension, density and drying rate) that affect the printing process and quality. High viscosity, nozzle clogging, agglomeration, precipitation, and uncontrollable drying patterns are among the frequently challenges encountered with inkjet printing. A good inkjet-printed droplet results from a balance between ink viscosity and surface wetting. Moreover, vapor pressure, boiling point, and surface tension of the inks are also critical parameters for inkjet printing technology.

In general, an inkjet printable ink consists of a nanoparticle-ink derived from a liquid metal dispersed in a non-metallic carrier-solvent (e.g., water, ethanol). Ultrasound sonication is generally used to break the bulk liquid metal into nanoparticles to make the ink compatible with inkjet printing. Indeed, native liquid metal is not inkjet-able, while liquid metal nanoparticles are small enough to pass through an inkjet nozzle. Thus, by printing the metal nanoparticle-ink onto any substrates the solvent evaporates and the liquid metal nanoparticles are left on the substrates surface.

To produce a functional inkjet printable ink, some crucial features need to be taken into account (Schlatter et al., 2017). First, the material must be prepared as a liquid that is homogeneous and stable over time in order to have a reproducible jetting. The ink formulation has to let the ink pass through the nozzle. Thus, viscosity, surface tension, and particle size need to be optimized to let the solution be expelled by the nozzle.

The dimensionless Ohnesorge number (Oh) is an index of the good fluid jettability. It is calculated as in Eq. (6) (McKinley and Renardy, 2011)

$$Oh = \frac{\eta}{\sqrt{\rho \bullet \sigma \bullet d}} \tag{6}$$

where η is the shear viscosity, ρ is the density, σ is the surface tension, and d is the jet diameter.

For a good inkjettable ink *Oh* number must be in the range of 0.1–1 (Antonopoulou et al., 2020). A value of $Oh < 0.1$ indicates the formation of satellite droplets (i.e., unwanted secondary droplets) while $Oh > 1$ suggests elongated ligaments that may break up into satellite droplets, or even lead to non-jetting (Torrisi et al., 2012).

Liquid metal-based inks are the most used due to their unique advantage of combining conductivity and deformability. Conductive silver inks, in particular silver nanoparticles (AgNPs), have been the most applied material for printed soft and/or flexible electronics (Fernandes et al., 2020). This is mainly due to the silver high electrical and thermal conductivity, chemical stability, relatively low cost (Ren et al., 2015). Usually, conductive inks are formulated with metallic particles (e.g., silver, copper, and gold) or carbon particles (such as graphene and carbon nanotubes) in a retention matrix (Fernandes et al., 2020). Silver nanoparticles have a low melting point, which promotes the generation of conductive thin films using relatively low temperatures, which is a vital working condition for flexible substrates for applications in soft robotics.

Conducting and semiconducting polymeric inks are also widely used in printed electronics. The inkjet printability of polymers correlates with polymer structure and molecular weight, concentration and solvent used (Bernasconi et al., 2019; De Gans et al., 2004). Polymers can be printed from the melt when the complete inkjet system is heated. Another possibility for inkjet printing of polymers is represented by the utilization of colloidal suspensions of polymer lattices, which has the advantage of presenting a high-molecular-weight polymer in a low-viscosity form. Overall, inkjet printing of conducting polymers is challenging due to their small solubility and miscibility (Simaite et al., 2016).

PEDOT:PSS (poly(3,4-ethylenedioxythiophene):poly(styrenesulfonate)) is a commercially available polymer ink extensively used in flexible and printed electronics. Nevertheless, various additives are often needed in order to adjust the rheological properties of the ink, as well as the electrical and mechanical properties of the printed films.

A multitude of other materials can be used as inks for inkjet printing technology. Examples include graphene based inks are used for flexible strain sensors (Kang et al., 2017), Gallium–Indium (GaIn) nanoparticle inks inkjet-printed directly onto elastomer glove surfaces to form arrays of strain gages with intricate wiring and contact pads (Boley et al., 2015), biological inks consisting of enzymes in water or other solvents, cells suspended in gelatin, proteins, as well as nucleic acids used as bioinks (Ratner et al., 2013).

Overall inks should have the following physical characteristics for a good jetting:

- Viscosity = 1–2 cPa s, at jetting temperature.
- Surface Tension = 32–42 dynes/cm at jetting temperature.
- Low Volatility—Boiling point >100 °C.
- Density—Specific gravity >1 is optimal.

The viscosity of inkjet printable inks is much lower than that of the screen paste. The suitably low viscosity lets the ink be pulled into and pushed out of the nozzle chamber. When it is too high, the kinetic energy is viscously dissipated and no droplets are ejected. Viscosity can be altered by heating the ink (cartridge temperature control) or by using additives such as the humectants, ethylene glycol or glycerol. For a given pressure wave at the nozzle, the lower is the viscosity the greater is the velocity and the amount of liquid propelled forward which leads to the formation of long tails behind the head of the drop. A comparison between typical viscosities of inks and pastes used for inkjet printing and screen printing respectively are summed up in Table 3 (Hu et al., 2018).

The surface tension should be high enough to hold the ink in the nozzle without dripping. Surface tension is also responsible for the spheroidal shape of the liquid drop emerging from the nozzle. For organic solvents, good choices

Table 3 Typical viscosity values for inks used in inkjet printing and pastes used in screen-printing technologies.

Printing technology	Ink/Paste viscosity (MPa s)
Inkjet Printing	4–30
Screen Printing	1k—10 k

are chlorobenzene (33.28 dyn/cm at 20 °C) and ethanol (46.03 dyn/cm at 25 °C). If the surface tension is too high a surfactant can be added to the ink to decrease it.

The high boiling point of the used solvent for inkjet printable inks guarantees that the ink not dry quickly in order to avoid the nozzles block. This issue is often referred to as a "skinning" or "crusting" effect. In the first case a hardened film develops over the nozzle, while the latter case is related to a build-up of particles around the nozzle. Screen printing requires slightly less volatile solvents with reasonably low evaporative rates (i.e., aromatic distillates and butoxyethanol) to avoid clogging of the screen mesh due to the fast ink drying.

Optimal inks are composed of solutes that are completely dissolved in the solvent system. Then the prepared ink needs to be filtered (usually though a 0.2 μm filter) before being filled in the inkjet printer cartridges, in order to avoid that cluster of particles will block the nozzles. A degassing process (by applying vacuum, sonication in water bath or centrifugation) is also recommended, especially for aqueous inks, combined with 2–24 h of resting time of the ink filled inside the cartridge. In fact, air bubbles that form in nozzles will block the jetting.

A common profile for inkjet printable inks is typically represented by the so-called (unwanted) "coffee ring" shape, where the deposited material dries to be concentrated on the periphery of the print, leaving a concave central area, as shown in Fig. 9. A widely accepted explanation attributes this effect to a non-uniform solvent evaporation across the droplet during the ink drying process (Deegan et al., 1997). Indeed, when a droplet is deposited onto a substrate, the evaporation rate is typically highest at the edge of the droplet–substrate interface (also known as the contact line) due to the highest surface area to volume ratio.

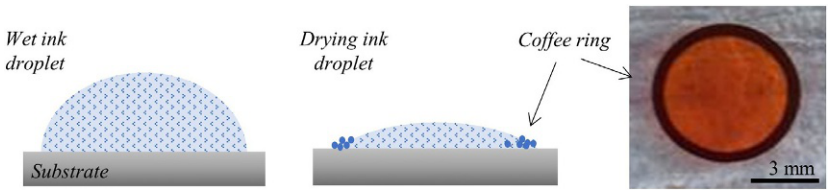

Fig. 9 Ink wetting and drying effect on inkjet-printed droplet. Typical drying dynamic of inkjet printed drop, showing that low viscosity inks tend to form a coffee ring and a photograph of a dried coffee drop.

The interactions of the ink droplets with the substrate must also be considered. When a droplet hits the substrate, the behavior of the drop is influenced by the bulk material properties, the surface properties, and the environment. Bulk properties are important when the solvent is absorbed by the substrate. The surface properties are important if the droplet rests on the surface. The affinity of the materials determines whether droplets wet the surface or coalesce into larger droplets. The spreading and wetting of the liquid-ink on the substrate and the drying behavior of the printed component are controlled by the solvent formulation and the temperature of the inkjet printing stage.

4. Examples of printed devices for soft robotics

Soft robotics usually includes three main components: the soft actuator, the control module with the power, and the soft sensors. The latter is essential for feedback-control, in terms of proprioception and exteroception of soft robots (Wang et al., 2018). These sensors have to fulfill the requirements of elasticity and durability to be suitable for integration with soft materials. In this perspective, screen printing is a good candidate to fulfill these needs. As explained in the above sections, this printing method is best suited to process intrinsically stretchable conductive materials on soft substrates. Indeed several examples of screen printed sensor can be found in the recent literature, as shown in Fig. 10A and B, (Koivikko et al., 2018; Pinto et al., 2017; Yeo et al., 2016). On the other end inkjet printing is used to simplify the manufacturing process, and at the same time to reduce the materials waste and realize high resolution design, as shown in Fig. 10C.

4.1 Example: Stretchable screen printed nanocomposite sensors for feedback–loop control of a soft earthworm robot

A recent publication (Goldoni et al., 2020) demonstrated the complete integration of a wireless, screen printed strain sensor with a soft robotic earthworm for locomotion detection, as shown in Fig. 11. The authors realized a serpentine screen printed sensor on Ecoflex employing a strain-sensitive multiwalled CNTs nanocomposite, deposited using a screen process between two layers of a silicone elastomer (Ecoflex). The authors have chosen as functional fillers OH-functionalized CNTs, because the presence of the hydroxyl groups ensures good compatibility, and thereby dispersion, with the elastomeric matrix. The sensor was shaped using a serpentine shape,

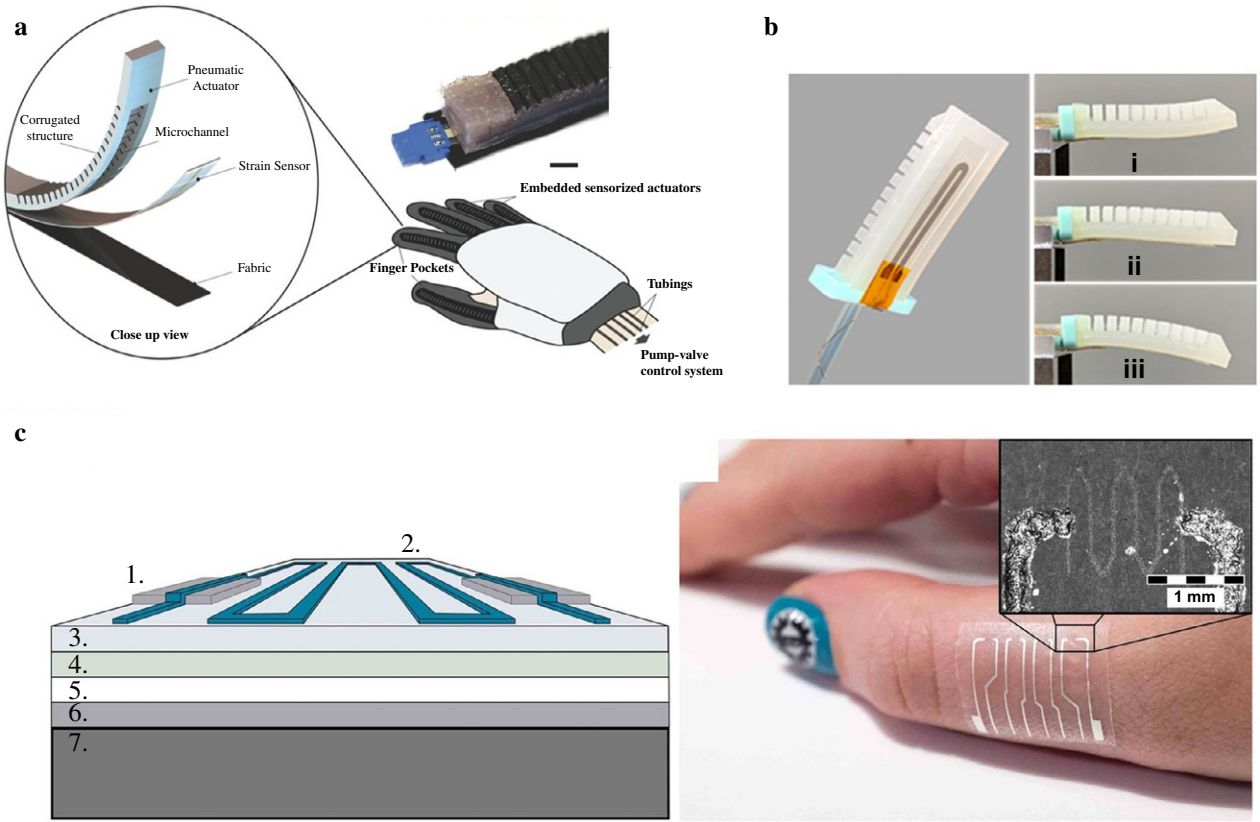

Fig. 10 See figure legend on opposite page.

as displayed in Fig. 11, in order to provide multiaxial stretchability. Indeed, the authors proved, by performing finite element analysis (FEA), the reliability of the screen printed strain sensor undergoing uniaxial and biaxial stretching up to 60% strain. Then the sensor was experimentally tested through static, cyclic electromechanical uniaxial tests and it proved a good ultimate stretchability (100%), cyclic reliability and stability (up to 500 cycles showing a marginal resistance drift). Moreover, the authors connected the sensor with a miniaturized circuit for wireless data acquisition using a stretchable nanomembrane, and the system was integrated onto a pneumatic elastomeric soft earthworm robot.

The sensorized-soft robot was tested through different motions, such as alternating left and right bending, elongation, compression, tactile sensing, simultaneous lateral compression, proving its ability to perceive internal and external stimuli and therefore the ability to interact with the surrounding environment. In conclusion, the described printed strain sensors system shows that thanks to the high elasticity of the screen printed CNTs nanocomposite, which can be pattern only employing screen printing technique, it is possible to guarantee excellent compliance for the whole range of movements (bending and stretching) that the robot needs to perform enabling the possibility to realize low cost and reliable devices in soft robotics applications.

Fig. 10 (A) Strain sensors for wearable soft robotic applications: schematic illustration of the sensor actuator within a hand (top); SEM image of metallic ink on silicone substrate (center); image of the as fabricated stretchable strain sensor (bottom). (B) Screen printed strain sensor attached to a soft robotic gripper. (C) Printed temperature sensor made of multilayered structure: (1) Screen printed silver conductors, (2) inkjet patterned graphene/PEDOT:PSS temperature sensor, (3) PU surface layer, (4) adhesive layer, (5) protective paper, (6) PET film and (7) cooling/heating element and photograph of the sample attached to the skin (Vuorinen et al., 2016). *Panel A reprinted with permission from Yeo JC, Yap HK, Xi W, Wang Z, Yeow CH, & Lim CT: Flexible and stretchable strain sensing actuator for wearable soft robotic applications, Adv Mater Technol 1:1–9, 2016 https://doi.org/10.1002/admt.201600018, Panel B reprinted by permission from Wang YF, Sekine T, Takeda Y, Hong J, Yoshida A, Matsui H, Kumaki D, Nishikawa T, Shiba T, Sunaga T, & Tokito S: Printed strain sensor with high sensitivity and wide working range using a novel brittle-stretchable conductive network, ACS Appl Mater Interfaces 12:35282–35290, 2020a https://doi.org/10.1021/acsami.0c09590.*

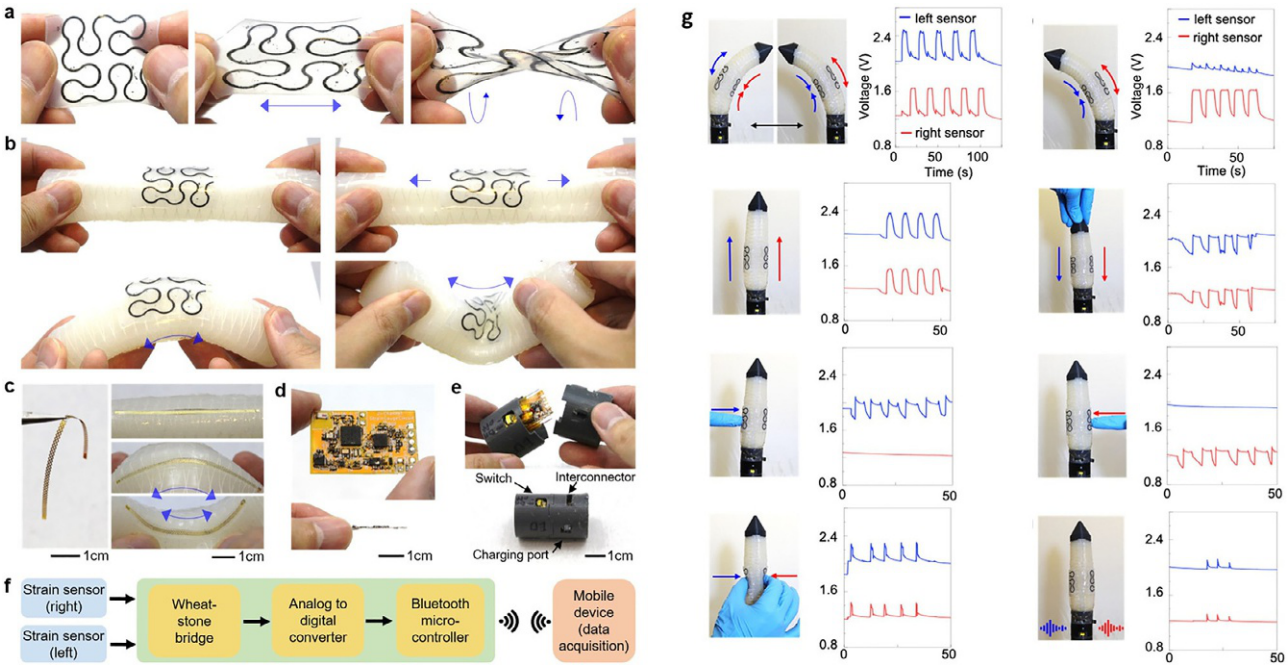

Fig. 11 Stretchable screen printed nanocomposite strain sensors, for feedback–loop control of a soft earthworm robot. Overview of a wireless strain sensing system integrated with a segment of a soft earthworm robot. (A) The nanocomposite strain sensor can endure multimodal stretching and bending on a soft robotic segment without mechanical fracture, (B) also when integrating onto the soft earthworm robot. (C and D) Photos of a miniaturized wireless circuit. (E) Plastic case of the wireless system. (F) Flowchart showing the signal path from strain sensors to the mobile device. (G) Proficiency of soft robot-embedded nanomembrane sensors in proprioception and exteroception. *Reprinted by permission from Goldoni R, Ozkan-Aydin Y, Kim YS, Kim J, Zavanelli N, Mahmood M, Liu B, Hammond FL, Goldman DI, & Yeo WH: Stretchable nanocomposite sensors, Nanomembrane interconnectors, and wireless electronics toward feedback-loop control of a soft earthworm robot, ACS Appl Mater Interfaces 12:43388–43397, 2020 https://doi.org/10.1021/acsami.0c10672 Copyright (2020) American Chemical Society.*

4.2 Example: Inkjet printed conductive gold electrodes for e-skin for soft robotics

One of the last research trends in soft robotic application is the development of a skin-like electronic system mimicking the thermo-sensation and mechano-sensation functionalities of natural skin.

A research team of University of California (Berkeley) in collaboration with Polymer Research Institute of Sichuan University (China) has developed a novel e-skin system by printing technology (Wu et al., 2021). The e-skin had ultrahigh sensitivity (non-contact sensing capability) and showed good capability for simultaneous monitoring/mapping of both thermal and mechanical stimulations. The e-skin system has been coupled with a soft robotic gripper for object manipulation. The sensing system for both thermo-sensation and mechano-sensation, analogous to that of natural human skin, paved the way for the future design of humanoid soft-robotics. The solution-processing inkjet fabrication of the e-skin assured scalability and cost efficiency. The inkjet printed skin sensory system is shown in Fig. 12.

This e-skin consists of arrays of potentiometric thermal sensors (3×3) and potentiometric mechanical sensors (4×4). The sensors working-principle is based on thermally or mechanically regulated variations in potential difference measured between two active electrodes well mimicking the natural skin sensory receptors so that the e-skin perceives even temperature and pressure variations caused by a finger touch. The description of the e-skin operation is outside the scope of this chapter. Interested readers can find full information in bibliography (Wu et al., 2021).

Here a description of the inkjet printing fabrication process of the e-skin will be provided. Kapton tape film was used as substrate, with gold nanoparticle ink employed to fabricate highly conductive gold connections on the substrate via inkjet printing. Briefly, conductive gold connections were inkjet printed on the Kapton substrate as the bottom electrode. Thermo-sensitive and mechano-sensitive prussian blue-modified graphite carbon (PB/carbon) electrode patterns were stencil printed on the gold connections. Then, the silver/silver chloride (Ag/AgCl) reference electrode pattern was printed by the side of the PB/carbon sensing electrodes with a gap of $\approx 750\,\mu m$. Thermal sensors are fabricated by casting polyvinyl alcohol/sodium chloride/glycerol-2% (PVA/NaCl/Gly-2%) ionic composite on the sensing regions, and mechanical sensors are constructed by placing PVA/NaCl/Gly-32% ionic composite microstructures on the sensing regions. Finally, the whole e-skin was fully encapsulated with a layer of

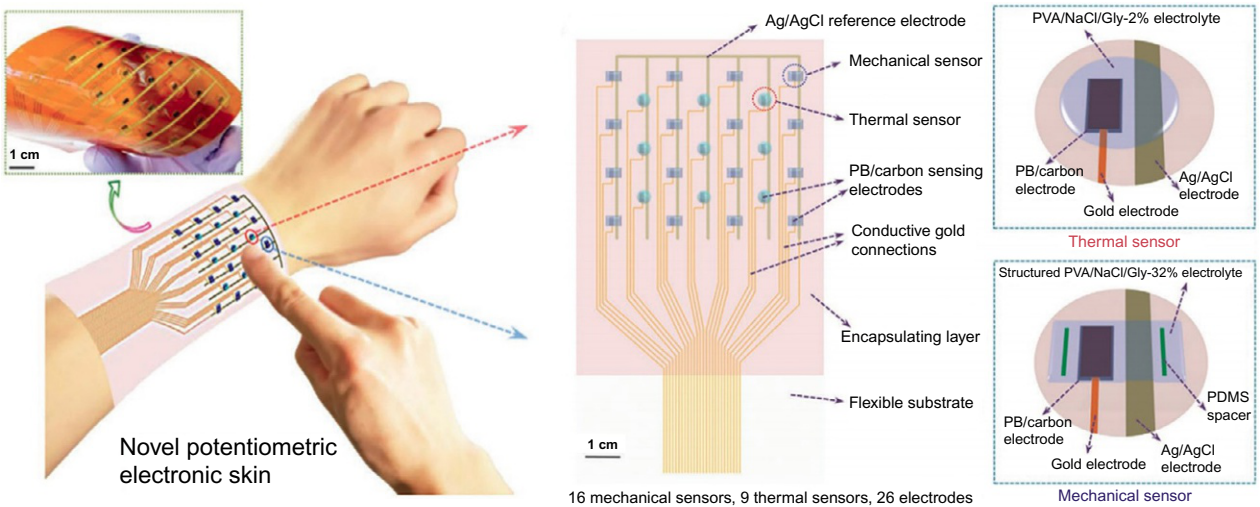

Fig. 12 Bioinspired design of potentiometric e-skin. Photograph and schematics showing the artificial e-skin based on a single potentiometric sensing scheme for both thermo-sensation and mechano-sensation (left). Structural layout of the potentiometric integrated 3×3 thermal sensors and 4×4 mechanical sensors (right). *Reprinted with permission from Wu X, Zhu J, Evans JW, Lu C, & Arias AC: A potentiometric electronic skin for thermosensation and mechanosensation, Adv Funct Mater 2021 https://doi.org/10.1002/adfm.202010824.*

Table 4 Values of viscosity, surface tension and density and Oh number for Gold nanoparticles ink used in inkjet printing (Begines et al., 2019; Cui et al., 2010; Rudolf et al., 2020).

Viscosity (mPa s)	Surface tension ($mN\,m^{-1}$)	Oh number	References
2	41.79	0.1	Begines et al. (2019)
2	n.a.	n.a.	Cui et al. (2010)
1.1	n.a.	n.a.	Rudolf et al. (2020)

polyimide film. Dimatix DMP 2800 inkjet printer was used for the e-skin gold connections fabrication. Cartridges of 10 pL volume and a drop spacing of 30 μm were used for the printing. The inkjet-printed gold electrode pattern was pre-dried on the printer hotplate at 60 °C for 30 min to stabilize the electrode pattern, then it was transferred to a vacuum hotplate and annealed at 250 °C for 1 h to fuse the gold nanoparticles into continuous conductive pattern. A commercial ≈60 μm thick Kapton with a typical surface tension of 50 mN m^{-1} was used as substrate. Used gold nanoparticle (AuNPs) ink was also purchased from a company. In this case, the company does not give details on the properties of the ink, however gold nanoparticles ink for inkjet printing are widely used. Thus, in Table 4 are listed some parameters for AuNPs ink.

In conclusion, through a careful material selection, component tuning, and structural engineering of sensor systems, the described printed e-skin presented by Wu et al., consisting in inkjet-printed gold electrodes on Kapton substrates, exhibits several advantages respect the state of art of e-skin, including, ultralow power consumption, simplified operation (i.e., only potentiometric measurement), ultra-high sensitivity, scalable fabrication, and economic efficiency. The latter two advantages are provided by the inkjet printing technology employed in the fabrication process.

5. Conclusions and outlook

In conclusion, screen and inkjet printing techniques offer a foundation for applications in soft robotics because of their powerful capacities to realize custom devices on intrinsic deformable and stretchable materials and curvilinear surfaces. Both the techniques stand out to be cost-effective, fast, and easy to use methods. Moreover, the recent development of printing has allowed exploring new avenues for materials processing, which otherwise are difficult to realize with conventional wafer-based fabrication techniques,

by establishing a close double link between the development of printing technique and the deformable and soft electronics.

Nevertheless, both printing techniques face some limitations for developing all layers of soft electronic devices. Regarding screen printing, these include the high material waste, indeed, differently to a drop-on-demand system, screen printing needs the employment of more ink than necessary to ensure a good print. Moreover, the screen printer is able to deposit high wet thickness of the film that usually is exposed to the atmosphere, which is not always desirable (Khan et al., 2015). It employs a mask, which can be easily deteriorated by the paste with time and which hinders the possibility to directly print the conductive soft device on the 3D object, as it is possible in the case of aerosol jet and spray coating techniques. On the other hand, since inkjet printers are designed for low volume printing, one of their main disadvantages is the relatively slow speed. Moreover, nozzle clogging and cartridge cost are a major problems. Even if this is the less material-consuming printing technique, printhead cleaning und flushing of the nozzles produces some ink waste. In addition, being a complex system, inkjet printer requires frequent maintenance.

Despite these limitations, the fabrication of flexible circuits, sensors, and other printed materials represents a great technological advancement compared with other standard methods and in the past few years, research in printing technologies has seen substantial developments. Moreover, these two techniques stand out among the other printing methods (such as gravure, flexography, aerosol, transfer printing, and spray coating) for the simplicity and the ability to pattern a wide range of soft materials, and the capability to print complex design with the best resolution. Employing these techniques, the current research is exploiting new routes of applications, such as bioimprinting, which has proven the possibility to provide a fast-growing breakthrough in tissue engineering and advanced soft-robotics for human health support (Li et al., 2021).

References

Abbott S: *How to be a great screen printer*, 2008, MacDermid Autotype.

Abellán-Llobregat A, Jeerapan I, Bandodkar A, et al.: A stretchable and screen-printed electrochemical sensor for glucose determination in human perspiration, *Biosens Bioelectron* 91:885–891, 2017. https://doi.org/10.1016/j.bios.2017.01.058.

Alias R, Mohd S: Rheological behaviors and their correlation with printing performance of silver paste for LTCC Tape, In *Rheology*, 2012, IntechOpen, pp 321–338. https://doi.org/10.5772/35004.

Amjadi M, Kyung KU, Park I, Sitti M: Stretchable, skin-mountable, and wearable strain sensors and their potential applications: a review, *Adv Funct Mater* 26:1678–1698, 2016. https://doi.org/10.1002/adfm.201504755.

Antonopoulou E, Harlen OG, Walkley MA, Kapur N: Jetting behavior in drop-on-demand printing: laboratory experiments and numerical simulations, *Phys Rev Fluids* 5:1–17, 2020. https://doi.org/10.1103/PhysRevFluids.5.043603.

Bandodkar AJ, Nuñez-Flores R, Jia W, Wang J: All-printed stretchable electrochemical devices, *Adv Mater* 27:3060–3065, 2015. https://doi.org/10.1002/adma.201500768.

Barmpakos D, Kaltsas G: A review on humidity, temperature and strain printed sensors—current trends and future perspectives, *Sensors (Switzerland)* 21:1–24, 2021. https://doi.org/10.3390/s21030739.

Barras R, Cunha I, Gaspar D, Fortunato E, Martins R, Pereira L: Printable cellulose-based electroconductive composites for sensing elements in paper electronics, *Flex Print Electron* 2(14006), 2017. https://doi.org/10.1088/2058-8585/aa5ef9.

Begines B, Alcudia A, Aguilera-Velazquez R, et al.: Design of highly stabilized nanocomposite inks based on biodegradable polymer-matrix and gold nanoparticles for inkjet printing, *Sci Rep* 9:1–12, 2019. https://doi.org/10.1038/s41598-019-52314-2.

Bernasconi R, Angeli MC, Mantica F, Carniani D, Magagnin L: SU-8 inkjet patterning for microfabrication, *Polymer (Guildf)* 185, 2019, 121933. https://doi.org/10.1016/j.polymer.2019.121933.

Boley JW, White EL, Kramer RK: Mechanically sintered gallium-indium nanoparticles, *Adv Mater* 27:2355–2360, 2015. https://doi.org/10.1002/adma.201404790.

Cahn G, Barrios A, Graham S, Meth J, Antoniou A, Pierron O: The role of strain localization on the electrical behavior of flexible and stretchable screen printed silver inks on polymer substrates, *Materialia* 10, 2020, 100642. https://doi.org/10.1016/j.mtla.2020.100642.

Cano-Raya C, Denchev ZZ, Cruz SF, Viana JC: Chemistry of solid metal-based inks and pastes for printed electronics—a review, *Appl Mater Today* 15:416–430, 2019. https://doi.org/10.1016/j.apmt.2019.02.012.

Chang J, Ge T, Sanchez-Sinencio E: Challenges of printed electronics on flexible substrates, In 2012 IEEE 55th international midwest symposium on circuits and systems (MWSCAS). 2012, pp 582–585. https://doi.org/10.1109/MWSCAS.2012.6292087.

Ciocca M, Giannakou P, Mariani P, et al.: Colour-sensitive conjugated polymer inkjet-printed pixelated artificial retina model studied via a bio-hybrid photovoltaic device, *Sci Rep* 10:1–15, 2020. https://doi.org/10.1038/s41598-020-77819-z.

Clement F, Linse M, Tepner S, et al.: 'Project FINALE'—screen and screen printing process development for ultra-fine-line contacts below 20µm finger width, In 36th European PV Solar Energy Conference and Exhibition. 2019, pp 259–262.

Costa Angeli M, Cramer T, Fraboni B, Magagnin L, Gastaldi D, Vena P: Reliability of inkjet printed silver nanoparticle interconnects on deformable substrates tested through an electromechanical in-situ technique, *MRS Commun* 9:1–8, 2019. https://doi.org/10.1557/mrc.2019.10.

Cruz S, Rocha LA, Viana JC: Piezo-resistive behaviour at high strain levels of PEDOT:PSS printed on a flexible polymeric substrate by a novel surface treatment, *J Mater Sci Mater Electron* 28:2563–2573, 2017. https://doi.org/10.1007/s10854-016-5832-3.

Cui W, Lu W, Zhang Y, Lin G, Wei T, Jiang L: Gold nanoparticle ink suitable for electric-conductive pattern fabrication using in ink-jet printing technology, *Colloids Surf A Physicochem Eng Asp* 358:35–41, 2010. https://doi.org/10.1016/j.colsurfa.2010.01.023.

Dang W, Vinciguerra V, Lorenzelli L, Dahiya R: Printable stretchable interconnects, *Flex Print Electron* 2:013003–013019, 2017. https://doi.org/10.1088/2058-8585/aa5ab2.

De Gans BJ, Duineveld PC, Schubert US: Inkjet printing of polymers: state of the art and future developments, *Adv Mater* 16:203–213, 2004. https://doi.org/10.1002/adma.200300385.

Deegan RD, Bakajin O, Dupont TF: Capillary flowasthe cause of ring stains fromdried liquid drops, *Nature* 389:827–829, 1997.

Derby B: Inkjet printing of functional and structural materials: Fluid property requirements, feature stability, and resolution, *Annu Rev Mat Res* 40:395–414, 2010. https://doi.org/10.1146/annurev-matsci-070909-104502.

Faddoul R, Reverdy-Bruas N, Blayo A: Formulation and screen printing of water based conductive flake silver pastes onto green ceramic tapes for electronic applications, *Mater Sci Eng, B* 177:1053–1066, 2012. https://doi.org/10.1016/j.mseb.2012.05.015.

Faddoul R, Reverdy-Bruas N, Blayo A: Printing force effect on conductive silver tracks: geometrical, surface, and electrical properties, *J Mater Eng Perform* 22:640–649, 2013. https://doi.org/10.1007/s11665-012-0245-9.

Falco A, Cinà L, Scarpa G, Lugli P, Abdellah A: Fully-sprayed and flexible organic photodiodes with transparent carbon nanotube electrodes, *ACS Appl Mater Interfaces* 6:10593–10601, 2014. https://doi.org/10.1021/am5022123.

Falco A, Petrelli M, Bezzecheri E, Abdelhalim A, Lugli P: Towards 3D-printed organic electronics: planarization and spray-deposition of functional layers onto 3D-printed objects, *Org Electron* 39:340–347, 2016. https://doi.org/10.1016/j.orgel.2016.10.027.

Fang Y, Tentzeris MM: Surface modification of polyimide films for inkjet-printing of flexible electronic devices, In *Flexible electronics*, 2018, IntechOpen, pp 137–144.

Fang C, Zhang J, Chen X, Weng GJ: Calculating the electrical conductivity of graphene nanoplatelet polymer composites by a Monte Carlo method, *Nanomaterials* 10:1–15, 2020. https://doi.org/10.3390/nano10061129.

Fernandes IJ, Aroche AF, Schuck A, et al.: Silver nanoparticle conductive inks: Synthesis, characterization, and fabrication of inkjet-printed flexible electrodes, *Sci Rep* 10:1–11, 2020. https://doi.org/10.1038/s41598-020-65698-3.

FlexiForce. 2021, https://www.tekscan.com/flexiforce-load-force-sensors-and-systems.

Galloway KC, Becker KP, Phillips B, et al.: Soft robotic grippers for biological sampling on deep reefs, *Soft Rob* 3:23–33, 2016. https://doi.org/10.1089/soro.2015.0019.

Gerboni G, Diodato A, Ciuti G, Cianchetti M, Menciassi A: Feedback control of soft robot actuators via commercial flex bend sensors, *IEEE/ASME Trans Mechatron* 22:1881–1888, 2017. https://doi.org/10.1109/TMECH.2017.2699677.

Giffney T, Bejanin E, Kurian AS, Travas-Sejdic J, Aw K: Highly stretchable printed strain sensors using multi-walled carbon nanotube/silicone rubber composites, *Sensors Actuators, A Phys* 259:44–49, 2017. https://doi.org/10.1016/j.sna.2017.03.005.

Goldoni R, Ozkan-Aydin Y, Kim YS, et al.: Stretchable nanocomposite sensors, Nanomembrane interconnectors, and wireless electronics toward feedback-loop control of a soft earthworm robot, *ACS Appl Mater Interfaces* 12:43388–43397, 2020. https://doi.org/10.1021/acsami.0c10672.

Gosselin D, Gougis M, Baque M, et al.: Screen-printed polyaniline-based electrodes for the real-time monitoring of loop-mediated isothermal amplification reactions, *Anal Chem* 89:10124–10128, 2017. https://doi.org/10.1021/acs.analchem.7b02394.

Grancarić AM, Jerković I, Koncar V, et al.: Conductive polymers for smart textile applications, *J Ind Text*:612–642, 2018.

Guinovart T, Bandodkar AJ, Windmiller JR, Andrade FJ, Wang J: A potentiometric tattoo sensor for monitoring ammonium in sweat, *Analyst* 138:7031–7038, 2013. https://doi.org/10.1039/c3an01672b.

He X, He R, Lan Q, et al.: *Screen-printed fabrication of PEDOT: PSS/Silver*, 2017 https://doi.org/10.3390/ma10030220.

Hu G, Kang J, Ng LWT, et al.: Functional inks and printing of two-dimensional materials, *Chem Soc Rev* 47:3265–3300, 2018. https://doi.org/10.1039/c8cs00084k.

Huttunen OH, Happonen T, Hiitola-Keinänen J, Korhonen P, Ollila J, Hiltunen J: Roll-to-roll screen-printed silver conductors on a polydimethyl siloxane substrate for stretchable electronics, *Ind Eng Chem Res* 58:19909–19916, 2019. https://doi.org/10.1021/acs.iecr.9b03628.

infinityPV., 2021, https://infinitypv.com/.
Jewell E, et al.: Deposition of high conductivity low silver content materials by screen printing, *Coatings* 5(2):172–185, 2015. https://doi.org/10.3390/coatings5020172.
Jung WB, Jang S, Cho SY, Jeon HJ, Jung HT: Recent progress in simple and cost-effective top-down lithography for ≈10 nm scale nanopatterns: from edge lithography to secondary sputtering lithography, *Adv Mater* 32:1–22, 2020. https://doi.org/10.1002/adma.201907101.
Kang H, Kim Y, Cheon S, Yi GR, Cho JH: Halide welding for silver nanowire network electrode, *ACS Appl Mater Interfaces* 9:30779–30785, 2017. https://doi.org/10.1021/acsami.7b09839.
Kapur N, Abbott SJ, Dolden ED, Gaskell PH: Predicting the behavior of screen printing, In *IEEE transactions on components, packaging and manufacturing technology*, 2013, pp 508–515.
Kaur M, Kim TH, Kim WS: New frontiers in 3D structural sensing robots, *Adv Mater* 33:1–15, 2021. https://doi.org/10.1002/adma.202002534. 2,002,534.
Khan S, Lorenzelli L, Dahiya RS: Technologies for printing sensors and electronics over large flexible substrates: a review, *IEEE Sens J* 15:3164–3185, 2015. https://doi.org/10.1109/JSEN.2014.2375203.
Kim J, Kumar R, Bandodkar AJ, Wang J: Advanced materials for printed wearable electrochemical devices: a review, *Adv Electron Mater* 3:1–15, 2017. https://doi.org/10.1002/aelm.201600260.
Koivikko A, Raei ES, Mosallaei M, Mäntysalo M, Sariola V: Screen-printed curvature sensors for soft robots, *IEEE Sens J* 18:223–230, 2018. https://doi.org/10.1109/JSEN.2017.2765745.
Kołodziej L, Ostrowski S, Maciejewski A, Jakubowska M, Wróblewski G: The influence of screen-printing parameters on properties of conductive layers for application in biomedical electrodes, In Szewczyk R, Krejsa J, Nowicki M, Ostaszewska-Liżewska A, editors: *Mechatronics 2019: Recent advances towards industry 4.0. Advances in intelligent systems and computing* (vol. 1044). Cham, 2020, Springer. https://doi.org/10.1007/978-3-030-29993-4_50.
Kumar R, Shin J, Yin L, You JM, Meng YS, Wang J: All-printed, stretchable Zn-Ag2O rechargeable battery via hyperelastic binder for self-powering wearable electronics, *Adv Energy Mater* 7:1602096–1602113, 2017. https://doi.org/10.1002/aenm.201602096.
Kun C, Kai C, Ziliang W: Optimization of screen printing process, In 2006 7th international conference on electronics packaging technology, ICEPT '06. 2007.
Larmagnac A, Eggenberger S, Janossy H, Vörös J: Stretchable electronics based on Ag-PDMS composites, *Sci Rep* 4:1–7, 2014. https://doi.org/10.1038/srep07254.
Lau GK, Shrestha M: Ink-jet printing of micro-elelectro-mechanical systems (MEMS), *Micromachines* 8:1–19, 2017. https://doi.org/10.3390/mi8060194.
Li K, Liu JK, Chen WS, Zhang L: Controllable printing droplets on demand by piezoelectric inkjet: applications and methods, *Microsyst Technol* 24:879–889, 2018. https://doi.org/10.1007/s00542-017-3661-9.
Li W, Yang S, Shamim A: Screen printing of silver nanowires: balancing conductivity with transparency while maintaining flexibility and stretchability, *Npj Flex Electron* 3, 2019, 13. https://doi.org/10.1038/s41528-019-0057-1.
Li M, Chen S, Fan B, Wu B, Guo X: Printed flexible strain sensor array for bendable interactive surface, *Adv Funct Mater* 30:1–7, 2020. https://doi.org/10.1002/adfm.202003214.
Li H, Liu H, Sun M, Huang YA, Xu L: 3D interfacing between soft electronic tools and complex biological tissues, *Adv Mater* 33:2004425–2004441, 2021. https://doi.org/10.1002/adma.202004425.
Liang J, Tong K, Pei Q: A water-based silver-nanowire screen-print ink for the fabrication of stretchable conductors and wearable thin-film transistors, *Adv Mater* 28:5986–5996, 2016. https://doi.org/10.1002/adma.201600772.

Liao X, Song W, Zhang X, Huang H, Wang Y, Zheng Y: Directly printed wearable electronic sensing textiles towards human-machine interfaces, *J Mater Chem C* 6:12841–12848, 2018. https://doi.org/10.1039/c8tc02655f.

Lipomi DJ, Lee JA, Vosgueritchian M, Tee BC, Bolander JA: Electronic properties of transparent conductive films of PEDOT:PSS on stretchable substrates, *Chem Mater* 24:373–382, 2012. https://doi.org/10.1021/cm203216m.

Liu WC, Watt AAR, Solvodynamic Printing AA: High resolution printing method, *Sci Rep* 9:1–12, 2019. https://doi.org/10.1038/s41598-019-47105-8.

Lugoda P, Costa JC, Garcia-Garcia LA, et al.: Coco stretch: strain sensors based on natural coconut oil and carbon black filled elastomers, *Adv Mater Technol* 6:1–9, 2021. https://doi.org/10.1002/admt.202000780.

Maleki H, Bertola V: Recent advances and prospects of inkjet printing in heterogeneous catalysis, *Cat Sci Technol* 10:3140–3159, 2020. https://doi.org/10.1039/d0cy00040j.

Marchese AD, Onal CD, Rus D: Autonomous soft robotic fish capable of escape maneuvers using fluidic elastomer actuators, *Soft Rob* 1:75–87, 2014. https://doi.org/10.1089/soro.2013.0009.

Market-Reports., 2020, https://www.marketsandmarkets.com/Market-Reports/printed-electronics-market-197.html.

Marra F, Minutillo S, Tamburrano A, Sarto MS: Production and characterization of graphene nanoplatelet-based ink for smart textile strain sensors via screen printing technique, *Mater Des* 198, 2021, 109306. https://doi.org/10.1016/j.matdes.2020.109306.

Matsui H, Takeda Y, Tokito S: Flexible and printed organic transistors: from materials to integrated circuits, *Org Electron* 75, 2019, 105432. https://doi.org/10.1016/j.orgel.2019.105432.

McKinley GH, Renardy M: Wolfgang von ohnesorge, *Phys Fluids* 23:127101–127107, 2011. https://doi.org/10.1063/1.3663616.

Mendes-Felipe C, Oliveira J, Etxebarria I, Vilas-Vilela JL, Lanceros-Mendez S: State-of-the-art and future challenges of UV curable polymer-based smart materials for printing technologies, *Adv Mater Technol* 4:1–16, 2019. https://doi.org/10.1002/admt.201800618.

Merilampi S, Laine-Ma T, Ruuskanen P: The characterization of electrically conductive silver ink patterns on flexible substrates, *Microelectron Reliab* 49(7):782–790, 2009. https://doi.org/10.1016/j.microrel.2009.04.004.

Metrohm, 2021. http://www.dropsens.com/en/screen_printed_electrodes_pag.html.

Mewis J, Wagner NJ: Thixotropy, *Adv Colloid Interface Sci* 147–148:214–227, 2009. https://doi.org/10.1016/j.cis.2008.09.005.

Ney L, Tepner S, Wengenmeyr N, et al.: Optimization of fine line screen printing using in-depth screen mesh analysis, *AIP Conf Proc* 2156:020006–020014, 2019. https://doi.org/10.1063/1.5125871.

Pan J, Tonkay GL, Quintero A: Screen printing process design of experiments for fine line printing of thick film ceramic substrates, *J Electron Manuf* 9:203–213, 1999. https://doi.org/10.1142/S096031319900012X.

Park YL, Chen BR, Pérez-Arancibia NO, et al.: Design and control of a bio-inspired soft wearable robotic device for ankle-foot rehabilitation, *Bioinspir Biomim* 9:016007, 2014. https://doi.org/10.1088/1748-3182/9/1/016007.

Phillips C, Al-Ahmadi A, Potts SJ, Claypole T, Deganello D: The effect of graphite and carbon black ratios on conductive ink performance, *J Mater Sci* 52:9520–9530, 2017. https://doi.org/10.1007/s10853-017-1114-6.

Pinto T, Cai L, Wang C, Tan X: CNT-based sensor arrays for local strain measurements in soft pneumatic actuators, *Int J Intell Robot Appl* 1:157–166, 2017. https://doi.org/10.1007/s41315-017-0018-6.

Plovie B, Bossuyt F, Vanfleteren J: Stretchability-the metric for stretchable electrical interconnects, *Micromachines* 9:7–10, 2018. https://doi.org/10.3390/mi9080382.

Potts SJ, Phillips C, Claypole T, Jewell E: The effect of carbon ink rheology on ink separation mechanisms in screen-printing, *Coatings* 10:1–17, 2020a. https://doi.org/10.3390/coatings10101008.

Potts SJ, Phillips C, Jewell E, Clifford B, Lau YC, Claypole T: High-speed imaging the effect of snap-off distance and squeegee speed on the ink transfer mechanism of screen-printed carbon pastes, *J Coat Technol Res* 17:447–459, 2020b. https://doi.org/10.1007/s11998-019-00291-6.

Qi X, Ha H, Hwang B, Lim S: Printability of the screen-printed strain sensor with carbon black/silver paste for sensitive wearable electronics, *Appl Sci* 10:1–10, 2020a. https://doi.org/10.3390/app10196983.

Qi D, Zhang K, Tian G, Jiang B, Huang Y: Stretchable electronics based on PDMS substrates, *Adv Mater* 33:1–25, 2020b. https://doi.org/10.1002/adma.202003155. 2,003,155:.

Quinsaat JEQ, Burda I, Krämer R, et al.: Conductive silicone elastomers electrodes processable by screen printing, *Sci Rep* 9:1–11, 2019. https://doi.org/10.1038/s41598-019-49939-8.

Ratner BD, Hoffman AS, Schoen FJ, Lemons JE: Bio-ink for on-demand printing of living cells, *Biomater Sci* 1:224, 2013. https://doi.org/10.1016/C2009-0-02433-7.

Ren HM, Guo Y, Huang SY, et al.: One-step preparation of silver hexagonal microsheets as electrically conductive adhesive fillers for printed electronics, *ACS Appl Mater Interfaces* 7:13685–13692, 2015. https://doi.org/10.1021/acsami.5b03571.

Riheen MA, Saha TK, Sekhar PK: Inkjet printing on PET substrate, *J Electrochem Soc* 166: B3036–B3039, 2019. https://doi.org/10.1149/2.0091909jes.

Roh E, Hwang B, Kim D, Kim B, Lee N: Stretchable, transparent, ultrasensitive, and patchable strain sensor for human? Machine interfaces comprising a nanohybrid of carbon nanotubes and conductive elastomers, *ACS Nano* 6252–6261, 2015.

Rudolf R, Majeric P, Golub D, Tiyyagura HR: Testing of novel nano gold ink for inkjet printing, *Adv Prod Eng Manag* 15:358–368, 2020. https://doi.org/10.14743/apem2020.3.371.

Schlatter S, Rosset S, Shea H: Inkjet printing of carbon black electrodes for dielectric elastomer actuators, In *Electroactive polymer actuators and devices (EAPAD)*, vol. 10163, 2017, p 1016311. 2017 https://doi.org/10.1117/12.2258615.

Shi H, Al-Rubaiai M, Holbrook CM, et al.: Screen-printed soft capacitive sensors for spatial mapping of both positive and negative pressures, *Adv Funct Mater* 29:1–10, 2019. https://doi.org/10.1002/adfm.201809116.

Shigemune H, Maeda S, Hara Y, Hosoya N, Hashimoto S: Origami robot: a self-folding paper robot with an electrothermal actuator created by printing, *IEEE/ASME Trans Mechatron* 21:2746–2754, 2016. https://doi.org/10.1109/TMECH.2016.2593912.

Simaite A, Mesnilgrente F, Tondu B, Souères P, Bergaud C: Towards inkjet printable conducting polymer artificial muscles, *Sens Actuators B* 229:425–433, 2016. https://doi.org/10.1016/j.snb.2016.01.142.

Sinha SK, Noh Y, Reljin N, et al.: Screen-printed PEDOT:PSS electrodes on commercial finished textiles for electrocardiography, *ACS Appl Mater Interfaces* 9:37524–37528, 2017. https://doi.org/10.1021/acsami.7b09954.

Søndergaard RR, Hösel M, Krebs FC: Roll-to-Roll fabrication of large area functional organic materials, *J Polym Sci B* 51:16–34, 2013. https://doi.org/10.1002/polb.23192.

Sridhar A, Blaudeck T, Baumann RR: Inkjet printing as a key enabling technology for printed electronics, *Mater Matters (Milwaukee, WI United States)* 6:12–17, 2011.

Stankovich S, Dikin DA, Dommett GHB, et al.: Graphene-based composite materials, *Nature* 442:282–286, 2006. https://doi.org/10.1038/nature04969.

Suresh RR, Lakshmanakumar M, Arockia Jayalatha JBB, et al.: Fabrication of screen-printed electrodes: opportunities and challenges, *J Mater Sci* 56:8951–9006, 2021. https://doi.org/10.1007/s10853-020-05499-1.

Ta TD, Umedachi T, Kawahara Y: Inkjet printable actuators and sensors for soft-bodied crawling robots, In Proceedings—IEEE International Conference on Robotics and Automation (ICRA). 2019-May. 2019, pp 3658–3664. https://doi.org/10.1109/ICRA.2019.8793827.

Tepner S, Wengenmeyr N, Linse M, Lorenz A, Pospischil M, Clement F: The link between Ag-paste rheology and screen-printed solar cell metallization, *Adv Mater Technol* 5:2000654–2000662, 2020. https://doi.org/10.1002/admt.202000654. 2,000,654:.

Tetsu Y, Yamagishi K, Kato A, et al.: Ultrathin epidermal strain sensor based on an elastomer nanosheet with an inkjet-printed conductive polymer, *Appl Phys Express* 10, 2017, 087201. https://doi.org/10.7567/APEX.10.087201.

Tian B, Yao W, Zeng P, et al.: All-printed, low-cost, tunable sensing range strain sensors based on Ag nanodendrite conductive inks for wearable electronics, *J Mater Chem C* 7: 809–818, 2019. https://doi.org/10.1039/c8tc04753g.

Torrisi F, Hasan T, Wu W, et al.: Inkjet-printed graphene electronics, *ACS Nano* 6:2992–3006, 2012. https://doi.org/10.1021/nn2044609.

Vaicekauskaite J, Mazurek P, Vudayagiri S, Skov AL: Mapping the mechanical and electrical properties of commercial silicone elastomer formulations for stretchable transducers, *J Mater Chem C* 8:1273–1279, 2020. https://doi.org/10.1039/c9tc05072h.

Vo TT, Lee HJ, Kim SY, Suk JW: Synergistic effect of graphene/silver nanowire hybrid fillers on highly stretchable strain sensors based on spandex composites, *Nanomaterials* 10:1–14, 2020. https://doi.org/10.3390/nano10102063.

Vuorinen T, Niittynen J, Kankkunen T, Kraft TM, Mäntysalo M: Inkjet-printed graphene/PEDOT:PSS temperature sensors on a skin-conformable polyurethane substrate, *Sci Rep* 6:1–8, 2016. https://doi.org/10.1038/srep35289.

Wagner S, Bauer S: Materials for stretchable electronics, *MRS Bull* 37:207–213, 2012. https://doi.org/10.1557/mrs.2012.37.

Wang H, Totaro M, Beccai L: Towards perceptive soft robots: progress and challenges, *Adv Sci* 5:1800541–1800557, 2018. https://doi.org/10.1002/advs.201800541.

Wang YF, Sekine T, Takeda Y, et al.: Printed strain sensor with high sensitivity and wide working range using a novel brittle-stretchable conductive network, *ACS Appl Mater Interfaces* 12:35282–35290, 2020a. https://doi.org/10.1021/acsami.0c09590.

Wang YF, Sekine T, Takeda Y, et al.: Fully printed PEDOT:PSS-based temperature sensor with high humidity stability for wireless healthcare monitoring, *Sci Rep* 10:1–8, 2020b. https://doi.org/10.1038/s41598-020-59432-2.

Weng B, Shepherd RL, Crowley K, Killard AJ, Wallace GG: Printing conducting polymers, *Analyst* 135:2779–2789, 2010. https://doi.org/10.1039/c0an00302f.

White EL, Yuen MC, Case JC, Kramer RK: Low-cost, facile, and scalable manufacturing of capacitive sensors for soft systems, *Adv Mater Technol* 2:1–10, 2017. https://doi.org/10.1002/admt.201700072.

Wilson DI: What is rheology? *Eye (Lond)* 32:179–183, 2017. https://doi.org/10.1038/eye.2017.267. Cambridge Ophthalmology Symposium, https://www.nature.com/articles/eye2017267.

Wu W: Stretchable electronics: functional materials, fabrication strategies and applications, *Sci Technol Adv Mater* 20:187–224, 2019. https://doi.org/10.1080/14686996.2018.1549460.

Wu L, Qian J, Peng J, et al.: Screen-printed flexible temperature sensor based on FG/CNT/PDMS composite with constant TCR, *J Mater Sci Mater Electron* 30:9593–9601, 2019. https://doi.org/10.1007/s10854-019-01293-1.

Wu X, Zhu J, Evans JW, Lu C, Arias AC: A potentiometric electronic skin for thermosensation and mechanosensation, *Adv Funct Mater* 31:2010824–2010834, 2021. https://doi.org/10.1002/adfm.202010824.

Yan K, Li J, Pan L, Shi Y: Inkjet printing for flexible and wearable electronics, *APL Mater* 8, 2020, 120705. https://doi.org/10.1063/5.0031669.

Yang W, Li NW, Zhao S, et al.: A breathable and screen-printed pressure sensor based on nanofiber membranes for electronic skins, *Adv Mater Technol* 3:1–7, 2018. https://doi.org/10.1002/admt.201700241.

Yeo JC, Yap HK, Xi W, Wang Z, Yeow CH, Lim CT: Flexible and stretchable strain sensing actuator for wearable soft robotic applications, *Adv Mater Technol* 1:1–9, 2016. https://doi.org/10.1002/admt.201600018.

Yokus MA, Foote R, Jur JS: Printed stretchable interconnects for smart garments: design, fabrication, and characterization, *IEEE Sens J* 16:7967–7976, 2016. https://doi.org/10.1109/JSEN.2016.2605071.

Yoon SS, Khang DY: Roles of nonionic surfactant additives in PEDOT:PSS thin films, *J Phys Chem C* 120:29525–29532, 2016. https://doi.org/10.1021/acs.jpcc.6b12043.

Yu H, Han H, Jang J, Cho S: Fabrication and optimization of conductive paper based on screen-printed polyaniline/graphene patterns for nerve agent detection, *ACS Omega* 4:5586–5594, 2019. https://doi.org/10.1021/acsomega.9b00371.

Yüce C, König M, Willenbacher N: Rheology and screen-printing performance of model silver pastes for metallization of si-solar cells, *Coatings* 8:1–17, 2018. https://doi.org/10.3390/COATINGS8110406.

Zabihipour M, Lassnig R, Strandberg J, et al.: High yield manufacturing of fully screen-printed organic electrochemical transistors, *Npj Flex Electron* 4:1–8, 2020. https://doi.org/10.1038/s41528-020-0078-9.

Zhao C, Zhou Y, Gu S, et al.: Fully screen-printed, multicolor, and stretchable electroluminescent displays for epidermal electronics, *ACS Appl Mater Interfaces* 12:47902–47910, 2020. https://doi.org/10.1021/acsami.0c12415.

Zhu L, Wang Y, Mei D, Ding W, Jiang C, Lu Y: Fully elastomeric fingerprint-shaped electronic skin based on tunable patterned graphene/silver nanocomposites, *ACS Appl Mater Interfaces* 12:31725–31737, 2020. https://doi.org/10.1021/acsami.0c09653.

Zhu Y, Joralmon D, Shan W, et al.: 3D printing biomimetic materials and structures for biomedical applications, *Bio-Des Manuf* 4:405–428, 2021. https://doi.org/10.1007/s42242-020-00117-0.

This page intentionally left blank

CHAPTER THREE

Metal-organic frameworks (MOFs) for sensing

Alessandro Sacchetti*, Arianna Rossetti, and Javier Martí-Rujas
Department of Chemistry, Materials and Chemical Engineering G. Natta, Politecnico di Milano, Milano, Italy
*Corresponding author: e-mail address: alessandro.sacchetti@polimi.it

Contents

1. Definition of MOF 92
   1.1 Definition of MOFs (1D–3D, generation, coordination polymers, etc.) 92
   1.2 Synthesis and most common building blocks (organic and inorganic) 94
   1.3 Mode of sensing 96
   1.4 BioMOFs 97
2. Sensing of gases, vapors and VOC 99
   2.1 Sensing of oxygen 100
   2.2 Sensing of water vapor 103
   2.3 Sensing of hazardous gases 105
   2.4 Sensing of VOC 106
   2.5 Sensing of small organic molecules 108
3. MOFs for sensing of biomolecules 109
4. Conclusions 118
References 118

Abstract

MOFs, (the acronym for Metal-Organic Frameworks) are a quite new family of materials resulting from the combination of organic ligands and metal ions. The coordination between the metal centers and the organic scaffolds give rise to complex assemblies which can develop into coordination polymers from 1D to 3D structures. These materials are usually porous with well-defined channels or pores. For this reason, MOFs are able to absorb a number of molecules with very high efficiency. Depending on the combination of the metal and organic components, selectivity toward different classes of gases or organic molecules (guests) can be achieved. The interaction of the MOF with the guest often results in a modification of the MOF crystalline structure which eventually produce a change in the physical properties of the materials. These variations can be exploited to detect the presence of a specific guest. In this chapter, the application of MOFs for the sensing of chemical species will be briefly illustrated. After an introduction on of the structures and synthesis of MOFs, the different mode of sensing will be

Advances in Chemical Engineering, Volume 57
ISSN 0065-2377
https://doi.org/10.1016/bs.ache.2021.03.002

described. Then a number of examples from the recent literature will be discussed. The focus will be on two issues: the sensing of small molecules as gases, VOC and organic compounds, and the sensing of biomolecules. The former can find many uses in the industry, whereas the latter is a promising topic for biomedical applications.

1. Definition of MOF

1.1 Definition of MOFs (1D–3D, generation, coordination polymers, etc.)

In the last 20 years or so, there has been a rapid upsurge in the research efforts to develop metal-organic frameworks (MOFs) (i.e., also known a porous coordination networks (PCNs)/coordination polymers (CPs)), and have consolidated into an important area of research in material sciences (Fig. 1) (Ding et al., 2019; Kitagawa et al., 2004; MacGillivray, 2010) In part, this is because MOFs are composed of metal ions and organic ligand molecules that are regarded as nodes and linkers respectively. The coordination nature of the chemical bonds between the organic ligands and the metal centers has given unique intrinsic properties that other porous materials did not show so far (Fig. 1).

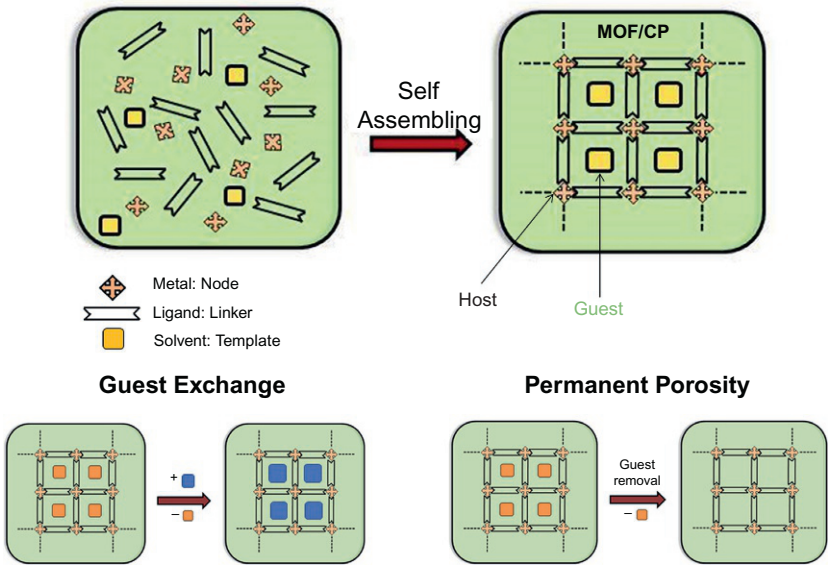

Fig. 1 Synthesis of a MOF by self-assembling of the building blocks in solution and guest exchange and formation of a guest "free" porous structure upon guest release.

Depending on the dimensionality of the metal-organic bonds, MOFs can be classified as zero-dimensional (0D), one-dimensional (1D), two-dimensional (2D) or three-dimensional (3D).

Structures that are formed by the self-assembling of metal ions and organic ligands that are discrete (i.e., that do not expand into the 3D of space) are regarded as 0D. Fundamental work has been carried out by Fujita and co-workers in the development of large nanospheres with volume voids of ca. 63,500 $Å^3$ able to encapsulate macromolecules such as proteins (i.e., ubiquitin, Fujita et al., 2012). 1D metal-organic structures are better regarded as coordination polymers since they do not form frameworks and compared to 2D and 3D counterparts are less robust because they have larger chances to move respectively. If the 1D chains are not parallel to each other but interwoven their rigidity can be important but if the 1D chains are parallel they can have a pronounced dynamic behavior in the presence of an external stimuli (Rossetti et al., 2018). The formation of rigid/stable channels/pores in 1D coordination polymers is challenging as it depends on the templating effect of guest molecules and the shape of the organic linkers. Two-dimensional metal-organic framework expand infinitely in two dimensions of space. The dynamic behavior of the layers can give also good properties such as pore breathing like or sliding of layers as response upon external stimuli. Among MOFs, those with intrinsic higher connectivity are the 3D MOFs as the nodes of connectivity metal-ligand are expanding in the three dimensions. This gives the possibility to form structures with rigid frameworks, large pores stable even in the absence of guest molecules and extremely high surface areas. Thermal stabilities from 350 °C to 400 °C can be achieved for some MOFs (MOF-5; Yaghi et al., 1995) providing wide range of thermal applicability.

Along with the ability to tune the nature of the organic building blocks (i.e., size, shape and chemical nature) and porosity, their dynamic behavior in presence of external stimuli is very important for the potential applications of MOFs in areas such as gas adsorption, proton conductivity, drug delivery, catalysis, and chemical sensing (Evans et al., 2020). Fine ligand length tuning has allowed the possibility to create structures that maintain the same MOFs reticular features but with a modulated pore dimension enlargement by applying the concept of isoreticular chemistry (Eddaoudi et al., 2002). MOFs synthesized through such approach are called isoreticular MOFs (IRMOFs). Large pores with diameters ranging from 1.4 to 9.9 nm and rigid structures have been prepared that allowed the diffusion of large proteins within the channels (Deng et al., 2012). The MOF framework is also

important to protect the included biomolecules from harsh environments such as high temperatures, adverse chemical environment, severe pH environments, and toxic substances.

Another aspect that has contributed significantly to MOFs development, has been their intrinsic good crystallinity which allowed the full atomic three-dimensional (3D) structural determination by X-ray crystallography. It is important to note that in many cases, because of their good crystallinity, it is possible to modify the organic linkers of an already crystallized MOF and still carry out full structure determination. This strategy is also referred as post synthetic modification (PSM) approach which is used for loading into MOFs biomolecules via ligand exchange (Cohen, 2017; Kim et al., 2012). In fact, the combination of rigidity and flexibility in MOFs lead to the definition of soft-porous MOFs (Horike et al., 2009; Krause et al., 2020). Soft-porous MOFs, are materials that can modify their structure upon external stimuli and can show breathing-like behavior, that means that the framework structure can adapt in the presence of new guests or can reduce its internal space when the guest molecules are removed completely. Adaptable framework behavior in the presence of new incoming molecules, specially large molecules such as proteins is very important as it might help in the preservation of protein activity (i.e., proteins maintain their function if their structure is not damaged during the inclusion process).

1.2 Synthesis and most common building blocks (organic and inorganic)

Since single crystal X-ray diffraction is the most reliable method for determining the 3D structural arrangement of atoms in a MOF, large MOFs single crystals are needed. The 3D atomic arrangement in a MOF is crucial to understand structure-function properties and to fine tune the building blocks in a MOF for improving its properties. Although several crystallization methods are being used for the preparation of MOFs (microwave synthesis, instant synthesis, solid-liquid interface synthesis…, Martí-Rujas and Kawano, 2013) most MOFs are prepared using "*one-pot*" reactions by slow crystallization methods. Layer diffusion or solvothermal synthesis are slow crystallization methods that usually gives large single crystals suitable for single crystal X-ray diffraction analysis. This step in the creation of MOFs is crucial as the formation of extended networks suffers from the so-called crystallization problem and the labile nature of metal-ligand bond formation plays a crucial role in this process.

From the earlier days, the most common building blocks for the synthesis of MOFs where based on nitrogen-based ligands (Fujita et al., 1994; Hoskins and Robson, 1989) and carboxylate organic ligands. The coordination among the organic ligand and the transition metals in pyridine-based MOFs takes place via a N–M whereas in the carboxylic based ligands, the coordination occurs among the deprotonated carboxylic group and the metals. Other ligands based on functional groups such as phosphonates, imidazolates are also being used in the preparation of MOFs.

Pyridine-based MOFs are less rigid if compared to carboxylate derived MOFs according to the metal-ligand bond energies. In the case of polytopic pyridine like ligand-based MOFs (i.e., metal-to-neutral Lewis base bonds), the bond energy is around 90–200 $kJ\,mol^{-1}$, whereas for carboxylate-based ligands (i.e., metal-to-charged ligand bonds), the bond energy is slightly higher about 150–350 $kJ\,mol^{-1}$ (Jiang et al., 2016). In the synthesis of carboxylate-based MOFs the development of inorganic clusters, referred usually as sub-building units (SBUs), has contributed to enhance the stability of such MOFs (Li et al., 1999) allowing the preparation of structures with giant unit cell volumes (ca. 702,000 $Å^3$) and very large pores observed in MIL-101 (Férey et al., 2005).

Thanks to the formation of 3D framework structures with such big pores, the introduction of huge molecules such as proteins has been possible. MIL-101 has been one of the first MOFs to be tested for biological applications with the inclusion of antitumor and antiretroviral drugs because of its large pores and biocompatibility with physiological conditions (McKinlay et al., 2010). Large-pore structures such as IRMOF-74 has allowed the inclusion of green fluorescent protein (GFP) in the pores via diffusion process just immersing the MOF in a solution containing the protein. Clearly, such sponge-like behavior has open the possibility to study many different aspects on the protein activity of on the protein loading within the MOFs.

Zinc-imidazolate frameworks (ZIFs) are another sub-class of MOFs that exploit the angles among the metal-imidazolate-metal in order to mimic the Si–O–Si bond angles seen in in rigid zeolites which is about 145°. Importantly, since imidazole is found in the side chains of endogenous amino acid histidine (His), derivates of imidazole can be used as organic linkers in biocompatible ZIFs. ZIFs have also intrinsic porosity and good thermal and chemical stability and show very good crystallinity. ZIFs have shown to have a rich chemistry with a wide variety of 3D topologies. One of the most studied ZIFs are the so-called ZIF-8 and ZIF-90 (Shieh et al., 2015) which have found applications in the de novo encapsulation of proteins

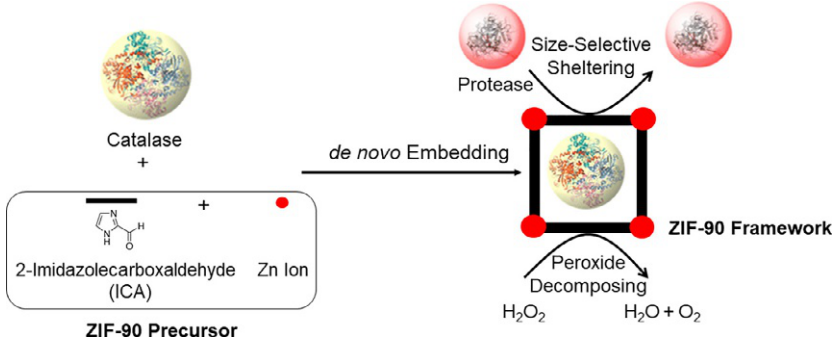

Fig. 2 Synthesis of ZIF-90 in aqueous environment with included catalase enzyme showing its functional activity.

(Fig. 2). ZIF-8 has been used to include hemeprotein cytochrome *c* (i.e., the protein is mixed with the MOF constituents and is included as guest during the crystallization) which showed 10-fold activity enhancement for the detection of peroxide species due to protein-ZIF interaction. Importantly, this de novo encapsulation of proteins method needs the interaction between protein being encapsulated and the building blocks forming the ZIF.

1.3 Mode of sensing

Self-assembling of metal ions with fluorophore organic molecules is a good approach to prepare fluorescent MOFs that can be used as sensors. A photoexcited fluorophore can transfer energy to the surrounding organic framework ligands but can also transfer such energy to included guest molecules (analytes). Thus, the interaction of included bioorganic guests and the fluorophore framework can give important changes on the quenching mechanisms, particularly as a function of the distance among the quencher and the fluorophore (i.e., host–guest interactions). Fluorescence can be used to study different protein conformations within the pores allowing a better understanding of protein encapsulation in a MOF (Chen et al., 2012). Using fluorescence, MOFs are being exploited for the detection of toxic and hazardous nitroaromatic compounds which have become a powerful sensing tool (Hu et al., 2020; Sharma et al., 2019).

In a similar approach but using the metal ions as the emitting part, MOFs can be utilized as luminescent probes taking the advantage of lanthanides. For instance, NIR-emiting lanthanides in biological environments can be used in applications as O_2 sensors with potential use in biological sensing (Fig. 3) (An et al., 2011; Muldoon et al., 2020).

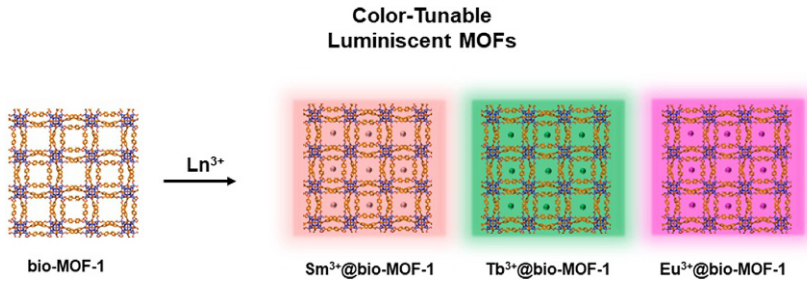

Fig. 3 Cation exchange reactions giving lanthanide luminescent MOFs.

A different sensing approach is by using metals such as Fe and Cu ions to construct MOFs that can oxidize chromogenic substances that with H_2O_2 to give as a product a colored reaction and this can be used as a signal to create sensors based on color changes (i.e., colorimetric sensors). For instance, Fe-MIL-88 can oxidize the chromogenic substrate 3,3′,5,5′-tetrametylbenzidine to give a blue color product, that was used to develop a DNA detector colorimetric sensor (Liu et al., 2015).

Considering the metal used in the synthesis of MOFs, paramagnetic metal ions such as Ga^{3+}, Fe^{3+} and Mn^{2+} can be used for applications such as magnetic resonance imaging (MRI). Thus, such magnetic properties make BioMOFs potential candidates to be used as contrasting agents for bioimaging in cancer cells (Wang, 2017).

1.4 BioMOFs

One line of research of MOFs that has attracted a huge interest is that oriented to biological applications, since MOFs can be prepared with organic molecules with biological activity. The biological activity in a MOF can be also due to the loading of guest molecules inside the channels/pores a MOF. In fact, the ability to prepare MOFs with extra-large pores by ligand synthesis applying isoreticular chemistry, has allowed the inclusion of biomolecules such as vitamins, nucleic acids, lipids and proteins although the inclusion and survival integrity of such large biomolecules has to be handled extremely well to avoid damage on the structure-function properties (Fujita et al., 2012). This sub-discipline of MOF chemistry has been regarded as BioMOFs and can have important applications in areas such as sensing or imaging.

BioMOFs are very important because of their intrinsic porous nature, they can be used in applications in areas such as drug delivery, imaging

and sensing depending in the nature of the building blocks used to self-assemble the BioMOF or the included guest biomolecules. The interactions among the organic molecules constituting in the framework with the guest molecules, can induce physical changes and hence be detected by various techniques. Also MOFs, can be coated and stabilized with lipids to give new functional properties such as the creation of lipid bilayer formation outside MOF structures with some cases good aqueous solution stabilization (He et al., 2015; Preiß et al., 2015; Wang et al., 2015). Cleary, BioMOFs that are not dangerous to the living organisms can be prepared if the metal ions and organic molecules are not toxic (i.e., biocompatible MOFs).

The self-assembly of MOFs with biological applications can be obtained using biologically related ligands such as peptides, aminoacids, saccharides, cyclodextrins and other biomolecules. Importantly bioorganic molecules have many salient features that render the MOF structure appealing for applications in biochemistry and medicine. Structurally speaking, biomolecules have a great diversity including flexible and rigid molecules. Using chiral biomolecules as building unit can lead to chiral MOFs with chiral pores that are useful in sensing of other chiral molecules (i.e., chiral recognition) (Fig. 4) (Saito et al., 2020; Sawada et al., 2014). The isolation inside of the MOF's chiral channels of chiral molecules that otherwise are not possible to

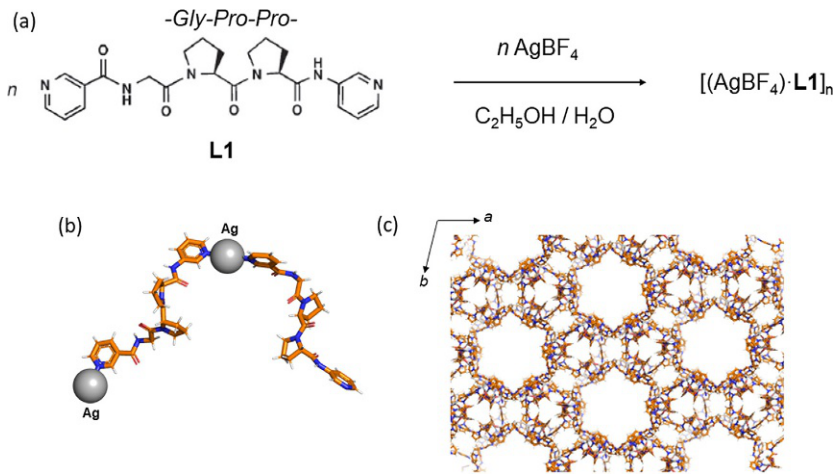

Fig. 4 (A) Bio-MOF synthesized using the tripeptide L1 and $AgBF_4$. (B) Asymmetric unit in [$(AgBF_4)$·**L1**] and the channel structure of the MOF structure. The Bio-MOF contains two types of helical nanochannels that are able to recognize chiral molecules from polar solutions.

be separated reminds of particular molecular recognition events taking place in more elaborated organic systems such as in proteins or enzyme pockets (Petsko and Ringe, 2004). Another important aspect of using biomolecules is that many are found in nature, they are readily available and in large quantities.

BioMOFs can be prepared with a great variety of bioorganic molecules such as amino acids, peptides, proteins, carbohydrates (saccharides), nucleobases and other bioorganic molecules available in nature (i.e., formic acid, lactic acid, fumaric acid, etc.).

2. Sensing of gases, vapors and VOC

One of the most appealing characteristic of MOFs, is their exceptionally high porosity which lead to very high specific surface area and pore volume. It has been reported that experimental Brunauer–Emmett–Teller (BET) surface areas can span from 2750 up to 7000 m^2g^{-1}, and pore volumes can reach up to 4.4 cm^3g^{-1} (Farha et al., 2012). This feature, together with the great compositional and structural diversity, and highly tunable functionality, make MOFs a material with great potential in gas storage and adsorption applications. In the same way, the chemical sensing of gas or other volatile compounds based on MOF materials is promising. In this field, the advantages of MOFs are many. For example, the large surface area make the surface host–guest interaction more efficient and the confined pores produce a concentration of target molecules to high levels thus enhancing the sensitivity. The tunable pore size and chemical environment of MOFs can be exploited to produce sensing selectivity toward specific compounds. Finally, the reversibility of the adsorption and desorption process of guest molecules, make MOFs regenerable and recyclable. All these features make MOFs ideal candidates in designing new sensing devices for volatile compounds. In Table 1 a representative list of molecules that can be detected by means of MOFs is reported. This list is not exhaustive and many other targets are continually added as the research in this field goes further.

The most common mode of sensing is based on the luminescence properties of the MOF. In the same way, colorimetric sensing is also very useful for its easy naked eye detection as other less common methods based on the magnetic properties of the material. All these features are the result of complex design of the MOFs which relies on the correct combination of metal ions and organic ligands. The organic ligands play a crucial role in the activation of the sensor and many different ligands has been proposed.

Table 1 List of representative class of compounds that can be detected by MOFs.

Gases	Aromatic VOC	Alyphatic VOC	Other
O_2	Benzene	Methanol	Organic amine
CO	Toluene	Acetone	Aniline
NO_x	Xylene and isomers	DMF	Drugs
SO_x	Nitrobenzene	Formaldehyde	Pesticides
NH_3	Trinitrotoluene	Acetaldehyde	
H_2S	Dinitrotoluene	Benzaldehyde	
HCl	Pyridine	Olefins	
H_2O vapors	Phenol		
	Dichlorophenol		

Usually, these ligands contains coordinating atoms or groups (as the carboxylate) and aromatic rings or C=C double bonds in order to exploit the presence of π electrons for interaction with the metal ion and the guest. Some of them present a quite complex molecular structure as the result of fine tuning of the properties. For these reasons, the molecular structures of the organic ligands will be showed within the text. In the next sections a selection of recent examples of this application will be discussed with particular regard to the structure of the MOF and the way of sensing through the mode of interaction of the target.

2.1 Sensing of oxygen

Molecular oxygen finds many applications as reactant in the chemical industry and for medical treatment. Oxidation reactions play an important role in the manufacturing of many chemicals, for example in the synthesis of ethylene oxide from ethylene or in the oxy-cracking process. The metallurgic industry consumes huge amount of oxygen in the smelting of iron ore into steel to remove sulfur and carbon impurities through the formation of their respective oxides. Oxygen is also the essential element for life, providing metabolic energy to cells through respiration. In the organisms, the concentration of oxygen must be maintained within a certain range. When the concentration of oxygen is altered, pathological conditions such as hypoxia can causes several diseases. Therefore, the detection of oxygen is very important in all that cases in which the required oxygen detection level ranges from the ppm level to ambient pressure.

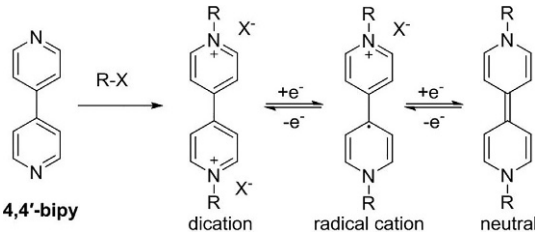

Fig. 5 Viologens and their redox reactivity.

The design of chromism-based oxygen sensors composed of MOFs have focused on viologen-functionalized MOFs. Viologens are a family of organic compounds based on the 4–4′-bipyridyl (**4,4′-bipy**) group. The alkylation of the nitrogen atoms produces a di-cation that undergoes highly reversible redox reaction (Fig. 5).

The di-cation form is usually colorless but after the first electron transfer a radical cation which displays a blue to green color is produced, depending on the alkyl group R. A second electron transfer yields a neutral yellow molecule. Viologen reacts fast with oxygen hence they represent an ideal sensor for this gas. A porous MOF based on methyl viologen cations has been reported by Gong and Lu (2013) as a fast and selective sensor for oxygen that is visible to the naked eye. The MOF contains cadmium ions and has the composition $(Me_2NH_2)_3(MV)_{1.5}[Cd_9(TTCA)_8]\cdot 15EtOH$, (MV = methylviologen and TTCA = triphenylene-2,6,10-tricarboxylate) (see Fig. 6).

Due to the effective photoresponse of the viologen compound, the color of MOF changes from dark-yellow to black after activation through X-ray irradiation. Upon exposure of the colored MOF to pure oxygen or to an oxygen containing atmosphere, the color returns to dark-yellow within 5 s and is visible with the naked eye. Notably, the color fails to change in the presence of other gases as N_2 and CO_2. Similar, porous and nonporous, cadmium-viologen-based MOFs showed good photochromic properties (Li et al., 2018). Notably the nonporous MOF changes both under in the presence or not of oxygen, whereas the porous MOF only changes color under anaerobic conditions and recovers immediately. Recently, phosphorescent coordination complexes of transition metals such as Ir^{3+}, Pt^{2+}, Pd^{2+}, and Ru^{2+} have been studied as oxygen sensors. A MOF containing a Pt(II)-porphyrin ligand (DBP-Pt; see Fig. 7) as an O_2-sensitive probe and a Rhodamine-B isothiocyanate (RhB; see Fig. 7) ligand as an O_2-insensitive

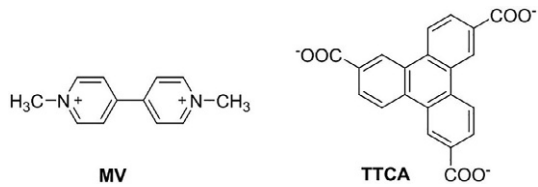

Fig. 6 Structures of the ligands MV and TCCA.

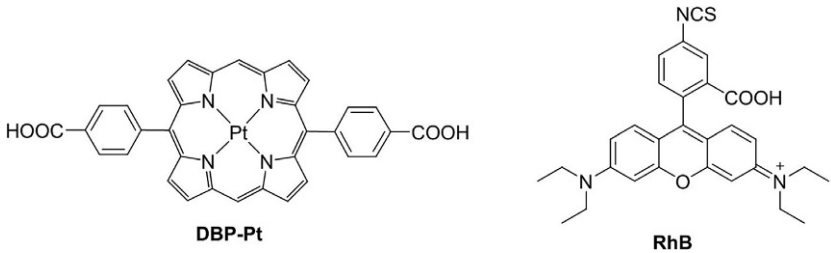

Fig. 7 Structures of the ligands DBP-PT and RhB.

reference probe, was designed by Xu et al. (2016). This phosphorescence/fluorescence dual-emissive MOF), was demonstrated to be useful as an intracellular oxygen sensor. This was the first example of an in vitro applicability of MOFs as intracellular oxygen biosensor.

Another type of MOF with excellent luminescence are transition metal-based MOFs, such as Zn^{2+}, Cu^{+}, and Cd^{2+} based MOFs. The use of metal as zinc or copper is very attractive for their low cost if compared with other noble metals commonly used. In this view, a highly porous and fluorescent MOF based on zinc ([Zn4O(bpz)2(abdc)] guest (bpz = 4-(3,5-dimethylpyrazol-1-id-4-yl)-3,5-dimethyl-pyrazol-1-ide, H2abdc = 2-aminoterephthalic acid; see Fig. 8), has been reported (Lin et al., 2013).

The material exhibits a blue photoluminescence and its application in sensing was tested with different gases. Oxygen was able to selectively quench the fluorescence of the MOF, and photoluminescence experiments showed a fast response. At 1 bar of oxygen, the fluorescence intensity was quenched by 96.5%, thus confirming the high oxygen-sensing efficiency. It was also demonstrated that the oxygen sensing process is rapid, reversible, and highly stable: these results are possible thanks to the presence of an appropriate size of the cavity which allow oxygen to efficiently enter and interact with the MOF. Recently, a new type of MOFs has been reported by Huang et al. (2017) combining the silver(I) chalcogenide/chalcogenolate clusters (SCCs) with a metal–organic framework to construct rigid SCC-based

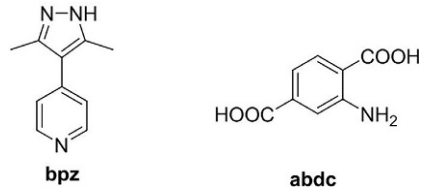

Fig. 8 Structures of the ligands bpz and abdc.

MOFs. Chalcogenide are compounds containing one chalcogen anions (usually a sulfide or a selenide), and in this case the silver cation is combined with the organic *tert*-butyl sulfide. When this cluster is combined with 4,4-bipyridine (4,4′-bipy; see Fig. 5), a stable porose MOF is obtained. The SCCs remain stable in air for more than 1 year and functions as an ultrafast visual fluorescence turn-off oxygen sensor. The luminescent response was reversible and tested for 100 cycles without performance loss.

2.2 Sensing of water vapor

The quantitative detection of water vapor is of great importance in many industrial manufacturing processes. Humidity must be controlled to maintain the quality, yield, or reliability of the final product. In some cases, material development and device fabrication must take place in specially designed ultralow-humidity dry rooms. Moreover, water is closely related to almost all conditions required to sustain life. Water sensors are widely applied in chemical industrial processes, environmental monitoring, food and pharmaceutical processes. Thus, an easy, rapid and highly sensitive water sensor is highly desirable. Magnetic MOF-based water sensors have been widely studied in the past few years. Microporous magnets compose a class of multifunctional molecule-based materials where desolvation-driven structural transformation leads to the switching of magnetic properties. An example (Xin et al., 2019) is the cyanido-bridged dysprosium-cobalt bimetal MOF $\{[Dy^{III}(H_2O)_2][Co^{III}(CN)_6]\}$. Upon dehydration and rehydration, an important change in the coordination geometry of Dy^{3+} occurs in a reversible SCSC (single crystal to single crystal) transformation. This results in a switch in the SMM (single-molecule magnet) behavior. The hydrated compound does not show SMM behavior whereas the dehydrated one has the desired SMM property. Colorimetric water sensors have been investigated by some groups. A cobalt based MOF (Chen et al., 2013a,b) with the formula of [Co1.5(tipb)(SO_4)(pta)0.5] (DMF)1.7 (1,3,5-tris(*p*-imidazolylphenyl)benzene (tipb), and terephthalic acid = H2pta) was obtained in a stable porous form displaying a blue color (Fig. 9).

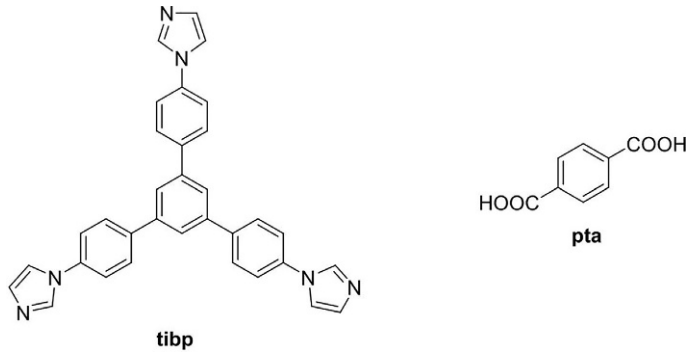

Fig. 9 Structures of the ligands tibp and pta.

When this material is exposed to air, the blue crystals gradually turn to red without losing crystallinity. It has been demonstrated that the MOF undergoes a reversible SCSC transformation as the consequence of the displacement of the pta ligand by water present in the air as moisture. The color change is caused by the changing of the coordinated configuration of the Co^{2+} ions from a four-coordinate tetrahedral coordination geometry to a six-coordinate octahedral coordination geometry. Notably, this change of coordination is reversible, thus making this MOF a good candidate as a colorimetric water-sensing material. An interest application of copper based sensor has been reported by Ullman et al. (2018) for the MOF $Cu_3(BTC)_2$ (BTC = 1,3,5-benzenetricarboxylate). The material was made in form of thin films using the spin coating method. The films worked as a colorimetric sensor for water vapors. The color change is attributed to the alterations in the d–d electrons transitions by the coordinated interaction between water and the metal center. The copper-based 3D-MOF [Cu(HL)-(DMSO) (MeOH)]n (H_3L = triphosphaazatriangulene; see Fig. 10) was reported by Nakatsuka et al. (2020) to have a reversible stimuli-responsive SCSC transformation. After exposition to water molecules, the color of the crystal slowly changes from yellow to blue-green, as a consequence of the coordination of water molecules by the Cu^{2+} ion. Again, notably these transformations are reversible, even within the single crystal.

The use of luminescent MOF (LMOFs) has been also widely investigated. An interest example (Chen et al., 2017) is the microporous Zn-MOF ($Zn(hpi_2cf)(DMF)(H_2O)$, H_2hpi_2cf = (5-(2-(5-fluoro-2-hydroxyphenyl)-4,5-bis(4-fluorophenyl)-1*H*-imidazol-1-yl)isophthalic acid) see Fig. 11). Thanks to the presence of an excited state intramolecular proton transfer (ESIPT) of the ligand, this Zn-MOF, which contains micropores (<3 Å),

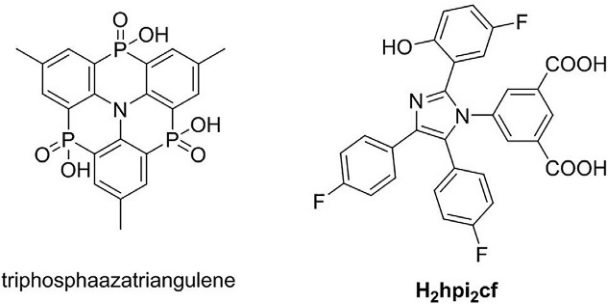

Fig. 10 Structures of the ligands triphosphaazatriangulene and H_2hpi_2cf.

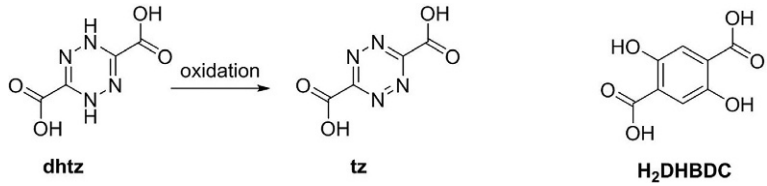

Fig. 11 Structures of the ligands dhtz, tz, and H_2DHBDC.

undergoes extremely facile SCSC transformation driven by reversible removal/uptake of coordinating water molecules simply stimulated by dry gas blowing or gentle heating at 70 °C. The reversible interconversion between the hydrated and dehydrated phases, activate the ESIPT process on the ligand thus resulting in sensitive two-color photoluminescence with the emission from blue at 463 nm to a cyan color at 493 nm. The blue emission rapidly shifts to a cyan color in a matter of seconds when blowing dry gases, and the color is easily restored upon exposure to wet gases or air.

2.3 Sensing of hazardous gases

Toxic gases such as H_2S, SO_2, NH_3, CO, NO, and NO_2 are detrimental to the environment and human health. They can be produced from industrial activity, but combustion exhaust is the largest source of these pollutant. These compounds are toxic, and in the case of NO_2 and SO_2, they contribute to acid rain. Thus, the detection of these destructive gases is a substantial component of air quality monitoring. The most important results have been obtained with the use of luminescent MOFs. For example (Nickerl et al., 2015), a LMOF based on the stable structure UiO-66 ($Zr_6O_4(OH)_4(pta)_6$, for pta; see Fig. 9) was modified with the introduction of dihydro-1,2,4,5-tetrazine-3,6-dicarboxylate (dhtz; see Fig. 11) ligand

molecules at approximate a 5:1 pta/dhtz. This dihydro-1,2,4,5-tetrazine unit can be easily oxidized to 1,2,4,5-tetrazine (tz; see Fig. 11), producing a clear colorimetric shift from yellow to pink as a result of increased blue-green light absorbance. Upon exposure to NO, NO_2, and Br_2 gas, the dhtz ligands were oxidized giving a clear color change from yellow to pink. This oxidation could be fully reversed by suspending the material in an aqueous solution with the reducing agent sodium dithionite, allowing the material to be used again. Ammonia can be detected selectively (Shustova et al., 2013) at high temperatures through with the Mg^{2+} containing MOF Mg(H_2DHBDC) (H_2DHBDC^{2-} = 2,5-dihydroxybenzene-1,4-dicarboxylate; see Fig. 11) that induces a significant redshift in emission from the LMOFs. At room temperature, emission from the material redshifts when exposed to NH_3, triethylamine, and ethylene diamine, but once heated to 100 °C, redshifted emission is only observed when the material is exposed to NH_3. Then ammonia could be removed under vacuum for 15 min, allowing the sensor material to be reused.

2.4 Sensing of VOC

Volatile organic compounds (VOCs) are defined as organic pollutants with the boiling points between 50 and 260 °C at room temperature and atmospheric pressure. They are widely applied in numerous ways by various industries and as component of many products of everyday use. VOCs mainly contain aliphatic hydrocarbons, aromatic hydrocarbons (benzene, toluene, xylene, etc.), ketone (acetone and butanone), alcohols (methanol, ethanol, butanol), aldehydes (formaldehyde, acetaldehyde), and chlorinated hydrocarbons (dichloromethane, chloroform). Large amounts of VOCs compounds are released to the environment each year. Most of the VOCs are toxic pollutants that substantially compromise human health and the ecosystem. Aromatic VOCs comprise benzene an its derivatives as nitrobenzene, anilines, and halogenated aromatic compounds. They are significantly used in a variety of industries as solvents or as components in coatings. Aromatics are also important precursor for the production of a large number of chemicals as pesticides and medicinal precursors or for the synthesis of monomers useful for the preparation of many materials. Vehicle exhaust is another common source of aromatic VOCs. Exposure to aromatic VOCs can be an hazard for employees working in industries and an environmental threat. Among them, chlorinated volatile organic compounds (Cl-VOCs) have more severe toxicity, high chemical stability,

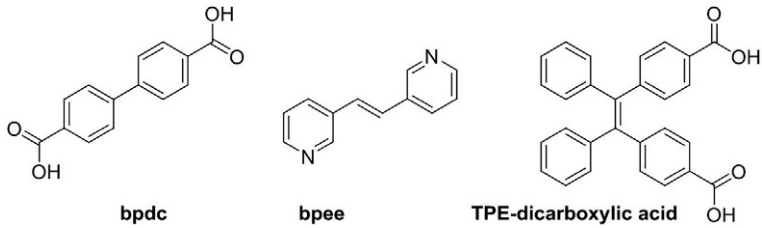

Fig. 12 Structures of the ligands bpdc, bpee and TPE-dicarboxylic acid.

and low biodegradability that are regarded as hazardous gas pollutants and listed as targeted highly harmful emissions in most countries. Nitroaromatic compounds (NACs) were can be efficiently detected in the vapor phase by LMOF materials. The luminescent MOF $Zn_2(bpdc)_2(bpee)$ (bpdc = 4,4′-biphenyldicarboxylate, bpee = 1,2-bipyridylethene; see Fig. 12), a porous and strongly LMOF with blue emission (Lan et al., 2009). This material is able to detect highly explosive vapors of dinitrotoluene (DNT) or nitrobenzene (NB) low ppm concentrations after a 10 s exposure. This behavior was fully by heating the sensor LMOF at 150 °C for about 1 min. An interesting LMOF-based sensor of aromatic VOC was reported constructed used a tetraphenylethene (TPE) derivative (Zhang et al., 2014). In this work, a responsive turn-on fluorescence was introduced into a zinc based MOF by using the TPE-based ligand 4,4′-(2,2-diphenylethene-1,1-diyl)dibenzoic acid (see Fig. 12). The phenyl rings were incorporated into the MOF to detect the aromatic guest molecules through the interactions between the host and guest. Different types of aromatic hydrocarbons, as benzene, toluene, xylene, and mesitylene, induce various emission peaks by altering the conformation of the ligand.

An example of a moisture-stable LMOF able to detect nitroaromatic compounds was prepared by Qin et al. (2015) using the metal ion Tb^{3+} with the ligand 5-(4-carboxyphenyl)pyridine-2-carboxylate (cppa, see Fig. 13). When exposed to nitrobenzene and meta nitrobenzene vapors, the emission from the LMOF was quenched. Due to its water stability, the LMOF shows high selectivity and sensitivity toward nitroaromatic explosives in both aqueous and vapor phases. Some LMOFs are also able to detect amine and aldehyde vapors (Zhang et al., 2016). With the use of a resorcin[4]arene-based octacarboxylate ligand H_8L (see Fig. 13), two family of MOFs have been prepared, one with cadmium and the other with zinc ions. These materials exhibited blue-green ligand-based emission, which was quenched following short exposure to amine and aldehyde vapors. These

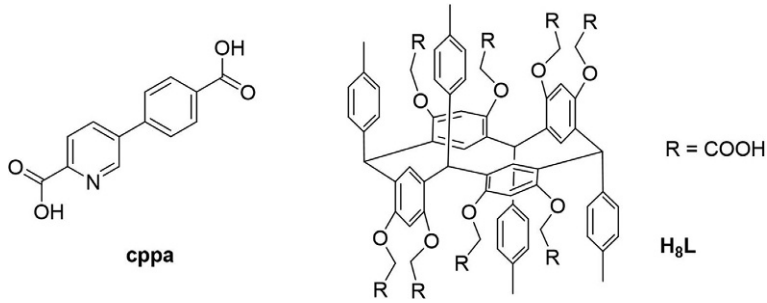

Fig. 13 Structures of the ligands cppa and of resorcin[4]arene-based ligand H_8L.

sensors were able to recognize different class of volatile organic compounds as formaldehyde, ethanal, propanal, butanal, pentanal, hexanal, and benzaldehyde. Interestingly, also some amines as ammonia, ethylamine, diethylamine, trimethylamine, propylamine, butylamine, and aniline were detected.

2.5 Sensing of small organic molecules

MOFs have shown to be useful also in the detection of more complex small organic molecules. These materials can find application in the sensing of biological active molecules as pesticides or even drugs. The detection of polychlorinated dibenzo-*p*-dioxins (PCDDs; see Fig. 14), an important class of persistent and highly toxic organic pollutants, has been efficiently achieved with a zirconium-based MOF embedding the CPTTA ligand (Wang et al., 2019; see Fig. 14). The interaction of this MOF with diverse PCCD caused the fluorescence-quenching of the system thus allowing the detection with high sensitivity. The process is a consequence of the π-π interaction of the host with the aromatic ligand.

Dopamine (3,4-dihydroxyphenylethylamine), an important neurotransmitter that is involved in the activity of the central nervous system, can be detected with the water stable Tb^{III} MOF $\{[Tb(Cmdcp)(H_2O)_3]_2(NO_3)_2 \cdot 5H_2O\}_n$ ($H_3CmdcpBr$ = *N*-carboxymethyl-(3,5-dicarboxyl)pyridinium bromide; see Fig. 15) (Wu et al., 2021). The mechanism relies on the spontaneous polymerization of dopamine. Under optimized conditions, the formed poly-dopamine interacts with MOF and quenches its green luminescence with high sensitivity and selectivity. Interestingly, this process is not interfered by other bio-related organic substances or metal ions, making the system applicable in biological fluids as serum and urine. Another example of sensing with potential medical application (Liu et al., 2020) is the use

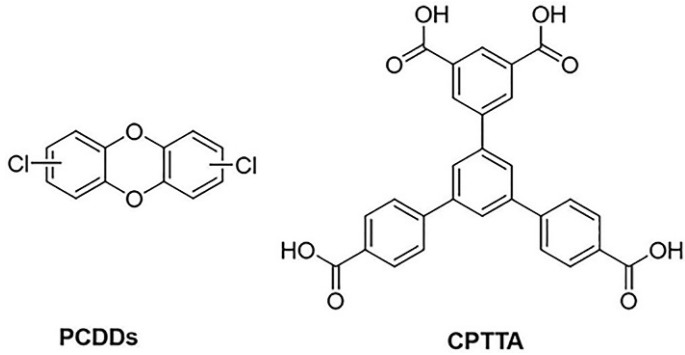

Fig. 14 Structures of the ligands CPTTA and of PCCDs.

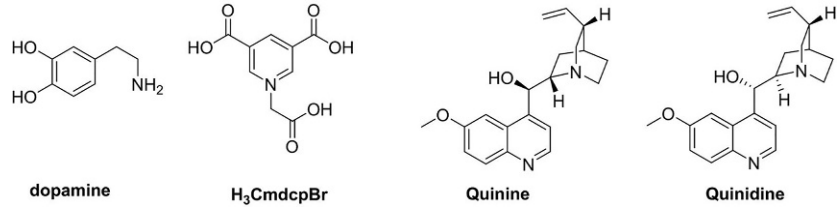

Fig. 15 Structures of the ligands H_3CmdcpBr and of dopamine, quinine and quinidine.

of a fluorescent probe based on a cadmium MOF embedding the ligand bpdc (see Fig. 12). This MOF is chiral, and this property can be exploited to selectively recognize the different enantiomers of a molecule.

In this case, the material was used in the recognition and detection of quinine and quinidine (see Fig. 15), a class of important antimalarial drugs, which can be applied as antipyretics, painkillers, anti-inflammatory agents and even certain heart diseases. The detection occurs through to multiple quenching mechanisms, including the competitive absorption of excitation light.

3. MOFs for sensing of biomolecules

Metal-organic frameworks (MOFs) are a novel kind of highly porous crystalline material, constructed by the self-assembly of inorganic metal-containing nodes and organic ligands through coordination linkage. They can be described as a class of porous coordination polymers based on metals and organic ligands (Furukawa et al., 2013; Zhou and Kitagawa, 2014). The

metal-organic connections are able to produce one, two and tri-dimensional structures thus allowing the design of new materials with different behaviors.

Several methodologies have been reported in the attempt to miniaturize MOFs to the nanoscale, which is vital for their use in biomedical applications. Porous nano-MOFs must be designed to display other excellent properties, such as drug storage–release capabilities, high biocompatibility and degradability, in order to make them appealing candidates for biomedical utility (Anderson and Stylianou, 2017; Imaz et al., 2011; McKinlay et al., 2010; Zhang et al., 2015b). Moreover, sensing biorelevant species, as required by advanced biological devices, in imaging applications, and for more basic understanding of biological functions, is of increasing interest, as is monitoring temperature and pH using fluorescent probes.

Due to the progressive development of MOFs synthetic processes and their considerable potential applications, integrating biomolecules into MOFs has recently gain considerable attention. Biomolecules, including lipids, oligopeptides, nucleic acids, and proteins have been readily incorporated into MOF systems exploiting different formulation methods. The formed biomolecule-MOF hybrid structures have shown promising applicability in various fields, such as antitumor treatment, gene delivery, biomolecular sensing, and nanomotor devices (Zhuang et al., 2017).

The ability to exchange the metal centers and insert different organic linkers provide a potential infinite library of MOFs materials. Beside this feature, the integration of small guest molecules within the MOFs pores, from small molecules to drugs and biomolecules, could be of particular interest for delivery applications in the field of nanomedicine (Horcajada et al., 2010). Indeed, several of the key inherent properties of MOFs make them great candidates for such drug delivery systems (DDSs). Among the advantages in their use, worth to be mentioned are the fact that multiple strategies are available to incorporate the guest molecules within the MOFs structures (Fujita et al., 2012) and, secondly, that the interactions between the guests and MOF linkers or metal nodes allow a high drug loading capacity. Additionally, the tunable sizes of MOF crystals can be optimized for a specific cellular uptake, (Zhuang et al., 2014) or for inducing a guest-MOF dissociation in stimuli-responsive materials, thus triggering the guest release.

The biosensing potential of MOFs has been greatly expanded by recent post-synthetical methods that allow the addition of pendent functional groups on some of the pre-existing MOFs and NMOFs structures; these strategies may be employed to tag MOFs with biomolecules (e.g., nucleic

acids, proteins, antibodies and enzymes) (Feng et al., 2015; Kumar et al., 2015; Zhuang et al., 2017). As an example, Kumar et al. (Kumar and Deep, 2014) reported the activation of MOFs tagged with an anti-BSA antibody and used for specific sensing of bovine serum albumin (BSA) in an aqueous medium.

Recently, the integration of big guest biomolecules within MOF materials has also driven great attention (Deng et al., 2012). Such biomolecules and macromolecules include vitamins and oligopeptides, as well as nucleic acids, lipids and proteins (Fujita et al., 2012; Zhuang et al., 2017). Due to their vast diversity and usual large size, their loading inside MOFs structures is more complicated. For example, integrating the guest macromolecules via electrostatic interactions or linking them to the structure by covalent bonding, which are common approaches used for small molecules, might not be ideal due to their larger sizes and complicated structures, which could impair a proper surface functionalization. Moreover, avoiding loss of functionality of the guest upon formation of the bio-MOF is challenging, since the incorporation process can affect the biomolecules delicate secondary or tertiary structures. Several pioneering works on integrating biomolecules with polymeric or inorganic materials have demonstrated the importance of these requirements and shed light on the design of MOF-based biomolecule delivery systems (Algar et al., 2011; Katz and Willner, 2004). A crucial factor remains the design of proper MOF carriers to improve biocompatibility.

Another valuable approach to modify MOFs for the design of DDSs consists in their post-synthesis surface functionalization. As an example, it is reported in literature that different oligopeptides have been conjugated to the external surface of MOF particles. Taylor et al. and Yang et al. both reported methods to graft specific peptides onto MOF nanoparticles (Taylor et al., 2009; Yang et al., 2014). These MOFs are synthesized first with encapsulated imaging agents or desired drugs; then, a layer of silica is coated on the surface of the MOF nanoparticles and grafted by silyl derived cyclic oligopeptide c(RGDfK); this fragment is able to target the αvβ3 integrin, a protein that is overexpressed in many tumor cells (Janssen et al., 2002). As a consequence, this system shows enhanced cellular uptake in cancer regions, as observed for c(RGDfK)-integrated MOF particles exploited for imaging and drug delivery.

Zhang et al. reported another work on grafting SGDEVDK oligopeptide onto MOF particles' surfaces also utilizing a silica coating (Fig. 16) (Zhang et al., 2015a). Firstly the oligopeptide chain is grafted to the silica shell, then a

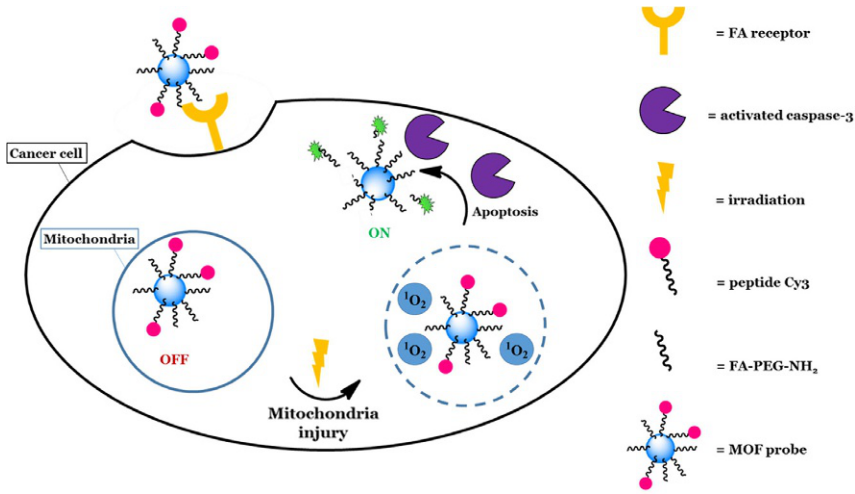

Fig. 16 MOF the for detection of cellular apoptosis activity: oligopeptide-Cy3 conjugated MOF and its fluorescence after caspase-3 cleavage (Zhang et al., 2015a).

dye, in this specific case Cy3, is coupled to the oligopeptide and the fluorescence is quenched when coupled. Since the oligopeptide is cleaved by caspase-3, which is activated during cell apoptosis, this MOF system can be used as a tool for the detection of cellular apoptosis activity. In fact, after its cleavage from the framework, the Cy3 fluorescence activity reappears, and this allows the monitoring of cellular apoptosis. However, up to now, it seems that a silica shell is necessary for the oligopeptide coating, so only the MOFs suitable for silica coating can be selected for this method.

Rosi et al. made pioneering achievements on metal–nucleobase syntheses (An et al., 2009, 2012). They synthesized a MOF including Zn2+, adenine and biphenyldicarboxylate (An et al., 2009). The anionic zeta-potential of the synthesized bio-MOF, due to the presence of nucleobases, facilitates the subsequent guest loading, especially of cationic molecules. In their experiments (An et al., 2009), Rosi et al. selected a antiarrhythmic drugs, such as procainamide in the form of HCl salt, encapsulated inside the framework through electrostatic interactions and released by simple cation exchange processes (Fig. 17). This kind of DDSs could be able to sense a variation in the ionic concentrations in different body districts, leading to the release of the drug in specific sites.

More complex is the case of using oligonucleotides and coupling them with MOF linkers. Oligonucleotides can indeed diffuse from the MOF surface to the inner core, due to their affinity toward the metal centers

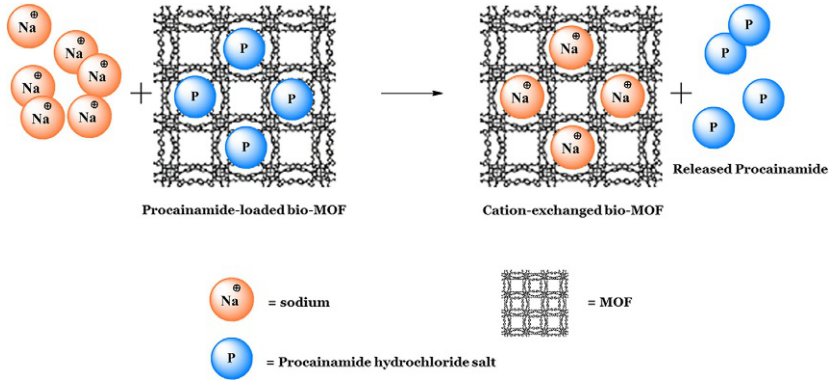

Fig. 17 Scheme depicting cation-triggered procainamide release from bio-MOF (An et al., 2009).

and MOF inner microenvironments. When this drawback is overcome, oligonucleotide-MOF complexes can be interestingly used as platforms for nucleic acid detection and gene delivery.

Different affinities of ss- and dsDNA (single-stranded and double-stranded) to MOF-based complexes are used in an elegant system for DNA sensing (Müller-Buschbaum et al., 2015; Wang et al., 2014) (Fig. 18). In general, the luminescence of a fluorescent labeled ssDNA probe is completely quenched after incorporation in the MOF via a contact quenching mechanism. However, the addition of a complementary ssDNA results in a stable helix formation, followed by the release of the dsDNA due to the lower affinity for the MOF platform. This allows a turning-on of the luminescence with a selectivity down to a single nucleotide mismatch and nanomolar detection limits (Müller-Buschbaum et al., 2015; Zhu et al., 2013).

With this aim, a fascinating *N,N′*-bis(2-hydroxyethyl)dithiooxamidato copper(II) (H2dtoaCu) MOF for DNA/RNA detection has been reported in literature (Chen et al., 2013a,b; Ye et al., 2014; Zhu et al., 2013). Carboxyfluorescein (FAM)-labeled oligonucleotide probe sequences have been adsorbed and complexed with the MOF structure via hydrophobic and π-stacking interactions. The fluorescence of FAM is quenched when in proximity to MOF due to a phenomenon involving photoinduced electron transfer (PET) from FAM to the paramagnetic Cu2+ nodes present in the MOF. Once the complex is employed, if the target DNA/RNA sequence is present in solution, it couples with the adsorbed probe strand. The hybridized DNA/RNA complex maintains a distance from the MOF structure which is sufficient for FAM to recover its fluorescence (Fig. 18).

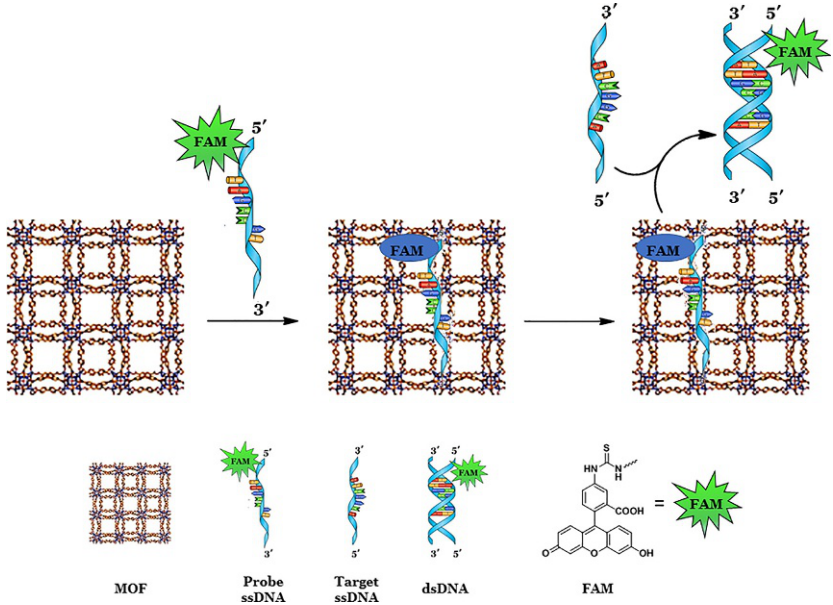

Fig. 18 Illustration of the "turn-on" detection of ssDNA based on MOF sensors. In the dark state, encapsulation of the FAM-labeled probe DNA results in fluorescence quenching, whereas after double-strand formation with the target ssDNA, dsDNA is released, and fluorescence is "switched on" (Wang et al., 2014).

This method has been used, for instance, in the detection of HIV-1 RNA, (Chen et al., 2013a,b) HIV DNA, (Zhu et al., 2013) HIV/HBV DNA, (Ye et al., 2014) and many more (Zhuang et al., 2017). The fields of applications of luminescent MOFs (LMOFs) has been recently extended to various types of biosensing, especially when they display properties like dispensability, biocompatibility and biodegradability, like in the case of some nanocrystal-MOFs (NMOFs); this research area appears to be attractive but still remains largely unexplored (Kumar et al., 2015).

Another MOF scaffold, namely UiO-66, has been also used as a platform for the detection of miRNA (Wu et al., 2015a). Similarly, FAM-labeled peptide nucleic acid probe has been adsorbed and confined inside the MOF pores. The complex was thus able to in situ monitor the dynamic change of miRNA expression in living cancer cells based on the amount of target miRNA present and subsequent fluorescence change. Besides using fluorescence recovery assay as a tool to detect the target DNA/RNA amounts, fluorescence anisotropy (FA) is also tested for the detection of

target DNA in oligonucleotide-MOF system (Guo et al., 2014). In addition to DNA/RNA detection, oligonucleotide adsorbed MOF platforms can also facilitate delivery of nucleic acids.

Apart from oligonucleotides, proteins are other biological macromolecules with delicate conformational structures. They display a variety of essential roles in metabolism, DNA replication, cellular signaling and stimuli-responsiveness, and in molecular transports. Unlike oligopeptide or oligonucleotide incorporation, it is challenging to directly adsorb or encase proteins in a microporous MOF core, due to the bulky structures these macromolecules usually have. Therefore, new strategies to accommodate proteins inside the MOFs have been developed in the last years (Zhuang et al., 2017). De novo protein encapsulation is a new approach to this aim: proteins are dispersed in the solution where MOF formation is taking place. MOF particles tend to grow around proteins and eventually encapsulate them (Fujita et al., 2012). As an example of this technique, Lyu et al. reported the embedment of cytochrome *c* (Cyt *c*) into MOF ZIF-8, (Lyu et al., 2014) forming a structure where Cyt *c* is found on the surface region of ZIF-8 crystals, which has a greater Zn2+ abundance. This occurs due to the strong coordination interaction between the metals and the amidic bonds of the protein, resulting in a successful encapsulation. Interestingly, embedded Cyt c shows 10-fold activity enhancement for the detection of peroxide species with respect to the wild-type. This feature can be therefore exploited for a practical sensing application of this protein-MOF interaction.

The synthetic approach has been applied by the same group, by co-entrapping two proteins inside the MOF structure (Wu et al., 2015b). In this case, a glucose oxidase (GOx) and a horseradish peroxidase (HRP) were encapsulated inside MOF ZIF-8; they were observed to localize in different MOF regions, due to their chemical-physical peculiarities. What is to be underlined, is the fact that the embedment of these two enzymes has a synergetic effect on the detection of hydrogen peroxide by UV–Vis assay.

Other ZIF-family MOFs, like ZIF-90 or ZIF-8, have been selected for embedding different proteins via the de novo approach: BSA, catalase, ovalbumin, and many more have been exploited for testing new biological sensing platforms (Cui et al., 2017; Zhuang et al., 2017).

For proteins with rigid conformation and large size, it is unlikely to be able to immobilize them within MOF pores. Therefore, the main approach to synthesize these complexes is usually to adsorb the proteins outside MOFs. These formed protein-coated MOF systems find an application as

a tool for protein detection and delivery. In this context, Ma et al. reported the synthesis of methylene green (MG) and glucose dehydrogenase (GDH) co-adsorbed onto the external surface of five ZIF-type MOFs (Jiang et al., 2013). In particular, it was observed a high GDH adsorption capacity on ZIF-70, caused by strong interactions between the proteins and ZIF-70, which include hydrophobic and electrostatic forces. Lastly, an electrochemical detecting system has been built, based on the MG/GDH-loaded ZIF-70, and real-time glucose levels in guinea pig brains have been successfully monitored (Fig. 19).

In other interesting applications, nano-sized MOFs can be efficiently used as contrast agents for magnetic resonance imaging (MRI), with a large number of highly paramagnetic metal ions that can be added to their structures both as connectivity centers and within the pores (Müller-Buschbaum et al., 2015). Both Gd3+ and Mn2+-based nanoMOFs have shown impressive relaxivities (Taylor et al., 2008a), with the main drawback of toxicity due to Gd3+ leaching solved by its possible substitution with the well-tolerated Mn2+, like in the nanoMOFs Mn(BDC)(H2O)2 and Mn3(BTC)2(H2O)6 (Taylor et al., 2008b). These MOFs were coated with a thin silica shell, and their surfaces were functionalized with a peptide for tumor-specific targeting (cyclic arginine-glycine-aspartate RGD), enhancing their cellular uptake. MOFs have also been investigated regarding CT-imaging techniques; for example, different iodinated MOFs, like [Cu(I4-BDC)(H2O)2].2H2O and [Zn(I4-BDC)(EtOH)2].2EtOH, contain exceptionally high iodine contents, up to 63 wt%, and display a X-ray attenuation coefficient comparable to the reference molecular contrast agent Iodixanol (DeKrafft et al., 2009). Different affinities of lumophores to healthy and damaged tissues can be employed in optical imaging as a mild and non-invasive

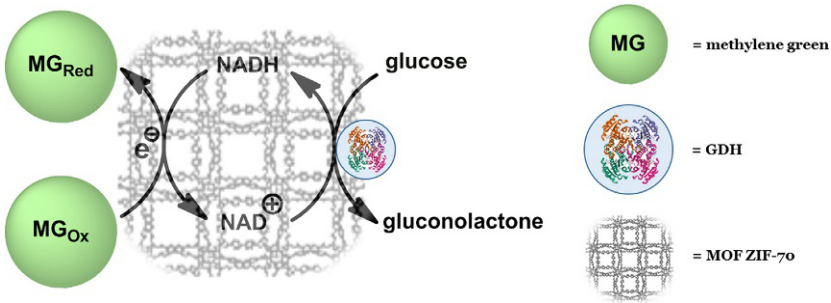

Fig. 19 Scheme of the electrochemical detecting system for in vivo glucose monitoring (Jiang et al., 2013).

method for the identification of tumors, like the nanoscale coordination polymer containing [Ru(5,5′-COO-biby)(biby)2] units as luminescent ligands, that was established as an imaging contrast agent with an enhanced uptake of the nanostructures in H460 human non-small cell lung cancer cells, highlighting the potential of MOF nanostructures as highly emissive optical contrast agents for non-invasive bioimaging.

An interesting potential biosensing application involves the detection of dipicolinic acid (DPA), a major component of the bacterial endospores, among which *Bacillus anthracis* is a prominent example. In this regard, a europium containing MOF has been employed for biosensing via luminescence detection. In details, the MOF [Eu2(FMA)2(OX)(H2O)4].4H2O exhibited sensitive, selective and instant "turn-on" sensing of dipicolinic acid (Xu et al., 2012). The nanoscale nature of this MOF enables dispersion in solvents and significantly enhanced the sensitivity level up compared to the normal bulk material by 90 times for sensing of 2 ppm of DPA. The limit threshold seems to be around only 0.1 ppm. It is worth noticing that this sensing is almost unaffected by the other co-existing components in the bacterial endospores such, as for instance, phthalic acid, isophthalic acid, terephthalic acid, riboflavin, D-phenylalanine, and several ions.

Luminescent MOFs have recently found new application in the intracellular sensing of the biologically relevant species NO radical and Fe2+. In the first case, a Cu-based MOF is employed: after addition of NO radicals, reduction of Cu2+ to Cu+ resulted in a significantly enhanced luminescence, that could be utilized for the intracellular detection of NO radicals. In fact, the triphenylamine emission in Cu-tca [Cu3(H2O)3(tca)2] is usually quenched by the paramagnetic Cu2+ centers. Interestingly, the luminescence occurs without any interference with other small molecules of biological relevance such as H2O2, nitrites, N-peroxides, and hypochlorite (Wu et al., 2012). Intracellular ferrous sensing was instead obtained by the selective quenching of MOF [Al(OH)(bpydc)] fluorescence in the presence of Fe2+ ions in HeLa cells, monitored by confocal fluorescence microscopy (Lu et al., 2014).

Other intracellular sensing assays developed involved, for instance, the in vitro detection of H2S in HeLa cells; it occurred by turn-on fluorescence observed for malonitrile and azide-functionalized MOFs (MN-ZIF-90 (Li et al., 2014) and UiO-66@N3 (Müller-Buschbaum et al., 2015), respectively). Real-time sensing of intracellular pH-values was instead achieved with Zr-based UiO-type MOFs containing covalently attached fluorescein moieties (He et al., 2014): the monitoring of the intracellular pH-change

occurred through confocal laser scanning microscopy, since processes such as the nano-MOF endocytosis and its endosomal maturation could be followed in real-time measuring the fluorescence of the dye.

4. Conclusions

Bio-ligands are an attractive family of molecules that can be incorporated into MOF structures, with beneficial features such as multiple coordination sites, preinstalled chirality, tunable hydrophobic/hydrophilic features, specific recognition/self-assembly capabilities, and they provide ideal characteristics for biomedical applications, sensing as well as drug delivery. Bio-ligands are commercially available in high purities, or can be easily synthesized, providing a nearly endless variety of possible ligands, and therefore potential infinite MOF scaffolds. Their ability to bind through multiple coordination sites can afford the formation of flexible or robust BioMOFs frameworks, where both families are important in different applications (Anderson and Stylianou, 2017). BioMOFs have two major advantages that make them useful as novel sensors. First, they usually exhibit high surface areas, and second, interactions between guest molecules and the MOFs pores are able to induce changes in their physical properties. Thus far, however, few BioMOFs sensors or biosensors based on MOFs scaffolds have been reported in literature. The general current challenges to be overcome include: the loading capability optimization inside the MOFs structures, evidences of MOF scaffold biocompatibility and, concerning BioMOFs, the biomolecules structure-functionality preservation of macromolecules during encapsulation or grafting processes for BioMOF synthesis (Imaz et al., 2011).

References

Algar WR, Prasuhn DE, Stewart MH, et al.: The controlled display of biomolecules on nanoparticles: a challenge suited to bioorthogonal chemistry, *Bioconjug Chem* 22: 825–858, 2011.

An J, Geib SJ, Rosi NL: Cation-triggered drug release from a porous zinc – adeninate metal – organic framework, *J Am Chem Soc* 131:8376–8377, 2009.

An J, Shade CM, Chengelis-Czegan DA, et al.: Zinc-adeninate metal – organic framework for aqueous encapsulation and sensitization of near-infrared and visible emitting lanthanide cations, *J Am Chem Soc* 133:1220–1223, 2011.

An J, Farha OK, Hupp JT, et al.: Metal-adeninate vertices for the construction of an exceptionally porous metal-organic framework, *Nat Commun* 3:604, 2012.

Anderson SL, Stylianou KC: Biologically derived frameworks, *Coord Chem Rev* 349: 102–128, 2017.

Chen Y, Lykourinou V, Vetromile C, et al.: How can proteins enter the interior of a MOF? Investigation of cytochrome c translocation into a MOF consisting of mesoporous cages with microporous windows, *J Am Chem Soc* 134:13188–13191, 2012.
Chen Q, Chang Z, Song WC, et al.: A controllable gate effect in cobalt(II) organic frameworks by reversible structure transformations, *Angew Chem Int Ed Engl* 52: 11550–11553, 2013a.
Chen L, Zheng H, Zhu X, et al.: Metal–organic frameworks-based biosensor for sequence-specific recognition of double-stranded DNA, *Analyst* 138:3490–3493, 2013b.
Chen L, Ye JW, Wang HP, et al.: Ultrafast water sensing and thermal imaging by a metal-organic framework with switchable luminescence, *Nat Commun* 8:1–10, 2017.
Cohen SM: The postsynthetic renaissance in porous solids, *J Am Chem Soc* 139:2855–2863, 2017.
Cui J, Feng Y, Lin T, et al.: Mesoporous metal-organic framework with well-defined cruciate flower-like morphology for enzyme immobilization, *ACS Appl Mater Interfaces* 9:10587–10594, 2017.
DeKrafft KE, Xie Z, Cao G, et al.: Iodinated nanoscale coordination polymers as potential contrast agents for computed tomography, *Angew Chem Int Ed Engl* 48:9901–9904, 2009.
Deng H, Grunder S, Cordova KE, et al.: Large-pore apertures in a series of metal-organic frameworks, *Science* 336:1018–1023, 2012.
Ding M, Flaig RW, Jiang H, et al.: Carbon capture and conversion using metal–organic frameworks and MOF-based materials, *Chem Soc Rev* 48:2783–2828, 2019.
Eddaoudi M, Kim J, Rosi N, et al.: Systematic design of pore size and functionality in isoreticular MOFs and their application in methane storage, *Science* 295:469–472, 2002.
Evans JD, Bon V, Senkovska I, et al.: Four-dimensional metal-organic frameworks, *Nat Commun* 11:2690–2700, 2020.
Farha OK, Eryazici I, Jeong NC, et al.: Metal-organic framework materials with ultrahigh surface areas: is the sky the limit? *J Am Chem Soc* 134:15016–15021, 2012.
Feng D, Liu TF, Su J, et al.: Stable metal-organic frameworks containing single-molecule traps for enzyme encapsulation, *Nat Commun* 6:5979, 2015.
Férey G, Mellot-Draznieks C, Serre C, et al.: Chromium terephthalate-based solid with unusually large pore volumes and surface area, *Science* 309:2040–2042, 2005.
Fujita M, Kwon YJ, Washizu S, et al.: Preparation, clathration ability, and catalysis of a two-dimensional square network material composed of cadmium(II) and 4,4′-bipyridine, *J Am Chem Soc* 116:1151–1152, 1994.
Fujita D, Suzuki K, Sato S, et al.: Protein encapsulation within synthetic molecular hosts, *Nat Commun* 3:1093–1097, 2012.
Furukawa H, Cordova KE, O'Keeffe M, et al.: The chemistry and applications of metal-organic frameworks, *Science* 341:6149, 2013.
Gong YN, Lu TB: Fast detection of oxygen by the naked eye using a stable metal–organic framework containing methyl viologen cations, *Chem Commun* 49:7711–7713, 2013.
Guo JF, Li CM, Hu XL, et al.: Metal–organic framework MIL-101 enhanced fluorescence anisotropy for sensitive detection of DNA, *RSC Adv* 4:9379–9382, 2014.
He C, Lu K, Lin W: Nanoscale metal–organic frameworks for real-time intracellular pH sensing in live cells, *J Am Chem Soc* 136:12253–12256, 2014.
He C, Liu D, Lin W: Self-assembled core-shell nanoparticles for combined chemotherapy and photodynamic therapy of resistant head and neck cancers, *ACS Nano* 9: 991–1003, 2015.
Horcajada P, Chalati T, Serre C, et al.: Porous metal–organic-framework nanoscale carriers as a potential platform for drug delivery and imaging, *Nat Mater* 9:172–178, 2010.
Horike S, Shimomura S, Kitagawa S: Soft porous crystals, *Nat Chem* 1:695–704, 2009.
Hoskins BF, Robson R: Infinite polymeric frameworks consisting of three dimensionally linked rod-like segments, *J Am Chem Soc* 111:5962–5964, 1989.

Hu ML, Razavi SAA, Piroozzadeh M, et al.: Sensing organic analytes by metal–organic frameworks: a new way of considering the topic, *Inorg Chem Front* 7:1598, 2020.
Huang RW, Wei YS, Dong XY, et al.: Hypersensitive dual-function luminescence switching of a silver-chalcogenolate cluster-based metal-organic framework, *Nat Chem* 9:689–697, 2017.
Imaz I, Rubio-Martínez M, An J, et al.: Metal-biomolecule frameworks (MBioFs), *Chem Commun* 47:7287–7302, 2011.
Janssen ML, Oyen WJ, Dijkgraaf I, et al.: Tumor targeting with radiolabeled alpha(v)beta(3) integrin binding peptides in a nude mouse model, *Cancer Res* 62:6146–6151, 2002.
Jiang Q, Yu P, Yang L, et al.: Zeolitic imidazolate framework-based electrochemical biosensor for in vivo electrochemical measurements, *Anal Chem* 85:7550–7557, 2013.
Jiang J, Zhao Y, Yaghi OM: Covalent chemistry beyond molecules, *J Am Chem Soc* 138:3255–3265, 2016.
Katz E, Willner I: Integrated nanoparticle–biomolecule hybrid systems: synthesis, properties, and applications, *Angew Chem Int Ed Engl* 43:6042–6108, 2004.
Kim M, Cahill JF, Fei H, et al.: Postsynthetic ligand and cation exchange in robust metal–organic frameworks, *J Am Chem Soc* 134:18082–18088, 2012.
Kitagawa S, Kitaura R, Noro S: Functional porous coordination polymers, *Angew Chem Int Ed* 43:2334–2375, 2004.
Krause S, Hosono N, Kitagawa S: Chemistry of soft porous crystals: structural dynamics and gas adsorption properties, *Angew Chem Int Ed Engl* 59:15325–15341, 2020.
Kumar P, Deep A: Bioconjugation of MOF-5 for molecular sensing, *J Porous Mater* 21:99–104, 2014.
Kumar P, Deep A, Kim KH: Metal organic frameworks for sensing applications, *TrAC Trends Anal Chem* 73:39–53, 2015.
Lan A, Li K, Wu H, et al.: A luminescent microporous metal-organic framework for the fast andreversible detection of high explosives, *Angew Chem Int Ed Engl* 48:2334–2338, 2009.
Li H, Eddaoudi M, O'Keeffe M, et al.: Design and synthesis of an exceptionally stable and highly porous metal-organic framework, *Nature* 402:276–279, 1999.
Li H, Feng X, Guo Y, et al.: A malonitrile-functionalized metal-organic framework for hydrogen sulfide detection and selective amino acid molecular recognition, *Sci Rep* 4:4366, 2014.
Li SL, Han M, Wu B, et al.: Photochromic porous and nonporous viologen-based metal-organic frameworks for visually detecting oxygen, *Cryst Growth Des* 18: 3883–3889, 2018.
Lin RB, Li F, Liu SY, et al.: A noble-metal-free porous coordination framework with exceptional sensing efficiency for oxygen, *Angew Chem Int Ed Engl* 52:13429–13433, 2013.
Liu YL, Fu WL, Li CM, et al.: Gold nanoparticles immobilized on metal-organic frameworks with enhanced catalytic performance for DNA detection, *Anal Chim Acta* 861:55–61, 2015.
Liu TY, Qu XL, Yan B: A sensitive metal-organic framework nanosensor with cation-introduced chirality for enantioselective recognition and determination of quinine and quinidine in human urine, *J Mater Chem C* 8:14579–14586, 2020.
Lu Y, Yan B, Liu JL: Nanoscale metal–organic frameworks as highly sensitive luminescent sensors for Fe2+ in aqueous solution and living cells, *Chem Commun* 50:9969–9972, 2014.
Lyu F, Zhang Y, Zare RN, et al.: One-pot synthesis of protein-embedded metal–organic frameworks with enhanced biological activities, *Nano Lett* 14:5761–5765, 2014.
MacGillivray LR: *Metal organic frameworks: design and application*, 2010, Wiley.
Martí-Rujas J, Kawano M: Kinetic products in coordination networks: Ab initio X-ray powder diffraction analysis, *Acc Chem Res* 46:493–505, 2013.

McKinlay AC, Morris RE, Horcajada P, et al.: BioMOFs: metal-organic frameworks for biological and medical applications, *Angew Chem Int Ed Engl* 49:6260–6266, 2010.
Muldoon PF, Collet G, Eliseeva SV, et al.: Ship-in-a-bottle preparation of long wavelength molecular antennae in lanthanide metal–organic frameworks for biological imaging, *J Am Chem Soc* 142:8776–8781, 2020.
Müller-Buschbaum K, Beuerle F, Feldmann C: MOF based luminescence tuning and chemical/physical sensing, *Microporous Mesoporous Mater* 216:171–199, 2015.
Nakatsuka S, Watanabe Y, Kamakura Y, et al.: Solvent-vapor-induced reversible single-crystal-to-single-crystal transformation of a triphosphaazatriangulene-based metal–organic framework, *Angew Chem Int Ed Engl* 59:1435–1439, 2020.
Nickerl G, Senkovska I, Kaskel S: Tetrazine functionalized zirconium MOF as an optical sensor for oxidizing gases, *Chem Commun* 51:2280–2282, 2015.
Petsko GA, Ringe D: *Protein structure and function*, London, 2004, New Science Press.
Preiß S, Wuttke S, Braig T: MOF nanoparticles coated by lipid bilayers and their uptake by cancer cells, *Chem Commun* 51:15752–15755, 2015.
Qin J, Ma B, Liu XF, et al.: Aqueous- and vapor-phase detection of nitroaromatic explosives by a water-stable fluorescent microporous MOF directed by an ionic liquid, *J Mater Chem A* 3:12690–12697, 2015.
Rossetti A, Lippi M, Martí-Rujas J, et al.: Highly dynamic and tunable behavior of 1D coordination polymers based on the bispidine ligand, *Chem A Eur J* 24:19368–19372, 2018.
Saito A, Sawada T, Fujita M: X-ray crystallographic observation of chiral transformations within a metal–peptide pore, *Angew Chem Int Ed* 59:20367–20370, 2020.
Sawada T, Matsumoto A, Fujita M: Coordination-driven folding and assembly of a short peptide into a protein-like two-nanometer-sized channel, *Angew Chem Int Ed* 53:7228–7232, 2014.
Sharma A, Kim D, Park JH, et al.: Mechanistic insight into the sensing of nitroaromatic compounds by metal-organic frameworks, *Commun Chem* 2:39, 2019.
Shieh FK, Wang SC, Yen CI, et al.: Imparting functionality to biocatalysts via embedding enzymes into nanoporous materials by a de novo approach: size-selective sheltering of catalase in metal-organic framework microcrystals, *J Am Chem Soc* 137:4276–4279, 2015.
Shustova NB, Cozzolino AF, Reineke S, et al.: Selective turn-on ammonia sensing enabled by high-temperature fluorescence in metal-organic frameworks with open metal sites, *J Am Chem Soc* 135:13326–13329, 2013.
Taylor KML, Rieter WJ, Lin W: Manganese-based nanoscale metal – organic frameworks for magnetic resonance imaging, *J Am Chem Soc* 130:14358–14359, 2008a.
Taylor KML, Jin A, Lin W: Surfactant-assisted synthesis of nanoscale gadolinium metal–organic frameworks for potential multimodal imaging, *Angew Chem Int Ed Engl* 47:7722–7725, 2008b.
Taylor KML, Della Rocca J, Xie Z, et al.: Postsynthetic modifications of iron-carboxylate nanoscale metal – organic frameworks for imaging and drug delivery, *J Am Chem Soc* 131:14261–14263, 2009.
Ullman AM, Jones CG, Doty FP, et al.: Hybrid polymer/metal-organic framework films for colorimetric water sensing over a wide concentration range, *ACS Appl Mater Interfaces* 10:24201–24208, 2018.
Wang HS: Metal–organic frameworks for biosensing and bioimaging applications, *Coord Chem Rev* 349:139–155, 2017.
Wang GY, Song C, Kong DM, et al.: Two luminescent metal-organic frameworks for the sensing of nitroaromatic explosives and DNA strands, *J Mater Chem A* 2:2213–2220, 2014.
Wang S, Morris W, Liu Y, et al.: Surface-specific functionalization of nanoscale metal-organic frameworks, *Angew Chem Int Ed* 54:14738–14742, 2015.

Wang B, Wang P, Xie LH, et al.: A stable zirconium based metal-organic framework for specific recognition of representative polychlorinated dibenzo-p-dioxin molecules, *Nat Commun* 10:1–8, 2019.
Wu P, Wang J, He C, et al.: Luminescent metal-organic frameworks for selectively sensing nitric oxide in an aqueous solution and in living cells, *Adv Funct Mater* 22:1698–1703, 2012.
Wu Y, Han J, Xue P, et al.: Nano metal–organic framework (NMOF)-based strategies for multiplexed microRNA detection in solution and living cancer cells, *Nanoscale* 7:1753–1759, 2015a.
Wu X, Ge J, Yang C, et al.: Facile synthesis of multiple enzyme-containing metal–organic frameworks in a biomolecule-friendly environment, *Chem Commun* 51:13408–13411, 2015b.
Wu KY, Chen M, Huang NH, et al.: Facile and recyclable dopamine sensing by a label-free terbium(III) metal – organic framework, *Talanta* 221:121399, 2021.
Xin Y, Wang J, Zychowicz M, et al.: Dehydration-hydration switching of single-molecule magnet behavior and visible photoluminescence in a cyanido-bridged DyIIICoIII framework, *J Am Chem Soc* 141:18211–18220, 2019.
Xu H, Rao X, Gao J, et al.: A luminescent nanoscale metal–organic framework with controllable morphologies for spore detection, *Chem Commun* 48:7377–7379, 2012.
Xu R, Wang Y, Duan X, et al.: Nanoscale metal-organic frameworks for ratiometric oxygen sensing in live cells, *J Am Chem Soc* 138:2158–2161, 2016.
Yaghi OM, Li G, Li H: Selective binding and removal of guests in a microporous metal–organic framework, *Nature* 378:703–706, 1995.
Yang H, Qin C, Yu C, et al.: RGD-conjugated nanoscale coordination polymers for targeted T1- and T2-weighted magnetic resonance imaging of tumors in vivo, *Adv Funct Mater* 24:1738–1747, 2014.
Ye T, Liu Y, Luo M, et al.: Metal–organic framework-based molecular beacons for multiplexed DNA detection by synchronous fluorescence analysis, *Analyst* 139: 1721–1725, 2014.
Zhang M, Feng G, Song Z, et al.: Two-dimensional metal-organic framework with wide channels and responsive turn-on fluorescence for the chemical sensing of volatile organic compounds, *J Am Chem Soc* 136:7241–7244, 2014.
Zhang L, Lei J, Ma F, et al.: A porphyrin photosensitized metal—organic framework for cancer cell apoptosis and caspase responsive theranostics, *Chem Commun* 54:10831–10834, 2015a.
Zhang M, Gu ZY, Bosch M, et al.: Biomimicry in metal–organic materials, *Coord Chem Rev* 293–294:327–356, 2015b.
Zhang H, Yang J, Liu YY, et al.: A family of metal-organic frameworks with a new chair-conformation resorcin[4]arene-based ligand: selective luminescent sensing of amine and aldehyde vapors, and solvent-mediated structural transformations, *Cryst Growth Des* 16:3244–3255, 2016.
Zhou HCJ, Kitagawa S: Metal-organic frameworks (MOFs), *Chem Soc Rev* 43:5415–5418, 2014.
Zhu X, Zheng H, Wei X, et al.: Metal-organic framework (MOF): a novel sensing platform for biomolecules, *Chem Commun* 49:1276–1278, 2013.
Zhuang J, Kuo CH, Chou LY, et al.: Optimized metal-organic-framework nanospheres for drug delivery: evaluation of small-molecule encapsulation, *ACS Nano* 8: 2812–2819, 2014.
Zhuang J, Young AP, Tsung CK: Integration of biomolecules with metal–organic frameworks, *Small* 13:1–14, 2017.

CHAPTER FOUR

Hydrogels for sensing applications

Fabio Pizzetti[a] **and Giuseppe Perale**[b,c,*]

[a]Department of Chemistry, Materials and Chemical Engineering "Giulio Natta", Politecnico di Milano, Milano, Italy
[b]Faculty of Biomedical Sciences, University of Southern Switzerland (USI), Lugano, Switzerland
[c]Ludwig Boltzmann Institute for Experimental and Clinical Traumatology, Vienna, Austria
*Corresponding author: e-mail address: giuseppe.perale@usi.ch

Contents

1. Introduction 124
2. Physical, chemical and biosensors 125
3. Hydrogels 126
4. Physicochemical sensing mechanism 129
   4.1 Temperature sensors 130
   4.2 pH, ions and ionic strength sensors 132
   4.3 Pressure and strain sensors 135
   4.4 Gas sensors 136
   4.5 Hygrometers 138
5. Biochemical sensing mechanism 138
   5.1 Sensors based on molecular interactions 139
   5.2 Sensors based on living cells and bacteria 144
6. Hydrogel-based sensors for biomedical applications 145
   6.1 Cancer monitoring 146
   6.2 Cardiac rhythm monitoring 146
   6.3 Cell metabolite detection 148
   6.4 Tissue engineering 149
   6.5 Wound healing monitoring 149
7. Conclusions 150
References 150

Abstract

In recent years, a series of developments have taken place in the field of sensors. One of the most important one is represented by the hydrogel-based sensors, constituting a class of smart sensing devices of pivotal importance for different applications. Hydrogels are three-dimensional structure made up from crosslinked polymers showing a hydrophilic behavior, biocompatible and able to swell in the presence of a thermodynamic compatible solvent. Furthermore, hydrogels are able to respond to different external

Advances in Chemical Engineering, Volume 57
ISSN 0065-2377
https://doi.org/10.1016/bs.ache.2021.03.001

stimuli; this peculiarity has ensured them great recognition for sensing application and diagnostics. This chapter is focused on the advantages reached in the last years for hydrogel-based sensors, separating them in physicochemical sensors and biosensors.

1. Introduction

Sensors are devices that are able to detect and respond to different inputs or signals from an external environment (Dincer et al., 2019). The name sensor comes from the five senses present in the human body (sight, hearing, touch, smell, taste), and their classification can be carried out following different pathways. One of the simplest classification methods is the one based on the types of inputs that need to be detected, which can be chemical or physical. The IUPAC (International Union of Pure and Applied Chemistry) proposed in 1991 a sensors' classification based on the different types of signal transduction; in this case, sensors can be classified as (Hulanicki et al., 1991):

(1) Optical sensors: they are focused on optical phenomena, such as light scattering, absorbance, reflectance, fluorescence, luminescence, optothermal effects, and refractive index. They are able to report changes in these properties.

(2) Electrochemical sensors: these sensors can detect electrochemical interactions between the analyte and an electrode.

(3) Electrical sensors: differently from the previous type, they do not involve electrochemical processes, but instead they exploit some metal oxide or organic semiconductors.

(4) Mass-sensitive sensors: they are based on effects able to transform a change in mass into a change of some analyte's properties. Some examples are piezoelectric and surface acoustic wave effects.

(5) Magnetic sensors: as the name suggests, they are based on a change in the magnetic properties of analyte gas.

(6) Thermometric sensors: they exploit the peculiarity of different reactions or adsorption processes able to generate or consume heat.

(7) Radiation sensitive sensors: they are based on physical properties (X-, β-, Γ- radiations) generically used for the determination of chemical composition.

As it can be observed from this classification, no clear distinction between chemical and physical sensors exists. The problem here is related to the difficulty of such separation since often both of them are present in a single

analyzed case. Shifting to their structure, a deductive sensor is composed of two parts: the receptor and the transducer. The receptor is that part that senses the stimulus and transforms it into energy, while the latter converts the energy from one form to another in order to produce a signal representing the information about the system. An important parameter is the sensitivity of such material, i.e., how much the sensor output is influenced by quantity changes in the input. In order to be classified as a good sensor, three generic rules must be followed:

(1) The sensor must be sensitive to the measured property.
(2) The sensor must be insensitive to any other properties, i.e., selectivity toward the desired quantity.
(3) The sensor must not influence the measured property, otherwise the output will be disturbed.

Sensors exist both as active and passive sensors. As far as active sensors are concerned, they require an external excitation or power signal for operating. Differently, passive sensors do not require any external power signals and are able to directly generate an output response.

2. Physical, chemical and biosensors

As reported in the previous paragraph, one of the first classifications of sensors was reported by the IUPAC in 1991 as physical and chemical sensors. According to their definition, the formers are "a device that provides information about a physical property of the system" while for the latter, they are "devices that transforms chemical information, ranging from the concentration of a specific sample component to total composition analysis, into an analytically useful signal" (Hulanicki et al., 1991). A few years later, in 1999, another definition was introduced by the IUPAC, that of biosensors.

Biosensors are devices that place themselves between physical and chemical sensors, possessing the peculiarity of possessing a physicochemical detector combined with a biological element, such as cell receptors, enzymes, antigen or nucleic acids. According to the IUPAC definition, they are "an integrated receptor-transducer device, which is capable of providing selective quantitative or semi-quantitative analytical information using a biological recognition element". In recent years biosensors are gaining more and more importance, thanks to their specific characteristics, i.e., the coupling of stability, reproducibility, sensitivity and a fast response (Bhalla et al., 2016). Different conditions and parameters should be taken

into consideration when designing these novel sensors; for instance, it is of pivotal importance the immobilization of the bio-element and the accessibility of receptors to the target should be guaranteed. Generically, a biosensor is constituted of a bio-receptor, a bio-transducer and an electronic system, able to allow the amplification of the signal and its display (Vigneshvar et al., 2016). The bio-receptor is the part that interacts with the analyte, producing an effect measured by the bio-transducer that can be of different typologies (electrochemical, electronic, optical, etc.). The selection of the biological recognition element is of pivotal importance, since they are responsible for the selectivity and should be selective toward the analyte while insensitive to other molecules. Biosensors can work both directly and indirectly: in the formers the signal coming from the production of the physicochemical agent has an intensity that is directly proportional to the analyte concentration, while for the latter the chemical compound whose concentration is sensed has its production influenced from the analyte (the analyte is not directly sensed, from this the name indirect). It should be pointed out that, as always, the biological recognition element has detection limits that are connected to the signal variation produced. In general, such limits are detected with the linear dependence range between signal recognition and signal intensity, usually derived from a calibration curve of its response to different analyte concentrations. Biosensors can have a variety of applications, and some of them will be discussed in this chapter; their main requirement is the identification of the target molecule and the availability of a suitable recognition element (Justino et al., 2015; Mehrotra, 2016).

3. Hydrogels

Hydrogels are materials that are gaining more and more importance in recent years in biomedical and tissue engineering applications, they are defined as colloidal structure of polymeric chains characterized by a three-dimensional crosslinked network (Fu and In Het Panhuis, 2019; Shetye et al., 2015). They show different peculiar properties, one of the most important being the so called "swelling behavior": the ability to absorb and retain large quantities of water (or a thermodynamically favorable solvent) and the subsequent volume increase. Hydrogels can be classified following different approaches, one of the most used is that following the typology of crosslinking, that can be either chemical or physical (Maitra and Shukla, 2014). Chemical crosslinked hydrogels show a network composed by covalent bonds and they are stable in water since they do not

dissolve, while physical crosslinked hydrogels are held together by dynamic interactions based on non-covalent interactions, such as electrostatic or hydrogen bonding. Furthermore, they can also be classified based on the typology of the material used for their production (natural, synthetic and semi-synthetic), or on the basis of their stability in physiological environment (durable/biostable or biodegradable), or according to the typology of ionic charges on the networks (Mahinroosta et al., 2018). Another important aspect that can be tuned in hydrogels' preparation is their shape: different applications may require different shapes and dimensions (Shibata, 2010; Tsuchiya et al., 2019). As an example, in recent years microbead hydrogels are gaining relevant importance in body implantation applications, thanks to their low angle dependent structures. Shifting to other applications, sheet-shaped gels are useful for surface applications in order to obtain a good adhesion with the surface (Sun et al., 2021), while fiber-based gels or hydrogel microfibers constitutes a good solution for soft actuators and soft robots thanks to their high framework's tunability and the great control that can be realized during synthesis (Hines et al., 2016). One of the characteristics that make hydrogels so interesting for a series of applications is their ability to respond to external stimuli thanks to their permeability and swelling behavior. Furthermore, this ability can also be tuned, for instance by inserting particular moieties inside the polymeric framework, thus making the structure more responsive to particular environmental stimuli, such as temperature or pH.

Also other parameters are able to influence the hydrogel sensitivity to such variables, such as the mesh size, the crosslinking density or the ionic charge. Thanks to all the characteristic listed, it can be noticed how hydrogels can be effectively useful in sensing applications. Different applications methods exist, varying on the hydrogel utility. The hydrogels can be used as host-network thanks to their inert and semiwet structure, alternatively they can be used as amplification devices analyzing properties such as a changing in the swelling degree. Finally, hydrogels can also be used as helper, able to control the diffusion of molecules throughout the polymeric matrix. Before moving to applications involving hydrogels in sensing, it is important to have a brief overview on hydrogels swelling. As expressed before, swelling is a phenomenon that occurs as soon as the hydrogel enters in contact with water or a thermodynamically compatible solvent, and the solvent molecules start entering inside the polymeric network (Ganji et al., 2010). This phenomenon can be referred to as hydration, and thanks to this the polymeric chains relax and the structure starts to enlarge. Two different forces are present during

this process: osmotic forces and elasticity forces of the network. The former favor the process, while the latter play a negative role and prevent excessive deformation. As soon as these two forces balance themselves, the system will be in equilibrium conditions and the quantity of water contained in the polymeric network takes the name of equilibrium water content. Different parameters play a relevant role in the swelling dynamic and equilibrium, such as polymer nature, crosslinking density and moieties inside the polymer. One of the most used models able to describe swelling behavior of neutral hydrogels is the Flory-Rehner theory (Flory and Rehner, 1943), that consider forces from three main contributions: the entropy change determined by the mixing between polymer and solvent, the heat determined by the same process, and the entropy change due to the reduction of numbers of the possible chain conformations through swelling.

The Flory-Rehner governing equation has the following expression:

$$-\left[\ln\left(1-\nu_2\right)+\nu_2+\nu_2^2\right]=\frac{V_1}{\nu_s M_C}\left(1-\frac{2M_C}{M}\right)\left(\nu_2^{1/3}-\frac{\nu_2}{2}\right) \qquad (1)$$

where ν_2 is the polymer volume fraction in the swollen hydrogel, ν_s is the polymer specific volume, V_1 is the solvent molar volume, M_C is the average molecular mass and M is the primary molecular mass. This equation is able to completely describe the swelling behavior of the hydrogel in terms of crosslinking density and the solvent typology. As anticipated, one of the greatest characteristics of hydrogels is their ability to respond to external stimuli (Echeverria et al., 2018). Different responses, that can be present, are a volume phase transition of the network, a change in shape and size (such as for instance during swelling), or a change in some optical, electrical or mechanical properties. Furthermore, hydrogels are sensitive to a variety of external stimuli (temperature, pH, light, presence of molecules etc.). One of the most used stimuli is the temperature variation: usually, the temperature at which a response is observed is called critical temperature (T_C), and in general at that temperature is possible to observe a phase change between polymer and solvent. Two different critical temperatures can be detected: the polymer exhibits an upper critical solution temperature (UCST) if the phase separation occurs below the critical temperature, while if the transition happens above the critical temperature a lower critical solution temperature is present (LCST). Other than temperature, also pH-responsive hydrogels are of great interest, in which a pH variation induces a volume phase transition. Here there will be a different behavior based on the type of hydrogel present: anionic or cationic. In the case of anionic hydrogels,

if the environmental pH is higher than structure's pK_a ionization occurs, and the hydrogel response corresponds to a higher hydrophilicity of the network, an increase in the number of fixed charges and in the electrostatic repulsion between chains. If instead the pH of the external solution is lower, protonation occurs, and the network gains a hydrophobic behavior and the structure will be more compact. Shifting to the cationic hydrogel, it is possible to observe the same response, but with a different trend.

Recently, light-responsive hydrogels are gaining importance in this field (Li et al., 2019). In general, they are formed by a polymeric network with a photoreactive moiety. Such molecule is able to capture the optical signal and converts it to a chemical signal through a photoreaction. The advantage of using this hydrogel for sensing applications is that the stimuli are non-invasive and do not require any contact with the material. Finally, also other types of responsive hydrogels can be described: the analyte-responsive (Culver et al., 2017) and the redox-responsive hydrogels (Cheng and Liu, 2017). The formers are able to recognize target molecules thanks to particular biomolecules incorporated in the hydrogel network, while the latters respond to reduction or oxidation of their constituent molecular components through an electrochemical or chemical activation determining an ion mobility between two electrodes and so the generation of a signal. From this brief introduction, it is clear how stimuli responsive hydrogels can be successfully applied as active sensing materials, thanks to their ability to respond to small variation of external conditions and give the response to external stimuli that can be of different typologies (physical, chemical, biological). All the hydrogels' properties can be tuned during the production according to the final utilization or applications. All these peculiarities, along with the possibility to employ hydrogels as support structures for sensing devices or as immobilization matrixes for biosensor elements, enabled the growing utilization of hydrogels for sensing applications.

4. Physicochemical sensing mechanism

The principal physicochemical mechanisms for sensing has been proposed by (Buenger et al. (2012); in recent years, new methods and technologies have been developed for hydrogels in sensing applications using this employing this kind of mechanism. Few examples will be analyzed in the following paragraphs, in particular attention will be shifted to temperature, pH, pressure, gas, and humidity sensors.

4.1 Temperature sensors

They are probably one of the most important and used type of sensors, having applications in different fields, such as industrial production processes, biotechnologies, medicine and everyday life. It should be highlighted that these types of sensors need to be extremely precise, highly responsive and able to work under different conditions. Among all the typologies of temperature sensors, hydrogel-based ones are of outstanding interest thanks to their peculiar features: first of all biocompatibility and the possibility to tune the hydrogel properties, in particular their structure. Furthermore, even the output signal can be tuned according to the desired behavior. For this application, two families of hydrogels seem to be promising: hydrogel photonic crystals (PCs) and intelligent polymerized crystalline colloidal arrays (IPCCAs). PCs are structures in which the dielectric constant varies periodically, determining the generation of a photonic band structure that the electromagnetic waves can or cannot proceed depending on their characteristic wavelength. Generally, the applications of PCs involve a change in their structure, determined by an external stimulus; in this case the introduction of a thermo-responsive material inside the photonic crystal makes the whole framework sensible to changes in temperature. Similarly, IPCCAs, that are crystal colloidal arrays of polymer spheres of different nature polymerized in a hydrogel matrix, can be used for temperature change detection. IPCCAs work in a similar way to PCs: they diffract the light determining different colors. As before, also here the introduction of a thermo-responsive material inside the network makes the whole framework sensitive to temperature variation. The reason behind this is that a temperature variation will determine a volume transition inside the polymer matrix, and this will induce a color change due to diffraction properties of the IPCCAs dispersion. The hydrogel technologies here reported rely on optical properties of the material. In the recent years, different hydrogel temperature sensors have been developed, and few examples will be discussed in the following part of the paragraph.

As an example, in 2018 Choe et al. (Choe et al., 2018) developed a thermo-responsive plasmonic microgel embedded in a stretchable hydrogel film. The microgel was produced using poly(N-isopropylacrylamide) (PNIPAM) decorated by gold nanoparticles (NPs). In literature this application is used in a variety of applications, since PNIPAM in combination with plasmonic nanoparticles as thermo-responsive sensors, thanks to the NPs low critical solution temperature close to that of human body and to a significant and reversible volume change. In the experiments from

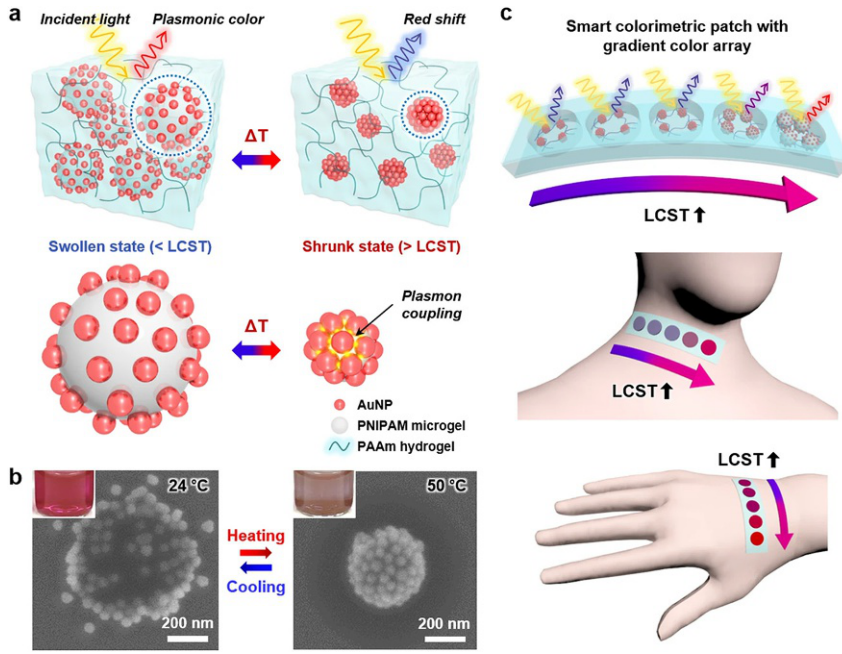

Fig. 1 (A) Schematic illustration of the plasmonic microgels in the PAAm hydrogel under swollen and shrunk states. (B) SEM images of the plasmonic microgels with 51 nm AuNPs under the swollen state at 24 °C (left) and under the shrunken state at 50 °C (right); the inset images show pictures of the plasmonic microgel dispersions under each condition. (C) Schemes of the sensor array patches attached to human skin at different positions (neck and hand). *Reprinted from Choe A, Yeom J, Shanker R, Kim MP, Kang S, Ko H: Stretchable and wearable colorimetric patches based on thermoresponsive plasmonic microgels embedded in a hydrogel film,* NPG Asia Mater *10:912–922, 2018. doi:10.1038/s41427-018-0086-6.*

Choe the microgels shown a large extinction peak shift, 176 nm, in a short time. Furthermore, the detection range was extremely large (from 29 °C to 40 °C) and with a good resolution of 0.2 °C. Color changing sensors are not the only technologies that can be found in literature (Fig. 1). Li et al. (2020) published in 2020 a work on polyvinyl alcohol (PVA) hydrogel with silver nanofibers (AgNWs) as temperature sensor. This is due to the ability of this structure to modify its electric conductivity varying the temperature of the external environment, in particular it increases linearly with T. They tried to explain this phenomenon with a variation of the electrons motion: it becomes more intense with increasing temperature, so the electrons energy is higher allowing some electrons to pass through some uncontacted AgNWs. In order to demonstrate this process, the authors realized

and tested a sensor based on this gel, connecting a copper wire to both ends of a rectangular hydrogel and then they connected the two ends of the wire to the two electrodes of a digital source meter recording the current change through the gel when stimulated by an external temperature variation. The conductivity of the gel was recorded, and they were able to convert it to temperature thanks to a conductivity-temperature relationship that was obtained by previous experiments. For these applications, the hydrogel has always been used as sensing network. Unfortunately, even if hydrogels possess good qualities such as biocompatibility, good flexibility and light weight, this type of network has poor mechanical strength and it can hardly resist to external forces. Due to these peculiarities, attention has also been shifted to dual-network (DN) hydrogels, thanks to their higher mechanical strength, toughness and modulus.

As an example, in 2020 An et al. (2020) developed a T-sensor based on multi-wall carbon nanotubes (MWCNTs) composite polyacrylamide/Fe^{3+}-polyacrylic acid double network hydrogels combining flexibility, thermal sensitivity and self-healing ability. Here the polyacrylamide was used as first network, while Fe^{3+} and polyacrylic acid complexation was used as second one in order to prepare DN hydrogels. The addition of MWCNTs allowed an increase in the toughness of the structure and was able to make the whole system highly resistive to tensile stresses and it improves also its conductivity. A calibration curve can be produced measuring the electrical conductivity as a function of different external temperature values. Once obtained such relation, it is possible to use these DN hydrogels as temperature sensors.

Other applications of hydrogels in T-sensors involve the utilization of hydrogels not as primary sensing elements, but for instance as 3D environment able to extend the lifetime of other sensing elements, generally in case of luminescence and fluorescent-based temperature sensors.

4.2 pH, ions and ionic strength sensors

pH sensing is probably one of the most important applications for stimuli responsive hydrogels, this is due to the hydrogel property of quickly react to a pH variation modifying different parameters of its structure. In literature a very exhaustive work on this topic is present, published in 2008 by Richter et al. (2008). In this work, Richter completely describes the physical and theoretical aspects of pH-sensitive hydrogels sensors, together with transducer, design rules and general conditions for the applications of these

structures. In 2010 Shin et al. (Shin et al., 2010) were able to produce a fast-responding photonic crystal pH sensor using inverse opal hydrogel structures. The measurements were possible coupling a fiber optic UV–vis spectrometer with a reflected light microscope. After few years, they proposed an improvement in the synthesis of these sensors, using different vinyl monomers containing acidic or basic substituents (Shin et al., 2012).

As an example, they used acrylic acid, vinylphosphonic acid, vinylimidazole, dimethylaminoethylmethacrylic acid copolymerized with hydroxyethylmethacrylate through photopolymerization. Then, the opal templating and subsequent opal template removal, allowed the fabrication of four different types of inverse opal hydrogels (IO). The colorimetric response was based on a pH-dependent swelling behavior that determine a different colorimetric response based on the substituents inside the structure. Another example that can be reported is that of Pathak and Singh (2017), that developed no-core fiber sensors (NCFS) using smart hydrogel coating. The hydrogel was prepared using aqueous solutions of acrylamide and bisacrylamide, using ammonium persulfate as initiator and tetramethylethylenediamine as catalyst. The polymerization was started using light and then the NCF was stubbed between two single-mode fibers with connector before the immobilization the smart hydrogel. This sensor showed a good sensitivity for a very large range of pH values with a linear response, showing also a good stability and reproducibility. Zhao et al. (2018) synthetized a hydrogel-coated optical fiber surface plasmon resonance (SPR) sensor. In their work, the system was produced with a multimode-singlemode-multimode (MMF-SMF-MMF) structure, where the singlemode one was prepared with a coating of silver film and the hydrogel prepared with acrylamide and bisacrylamide. In this case, the hydrogel's refractive index decreased with an increase in the environmental pH, causing the resonance wavelength to show a blue shift. Unfortunately, hydrogel smart sensors not only bring advantages, but they carry on also some drawbacks. In the work of Deng et al. (2018) they highlighted how in open-loop hydrogel-based pH sensors the performance is usually limited by the slow cooperative diffusion process of hydrogels. They tried to overcome this problem inserting a force compensation: an external actuator will exert a compensating pressure, able to suppress the hydrogel swelling, thus accelerating the diffusion process and improving the sensor's dynamic behavior. The typologies of hydrogel-based sensors described so far can also be applied in other sensing applications just modifying the hydrogel formulation. For instance, ions recognition hydrogel-based sensors work in a similar way to pH sensors.

Just to analyze some examples, Sannino et al. (2007) used quartz crystal microbalance (QCM) in order to recognize small changes in the pH values. Then, they spin-coated onto the QCM some cellulose-based hydrogels for obtaining a smart hydrogel sensor. Later on, in 2020 after observing the versatility of these devices, Tokuyama et al. (2020) proposed the application of a QCM hydrogel-coated sensor as arsenic ions sensor. This was possible preparing the hydrogel with *N*,*N*-dimethylacrylamide, using *N*,*N*′-methylenebisacrylamide as crosslinking monomer and loading some zirconia NPs inside this system. This solution was then deposited onto the QCM sensor and rinsed with water. The investigation of the ions adsorption was based on the resonance frequency of the hydrogel-coated QCM, since the zirconia NPs were demonstrated to be able to adsorb As(III) and As(V). Other types of sensors that can be useful in these applications are naked-eye sensors, and as an example Ozay and Ozay (2013) developed a reusable hydrogel-based naked-eye sensor for ions sensing. In their work, the hydrogel was synthetized using 2-hydroxyethylmethacrylate and acrylamide as primary monomer and N-(Rhodamine-6G)lactam-N′-acryloylethylenediamine as comonomer, and then they demonstrate that the system was sensitive to Fe^{3+} ions through UV light. Furthermore, these sensors showed chemo-sensor for Fe^{3+} in the visible light. In their study, the sensor was demonstrated to be very responsive, showing a color change in less than 2 s and able to detect also small concentrations of Fe^{3+} in the solution (in the order of 0.1 ppm). Other technologies used in the field of sensors involved the applications of quantum dots (QDs). QDs are nanomaterials that emerged in the recent years thanks to their photostability, high quantum yields and very broads absorption bands. Unfortunately, QDs shows also some limitations, in particular they have to be mixed in aqueous samples in order to perform fluorescence measurements. In order to overcome this problem, one solution that has been proposed is that of immobilize the QDs in a matrix that will not affects their properties and that allows the penetration of the analyte. In these applications, hydrogels are a very useful class of materials.

As an example, Zhou et al. (2018) developed a ratiometric fluorescence sensor based on QD-doped hydrogel optical fiber for Fe^{3+} ions detection. They synthetized two different classes of water soluble QDs, showing two different photoluminescence wavelengths: the first was capped with thioglycolic acid showing green emissions (gQDs), while the other was capped with N-acetyl-L-cysteine and possessed a red emission (rQDs). Then, they were inserted in a hydrogel matrix prepared using 30% w/v polyethyleneglycol diacrylate and 1% w/v 2-hydroxyl-2-methyl-propiophenone

in deionized water. Fe^{3+} ions are able to diffuse into the hydrogel matrix, and they can selectively quench the rQDs, while leaving unaffected the gQDs, thus exhibiting a stable fluorescence emission. Concluding this paragraph, the importance of pH sensors is not only related to the sample measurements of some pH values, but to the possibility of investigating also specific biological processes responsible of a pH variation in aqueous environments.

4.3 Pressure and strain sensors

Hydrogels are a class of materials that can be applied also for pressure-based sensors, thanks to their ability of modifying some properties after the application of external stresses; furthermore, it possible to detect the magnitude of such external stresses evaluating the systems' variation. Generally, hydrogels used in this type of applications present a good flexibility, high sensitivity and a good repeatability, able to guarantee their enforceability both in single pressure measurements and in strain cyclic evaluations. A first example for these applications can be the work of Xia et al. (2019)) that in 2019 developed a high performance wearable sensor based on an ionic conductive hydrogel. They synthetized the hydrogel through micellar copolymerization method, dissolving LiCl and sodium-dodecyl-sulfate (SDS) in deionized water; then, lauryl methacrylate was added together with hybrid latex NPs. The system presented skin-like mechanical properties and characteristics, such as low modulus and robust elasticity. This system can be used as pressure sensor thanks to its sensitivity to external stimuli, durability and reproducibility.

Zhu et al. (2020)) in 2020 were able to develop an ionic conductor hydrogel synthetized with interpenetrating sodium carboxymethylcellulose micro-sheets in a polyacrylamide network. The hydrogel is here the core part of the sensor, fixed onto an elastic surface that encapsulate the system preventing water evaporation. A copper foil was attached to the hydrogel, ensuring electrical connections. This hybrid hydrogels can be worn as strain sensor to monitor distinguish the normal motion of human body from large strain to subtle pressure change caused by human breath. As a last example, the work of Zhang et al. (2019a) can be analyzed. They were able to produce a MXene-containing hydrogel as smart compressor sensor. MXenes are a class of 2D inorganic structures that are gaining much relevance in electrochemical and sensing applications. In their work, they used MXene nanosheets entrapped in a hydrogel matrix, prepared using PNIPAM and physical crosslinking Fig. 2.

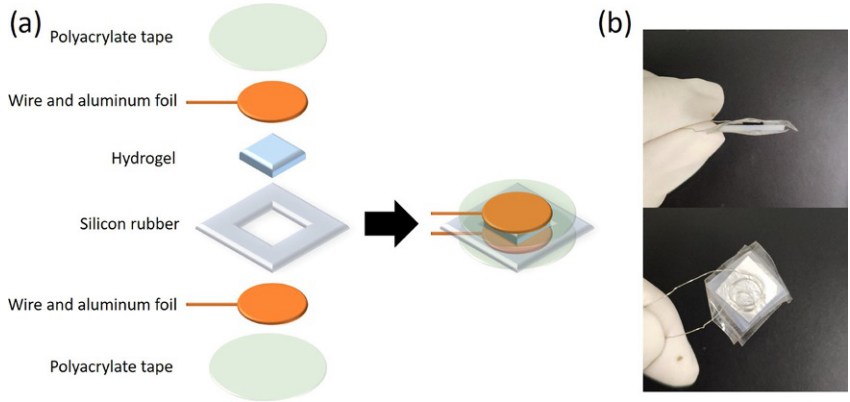

Fig. 2 (A) Assembly schematic diagram and (B) photograph of the compression sensor. *Reprinted with the permission of ACS Publications Zhang Y, Chen K. Li Y, Lan J, Yan B, Shi L, Ran R: High-strength, self-healable, temperature-sensitive, MXene-containing composite hydrogel as a smart compression sensor,* ACS Appl Mater Interfaces *11:47350–47357, 2019a. doi:10.1021/acsami.9b16078.*

4.4 Gas sensors

A gas sensor is defined as a device able to detect the presence of certain gases in a controlled volume. These types of sensor are of pivotal importance in a series of industrial applications, and a large number of sensors are available on the market. The challenge that is dealt with in recent years is the combination of different features for gas sensors, such as responsivity, selectivity and biocompatibility. Generally, the hydrogel-based sensor for gas detection can be divided into three different classes: hydrogels used as passive protecting elements for a primary sensor, hydrogels modified with sensitive molecule able to make the system sensitive to certain gases and eventually hydrogels which exploit their stimuli responsive swelling ability for sensing. The first of the list is probably the less interesting one, since the hydrogel do not participate actively in the sensing process, the hydrogel is merely present as a support element, able to improve the device's performance.

As an example for this kind of application, Puttasakul et al. (2019) applicated a polyacrylamide hydrogel as sensitive layer for vapor sensing. Such gel was characterized with a high degree of porosity, able to absorb explosive vapors. The hydrogel was deposited onto a screen-printed gold electrode connected to a potentiostat in order to carry out electrochemical measures. The second typology of hydrogel application in gas sensors is represented by the synthesis of novel hydrogel systems with peculiar sensitive

molecules, enabling them to be sensitive to particular gases. One of the classical solutions usually used is the incorporation of a fluorescent tracer inside the hydrogel matrix that is able to react with a target gas. One example of this type of application can be found in the work of Wu et al. (2018), that developed a novel fluorescent dual pH and oxygen sensor loaded in multi-well plates for *in situ* monitoring of oxygen respiration and extracellular acidification during microbial cell growth. The hydrogel was synthetized using poly(2-hydroxyethyl methacrylate)-*co*-polyacrylamide (PHEMA-*co*-PA), and then it was conjugated with a polymerizable oxygen probe, produced from Pt(*II*)*meso*-tetra(pentafluorophenyl)porphine and a polymerizable pH probe derived from fluorescein. As another example, Hong et al. (2013) developed an IO hydrogel applicable in CO_2 gas sensing using amines. The mechanism is based on the reactivity of carbon dioxides with amines forming carbamates, bicarbonates or other ionic liquids; thus, it is possible to sense the presence of CO_2 through a photonic hydrogel with amino groups monitoring the changes in light diffraction. Eventually, the last class of hydrogel sensors in gas sensing applications is based on hydrogels that exploit their stimuli responsive characteristics directly for gas sensing. In this class, a lot of innovative systems are available in literature. As an example, Zhi et al. (2020) developed a self-responding sensing system in NO_2 and NH_3 sensing. These hydrogels, in this work, were hydrogen-bond-based supramolecular conductive hydrogels, that shown good self-responding ability to those target gases. In particular, three different supramolecular interactions are present in these hydrogel-based sensors: hydrogen bonding, molecule crystallization and electrostatic interactions.

Among these, hydrogen bonding and molecule crystallization are self-responsive to NO_2 and NH_3, while the electrostatic interactions are present just to provide conductivity and increase the system stability. In their work, the hydrogel was produced dissolving poly(vinyl alcohol) and carrageenan in distilled water together with 3-butylimidazolium and p-styrenesulfonate hydrate, later also *N*,*N*′-methaylenbis-(acrylamide) was added. Another example that can be reported is the work of Wu et al. (2019a), which developed a different method for sensing the same gases, based on DN hydrogels. They produced an ionic conductive polyacrylamide and carrageenan DN hydrogel, that was characterized through UV–vis spectra. They carried out gas sensing in gas chambers with electrical feedthroughs. The sensor exhibited high sensitivity, selectivity and linearity. Furthermore, the nitrogen oxide detection had very low detection limits, in the order of ppb.

4.5 Hygrometers

Hygrometers are sensors that are able to measure the humidity present in the air, in recent years most of them evaluate it through electrical measurements. Hydrogels can potentially improve these sensing devices thanks to their ability to absorb water in their meshes. The hydrogels' properties are strictly related to their humidity of the environmental air; thus, they can be useful for humidity detection. An example of this technology can be found in the work of Buchberger et al. (2019), were they proposed hydrogel thin films as fast optical humidity sensors. Their hydrogels were produced through chemical vapor deposition technique, fabricated using 2-hydroxyethylmethacrylate and tert-butyl peroxide. A variation in the relative humidity of the surrounding air will lead to a variation in the film thickness, thus just an optical evaluation allowed such variation. Later, two implementations of the optical setup were introduced. The first one was based on a laser and a photo detector able to precisely measure the thickness change, while the latter was based on a broadband light source together with a spectrometer, able to allow the spectral recording yield to absolute thickness values.

An innovative solution in humidity measurements can be found in the work of Zhang and Zhang (2015) were they developed a new intensity-based fiber optic humidity sensor, formed by solidification of mini hydrogel spheres on bare fiber cores. Their hydrogel was produced using drops of poly(ethylene glycol) dimethacrylate mixed with a 0.5%wt curing agent, and crosslinked through the usage of UV lamp. A variation in the external relative humidity will translate in a variation of the refractive index of the hydrogel spheres, and it can be detected through the intensity change of the transmitted light through the fiber. Jang and Jeong (2020) synthetized a humidity sensor with chitosan based plasmonic metal-hydrogel-metal filters. Chitosan was chosen because it gives the hydrogel the ability to swell upon a change in the environmental humidity. This system was used in the implementation of a tunable resonator that, combined with a photovoltaic cell, allows the estimation of a precise humidity value through the evaluation of a change in current.

5. Biochemical sensing mechanism

As far as now, sensing mechanisms based on physicochemical parameters have been analyzed. They are not the only one present, since also some

complex biochemical mechanisms are available for hydrogel-based sensors. Initially, the basic concepts behind molecular and biological interactions will be introduced, then some techniques available or recently developed in literature will be discussed.

5.1 Sensors based on molecular interactions

The interaction between an enzyme and the substrate is a very important topic in this field. A large number of references is available in literature, but here just the basic concept will be reported and will be schematized, in order to give the reader principal information so that it will be easier to understand some applications.

Enzymes are defined as highly specific molecules that act as biological catalysts, accelerating chemical reactions and lowering the activation energies. The molecules upon which they are able to act are the so-called substrates; usually, the first step in a chemical reaction that involves enzymes is the formation of an enzyme-substrate complex: this represents the reactive transition state of the process. Then the chemical products are formed, and the enzyme can be restored. One of the most important tasks to study is the enzyme kinetics, i.e., how they are able to bind substrate and generate the product. To recent days, one of the theory that is largely used is the one developed by Michaelis and Menten (Johnson and Goody, 2011): it was originally derived into 1913, considering the reactions divided into the two stages mentioned before. They were able to notice that the enzyme rates depend on the enzyme and substrate concentration: as a matter of fact, if the substrate concentration is very high, the enzyme becomes saturated and the reaction rate depends only on the velocity of the conversion from substrate to the products. The governing equation giving the reaction rate in an enzyme catalyzed chemical reaction in the Michaelis-Menten model is the following:

$$r = \frac{k_{cat}[E_0][S]}{K_m + [S]} \tag{2}$$

where k_{cat} is the kinetic constant, K_m is the Michaelis-Menten constant (i.e., the substrate concentration required for an enzyme to reach one half its maximum reaction rate) and $[E_0]$ and $[S]$ are the initial concentration of the enzyme and the substrate concentration respectively. The kinetic constant in this model represents the reaction's turnover number, that is the number of substrate molecules converted by one active site per unit time.

Of course, in some real cases, more complex kinetic schemes describe the interaction between substrate and enzyme, involving for instance some rearrangements. Here this model has been reported since it describes the idea behind a generic enzyme catalyzed reaction and allow the reader to understand how the enzyme and substrate interactions can allow the determination of an analyte concentration.

Now, some examples of hydrogel-based sensors based on enzyme-substrate interactions will be reported, separated between the different types of analyte detected:

(1) *Alcohol detection*. In recent years, enzymatic biosensors are largely used for this application. In this case, a hydrogel matrix can be applied. A series of different sensors are available in literature; as an example, in the work of Buenger et al., they reported a hydrogel-based enzyme alcohol sensor based on the alcohol oxidase (AOX) and the horseradish peroxidase (HRP) blocked in an ionotropic polymeric hydrogel and in a polyethyleneglycol hydrogel obtain from microparticles (Jang and Koh, 2010; Wu et al., 2007). A different example can be found in the work of Burrs et al. (2015), were they studied and compare four different hydrogel matrixes for alcohol sensing: the AOX was encapsulated in chitosan hydrogel, cellulose nanocrystals, PNIPAM and silk fibroins hydrogels. They demonstrated that chitosan and PNIPAM hydrogels were the one showing greater sensitivity and faster response time.

(2) *Glucose detection*. High value of glucose concentration in the bloodstream is the reason behind the diabetes mellitus disease. It affects more than 400 million people worldwide, and it can be noticed how the glucose concentration monitoring is an important task (Vashist, 2013). The majority of self-monitoring devices present in the market provides generically point measurements, without provide essential information such as glucose trends and possible peaks. Due to this problem, the demand of smart continuous glucose monitoring system has increased and hydrogel-based biosensors have been proposed as interesting solution (Liang et al., 2020). Recently, the most used and effective hydrogel-based biosensors are the one exploiting glucose oxidase (GOX), an oxido-reductase able to catalyze the oxidation of glucose. Generally, it is immobilized in pH-sensitive hydrogel matrix, able to swell upon contact with glucose molecules. It can be noticed how the most important parameter in this process is the hydrogel ability to swell. An example can be found in the work of Mugweru et al. (2007), that

were able to entrap GOX in a polyethyleneglycol diacrylate hydrogel, and then fabricated glucose sensor arrays on gold electrodes on flexible polyimide sheets.

The mechanism of this sensor is based on the reaction between GOX and glucose, analyzing the catalytic current produced that is proportional to the analyte concentration. Of course, this is not the only method available; differently, Kim et al. (2011) developed an optical biosensor, encapsulating GOX in a peptide hydrogel, together with fluorescent molecules. Their fluorescent tracers were functionalized QDs and the photoluminescence quenching of the hybridized QDs allowed the evaluation of glucose concentration. In recent years, also other fluorescence based biosensors are available, for instance in the work of Kim et al. (2016) they developed a hydrogel biosensor based on a copolymer between acrylamide and fluorescent monomers of fluorescein and rhodamine B. They immobilized GOX in the pH-responsive hydrogel matrix and it was able to change color changing pH, enabling also a possible naked-eye application. Unfortunately, one of the biggest limitations in this type of sensors is the low responsibility, generally related to the hydrogel volume. In order to overcome this limitation, Wang et al. (2016) proposed in 2016 a glucose-sensitive hydrogel film. Such film was produced through layer-by-layer assembly, using partially oxidized dextran, chitosan and GOX. The mechanism in this sensor is the following: the GOX reacts with glucose converting it to gluconic acid, lowering the pH and thus making the hydrogel film swelling. An interesting innovation in this field was proposed by Zhao et al. (2019a): they developed a device able to monitor and decrease the glucose concentration while controlling the bacterial infection in diabetic wound. This is a good innovation, being that usually diabetic patients suffer from bacterial infections that can force them to go limb amputation. They developed a GOX-loaded antimicrobial peptide hydrogel, formed from self-assembly of a heptapeptide. In this case, the GOX is able to convert glucose into hydrogen peroxide, thus decreasing the glucose concentration, and the produced hydrogen peroxide can act against the microbial activity thanks to its antimicrobial properties.

(3) *Urea and ammonia detection*. These applications can be useful, since they can replace single-point blood urea nitrogen or urea clearance tests in order to check renal and hepatic functions. As an example, Quinn et al. (2019) developed a hydrogel made of polyelectrolyte multilayer

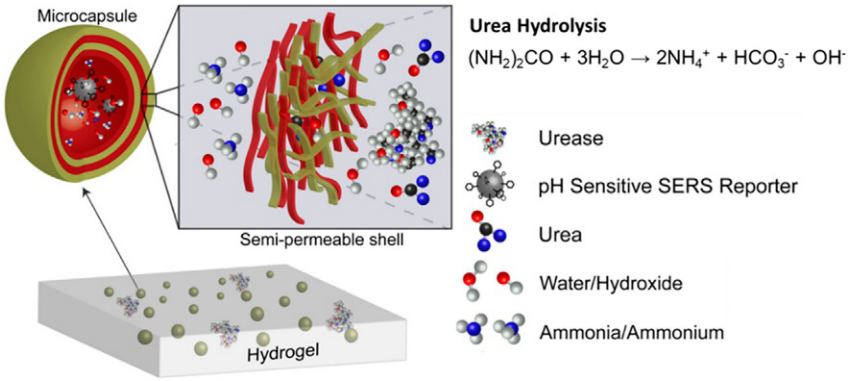

Fig. 3 Microcapsules containing surface-enhanced Raman spectroscopy (SERS) pH reporter, immobilized in an alginate hydrogel. *Reprinted from Quinn A, You Y-H, McShane MJ: Hydrogel microdomain encapsulation of stable functionalized silver nanoparticles for SERS pH and urea sensing,* Sensors *19:3521, 2019. doi:10.3390/s19163521.*

microcapsules containing a SERS-sensitive pH reporter. The mechanism behind this sensor is the incorporation of the urease inside the hydrogel matrix, thus enabling the recognition of urea in different concentrations. A schematic representation of this structure can be observed in Fig. 3. As another example, Erfkamp et al. (2019) developed an enzyme-based piezoresistive ammonia sensor based on alkaline pH change sensitive hydrogel. The gel was produced using acrylic acid and 2-(dimethylamino)ethyl methacrylate, fixed in the center of a circuit board and a pressure sensor chip was put on top of the synthetized hydrogel. For all these types of sensors, it is of pivotal importance the immobilization of the urease enzyme, since thanks to its presence the hydrogel is able to swell in presence of urea. Then, the swelling can generate an output signal that can be correlated to the urea concentration.

Not only the interactions between an enzyme and its substrate are of importance in these kinds of applications, since also other molecular interactions can be present, in particular antibody-antigen interactions and nucleotide and DNA interactions. As far as the formers are concerned, their working principle is based on the recognition of antigens or antibodies immobilized on a transducer to antibodies or antigen respectively; the signal is proportional to the concentration of the analyte. The preparation of these types of sensors are several: the antibodies or the antigens can be immobilized in a hydrogel matrix, or they can be chemically linked inside the network,

or a copolymerization between antibody antigen-binding fragments and the hydrogel can occur. Furthermore, several detection solutions can be applied in this type of sensing application, as an example, the quartz crystal microgravimetry with dissipation and the surface plasmon resonance can be cited (QCM-D and SPR respectively).

QCD-M is a technique that quantifies the decrease of the resonance frequency of the quartz crystal when the mass increases, while SPR is based on evanescent waves to examine surfaces through the change in the refractive index due to analyte binding. In general, hydrogels were mainly used as immobilizers of antigens or antibodies thanks to their peculiarities (Scarano et al., 2010). However, these techniques have recently become less importance since they are time consuming and require skilled operators; as a matter of facts, site-direct immobilization techniques are the ones that are recently gaining more importance. They are based on specific adsorption of the antigen or the antibody-binding protein modified surface, even if it is still possible to find some antibody-antigen based hydrogel sensing devices. As an example, Randriantsilefisoa et al. (2019) developed an hydrogel matrix based on polyethylene glycol (PEG) and dendritic polyglycerol (dPG). Their sensor was used for sensitive detection of antibodies, since the hydrogel matrix was customizable for antibody and peptide diffusion and it was able to covalently link any peptide for specifically recognizing its target antibody. As another example, one of the most recent work is that of Lim et al. (2020) that developed a bio-conjugated polyacrylamide-based hydrogel (HBPAAm) able to respond to the presence of hepatitis B core antigen (HBcAg) by a change of hydrogel weight. In this hydrogel, the affinity crosslinks produced by the bio-specific coupling between the bound HBcAg and its antibody are immobilized; in the presence of the analyte, they are disrupted and this induce the hydrogel's swelling, proportional to the concentration of free HBcAg. Nucleotide and DNA interactions have also been introduced previously. The devices exploiting these interactions offer several opportunities in different fields, such as biosensing, drug delivery and tissue engineering applications. Due to the scope of this chapter, here only the biosensing application will be dealt with. DNA biosensors hydrogels are generally formed by a synthetic polymer as a scaffold and analyte binding, functional DNA crosslinker as the sensing element. The dissociation of the crosslink (it takes place in the presence of the analyte) determine a change in the hydrogel swelling, mass or a release of some incapsulated substances, that represent the output signal of this system.

An example of this sensors can be found in the work of Mao et al. (2017) that developed a portable visual detector for different targets based on DNA crosslinked hydrogel. In their system, the hydrogel was the target-responsive unit, while gold nanorods have been used as multicolor signal readout circuit. The hydrogel was based on aptamers and the encapsulation of glucoamylase determined the molecular recognition and amplification. This system was based on a colorimetric method (since the gold nanorods were able to change color changing the analyte concentration), but this technique has some drawbacks, being the most important ones the low sensitivity and the semi-quantitative nature of this process. In order to overcome these limitations, in literature the use of a molecular imprinting approach to form hydrogel has been reported (Li et al., 2017). These hydrogels can be produced using polymerizable methacrylate groups carried by aptamers with bifunctional aptamer-protein complexes as crosslinker. Other than this possibility, also DNA-based electrochemical biosensors can be of great importance. As an example, Liu et al. (2018) developed an electrochemical biosensor based on hybrid DNA hydrogel entrapped on indium tin oxide/polyethylene terephthalate electrode.

5.2 Sensors based on living cells and bacteria

Using microorganisms for biosensing can bring useful benefits: they are able to detect a wide range of substances in different environmental conditions, such as pH, temperature or various oxygen concentrations. The exploitation of hydrogels in this kind of devices is evident, since hydrogels can guarantee a high gas exchange rate and transport of nutrients to cells or bacteria immobilized inside the matrix. Two different applications will be analyzed in this chapter: cells and bacteria. As far as the formers are concerned, different applications are present in literature. As an example, Qiao et al. (2015) developed a novel taste biosensor based on ligand-receptor interactions. In their work, they fixed a SD rat's taste bud tissue on a glassy carbon electrode using sodium alginate-starch gel. Here the tissue was blocked between two nuclear microporous membranes, thus creating a sandwich-type sensing membrane.

They were able to measure the current induced by the presence of capsaicin and gingerol that stimulate the receptors. Other works using cells can be found, such as that of Jiang et al. (2017) that produced a mast cell-based electrochemical sensor for detection of N-acylhomoserine lactones (AHLs): AHLs are bacterial quorum signaling molecules, and their

detection can be used for a primary evaluation of food-borne pathogenic bacteria. A novel challenge for this type of sensors is their application in the development of an assay method for the reflection of the real feelings of gustatory tissue; that is the development of an artificial tasting device for sensing and taste information standardization. Novel biosensors are produced using specific taste bud tissues as sensing elements and a hydrogel matrix can be used to encapsulate them and increase the stability of the device. As an example, Wei et al. (2017) developed a biosensor for the investigation of the kinetic characteristics of the receptor in taste using porcine taste bud tissue. Moreover, here a sandwich-type membrane was used, realized with aldehyde starch, and fixed on a glassy carbon electrode. This system was able to detect the response current induced by some specific molecules and then characterize the kinetic between the cells and their ligands. Shifting to bacteria-based biosensors, also they can be of great importance in hydrogel-based sensors. An example can be found in the work of Zhang et al. (2019b) that developed a toxicity test sensor for heavy ions through the bacterial enzymatic activity and viability induced from toxic heavy metal ions. The bacteria *Escherichia coli* was encapsulated inside a hydrogel matrix made from polyvinyl alcohol; such encapsulation allowed the enhancement of the viability and activity of the biological sensing agent and they improve the portability of the system itself. As another example, Alehosseini et al. (2019) developed a sensor for probiotic protection, made from an agarose-based hydrogel. In their work, they used the oil-induced biphasic hydrogel particle formation for encapsulate the sensitive strain *Bifidobacterium pseudocatenulatum* CECT 7765, thus guaranteeing the production of a protection for the bacterium.

This type of protection brings several advantages, such as the generation of a continuous layer around the bacteria and the optimal combination of materials make this system ideal for its application. Another application of bacteria-based biosensor has been reported by Gao et al. (2020), that applied it for concrete self-healing. Their hydrogel was produced from gelation of alginate and chitosan with calcium ions, and *Bacillus pseudofirmus* was used as bacterium, thanks to its ability to combine high alkalinity and the long-time survivability.

6. Hydrogel-based sensors for biomedical applications

In all the previous paragraphs of this chapter, the different sensing mechanisms have been proposed and introduced, separating them between

physicochemical and biochemical mechanisms. Now, hydrogel-based sensors for biomedical applications will be analyzed, dividing them between the applications they are used for and the mechanism they exploit. In general, it can be identified five main fields where hydrogel-based sensors can be applied: cancer monitoring, cardiac rhythm monitoring, cell metabolite detection, tissue engineering and wound healing monitoring.

6.1 Cancer monitoring

Cancer monitoring is probably one of the biggest tasks for sensing in biomedical fields. For an early cancer detection, it is important to notice the presence of some altered expression of biomolecules, such as proteins and glycans. It can be thus noticed how it is important to develop some biosensors able to couple selectivity and a good sensitivity. As an example, (Gao et al., 2020; Ngoepe et al., 2013) focused on H_2O_2 and TNF-α (a cytokine), two inflammatory molecules that can be used for the detection of different cancer pathologies. They decided to focus on enzyme-based biosensors for water peroxide detection, while on antibody-based biosensors for cytokines.

Another example has been reported by Crulhas et al. (2017), who developed hydrogel microstructures for the detection of superoxide anions released by cancer cells. In their work, they used an electrochemical biosensor based on ferrocene, coupled with superoxide dismutase in a poly(ethylene glycol) diacrylate hydrogel matrix. In order to characterize their biosensor, they opted for electrochemical impedance spectroscopy and cyclic voltammetry. A good application of hydrogel-based biosensors can also be found in the work of Wu et al. (2019b), that developed a visual sensor for glutathione detection, a molecule whose imbalance is the cause of various diseases such as cancers, Alzheimer's or Parkinson. Such sensor exploited a stimulus-responsive fluorescent hydrogel, using 5,6-bicarboxylic fluorescein crosslinked partly ammoniated polyacrylamide. Zhao et al. (2019b) show the applicability of these devices in cancer imaging. They worked on a ruthenium-albumin hydrogel that shows strong luminescence, applying it for imaging purposes. Furthermore, it showed good selectivity to cancer cells with respect to non-cancer ones.

6.2 Cardiac rhythm monitoring

The cardiac rhythm can be measured from the artery pulse, that is an indicator of different cardiovascular pathologies. In this case, the material should

fulfill different requirements: it should be smart, flexible and soft. Hydrogels seem to be one of the best solutions to this problem: they can fit the curvature of human skin and are sensitive to the detection of the three different pulse waves associated to wrist pulse, blood pressure and cardiac rhythm that are percussion wave (P1 wave), tidal wave (P2 wave) and diastolic wave (P3 wave) respectively. As a first example, Chen et al. (2019) developed a conductive polymer hydrogel suitable for different applications. They were able to incorporate multiple hydrogen bonding 2-ureido-4[1H]-pyrimidone groups as crosslinking points into a polyaniline/poly(4-styrenesulfonate) network, offering great conductivity, excellent stretchability and injectability. This can be observed in Fig. 4.

This hydrogel was then used as strain sensor able to monitor both large motions and subtle movements. Another example that can be reported is that of Wang et al. (2018), who developed a novel conductive hydrogel produced from interpenetrating polyaniline and poly(acrylamide-*co*-hydroxyethyl methyl acrylate), that showed a good strength and toughness to cyclic loading. For this application also DN hydrogels have been proposed, as it can be observed in the work of Hou et al. (2019). In their work, they proposed a DN hydrogel-based ionic strain sensor based on agar/NaCl/polyacrylamide double network that combined good sensitivity and mechanical properties. This device was useful for monitoring human motions, such

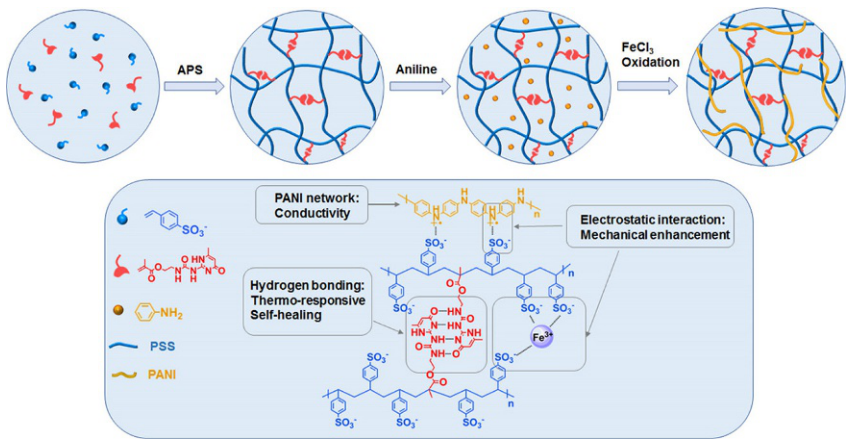

Fig. 4 Schematic illustration of synthesis process of the supramolecular conductive PANI/PSS–UPy hydrogels and the formation mechanism. *Reprinted with the permission of ACS Publications Chen J, Peng Q, Thundat T, Zeng H: Stretchable, injectable, and self-healing conductive hydrogel enabled by multiple hydrogen bonding toward wearable electronics,* Chem Mater *31:4553–4563, 2019. doi:10.1021/acs.chemmater.9b01239.*

as joint motions, slight wrist pulse and throat muscle movement. The problem related to these hydrogel-based sensors is that it was not always possible to distinguish between P1, P2 and P3 waves; furthermore, the frequency and precision of these devices can be rough. To overcome these limitations, new formulations of hydrogel-based sensor incorporating nanoparticles have been proposed. As an example, Han et al. (2017) developed a two-stage process for the production of an adhesive polydopamine-clay-polyacrylamide hydrogel. This system showed good properties, such as repeatable and durable adhesiveness thanks to which it can adhere to human skin without causing an inflammatory response, and can be used in wrist pulse measurements. A different solution for improving the sensitivity of these sensors has been proposed by Zhang et al. (2018), who developed an hydrogel matrix containing MXene ($Ti_3C_2T_x$). During the characterization of this system, they were able to notice that the strain sensitivity was higher compared to other hydrogel-based sensors.

6.3 Cell metabolite detection

Classical methods for cell metabolite detection are cell's cultivation and intermittent cells and media culture collection, but they present several disadvantages (Shi et al., 2019). They require a large number of cells, reactants and costly operations; furthermore, the information provided on the dynamics and time evolution of the system are not complete.

Due to these problems, efforts have been accomplished in the development of smart and innovative biological mechanism approaches for monitoring biosystem changes. In this application, hydrogel-based systems play an important role: this is due to the fact that cell metabolite detection can be performed monitoring the trend of various properties such as pH or molecules concentration. As an example, Yan et al. (2009) developed an optical enzyme-based biosensor for local detection of hydrogen peroxide secreted by stimulated macrophages. Their system presented an enzyme-carrying hydrogel structure, made from PEG. They added horseradish peroxidase (HRP) and amplex red in order to create the sensing system: amplex red has the ability to becoming fluorescent in the presence of HRP and H_2O_2. Another example is provided by Li et al. (2015), who developed a biosensor platform based on a Pt nanoparticle-modified conductive polymer hydrogel (CPH) electrode and using a polyaniline/PtNP-modified glassy carbon electrode as the working electrode. They used the amperometric response for the detection of metabolites, showing good performances

in a wide linear range, together with high sensitivity and rapid response time for a variety of molecules. Up to now, the only disadvantages of these type of biosensors is their stability over a long period of time, making them not very reliable over a large time span.

6.4 Tissue engineering

Tissue engineering is a novel biomedical practice that combine cells usage, engineering and innovative materials for the formation of new tissues. In this field, hydrogels are a class of useful materials, thanks to their ability as immobilizing scaffolds for bioreceptors so that they can detect, measure and monitor the concentration of specific molecules, their interactions and kinetics. An example of hydrogels in this field has been reported in the work of Wang et al. (2013), that developed an optical ATP sensor for *in situ* monitoring of extracellular ATP in biological tissue. ATP (adenosine triphosphate) is a key molecule in cellular metabolism thanks to its extracellular signaling activity. As a matter of fact, important in tissue engineering applications is the possibility to identify and monitor cellular activity: cells proliferation, migration, cytokine release and specific molecules production are some of the useful indicator that can be monitored for tracking the scaffold's efficiency (Shen et al., 2015). One of the most important aspects in tissue engineering application is the quantification of the activity of particular functional protein molecules.

6.5 Wound healing monitoring

Wound healing is probably one of the most important physiological process, that allow the reconstruction of destroyed tissue by living ones in a living being. Hydrogels have gained much importance also in this application thanks to their properties and can be used for activating immune cells to speed up wound healing (Xiang et al., 2020). Furthermore, in recent years different researchers have also proposed the possibility to use hydrogels also as wound healing monitoring device and not only as promoters (Sridhar and Takahata, 2009). Examples of negative phenomena that can take place during the treatment of the wounds are infections and bacteria proliferation: thus, their recognition is of pivotal importance for avoiding pain and complications. Generally, hydrogel-based sensors for wound healing monitor pH, temperature or humidity for controlling the wound. As far as the bacteria proliferations are concerned, they can be detected from the presence of particular molecules or compounds. Some examples for these applications

are already available in literature. For instance, Rahimi et al. (2016) developed a pH sensing array for wound assessment, working with sensors made from two-screen-printed electrodes with a conductive-selective polymeric membrane made from polyaniline. As another example, Jankowska et al. (2017) synthetized a fluorescent sensing system for the control of the wound status and to continuously monitor it.

7. Conclusions

This chapter has dealt with hydrogel applications in physicochemical sensors and biosensors. It can be noticed how hydrogel-based sensors have gained more importance in the recent years. This was possible thanks to the properties of hydrogels, that can be of pivotal importance in sensor applications: as an example, the high water content guarantees biocompatibility and allow the diffusion of different molecules through their network. Furthermore, important is also their tunability and their ability to respond to external stimuli that give hydrogels great versatility. Such versatility can be verified by the wide range of applications of hydrogel-based sensors: pH, temperature or pressure responsive sensors, but also enzyme or cell-based biosensors. Great importance has been given to the development of novel hydrogels' formulations and their synthesis, since the development of new hydrogels matrixes can be the "winning factor" for the preparation of new sensors in this field.

References

Alehosseini A, Gomez del Pulgar EM, Fabra MJ, et al.: Agarose-based freeze-dried capsules prepared by the oil-induced biphasic hydrogel particle formation approach for the protection of sensitive probiotic bacteria, *Food Hydrocoll* 87:487–496, 2019. https://doi.org/10.1016/j.foodhyd.2018.08.032.

An R, Zhang X, Han L, et al.: Healing, flexible, high thermal sensitive dual-network ionic conductive hydrogels for 3D linear temperature sensor, *Mater Sci Eng C* 107:110310, 2020. https://doi.org/10.1016/j.msec.2019.110310.

Bhalla N, Jolly P, Formisano N, Estrela P: Introduction to biosensors, *Essays Biochem* 60:1–8, 2016. https://doi.org/10.1042/EBC20150001.

Buchberger A, Maierhofer P, Bergmann A, et al.: Single particle detector using the evanescent field of a silicon nitride waveguide, In Proc. IEEE sensors. 2019, pp 2019–2022. https://doi.org/10.1109/SENSORS43011.2019.8956493. 2019-Octob.

Buenger D, Topuz F, Groll J: Hydrogels in sensing applications, *Prog Polym Sci* 37: 1678–1719, 2012. https://doi.org/10.1016/j.progpolymsci.2012.09.001.

Burrs SL, Vanegas DC, Bhargava M, et al.: A comparative study of graphene-hydrogel hybrid bionanocomposites for biosensing, *Analyst* 140:1466–1476, 2015. https://doi.org/10.1039/c4an01788a.

Chen J, Peng Q, Thundat T, Zeng H: Stretchable, injectable, and self-healing conductive hydrogel enabled by multiple hydrogen bonding toward wearable electronics, *Chem Mater* 31:4553–4563, 2019. https://doi.org/10.1021/acs.chemmater.9b01239.

Cheng W, Liu Y: 2—Redox-responsive hydrogels, In Jana S, Maiti S, Jana S, editors: *Biopolymer-based composites*, 2017, Woodhead Publishing, pp 31–60. ISBN 978-0-08-101914-6.

Choe A, Yeom J, Shanker R, Kim MP, Kang S, Ko H: Stretchable and wearable colorimetric patches based on thermoresponsive plasmonic microgels embedded in a hydrogel film, *NPG Asia Mater* 10:912–922, 2018. https://doi.org/10.1038/s41427-018-0086-6.

Crulhas BP, Recco LC, Delella FK, Pedrosa VA: A novel superoxide anion biosensor for monitoring reactive species of oxygen released by cancer cells, *Electroanalysis* 29: 1252–1257, 2017. https://doi.org/10.1002/elan.201600767.

Culver HR, Clegg JR, Peppas NA: Analyte-responsive hydrogels: intelligent materials for biosensing and drug delivery, *Acc Chem Res* 50:170–178, 2017. https://doi.org/10.1021/acs.accounts.6b00533.

Deng K, Bellmann C, Fu Y, Rohn M, Guenther M, Gerlach G: Miniaturized force-compensated hydrogel-based pH sensors, *Sens Actuators B* 255:3495–3504, 2018. https://doi.org/10.1016/j.snb.2017.09.183.

Dincer C, Bruch R, Costa-Rama E, et al.: Disposable sensors in diagnostics, food, and environmental monitoring, *Adv Mater* 31:1–28, 2019. https://doi.org/10.1002/adma.201806739.

Echeverria C, Fernandes S, Godinho M, Borges J, Soares P: Functional stimuli-responsive gels: hydrogels and microgels, *Gels* 4:54, 2018. https://doi.org/10.3390/gels4020054.

Erfkamp J, Guenther M, Gerlach G: Enzyme-functionalized piezoresistive hydrogel biosensors for the detection of urea, *Sensors* 19:1–15, 2019. https://doi.org/10.3390/s19132858.

Flory PJ, Rehner J: Statistical mechanics of cross-linked polymer networks I. Rubberlike elasticity, *J Chem Phys* 11:512–520, 1943. https://doi.org/10.1063/1.1723791.

Fu J, In Het Panhuis M: Hydrogel properties and applications, *J Mater Chem B* 7:1523–1525, 2019. https://doi.org/10.1039/c9tb90023c.

Ganji F, Vasheghani-Farahani S, Vasheghani-Farahani E: Theoretical description of hydrogel swelling: a review, *Iran Polym J* 19:375–398, 2010.

Gao M, Guo J, Cao H, et al.: Immobilized bacteria with pH-response hydrogel for self-healing of concrete, *J Environ Manage* 261:110225, 2020. https://doi.org/10.1016/j.jenvman.2020.110225.

Han L, Lu X, Liu K, et al.: Mussel-inspired adhesive and tough hydrogel based on nanoclay confined dopamine polymerization, *ACS Nano* 11:2561–2574, 2017. https://doi.org/10.1021/acsnano.6b05318.

Hines L, Petersen K, Lum G, Sitti M: Soft actuators for small-scale robotics, *Adv Mater* 29:1603483, 2016. https://doi.org/10.1002/adma.201603483.

Hong W, Chen Y, Feng X, et al.: Full-color CO2 gas sensing by an inverse opal photonic hydrogel, *Chem Commun* 49:8229–8231, 2013. https://doi.org/10.1039/c3cc44825h.

Hou W, Sheng N, Zhang X, et al.: Design of injectable agar/NaCl/polyacrylamide ionic hydrogels for high performance strain sensors, *Carbohydr Polym* 211:322–328, 2019. https://doi.org/10.1016/j.carbpol.2019.01.094.

Hulanicki A, Glab S, Ingman F: Chemical sensors definitions and classification, *Pure Appl Chem* 63:1247–1250, 1991. https://doi.org/10.1351/pac199163091247.

Jang JI, Jeong H-C: Shear induced TiO2 nano structure using brush-coating for liquid crystal alignment, *Crystals* 10:1–7, 2020. https://doi.org/10.3390/cryst10100860.

Jang E, Koh WG: Multiplexed enzyme-based bioassay within microfluidic devices using shape-coded hydrogel microparticles, *Sens Actuators B* 143:681–688, 2010. https://doi.org/10.1016/j.snb.2009.10.028.

Jankowska DA, Bannwarth MB, Schulenburg C, et al.: Simultaneous detection of pH value and glucose concentrations for wound monitoring applications, *Biosens Bioelectron* 87:312–319, 2017. https://doi.org/10.1016/j.bios.2016.08.072.

Jiang D, Feng D, Jiang H, et al.: Preliminary study on an innovative, simple mast cell-based electrochemical method for detecting foodborne pathogenic bacterial quorum signaling molecules (N-acyl-homoserine-lactones), *Biosens Bioelectron* 90:436–442, 2017. https://doi.org/10.1016/j.bios.2016.09.096.

Johnson KA, Goody RS: The original Michaelis constant: translation of the 1913 Michaelis-Menten paper, *Biochemistry* 50:8264–8269, 2011. https://doi.org/10.1021/bi201284u.

Justino CIL, Freitas AC, Pereira R, Duarte AC, Rocha Santos TAP: Recent developments in recognition elements for chemical sensors and biosensors, *TrAC Trends Anal Chem* 68:2–17, 2015. https://doi.org/10.1016/j.trac.2015.03.006.

Kim JH, Lim SY, Nam DH, Ryu J, Ku SH, Park CB: Self-assembled, photoluminescent peptide hydrogel as a versatile platform for enzyme-based optical biosensors, *Biosens Bioelectron* 26:1860–1865, 2011. https://doi.org/10.1016/j.bios.2010.01.026.

Kim Y, Namgung H, Lee TS: Synthesis of a glucose oxidase-conjugated, polyacrylamide-based, fluorescent hydrogel for a reusable, ratiometric glucose sensor, *Polym Chem* 7:6655–6661, 2016. https://doi.org/10.1039/c6py01120a.

Li L, Wang Y, Pan L, et al.: A nanostructured conductive hydrogels-based biosensor platform for human metabolite detection, *Nano Lett* 15:1146–1151, 2015. https://doi.org/10.1021/nl504217p.

Li XF, Wang TJ, Qian Y, Jiang GZ, Zhang DD, Liu WB: Dietary niacin requirement of juvenile blunt snout bream Megalobrama amblycephala based on a dose–response study, *Aquacult Nutr* 23:1410–1417, 2017. https://doi.org/10.1111/anu.12516.

Li L, Scheiger JM, Levkin PA: Design and applications of photoresponsive hydrogels, *Adv Mater* 31:1–17, 2019. https://doi.org/10.1002/adma.201807333.

Li Y, Hu C, Lan J, et al.: Hydrogel-based temperature sensor with water retention, frost resistance and remoldability, *Polymer* 186:122027, 2020. https://doi.org/10.1016/j.polymer.2019.122027.

Liang Z, Zhang J, Wu C, et al.: Flexible and self-healing electrochemical hydrogel sensor with high efficiency toward glucose monitoring, *Biosens Bioelectron* 155:112105, 2020. https://doi.org/10.1016/j.bios.2020.112105.

Lim SL, Ooi CW, Low LE, et al.: Synthesis of poly(acrylamide)-based hydrogel for bio-sensing of hepatitis B core antigen, *Mater Chem Phys* 243:122578, 2020. https://doi.org/10.1016/j.matchemphys.2019.122578.

Liu S, Su W, Li Y, Zhang L, Ding X: Manufacturing of an electrochemical biosensing platform based on hybrid DNA hydrogel: taking lung cancer-specific miR-21 as an example, *Biosens Bioelectron* 103:1–5, 2018. https://doi.org/10.1016/j.bios.2017.12.021.

Mahinroosta M, Jomeh Farsangi Z, Allahverdi A, Shakoori Z: Hydrogels as intelligent materials: a brief review of synthesis, properties and applications, *Mater Today Chem* 8:42–55, 2018. https://doi.org/10.1016/j.mtchem.2018.02.004.

Maitra J, Shukla V: Cross-linking in hydrogels—a review, *Am J Polym Sci* 4:25–31, 2014.

Mao Y, Li J, Yan J, et al.: A portable visual detection method based on a target-responsive DNA hydrogel and color change of gold nanorods, *Chem Commun* 53:6375–6378, 2017. https://doi.org/10.1039/c7cc01360d.

Mehrotra P: Biosensors and their applications—a review, *J Oral Biol Craniofac Res* 6:153–159, 2016. https://doi.org/10.1016/j.jobcr.2015.12.002.

Mugweru A, Clark BL, Pishko MV: Electrochemical sensor array for glucose monitoring fabricated by rapid immobilization of active glucose oxidase within photochemically polymerized hydrogels, *J Diabetes Sci Technol* 1:366–371, 2007. https://doi.org/10.1177/193229680700100308.

Ngoepe M, Choonara YE, Tyagi C, et al.: Integration of biosensors and drug delivery technologies for early detection and chronic management of illness, *Sensors (Switzerland)* 13:7680–7713, 2013. https://doi.org/10.3390/s130607680.

Ozay H, Ozay O: Rhodamine based reusable and colorimetric naked-eye hydrogel sensors for Fe3+ ion, *Chem Eng J* 232:364–371, 2013. https://doi.org/10.1016/j.cej.2013.07.111.

Pathak AK, Singh VK: A wide range and highly sensitive optical fiber pH sensor using polyacrylamide hydrogel, *Opt Fiber Technol* 39:43–48, 2017. https://doi.org/10.1016/j.yofte.2017.09.022.

Puttasakul T, Pintavirooj C, Sangma C, Sukjee W: Hydrogel based-electrochemical gas sensor for explosive material detection, *IEEE Sensors J* 19:8556–8562, 2019.

Qiao L, Jiao L, Pang G, Xie J: A novel pungency biosensor prepared with fixing taste-bud tissue of rats, *Biosens Bioelectron* 68:454–461, 2015. https://doi.org/10.1016/j.bios.2015.01.032.

Quinn A, You Y-H, McShane MJ: Hydrogel microdomain encapsulation of stable functionalized silver nanoparticles for SERS pH and urea sensing, *Sensors* 19:3521, 2019. https://doi.org/10.3390/s19163521.

Rahimi R, Ochoa M, Parupudi T, et al.: A low-cost flexible pH sensor array for wound assessment, *Sens Actuators B* 229:609–617, 2016. https://doi.org/10.1016/j.snb.2015.12.082.

Randriantsilefisoa R, Cuellar-Camacho JL, Chowdhury MS, Dey P, Schedler U, Haag R: Highly sensitive detection of antibodies in a soft bioactive three-dimensional bioorthogonal hydrogel, *J Mater Chem B* 7:3220–3231, 2019. https://doi.org/10.1039/c9tb00234k.

Richter A, Paschew G, Klatt S, Lienig J, Arndt KF, Adler HJP: Review on hydrogel-based pH sensors and microsensors, *Sensors* 8:561–581, 2008. https://doi.org/10.3390/s8010561.

Sannino A, Pappadà S, Giotta L, Valli L, Maffezzoli A: Spin coating cellulose derivatives on quartz crystal microbalance plates to obtain hydrogel-based fast sensors and actuators, *J Appl Polym Sci* 106:3040–3050, 2007. https://doi.org/10.1002/app.25899.

Scarano S, Mascini M, Turner APF, Minunni M: Surface plasmon resonance imaging for affinity-based biosensors, *Biosens Bioelectron* 25:957–966, 2010. https://doi.org/10.1016/j.bios.2009.08.039.

Shen X, Shamshina JL, Berton P, Gurau G, Rogers RD: Hydrogels based on cellulose and chitin: fabrication, properties, and applications, *Green Chem* 18:53–75, 2015. https://doi.org/10.1039/c5gc02396c.

Shetye SP, Ajeet G, Shilpa B, Pankaj G: Hydrogels: introduction, preparation, characterization and applications, *Int J Res Methodol* 1:47–71, 2015.

Shi J, Tong L, Tong W, et al.: Current progress in long-term and continuous cell metabolite detection using microfluidics, *TrAC Trends Anal Chem* 117:263–279, 2019. https://doi.org/10.1016/j.trac.2019.05.028.

Shibata D: Colorectal cancer: perspectives on treatment, survivorship, and outcomes, *Cancer Control* 17:4–5, 2010. https://doi.org/10.1177/107327481001700101.

Shin J, Braun PV, Lee W: Fast response photonic crystal pH sensor based on templated photo-polymerized hydrogel inverse opal, *Sens Actuators B* 150:183–190, 2010. https://doi.org/10.1016/j.snb.2010.07.018.

Shin J, Han SG, Lee W: Inverse opal pH sensors with various protic monomers copolymerized with polyhydroxyethylmethacrylate hydrogel, *Anal Chim Acta* 752:87–93, 2012. https://doi.org/10.1016/j.aca.2012.09.026.

Sridhar V, Takahata K: A hydrogel-based passive wireless sensor using a flex-circuit inductive transducer, *Sensors Actuators A Phys* 155:58–65, 2009. https://doi.org/10.1016/j.sna.2009.08.010.

Sun Z, Li Z, Qu K, et al.: A review on recent advances in gel adhesion and their potential applications, *J Mol Liq* 325:115254, 2021. https://doi.org/10.1016/j.molliq.2020.115254.

Tokuyama H, Kitamura E, Seida Y: Development of zirconia nanoparticle-loaded hydrogel for arsenic adsorption and sensing, *React Funct Polym* 146:104427, 2020. https://doi.org/10.1016/j.reactfunctpolym.2019.104427.

Tsuchiya M, Kurashina Y, Onoe H: Eye-recognizable and repeatable biochemical flexible sensors using low angle-dependent photonic colloidal crystal hydrogel microbeads, *Sci Rep* 9:1–10, 2019. https://doi.org/10.1038/s41598-019-53499-2.

Vashist S: Continuous glucose monitoring systems: a review, *Diagnostics* 3:385–412, 2013. https://doi.org/10.3390/diagnostics3040385.

Vigneshvar S, Sudhakumari CC, Senthilkumaran B, Prakash H: Recent advances in biosensor technology for potential applications—an overview, *Front Bioeng Biotechnol* 4:1–9, 2016. https://doi.org/10.3389/fbioe.2016.00011.

Wang C, Huang CYC, Lin WC: Optical ATP biosensor for extracellular ATP measurement, *Biosens Bioelectron* 43:355–361, 2013. https://doi.org/10.1016/j.bios.2012.12.027.

Wang X, Li Q, Guan Y, Zhang Y: Glucose oxidase-incorporated hydrogel thin film for fast optical glucose detecting under physiological conditions, *Mater Today Chem* 1–2:7–14, 2016. https://doi.org/10.1016/j.mtchem.2016.10.005.

Wang Z, Chen J, Cong Y, et al.: Ultrastretchable strain sensors and arrays with high sensitivity and linearity based on super tough conductive hydrogels, *Chem Mater* 30:8062–8069, 2018. https://doi.org/10.1021/acs.chemmater.8b03999.

Wei L, Qiao L, Pang G, Xie J: A kinetic study of bitter taste receptor sensing using immobilized porcine taste bud tissues, *Biosens Bioelectron* 92:74–80, 2017. https://doi.org/10.1016/j.bios.2017.01.064.

Wu XJ, Choi MMF, Chen CS, Wu XM: On-line monitoring of methanol in n-hexane by an organic-phase alcohol biosensor, *Biosens Bioelectron* 22:1337–1344, 2007. https://doi.org/10.1016/j.bios.2006.06.002.

Wu S, Wu S, Yi Z, et al.: Hydrogel-based fluorescent dual pH and oxygen sensors loaded in 96-well plates for high-throughput cell metabolism studies, *Sensors* 18:564, 2018. https://doi.org/10.3390/s18020564.

Wu J, Wu Z, Han S, et al.: Extremely deformable, transparent, and high-performance gas sensor based on ionic conductive hydrogel, *ACS Appl Mater Interfaces* 11:2364–2373, 2019a. https://doi.org/10.1021/acsami.8b17437.

Wu R, Ge H, Liu C, et al.: A novel thermometer-type hydrogel senor for glutathione detection, *Talanta* 196:191–196, 2019b. https://doi.org/10.1016/j.talanta.2018.12.020.

Xia S, Zhang Q, Song S, Duan L, Gao G: Bioinspired dynamic cross-linking hydrogel sensors with skin-like strain and pressure sensing behaviors, *Chem Mater* 31:9522–9531, 2019. https://doi.org/10.1021/acs.chemmater.9b03919.

Xiang J, Shen L, Hong Y: Status and future scope of hydrogels in wound healing: synthesis, materials and evaluation, *Eur Polym J* 130:109609, 2020. https://doi.org/10.1016/j.eurpolymj.2020.109609.

Yan J, Sun Y, Zhu H, Marcu L, Revzin A: Enzyme-containing hydrogel micropatterns serving a dual purpose of cell sequestration and metabolite detection, *Biosens Bioelectron* 24:2604–2610, 2009. https://doi.org/10.1016/j.bios.2009.01.029.

Zhang ZF, Zhang Y: Humidity sensor based on optical fiber attached with hydrogel spheres, *Opt Laser Technol* 74:16–19, 2015. https://doi.org/10.1016/j.optlastec.2015.05.006.

Zhang Y, Wang X, Xu C, et al.: Fabrication of chitosan gel droplets via crosslinking of inverse Pickering emulsifications, *Carbohydr Polym* 186:1–8, 2018. https://doi.org/10.1016/j.carbpol.2017.12.062.

Zhang Y, Chen K, Li Y, et al.: High-strength, self-healable, temperature-sensitive, MXene-containing composite hydrogel as a smart compression sensor, *ACS Appl Mater Interfaces* 11:47350–47357, 2019a. https://doi.org/10.1021/acsami.9b16078.

Zhang Y, Ren T, He J, Tian H, Jin B: Acute heavy metal toxicity test based on bacteria-hydrogel, *Colloids Surf A Physicochem Eng Asp* 563:318–323, 2019b. https://doi.org/10.1016/j.colsurfa.2018.12.016.

Zhao Y, Lei M, Liu SX, Zhao Q: Smart hydrogel-based optical fiber SPR sensor for pH measurements, *Sens Actuators B* 261:226–232, 2018. https://doi.org/10.1016/j.snb.2018.01.120.

Zhao Y, Du X, Jiang L, et al.: Glucose oxidase-loaded antimicrobial peptide hydrogels: potential dressings for diabetic wound, *J Nanosci Nanotechnol* 20:2087–2094, 2019a. https://doi.org/10.1166/jnn.2020.17189.

Zhao Z, Hu R, Shi H, et al.: Design of ruthenium-albumin hydrogel for cancer therapeutics and luminescent imaging, *J Inorg Biochem* 194:19–25, 2019b. https://doi.org/10.1016/j.jinorgbio.2019.02.002.

Zhi H, Gao J, Feng L: Hydrogel-based gas sensors for NO2 and NH3, *ACS Sens* 5:772–780, 2020. https://doi.org/10.1021/acssensors.9b02383.

Zhou M, Guo J, Yang C: Ratiometric fluorescence sensor for Fe3+ ions detection based on quantum dot-doped hydrogel optical fiber, *Sens Actuators B* 264:52–58, 2018. https://doi.org/10.1016/j.snb.2018.02.119.

Zhu T, Cheng Y, Cao C, et al.: A semi-interpenetrating network ionic hydrogel for strain sensing with high sensitivity, large strain range, and stable cycle performance, *Chem Eng J* 385:123912, 2020. https://doi.org/10.1016/j.cej.2019.123912.

This page intentionally left blank

CHAPTER FIVE

Integrated microsystems for bridging multiscale elements

Koki Yoshida and Hiroaki Onoe*
Keio University, Kanagawa, Japan
*Corresponding author: e-mail address: onoe@mech.keio.ac.jp

Contents

1. Introduction 158
2. Nano-scale function of hydrogels 158
   2.1 Stimuli responsiveness 158
   2.2 Imparting functions to polymer chains 160
3. Fabrication of hydrogel 161
   3.1 Physically cross-linked hydrogel: Calcium alginate hydrogel 162
   3.2 Chemically cross-linked hydrogel: Poly(*N*-isopropylacrylamide) 168
4. Multi-scale function of hydrogels with functional materials 173
   4.1 Magnetic nanoparticles 174
   4.2 Pt catalyst 175
   4.3 Graphene, carbon nanotube 176
   4.4 Photonic colloidal crystal 177
   4.5 Living cells 180
5. Integrated soft robots by bridging multiscale elements 181
   5.1 Integrated with rigid body 182
   5.2 Hydrogel patterning integrated systems 184
6. Discussion 186
   6.1 Problems of stimuli-responsive hydrogel 186
   6.2 Other functional hydrogels 189
7. Conclusion 190
References 191

Abstract

Hydrogels are emerging as enabling materials for a wide range of new applications for soft robots because of their flexibility. Some of the polymer chains that make up the hydrogel have a nano-scale function of swelling and contracting in response to external stimuli. In addition, because the network of polymer chains is on the nanometer order, it is possible to encapsulate various functional materials. Therefore, stimulus-responsive hydrogels and functional materials encapsulating hydrogels are also being actively studied for use as soft robot components. From a fundamentals point of view, the nano-scale functions of hydrogels, fabrication method, and integration with functional

Advances in Chemical Engineering, Volume 57
ISSN 0065-2377
https://doi.org/10.1016/bs.ache.2021.02.001

materials must be considered for each specific application. This section provides a basic understanding of hydrogels and the recent development of novel fabrication and integration of hydrogel with functional materials such as magnetic nanoparticles, Pt catalyst, graphene, photonic colloidal crystal, and living cells.

1. Introduction

Conventional robots are usually composed of sensors, driving sources, and controlling systems. Furthermore, in order to achieve specific motion, such as bending, twisting, or rotation, the soft robot needs to be constructed with structures and mechanisms adjusted to the purpose. For fabricating soft robots, actuators and sensors must be constructed from flexible materials, and these elements must be integrated.

Recently, hydrogels are widely used for soft chemical sensors and soft actuators (Liu et al., 2020). They have nanoscale functions due to their own polymer chains, and functional materials can be encapsulated in the network of polymer chains. Therefore, the hydrogels are expected to a candidate for an integrated component of multi-scale elements (Lee et al., 2020). In this section, we introduce the nanoscale functions of hydrogels, the fabrication method of hydrogels, the multi-scale function of hydrogels with functional materials, and finally integrated soft robots by bridging multiscale elements.

2. Nano-scale function of hydrogels

A hydrogel is a polymer network containing aqueous solution, and most hydrogel has flexibility and biocompatibility. Some of the polymer chains that make up the hydrogel have a nano-scale function of swelling and contracting in response to external stimuli (Mano, 2008). In addition, because the network of polymer chains is on the nanometer order (ex. network of calcium alginate gel: ~10 nm (Turco et al., 2011)), it is possible to encapsulate various functional materials. Therefore, stimulus-responsive hydrogels and functional materials encapsulating gels are also being actively studied for use as soft robot components.

2.1 Stimuli responsiveness

Among the properties of the hydrogel, stimuli-responsiveness has been widely applied to sensors (Buenger et al., 2012; Richter et al., 2008) and actuators (Cui et al., 2019; Ionov, 2013). Hydrogel's polymeric chains

produce volume changes in response to external stimuli such as temperature (Morales et al., 2016; Schild, 1992), pH (Bassik et al., 2010), light (Takashima et al., 2012), and chemical compounds (ex. glucose (Ye and Wang, 2010), acetone (Zhao et al., 2014), alcohol (Tsuchiya et al., 2019)). Here, we introduce in detail the volumetric change mechanism of temperature-responsive gels, which is one of the most widely used. The temperature-responsiveness of the thermal-responsive hydrogel is due to the changing the interaction between the polymer chains and the solvent in response to temperature changes. The swelling and contraction mechanisms of poly(*N*-isopropyl acrylamide) (pNIPAm) gels, which is the most widely studied of the temperature-responsive gels, are described (Schild, 1992). The pNIPAm gel has a lower critical solution temperature (LCST) around 33 °C. The pNIPAm gel absorbs a large amount of water and swells greatly at low temperatures (<33 °C). On the other hand, the pNIPAm gel shrinks discontinuously around the LCST at high temperature (>33 °C). The pNIPAm gel has a hydrophilic amide group and a hydrophobic isopropyl group, and the methylene and methane groups in the main chain of the polymer chain are also hydrophobic. At low temperature, the hydrophilic amide groups interact strongly with water by hydrogen bonding, and each chain is surrounding by water. The pNIPAm gel take up a large amount of water and largely swells due to the strong interaction between water and the polymer chains (Fig. 1A). This phenomenon is called hydration. On the other hand, the hydrogel bonds that drive hydration are thermally week, and the hydrogen bonds between the amide group and the water weaken as the temperature increases. Then, the water leaves

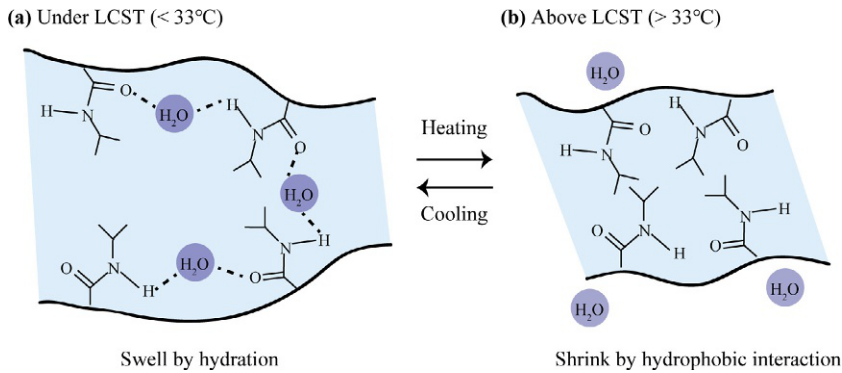

Fig. 1 (A) The pNIPAm gel swell by hydration. (B) The pNIPAm gel shrink by hydrophobic interaction.

the polymer chain as the temperature increases. The hydrophobic isopropyl group tend to gather with each other in water due to their low affinity for water. When the effect of aggregation due to the interaction of hydrophobic isopropyl groups exceeds the effect of reduced hydration by temperature increasing, the entire polymer chain aggregates. As a results, the pNIPAm gels shrinks with releasing the water (Fig. 1B). In other words, the temperature responsiveness is the balance between hydration and hydrophobic interaction. The various types of stimuli-responsiveness such as pH (Bassik et al., 2010), light (Takashima et al., 2012) and chemical compounds (Tsuchiya et al., 2019; Ye and Wang, 2010; Zhao et al., 2014) could be realized by modifying the functional groups of the polymer chains since the stimuli-responsive hydrogels swell and shrink by the interaction of the polymer chain.

2.2 Imparting functions to polymer chains

New functions could be realized by adding functional materials such as DNA to the polymer chains in addition to modifying the functional groups. Chemical-responsive hydrogels are also responsive to a molecule with the same functional group or similar chemical structure because of the chemical-responsive hydrogel swells or shrink due to the binding and interaction between the polymer chain and the target molecules. Thus, one of the challenges of the chemical-responsive hydrogel is the selectivity of detecting the specific molecules. In order to solve this problem, hydrogels with molecular recognition substances such as DNA (Gačanin et al., 2020; Shao et al., 2017), proteins (Banta et al., 2010), and peptides (Webber et al., 2015) have been reported. For example, DNA could detect target proteins, metal ions, organic compounds by adjusting the base sequence (Liu, 2011). In addition, DNA has the advantages of easy artificial synthesis and amplification and high thermodynamic stability. One of the methods for copolymerizing DNA into hydrogels is to use vinyl group modification and radical polymerization (Fig. 2A) (Jiang et al., 2019; Kahn et al., 2017). Both ends of DNA modified with vinyl groups play the role of cross-linking points in the polymer network and can be copolymerized with the radical-reactive functional groups of the polymer chain (Hayashi et al., 2019; Ono et al., 2008). There is a large distance between the ends of the DNA since the DNA copolymerized to the hydrogel has a linear structure when not bound to the target material (Fig. 2B top). When the target substance binds to the DNA, the structure changes into a hairpin shape and the distance between the ends

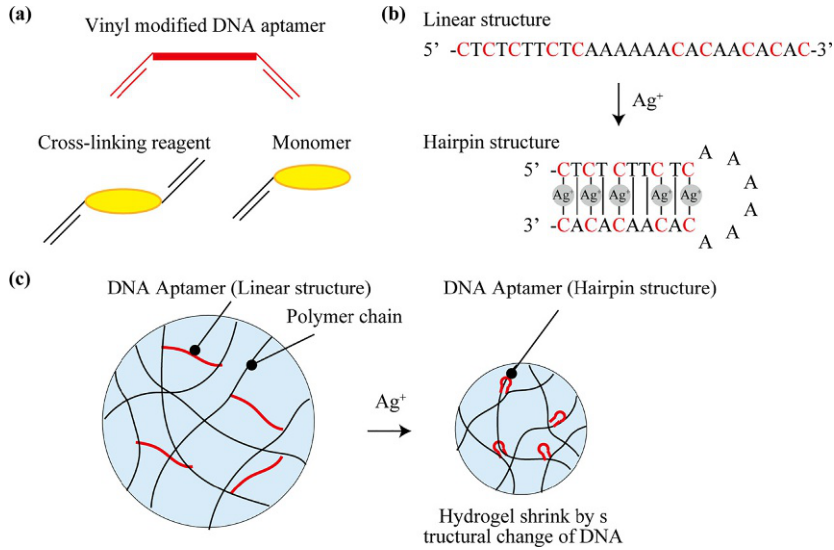

Fig. 2 (A) Copolymerization of vinyl modified DNA. (B) Structure change of DNA aptamer. (C) Volume change of DNA hydrogel.

largely decreases (Fig.2B bottom). In this process, the entire hydrogel shrinks because the copolymerized polymer chains are pulled by the structural change of the DNA (Fig.2C).

3. Fabrication of hydrogel

In order to apply hydrogel to soft robotics, it is necessary to fabricate the hydrogel into the desired shape and structure. Hydrogels are obtained by cross-linking polymer networks. There are two main types of cross-linking methods: physical cross-linking by intermolecular interactions such as hydrogen bonding and hydrophobic interactions, and chemical cross-linking by covalent bonding (Hennink and van Nostrum, 2012). When fabricating 3D structures using hydrogels, common processing methods such as machining and rolling cannot be used because hydrogels are brittle materials. Therefore, there has been a lot of research on forming hydrogels into various three-dimensional structures (Shafranek et al., 2019). In this section, we first explain the cross-linking methods of typical hydrogels commonly used in the construction of soft robots, and then we also explain the forming methods using each hydrogel.

3.1 Physically cross-linked hydrogel: Calcium alginate hydrogel

First, calcium alginate hydrogel, which is one of the typical physically cross-linked hydrogels, is described. Sodium alginate is a polymer of β-1,4-D-mannuronic acid (Man.) and α-1,4-L-glucuronic acid (Glu.) (Fig. 3A) (Lee and Mooney, 2012; Pawar and Edgar, 2012). Man. and Glu. have different steric structures and they are randomly bonded together to form linear polymers. The molecular chains of Glu. Glu. blocks are bent due to repulsion of carboxy groups, and ionic bonding occurs when divalent cations such as calcium ions enter between the chains. This ionic cross-linking occurs instantaneously between multiple sodium alginate chains and this polymerization results in gelation of calcium alginate hydrogels (Fig. 3B). Various methods to form various shapes of calcium alginate hydrogels with microfluidic devices have been reported by taking advantage of their instantaneous polymerization.

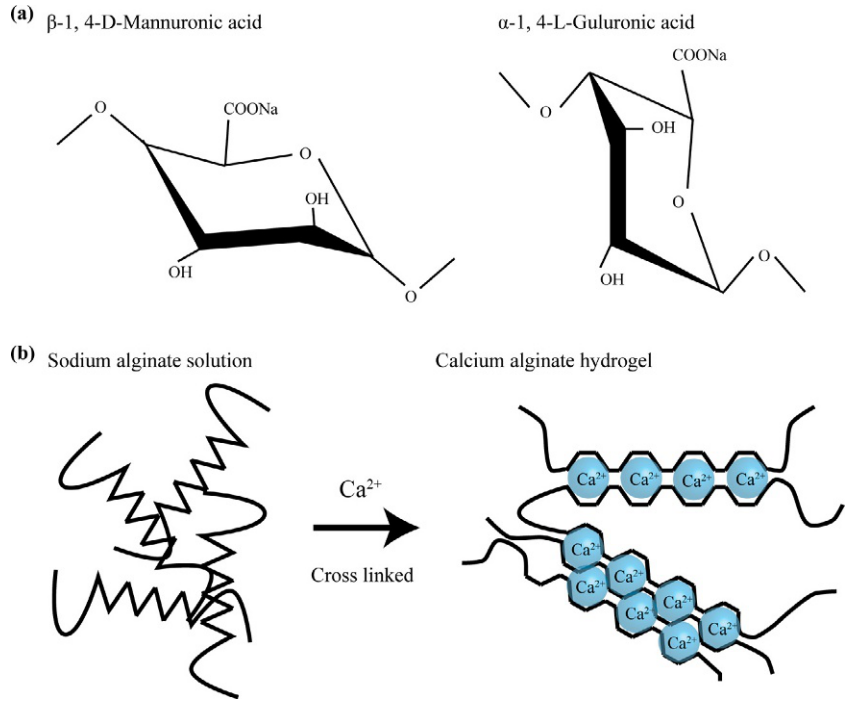

Fig. 3 (A) Molecular structures of β-1,4-D-mannuronic acid and α-1,4-L-glucuronic acid. (B) Physically cross-linked alginate hydrogel by calcium ions.

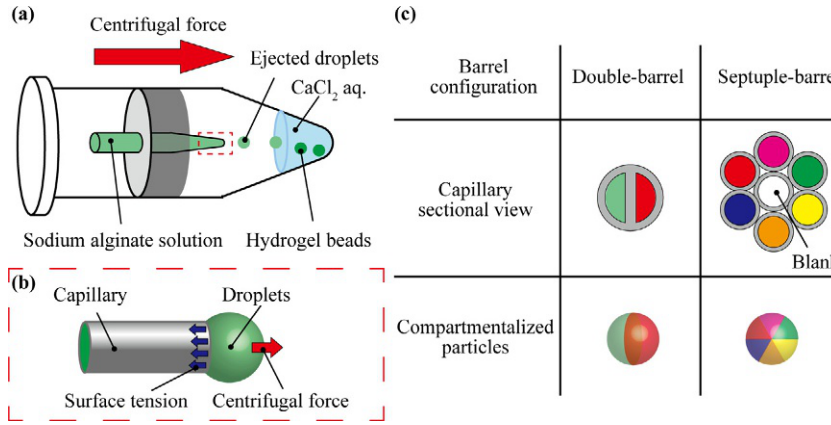

Fig. 4 (A) Centrifuge-based hydrogel beads formation. (B) Formation of micro-scale droplets. (C) Compatrmentalized particles.

For example, hydrogel beads can be fabricated by instantaneous cross-linking of droplets. Microfluidic devices using centrifugal force have been proposed for the production of micro-scale droplets (Fig. 4A) (Maeda et al., 2012). The pre-gel solution filled in the glass tube is ejected by applying centrifugal force. Then, the ejected pre-gel solution forms micro-scale droplets by the surface tension. As soon as the droplets contact with calcium chloride solution, the droplets are gelled with maintaining their geometry by rapid gelation. The size of the hydrogel beads can be adjusted by the diameter of the glass tube and the applied centrifugal force since the droplet size is determined by Tate's law (Fig. 4B). The advantage of this method is that the uniform hydrogel beads can be fabricated. In addition, hydrogel beads made of stimuli-responsive gels can quickly swell and shrink in response to external stimuli because the heat transfer and mass diffusion are rapid in microscale. Thus, the stimuli-responsive hydrogel beads are expected to use rapid chemical sensing. Compartmentalized hydrogel beads can be fabricated by compartmentalizing the cross-section of the tube (Fig. 4C). Other types of patterns such as marble or spiral can be applied to the hydrogel beads by rotating the injection tube (Yasuda et al., 2017) or droplet (Zhao et al., 2018). These compartmentalized and patterned hydrogel beads are also expected to be applied to building blocks for forming complex shapes (Glotzer and Solomon, 2007). Biochemical sensors (Tsuchiya et al., 2019), self-assembly of microgel beads(Yoshida et al., 2016), and autonomous driving robots(Hayakawa et al., 2016) have been reported by encapsulating functional materials such as colloidal crystals,

magnetic nanoparticles, and Pt catalysts in these calcium alginate beads respectively. Furthermore, this fabrication method is expected to be used for fabricating a scaffold for cell culture since the particles can be made without using oil, which harms cells (Yoshida et al., 2017; Zhao et al., 2018).

Next, we explain the fabrication method of the fiber-shaped hydrogel (Cheng et al., 2017). Hydrogel fibers have extensive applications in various fields including soft robotics, biomimetics, and biomedical application due to their capability to mimic many aspects of the physiological microenvironment. The hydrogel fibers are mainly fabricated by electrospinning or microfluidic devices. In this section, the forming method of the fiber-shaped calcium alginate hydrogels by microfluidic devices is described. The hydrogel fiber can be fabricated by continuously injecting and instant gelling the pre-gel solution (Fig. 5A) (Cheng et al., 2014). At the microscale, laminar flow is formed due to the small Reynolds number ($Re \ll 1$). Therefore, multiple liquids can flow in a microfluidic device without mixing. Using this property, hydrogel fibers with various cross-sectional patterns have been developed by forming bi-layered flow or double coaxial laminar flow inside the microfluidic device (Fig. 5B) (Cheng et al., 2014; Nakajima et al., 2017). The cross-sectional patterning of the stimuli-responsive hydrogel can be used to realize bimorph actuators with double-layered shapes and pumping with tubular structures (Fig. 5C).

Hydrogel fibers with axial patterning also have been developed by digitally controlled flow systems (Fig. 5D) (Kang et al., 2011; Takeuchi et al., 2020). The flow of the pre-gel solution is controlled by a computerized pneumatic valve system. The coding of diverse functional hydrogels on the microscale may offer new opportunities to generate a range of useful functions for soft robotics. In addition to controlling the flow, grooved fibers can be fabricated by varying the injection port of the pre-gel solution (Fig. 5E) (Kang et al., 2011; Shi et al., 2015). Since the grooved fiber is utilized for the alignment of neurons and other cells, it is expected to be applied to bio-hybrid robots in the future.

In addition, two fabrication methods of spiral-shaped hydrogels for soft robot applications have been reported: a rope-coil effect (Nie and Takeuchi, 2017; Tottori and Takeuchi, 2015) and an anisotropic gelation method (Yoshida et al., 2018; Yoshida and Onoe, 2017). A highly viscous liquid drips in a spiral due to the rope-coil effect and a spiral-shaped gel can be constructed by gelation at the same time (Fig. 6A). The materials that can be used for fabricating spiral-shaped hydrogel are limited due to the high viscosity required to cause the rope-coil effect. Next, we will introduce the

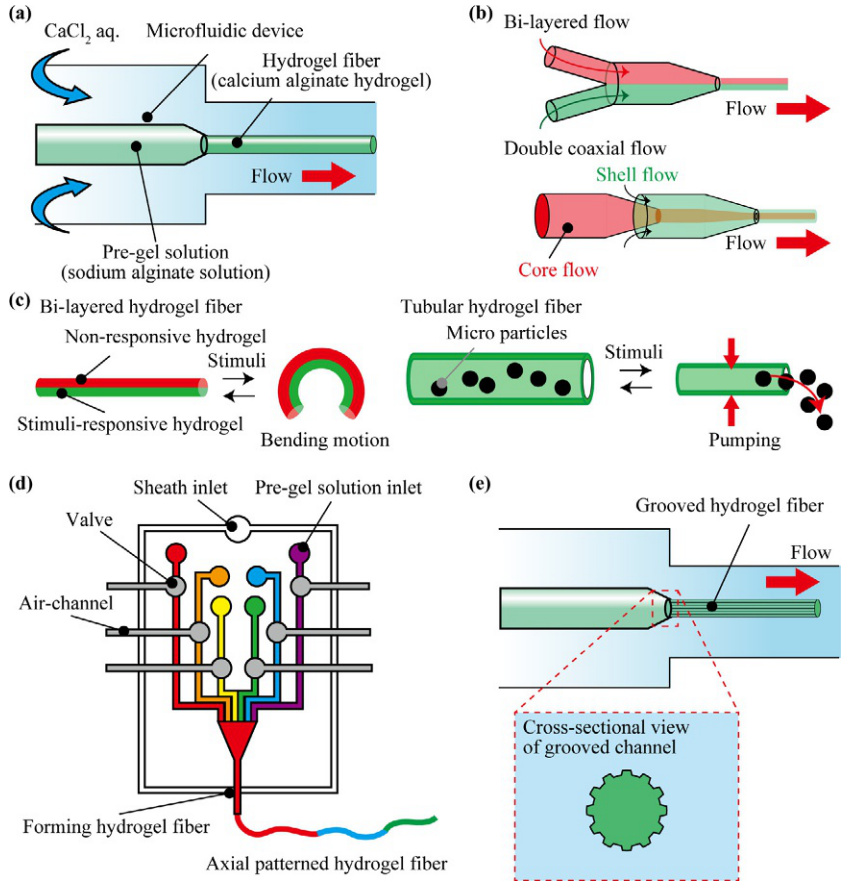

Fig. 5 (A) Fabrication of hydrogel fiber by using microfluidic device. (B) Cross-sectional patterning of hydrogel fibers: Bi-layered flow and double coaxial flow. (C) Application of patterned hydrogel fibers: bi-layered hydrogel fiber and tubular hydrogel fiber. (D) Flow control for forming axial patterning by pneumatic-valve system. (E) Fabrication of grooved hydrogel fiber.

fabrication of hydrogel microspring by the asymmetric gelation method. A microfluidic device with a bevel-tip capillary is used for the asymmetric gelation (Fig. 6B). Sodium alginate solution is injected into calcium chloride solution through the bevel-tip capillary. Asymmetric gelation occurs near the bevel-tip capillary and the hydrogel microspring can be constructed continuously. The wounding direction and pitch of the hydrogel microspring can be controlled by applying an external force such as buoyancy when ejecting pre-gel solution through the bevel-tip capillary (Fig. 6C).

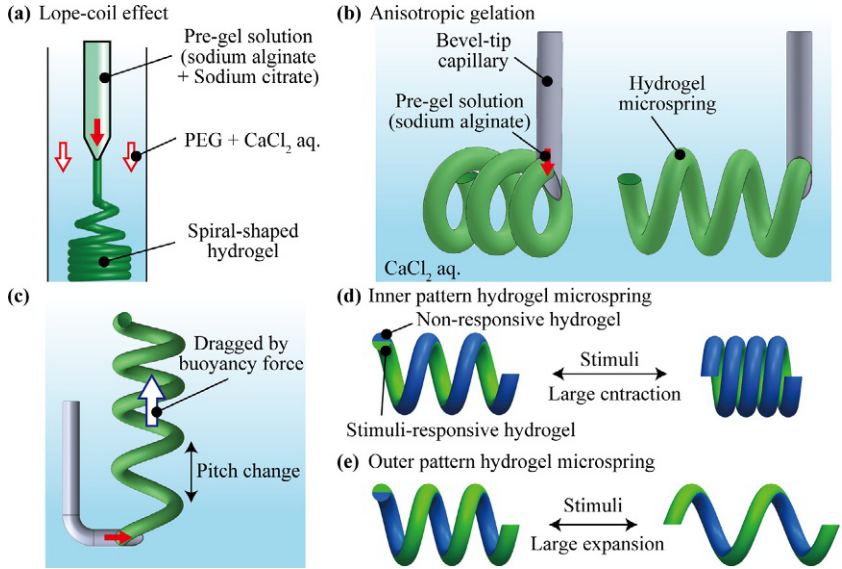

Fig. 6 (A) Fabrication of spiral-shaped hydrogel by lope-coil effect. (B) Fabrication of hydrogel microspring by anisotropic gelation. (C) Pitch of hydrogel microspring can be adjusted by bupyancy force. (D), (E) Double-layered hydrogel microspring for soft actuators: large contraction and expansion.

Hydrogel microsprings can also be patterned by forming bilayer or double coaxial laminar flows in the bevel-tip capillary. By patterning the stimuli-responsive hydrogel to the inner spring, the hydrogel microspring is largely contracted by applied stimuli (Fig. 6D). On the other hand, the hydrogel microspring is expanded by patterning the stimuli-responsive hydrogel to the outer spring (Fig. 6E). Since the spiral shape is widely used in engineering, the fabrication method of this hydrogel microspring is expected to be developed into various applications such as soft actuators.

Furthermore, polymer chains of calcium alginate hydrogel can be decomposed by the alginate lyase. Calcium alginate hydrogel can be utilized as a template for forming other hydrogels by using this enzyme. Other hydrogels can be formed into fiber or spring shapes by encapsulating inside the calcium alginate fiber (Onoe et al., 2013) or spring (Yoshida and Onoe, 2017) and then removing the outer calcium alginate hydrogel. For example, H. Onoe et al. showed that by using a microfluidic device with double-coaxial laminar flow, meter-long core-shell hydrogel microfibres encapsulating ECM proteins and differentiated cells or somatic stem cells can be fabricated and that the microfibres reconstitute intrinsic morphologies

and functions of living tissues. The method for fabricating cell fibers has three steps: formation of a core-shell hydrogel fiber using the double-coaxial laminar flow microfluidic device, culturing the cells in this core to form a fiber-shaped cellular construct, and removal of calcium alginate shell (Fig. 7A). In addition, fabrication of agarose hydrogel spring by using calcium alginate shell template has been proposed. The method is also three steps: formation of a core-shell hydrogel microspring by using double-coaxial laminar flow microfluidic device and the bevel-tip capillary, the gelation of agarose hydrogel by temperature change, and removal of calcium alginate shell (Fig. 7B). In summary, the use of alginate as a template enables the molding of materials that require time for gelation, such as collagen and agarose.

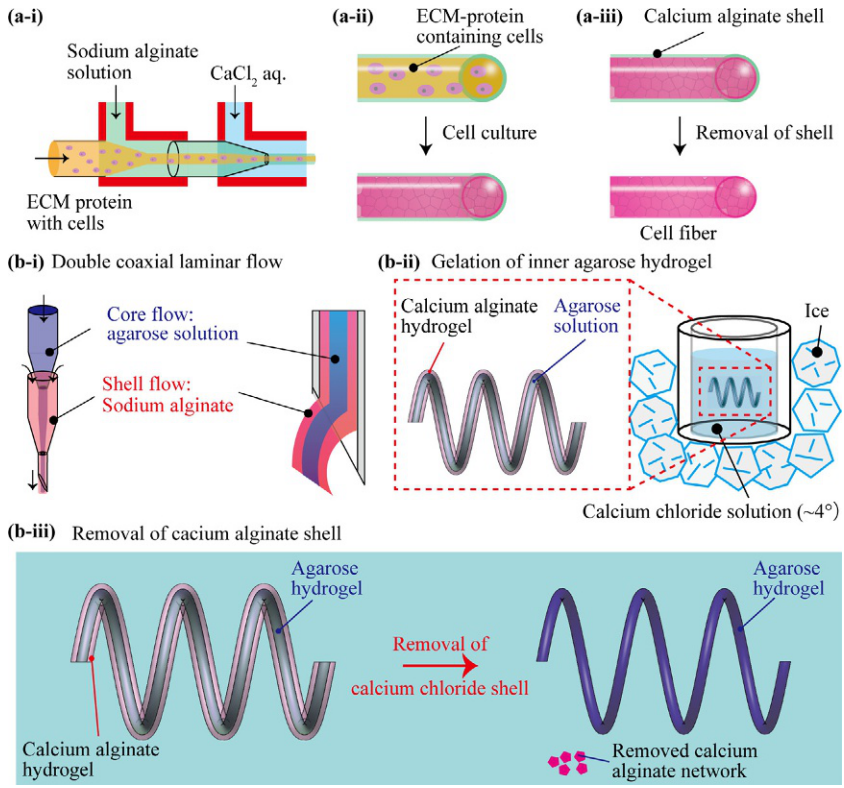

Fig. 7 (A) Fabrication process of cell fiber. (B) Fabrication process of agarose hydrogel microspring.

3.2 Chemically cross-linked hydrogel: Poly(*N*-isopropylacrylamide)

Next, we describe a typical chemically cross-linked hydrogel poly(*N*-isopropylacrylamide) (pNIPAm). pNIPAm gels are fabricated by cross-linking an acrylic monomer *N*-isopropylacrylamide. Acrylic monomers are low-molecular compounds with vinyl groups involved in polymerization. Acrylic monomers are mainly polymerized by radical reactions. Radical polymerization proceeds by initiation, propagation, and termination (Fig. 8A). Because the radicals generated by UV irradiation are highly reactive, radicals are quickly transferred to monomers and produce the

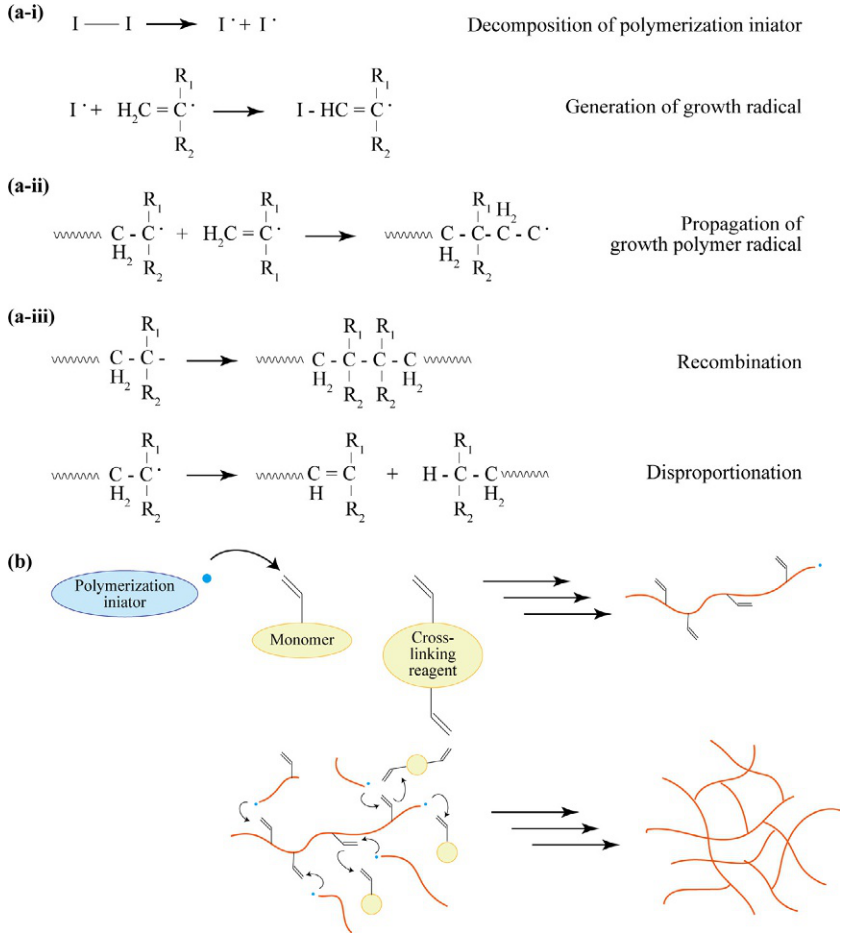

Fig. 8 (A) Reaction of radical polymerization. (B) Cross-linking of polymer network.

radical initiator for radical polymerization (Initiation). The generated radical initiator causes a rapid and continuous radical addition reaction to the double-bonded part of the vinyl group of another monomer (Propagation). This propagation reaction proceeds repeatedly until the termination reaction occurs, and a polymer with high molecular weight is obtained at once. The polymer chain can be cross-linked to create a polymer network structure by copolymerizing a divinyl compound with two vinyl groups during polymerization (Fig. 8B).

These UV cross-linked hydrogels are suitable for fabricating two-dimensional patterns by photolithography techniques. Specific pattern hydrogels can be fabricated by irradiating UV light to the pre-gel solution through a photomask (Fig. 9A) (Jeon et al., 2017). Various motions such as bending (Yoon et al., 2014) and twisting (Jeon and Hayward, 2017) caused by spatially nonuniform stresses have been reported by patterning the stimulus-responsive hydrogels and non-responsive hydrogels (Fig. 9B, C). Such bulking-driven morphogenetic processes are common in biology and have gained increasing attention for self-shaping materials for applications in soft robots (Ionov, 2015). In particular, the technique of constructing a complex three-dimensional structure by folding a planar structure is called "origami" (Fig. 9D) (Na et al., 2015; Silverberg et al., 2015). The essential characteristics of a piece of origami, that is a continuous sheet folded without cutting or gluing, are a pattern of creases that intersect in vertices, along with the "mountain"/"valley" assignment (the direction of bending) and folding angle for each crease. For realizing origami, photo-crosslinkable polymer trilayers (poly(*p*-methylstyrene) (PpMS) – pNIPAm – PpMs) have been developed, and the placement of open stripes of defined width in either of the rigid layers drives bending to an angle that can be controlled with excellent fidelity, and with control of mountain and valley assignments. It is expected that the combination of photolithography and origami strategy is powerful approach to realize the shape-morphing soft robots and soft actuators.

In addition to the photolithography technique, many types of research have been conducted to fabricate 3D structures by ejecting pre-gel solution from a nozzle and UV cross-linking, just like additive manufacturing commonly known as 3D printing (Fig. 10A) (Li et al., 2018; Shafranek et al., 2019). 3D printing is a form of digital products that can transfer objects created by computer-aided design (CAD) from the virtual world into the physical world. 3D printing using stimuli-responsive hydrogels is called 4D printing, which adds a time axis to the 3D coordinate axis, and is

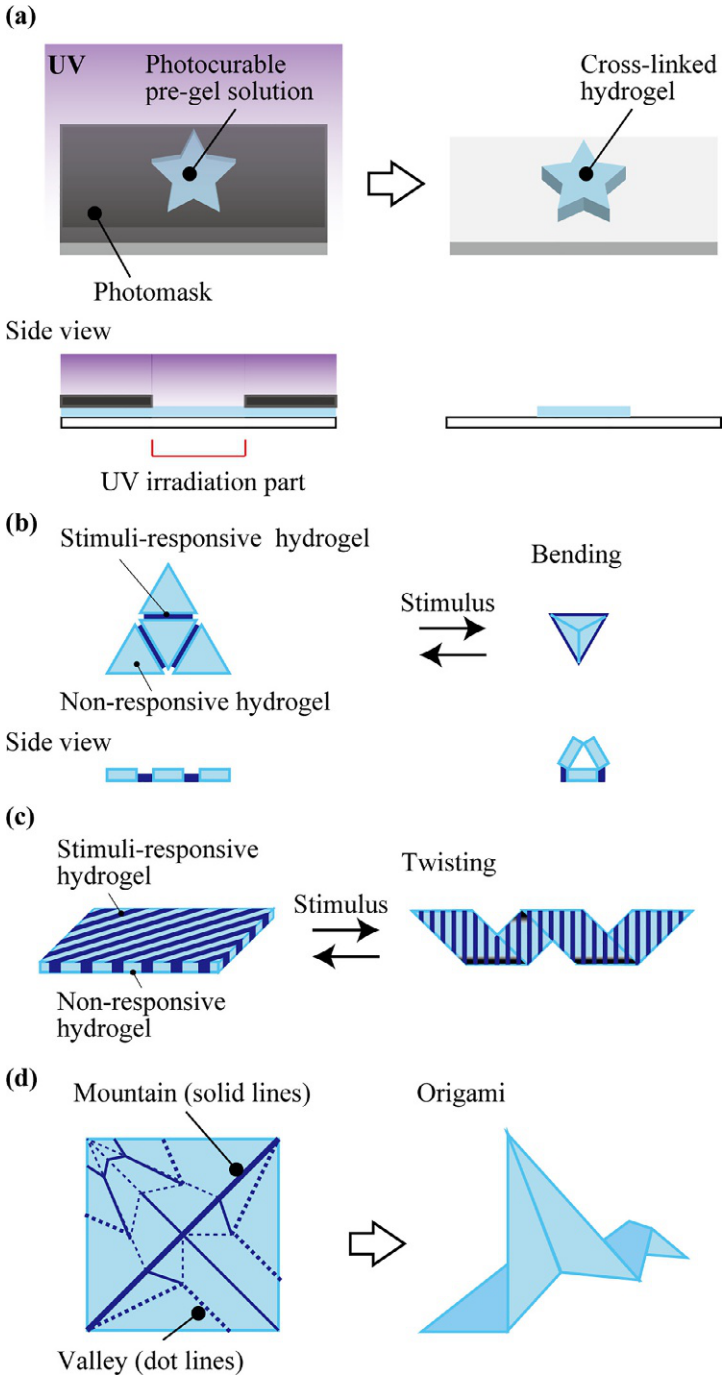

Fig. 9 (A) Photolithographic fabrication of photocurable hydrogel. (B) Bending motion of patterned stimuli-responsive hydrogel. (C) Twisting motion of stripe patterned stimuli-responsive hydrogel. (D) Origami hydrogel.

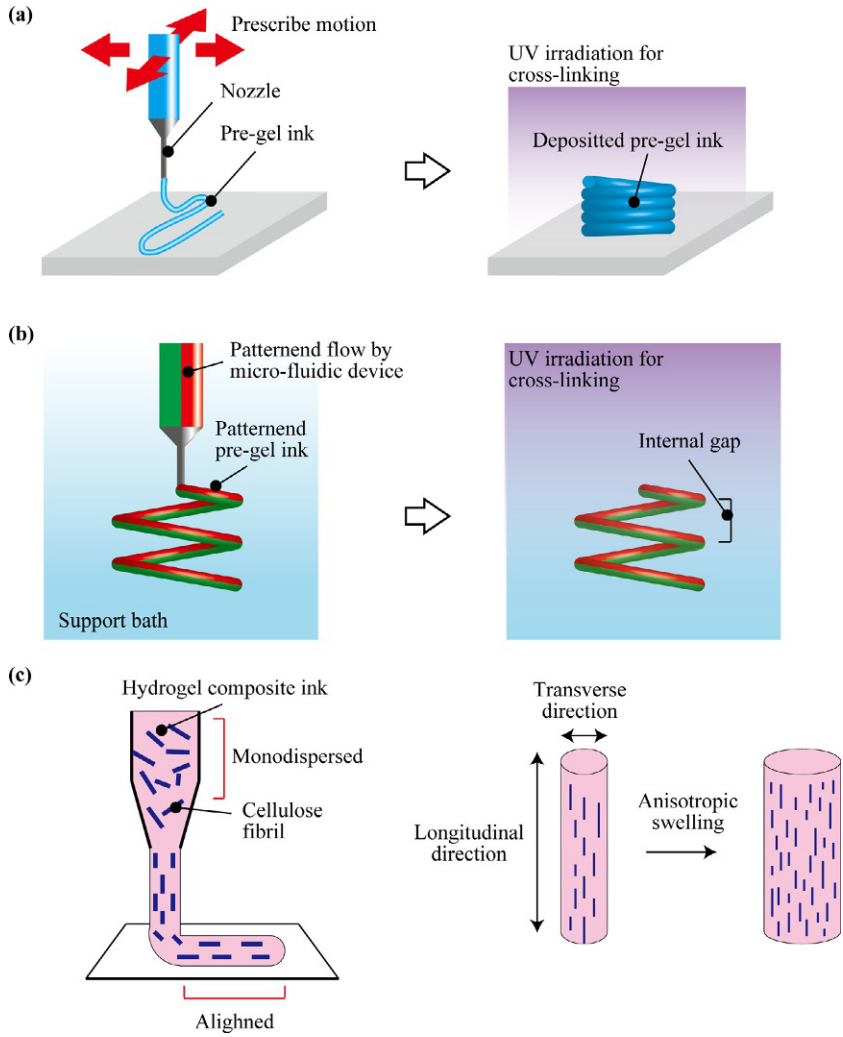

Fig. 10 (A) Direct ink writing. (B) Printing in the support bath. (C) Hydrogel composite ink composed of stiff cellulose fibrils for anisotropic swelling behavior.

expected to have various applications as a new processing method for soft materials (Momeni et al., 2017). The printing technologies are mainly divided into two categories: a direct ink writing (DIW) (Kirillova et al., 2017; Naficy et al., 2017) and a printing in a support bath (Uchida, 2019). During DIW, pressurized viscoelastic pre-gel inks are extruded out of the 3D printer's nozzles in form of printed fibers, which are deposited into patterns based on the prescribed motion of nozzles (Fig. 10A) (Yuk and

Zhao, 2018). Then deposited pre-gel ink can be cross-linked remaining its shape by UV irradiation because of its viscoelasticity. On the other hand, the pre-gel ink extruded into the support bath remains in place within the support bath because of the viscoelasticity of the support materials (Fig. 10B). The printed pre-gel-ink in the support bath can also be cross-linked. The advantage of printing in the support bath is that 4D structures with internal gap such as spiral shape could be fabricated. Furthermore, multi-layered hydrogel could be printed by utilizing the multi-flow micro-fluidic device because the pre-gel ink is extruded through the nozzle. So, these features enhance the variety of manufacturable structure. For further advancing of 3D printing technique, A. Sydney Gladman et al. have proposed hydrogel composite ink composed of stiff cellulose fibrils embedded in a soft acrylamide matrix for enabling shape change using a single material patterned in a one-step process (Fig. 10C) (Sydney Gladman et al., 2016). The composite architectures are printed using a viscoelastic ink that contains an aqueous solution of *N*,*N*-dimethylacrylamide (or *N*-isopropylacrylamide), a photoinitiator, a nanoclay, a glucose oxidase, a glucose, and a nanofibrillated cellulose (NFC). During printing, these fibrils undergo shear-induced alignment as the ink flows through the deposition nozzle, which leads to printed filaments with anisotropic stiffness, and swelling behavior in the longitudinal direction compared to the transverse direction. Harnessing anisotropic swelling allows precise control over the curvature in bilayer structures. In addition to printing technology, the development of multifunctional soft robots is expected through more study of materials.

The other types of 3D printing technology which is called stereolithography have been studied since the first commercialized 3D printing technique that was developed by Chuck Hull in 1986 (Li et al., 2020b). A stereolithography setup is made of a container that holds the photocurable pre-gel solution, a laser source (usually UV light) that induces the polymerization and cross-linking of the pre-gel solution, a system that permits the horizontal plane (X- and Y- directions) movement of the laser beam, and a system that controls the vertical plane (*Z*-direction) movement of fabrication platform (Fig. 11A). The surface of the photocurable pre-gel solution is irradiated laser source in a 2D pattern and gelled through absorbing a single photon. The fabrication platform moves layer by layer in the Z-direction after curing each layer of pre-gel solution to create the 3D construct hydrogel (Mondschein et al., 2017). In particular, two-photon polymerization (TPP) is utilized for fabricating micro- or nano-scale soft robots

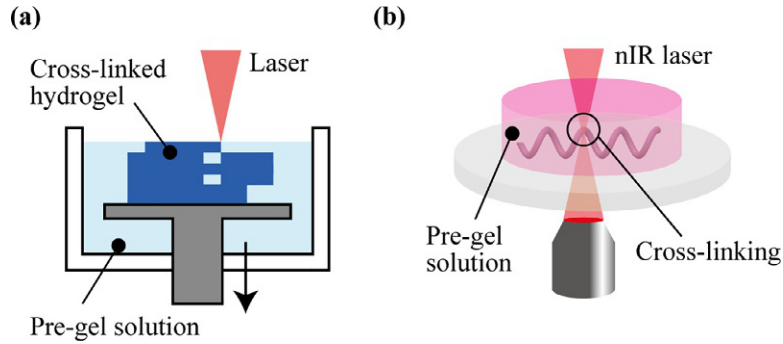

Fig. 11 (A) Stereolithography setup. (B) Two-photon polymerization.

(Huang et al., 2020; Lv et al., 2018; Peters et al., 2016; Wang et al., 2018). TPP uses near-infrared femtosecond laser (nIR laser) pulses in the focal volume particularly titanium: sapphire laser at 800 nm wavelength to initiate the polymerization of photosensitive hydrogels (Fig. 11B) (Xing et al., 2015). In the focal point of the nIR laser beam, a suitable photoinitiator can simultaneously absorb two photons within a small volume in the photosensitive pre-gel solution and let them serve as one photon to trigger the cross-linking reactions between photoinitiator molecules and monomers with a resolution of 30 μm (Liska et al., 2007). For example, Xiaopu Wang and coworkers have been developed a spiral-shaped micro-swimmer by TPP for biomedical applications (Wang et al., 2018). Huang and coworkers have proposed a programmable modular design that directly constructs 3D reconfigurable microstructures capable of sophisticated 3D-to-3D shape transformations by assembling 4D micro-building blocks which are fabricated by using two-photon polymerizable and stimuli-responsive hydrogels (Huang et al., 2020).

4. Multi-scale function of hydrogels with functional materials

In addition to the functions of its own polymer chains, hydrogels can obtain various functions by encapsulating functional materials in the polymer network. Thus, hydrogels encapsulating various functional materials on the nano- to micro-scale have been proposed. Functional materials include magnetic nanoparticles, Pt catalysts, graphene, CNTs, photonic colloidal crystals, and living cells.

4.1 Magnetic nanoparticles

Typical stimuli-responsive hydrogel actuator relies on the swelling/shrinking behavior caused by osmotic-pressure changes and one of the challenges is that the response speed is slow. To solve this problem, the development of hydrogel actuators that rapidly respond to external stimuli has been actively developed. A magnetic field is one of the external stimuli to achieve a rapid response. It is possible to fabricate hydrogels that respond to magnetic fields by encapsulating magnetic nanoparticles or grafting several functional groups onto the surface of the magnetic nanoparticles as cross-linkers (Fig. 12A) (Li et al., 2013). For example, hydrogel actuators that expand/contract (Fuhrer et al., 2009), or bend (Haider et al., 2015; Ramanujan

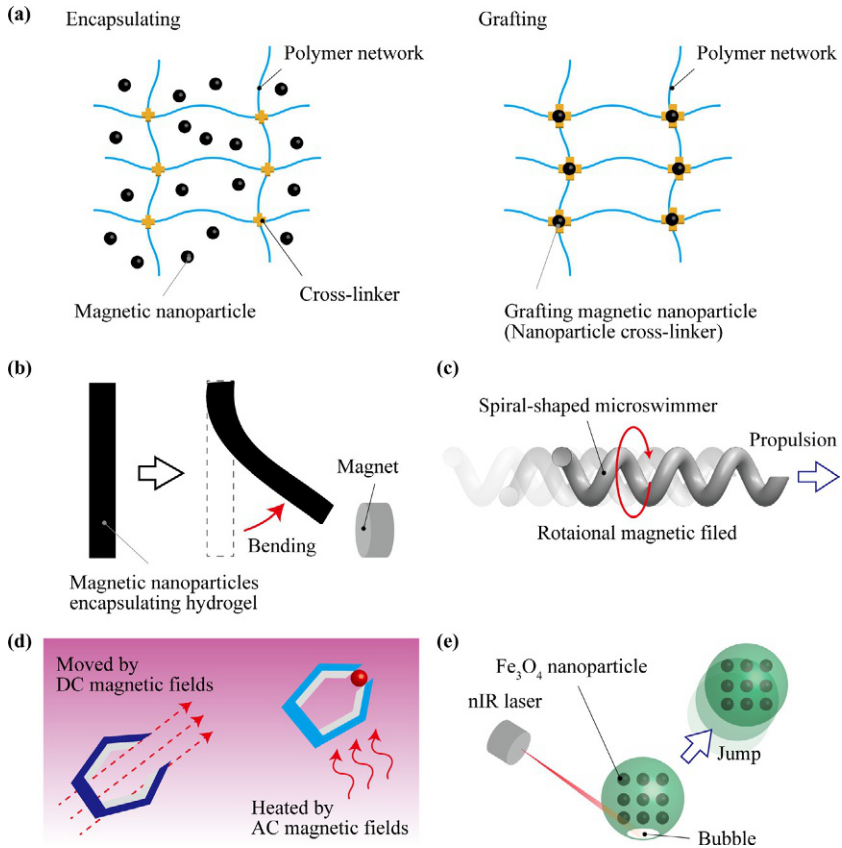

Fig. 12 (A) Magnetic response hydrogels. (B) Bending motion. (C) Propulsion of spiral-shaped micro-swimmer. (D) Remote actuation by AC magnetic fields. (E) Jumping motion by nIR irradiation.

and Lao, 2006; Yoshida and Onoe, 2017) in response to magnetic fields have been reported (Fig. 12B). Magnetic fields are also ideal candidates for driving soft robots in various environment including in vivo environment as i) untethered magnetic soft robots can be operated in any magnetically transparent environment (vacuum, gaseous environments, as well as conductive and non-conductive, Newtonian and non-Newtonian liquids) and ii) interaction with biological tissue is not problematic (Kim et al., 2011; Peters et al., 2016; Schenck, 2005). There has also been much research on microrobots that can be propelled like flagella by applying a rotating magnetic field (Fig. 12C) (Ceylan et al., 2019; Huang et al., 2016; Yoshida and Onoe, 2020). In the low Reynolds number, propulsion by flagellar rotation is highly efficient (Lighthill, 1976; Peyer et al., 2013). Thus, the spiral-shaped micro-swimmer propelled by rotating magnetic fields has the potential to use the untethered soft robots in the various micro-scale environment such as *in vivo*. In addition, magnetic fields are harmless to live organisms, and the use of biocompatible and biodegradable hydrogels is expected to be applied to *in vivo* therapies and drug deliveries (Bergeles et al., 2010; Soto et al., 2020).

In addition, the Brownian motion of magnetic nanoparticles such Fe_3O_4 in the gel can be induced by applied an AC magnetic field, which results in a heat generation (Fig. 12D) (Kuo et al., 2014). Therefore, it is possible to remotely swell and shrink the thermal-responsive hydrogel using magnetic fields. Furthermore, sphere-shaped micro-robots that can rapidly jump by the bubble caused by the photothermal effect of the embedded magnetic iron oxide nanoparticles have been proposed (Fig. 12E) (Li et al., 2020a). Therefore, magnetic nanoparticles encapsulating hydrogel could be widely used for components of soft robotics remotely driven by the various external sources.

4.2 Pt catalyst

Hydrogels contain a large amount of water, which allows the solution to diffuse into the polymer network. Therefore, the function of the catalyst encapsulated inside the hydrogel can be utilized (Lin et al., 2020). In this section, we will particularly discuss the Pt catalyst used to supply the driving source of the soft robot (Katuri et al., 2017). The Pt catalyst is nanoparticles of Pt that can accelerate the decomposition of aqueous hydrogen peroxide. The hydrogen peroxide water is instantly decomposed to produce oxygen when contact with the Pt catalyst encapsulated hydrogel such as

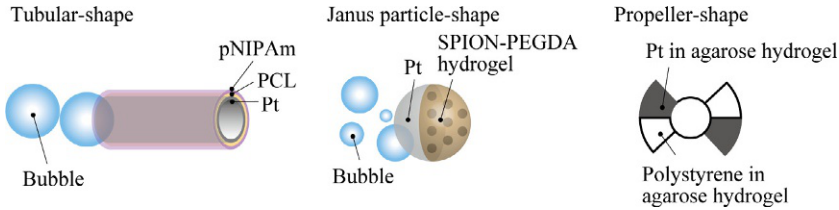

Fig. 13 Various shape of micro-robots driven Pt catalytic reaction.

$$2H_2O_2 \rightarrow 2H_2O + O_2 \quad (1)$$

This decomposition reaction is extreme and produces a large amount of oxygen. It has been proposed to use the generated oxygen as a driving source to propel tubular-shaped (Magdanz et al., 2014), Janus particle-shaped (Seo et al., 2015), and propeller-shaped (Hayakawa et al., 2016) hydrogel robots (Fig. 13). As the advantages of this catalytic reaction, untethered autonomous soft robotics and micro-scale motor could be realized. In addition, this catalyst reaction is also utilized not only for hydrogel-based soft robots but also for silicone-based pneumatic untethered soft robots (Wehner et al., 2016) since this catalytic reaction can rapidly generate oxygen.

4.3 Graphene, carbon nanotube

In general, the stimuli-responsive hydrogel actuators are driven by heat transfer and diffusion of the solution. Therefore, it is difficult to selectively swell/shrink only a part of the stimuli-responsive hydrogel because the external stimuli are uniformly transferred to the entire stimuli-responsive hydrogel. In order to solve this problem, the use of graphene, which generates heat by absorbing near-infrared light (nIR), has been reported (Robinson et al., 2011). For example, nIR-driven hydrogel actuators have been synthesized by interfacing genetically engineered elastin-like polypeptides with reduced-graphene oxide sheets (Fig. 14A) (Wang et al., 2013). The resulting nanocomposites exhibited rapid and tunable motions controlled by light position, intensity, and path, including finger-like flexing and crawling (Fig. 14B).

The CNTs, an allotropic form of carbon, are cylindrical nanostructures with a hexagonal arrangement of sp^2 hybridized carbon atoms. Basically, it is a rolled-up graphene sheet having one single-walled (Vashist et al., 2018). SWCNTs can also enhance the water molecule transport, dual-responsive actuators (thermal and optical) using poly(*N*-isopropylacrylamide)

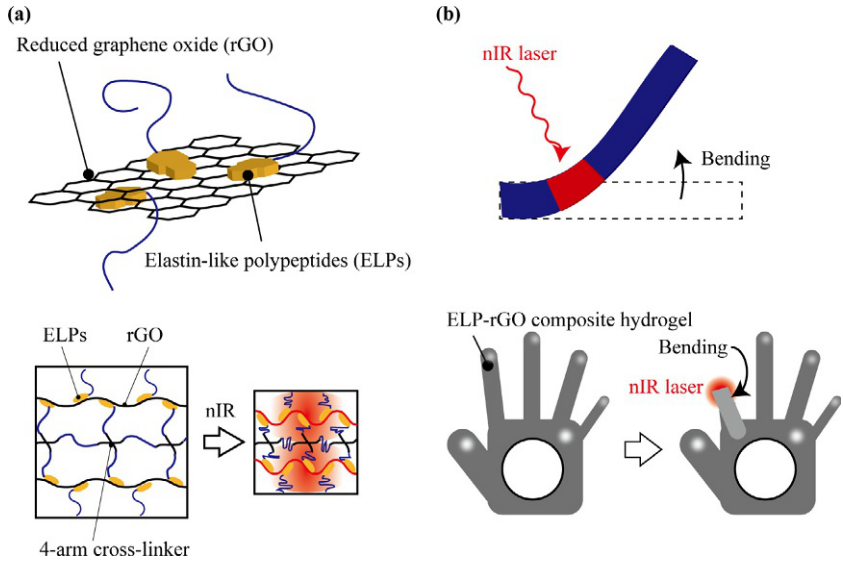

Fig. 14 (A) ELP-rGO composite hydrogel (B) ELP-rGO composite actuator for rapid and tunable motion by nIR laser.

(pNIPAM) have fabricated (Zhang et al., 2011), and the fast response speed was achieved. As graphene and CNTs constitute only carbon, hence have superior biocompatibility, low toxicity, and immunogenicity, which make them an ideal candidate to be used for biomedical applications. Near-infrared light has also biopermeability since water, which makes up 60–70% of the human body, is the most difficult to absorb nIR (~0.8–1.2 μm). Therefore, a driving method using graphene or CNTs and nIR is very promising as a remote control and energy source for micro-robots operating in living organisms.

4.4 Photonic colloidal crystal

For applying these stimuli-responsive hydrogels for biochemical sensors, it is necessary to convert the external stimulus to another type of information. A photonic colloidal crystal hydrogel, in which monodispersed colloidal particles (diameter: 1 nm–1 μm) are regularly arranged, is expected to be a powerful tool for sensors based on a stimuli-responsive hydrogel (Fig. 15A) (Ge and Yin, 2011). The photonic colloidal crystal hydrogel reflects visible-light wavelength through Bragg's diffraction as.

$$\lambda = 2dn \sin\theta \tag{2}$$

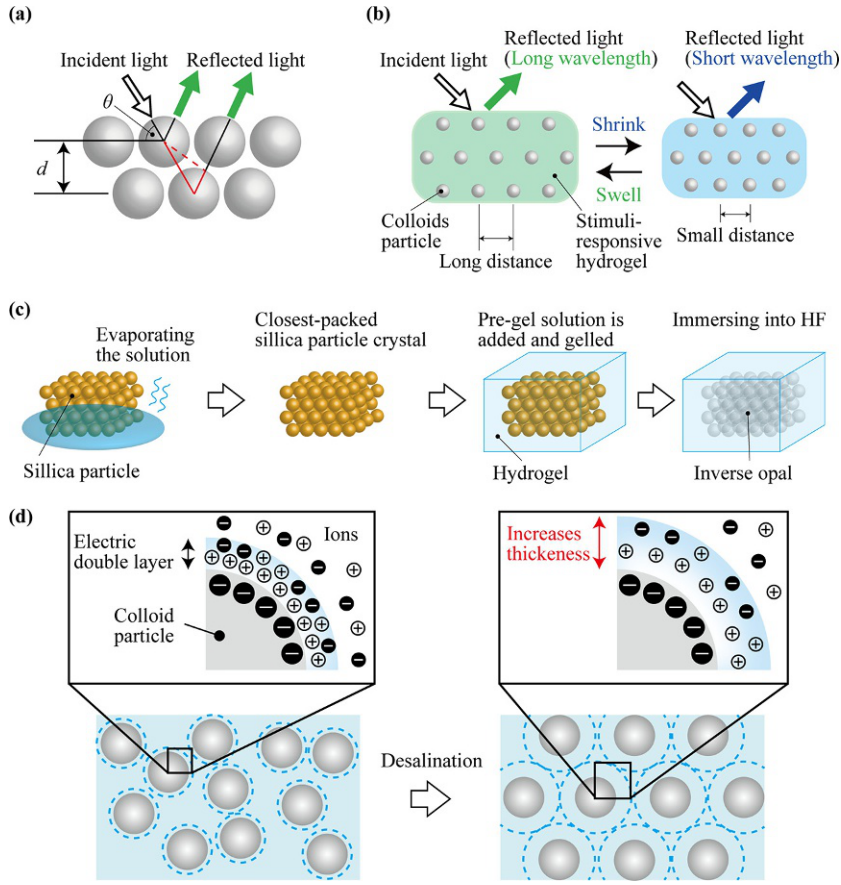

Fig. 15 (A) Photonic colloidal crystal. (B) Color change of photonic colloidal crystal hydrogel. (C) Fabrication process of vaporization method. (D) Arranged colloidal particles by electric double layer.

where d is the distance of the colloid particles, n is their effective refractive index, θ is the angle of the incident light. In this hydrogel, the intensity of the stimulus can be converted to visible color information by the change in the distance between the colloidal particles (Fig. 15B). Thus, it is possible to obtain the sensing information with the naked eye. In previous research, various types of photonic colloidal crystal hydrogel sensors have been proposed such as flexible skin temperature and alcohol sensor (Tsuchiya et al., 2019), humidity sensor (Tian et al., 2008), and certain analyzes (Ye et al., 2012).

As a method to align the colloidal particles, vaporization of solvent (Nakayama et al., 2003; Saito et al., 2003) and desalting by using ion

exchange resin (Tsuchiya et al., 2019) are proposed. In the vaporization method, photonic colloidal crystals are constructed by gradually evaporating a solution in which colloidal particles are dispersed (Fig. 15C). Then a pre-gel solution is added to the constructed colloidal crystals. After gelation, the inner colloidal crystal is dissolved by hydrofluoric acid. The porous structure which is called inverse opal created by the dissolution of the colloidal crystals can be used to reflect visible color. In the desalting method, the colloidal particles are arranged in the pre-gel solution by an electric double layer (Fig. 15D). The arraying method using an electric double layer of silica colloidal particles was described. The surface of silica colloidal particles is covered with silanol groups. Normally, the silanol groups are electronegative in solution such as.

$$\mathrm{Si-O-H \rightarrow Si-O^- + H^+} \tag{3}$$

The ionized H^+ is attracted to the colloidal particles by electrostatic interaction, while it tends to distribute uniformly by thermal motion. Therefore, H^+ is distributed in the vicinity of the colloidal particles while diffusing, which is called the electric double layer. The ions present in the solution are exchanged to H^+ and OH^- when the colloidal solution is mixed with the ion exchange resin and desalted. The concentration of ions in the colloidal solution decreases since the exchanged H^+ and OH^- become water (H_2O) molecules in the solution. As a result, the ions in the vicinity of the colloidal particles have a stronger force to diffuse uniformly in the solution, thus increasing the thickness of the electric double layer. The increasing thickness of the electric double layer causes strong repulsion to act between the particles, and the colloidal particles arrange themselves in a regular pattern.

One of the challenges of colloidal crystal structure color is that the observed color was changed depending on the observation angle because the wavelength of the reflected light is determined by the distance of the particles. To overcome this problem, a sensor with less angular dependence has been proposed by fabricating the spherical photonic colloidal crystal (Suzuki et al., 2017; Tsuchiya et al., 2019). Moreover, photonic colloidal crystals have the advantage of not color degradation because they are colored by their structure. Thus, photonic colloidal crystal hydrogels are expected to be used as a simple, wearable, and long term sensor because conventional analyzers are large, and small colorimetric sensors also have problems such as color degradation.

4.5 Living cells

At the end of this section, a hybrid system that integrates living cells and hydrogels are described (Ricotti et al., 2017). In previous research, biomimetic soft robots have been achieved by integrating cardiac muscle and soft materials through fibronectin (Fig. 16A) (Nawroth et al., 2012; Park et al., 2016). Cardiac muscles are an attractive driving source for soft robots since cardiac muscle beats spontaneously. However, integrating living cells

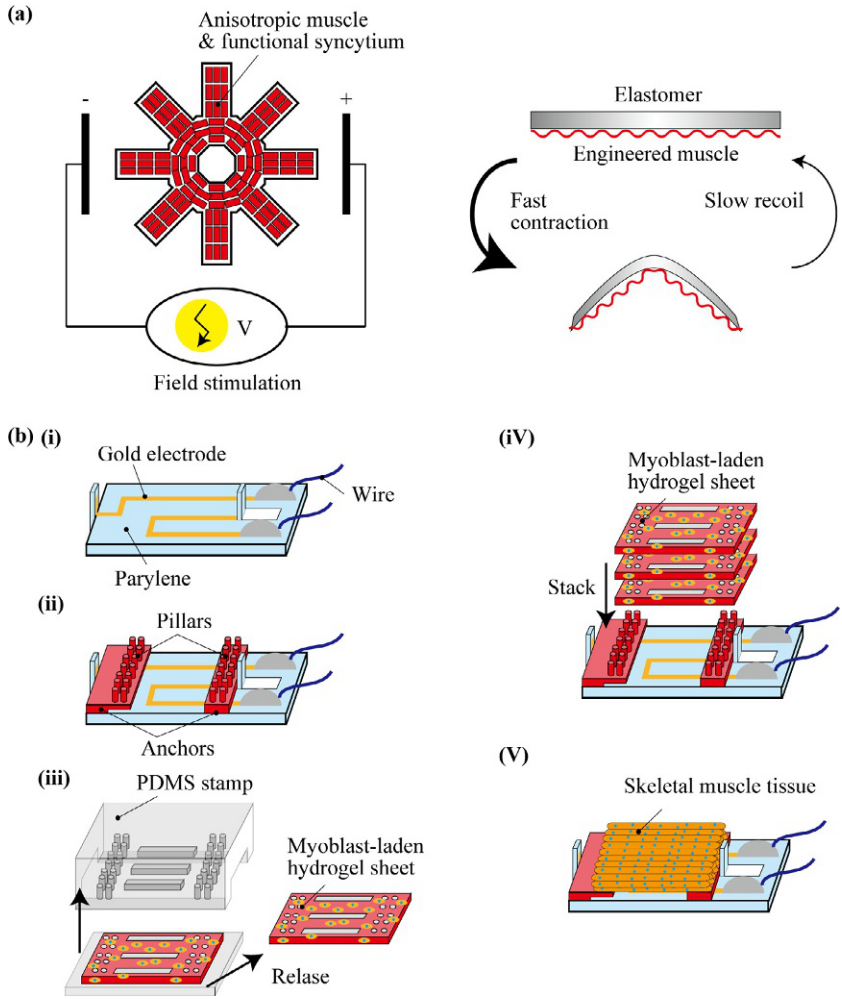

Fig. 16 (A) Biomimetic soft robots integrated cardiac muscle and soft materials trough fibronectin. (B) Bio-hybrid actuator that cultivates skeletal muscle on a device with pillars driven by electrical stimulation.

through fibronectin can only construct a two-dimensional actuator. Therefore, in order to realize more complex actuation, it is necessary to construct the three-dimensional tissue. Some hydrogels can be used as a support substrate for living cells. In particular, collagen gel is the most widespread protein in living organisms and constitutes connective tissues such as skin, tendons, and bones in the body. Living organisms are composed of many cells, and collagen gel plays an important role as a matrix between these cells. Therefore, research on constructing three-dimensional collagen gels has been actively conducted not only for soft robot applications but also for applications in regenerative medicine. For example, type I collagen is a protein consisting of three polypeptides with about 1000 amino acid residues, and these three polypeptides are twisted together to form a three-stranded helix structure. The outer part of the helix is composed of proline, a hydrophobic amino acid, and collagen is gelled by hydrophobic bonds formed by hydrophobic amino acids. The hydrophobic bond shows a higher binding force at a higher temperature, so collagen becomes a sol at low temperature and a gel at high temperature ($<\sim 37\,^{\circ}C$). Therefore, three-dimensional structures of collagen gel can be constructed by placing the chilled cell suspended pre-gel solution in a mold and heating it (Raman et al., 2016; Raman et al., 2017). Collagen gels with living cells also can be formed into three-dimensional tissues such as beads (Matsunaga et al., 2011), fibers (Onoe et al., 2013), and springs (Yoshida and Onoe, 2017) by using microfluidic devices. In fact, a bio-hybrid actuator that cultivates skeletal muscle on a device with pillars driven by electrical stimulation has been reported (Fig. 16B) (Morimoto et al., 2020). Muscle tissue is one of the potential candidates used as the driving element of bio-hybrid soft robots owing to its high contraction efficiency and superior power-to-weight ratio of contractions (Ricotti et al., 2017; Ricotti and Menciassi, 2012). The development of biochemical sensors using cells with odor receptors is also underway (Hirata et al., 2019), and the use of cells with various functions will open up new avenues for bio-hybrid soft robots.

5. Integrated soft robots by bridging multiscale elements

Finally, we present soft robots that integrate micro-scale elements constructed with hydrogels. By integrating the multiscale elements, it is possible to realize systems that cannot be realized by using only functional hydrogel elements. It has been reported that the volume changes of

stimuli-responsive gels by swelling and shrinking can be converted into motion control for soft robots. There are two main ways to integrate hydrogels. The first is to combine a functional hydrogel with a mechanism made of a rigid material such as elastomer or resin. The rigid mechanism can be driven by the volume change of the stimuli-responsive gel. The other method is to construct an integrated system by patterning multiple functional hydrogels. Taking advantage of the flexibility of hydrogels, the shape of the gel robot can be changed by the volume change of the stimuli-responsive gel to create new functions.

5.1 Integrated with rigid body

B. Xu et al. have proposed a system that integrates a propulsion mechanism using cardiac muscle and a propulsion control using stimuli-responsive hydrogel (Fig. 17A) (Xu et al., 2019). The system was composed of three elements: An airplane-shaped elastic body constructed with a 3D printer, cardiac muscle sheets arranged in a line as a propulsion source, and a temperature-responsive hydrogel (pNIPAM) with gold nanorods for propulsion control. The soft robot is actuated by a muscular tail fin that emulates the swimming of whales and works as a cellular engine powered by the synchronized contraction of striated cardiac microtissue constructs. For a transition of propulsion behavior, the soft robot can be optically triggered to transform from a spread to a retracted form, which effectively changes the

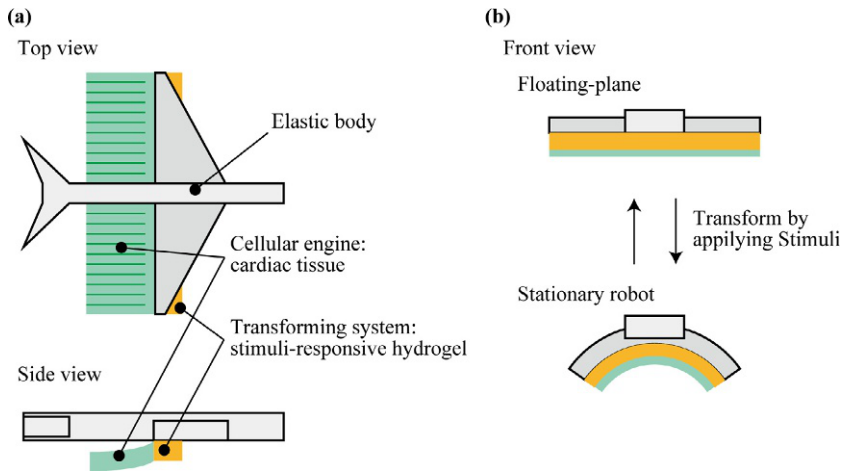

Fig. 17 (A) Integrated soft robots composed of elastic body, cardiac tissue, and stimuli-responsive hydrogel. (B) Transition of propulsion behavior by stimuli-responsive hydrogel.

bending stiffness of the tail fins, thus minimizing the propulsion force from the tail fin and effectively switching off the engine (Fig. 17B). There are several problems with conventional untethered microrobots: the robots can only propel at a specific condition such as the presence of hydrogen peroxide water, and it is difficult to control their propulsion behavior remotely. So, their work has taken a major step in solving the control problems by providing alternative programmable motion control strategies by integrating functional hydrogel, elastic body, and living cells. In addition, a targeted drug delivery strategy by using the floating-plane transformable robot as a cargo carrier was implemented by using the deformation of the soft robot.

Y. Morimoto et al. have developed a bio-hybrid robot actuated by an antagonistic pair of skeletal muscle tissues based on the concept of biological systems (Fig. 18) (Morimoto et al., 2018). Skeletal muscle tissues are attractive driving elements owing to the precise controllability of their contractions, in contrast to cardiac muscle tissues. However, the contractions of the skeletal muscle tissues on flexible substrates do not last for a long time due to spontaneous shrinkage of the tissues caused by their intrinsic traction force that increases through the course of culture (Cvetkovic et al., 2014). To overcome these issues, biological systems use antagonistic pairs of skeletal muscles. The bio-hybrid robot has a joint connected to the skeletal muscle tissues via flexible ribbons for taking the advantage of the antagonistic pair of

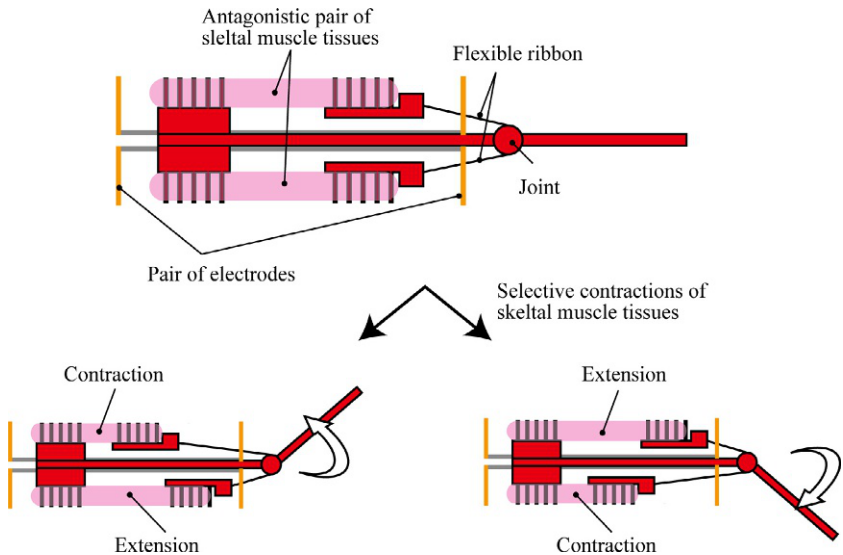

Fig. 18 Bio-hybrid robot actuated by an antagonistic pair of skeletal muscle tissues.

skeletal muscle tissues. When skeletal muscle tissues are selectively contracted by applying electrical stimulations with gold electrodes, linear contraction and extension of the skeletal muscle tissues can induce a smooth bidirectional rotation of the joint, leading to large actuation of the bio-hybrid robot. These achievements indicate that the proposed bio-hybrid robots would exceed the limitations of design in conventional bio-hybrid robots that have been restricted to actuate like a mollusk.

By combining soft and hard materials, integrated systems could be realized by taking advantage of each material, just like the structure of a living body. However, the hydrogel is a wet material, whereas most hard materials are dry. Therefore, it is desirable to develop a technology to bond hydrogels and hard materials.

5.2 Hydrogel patterning integrated systems

X. Du et al. have presented a new untethered soft millirobot with magnetic actuation in the head and function in the tail by implementing control, actuation, and sensing directly in the materials, thereby endowing robots with multimodal locomotion and environment-adaptive functions (Fig. 19A) (Du et al., 2020). The hydrogel-based millirobots were fabricated by two-step photopolymerization. Due to the soft and asymmetric structure, the millirobot achieved robust multimodal locomotion, including controllable and transformable crawling, swinging and rolling, and helical propulsion in

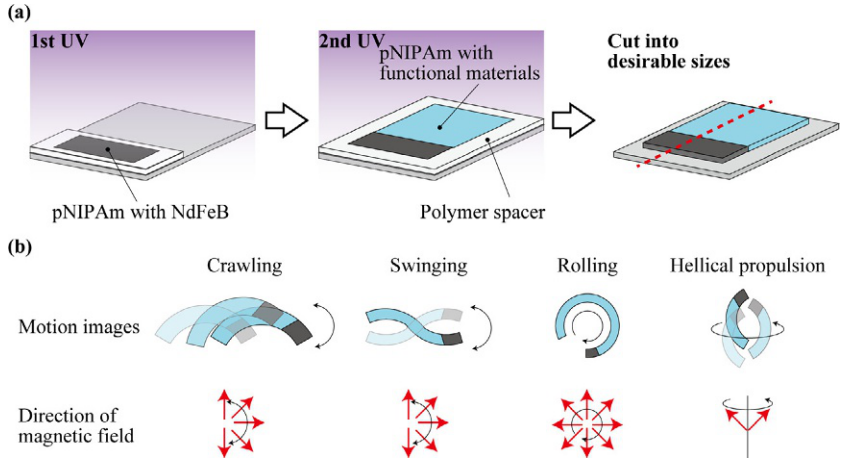

Fig. 19 (A) Fabrication of untethered soft millirobot with magnetic actuation in the head and function in the tail. (B) Multi-motion of soft millirobot: crawling, swinging, rolling, and helical propulsion.

water (Fig. 19B). The soft robot also possesses extraordinary functions, for example, optical camouflage in water, controllable delivery, and interaction with the changing environment via visible color–shifting. This seamless integration of bioinspired design and smart materials with hydrogels provides a powerful strategy for the development of the next-generation smart robot.

Finally, we will introduce soft spiral-shaped microswimmers that can autonomously control swimming behavior by detecting surrounding environments (Fig. 20) (Yoshida and Onoe, 2020). One of the most important characteristics of evolution has been motility, which became essential for survival or targeting activities like reproduction for many organisms. To this end, many microorganisms developed soft spiral-shaped flagella and their flagella can change the morphology of their spiral-shaped flagella to control swimming motility. The morphological change of the flagella achieves robust and adaptive chemotaxis responding to both attractants and repellents, such as nutrients, temperature, and pH. By mimicking these flagella systems, spiral-shaped rigid microswimmers have been developed for various applications, such as target drug delivery, micro-object transport, and micro-fluid manipulation. However, these microswimmers largely consist of metals and propel themselves by applied external rotational magnetic fields. So the swimming direction and velocity can be solely controlled by external systems because the morphology of their spiral bodies cannot be deformed. Features of the stimuli-responsive hydrogel, which are

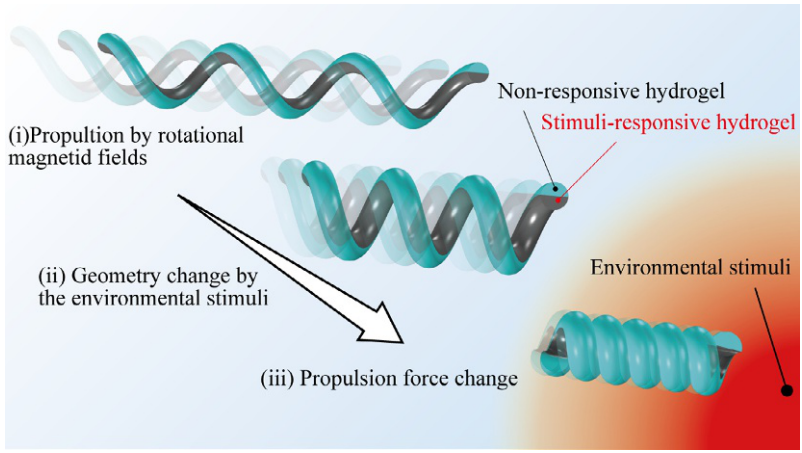

Fig. 20 Soft spiral-shaped microswimmers that can autonomously control swimming behavior by detecting surrounding environments.

flexibility and stimuli-responsiveness, are attractive functions for realizing the autonomous swimming motility control by the geometry of microswimmer change. By patterning the stimuli and magnetic responsive hydrogel through a bevel-tip based microfluidic device, the spiral shape changes in response to the environmental stimuli and, therefore, the swimming motility of the microswimmer as well. This multi-scale function integration strategy, which uses the morphology of soft robots, stimuli-responsiveness of the hydrogel, and functional materials, can open new avenues for various microscale biochemical applications, such as autonomous soft-robots and soft micro-probes for the intricate, minuscule environment.

Researches on the integration of multiple hydrogels to create new functions were explained. As described in this chapter, hydrogel could be characterized using the ability to encapsulate various functional materials, including other stimuli-responsive hydrogels. Moreover, complex compartmentalization characterized by a microfluidic device and photolithography technique can also contribute to the optimization of their internal structure and functionality enhancement.

6. Discussion

6.1 Problems of stimuli-responsive hydrogel

There are three important obstacles to stimuli-responsive hydrogel: the driving environment, the brittleness of hydrogel, and the slow responsiveness. Most stimuli-responsive hydrogels swell/shrink by osmotic-pressure change with aqueous solution transfer. Thus, most stimuli-responsive hydrogel-based soft robots can only drive in the presence of a solvent. To prevent the hydrogels from dehydrating, H. Yuk and coworkers have devised a method to robustly bind hydrogels to elastomers such as rubber and silicone that are stretchy like hydrogels yet impervious to water (Yuk et al., 2016). The first physically crosslink the dissipative network to form a hydrogel infiltrated with monomer/macromonomer solution of the stretchy network, which can be crosslinked in future steps (Fig. 21A). Then, an elastomer is also cured before bonding with hydrogels. Benzophenone in ethanol solution was treated to elastomer via swelling-driven surface absorption of benzophenone solution to address elastomers' oxygen inhibition effect (Fig. 21B). The benzophenone also acts as an ultraviolet-assisted grafting agent for covalently crosslinking hydrogel polymers on elastomer surfaces. Thereafter, the pre-shaped hydrogel and elastomer are assembled into a hybrid, and then the stretchy polymer network in the hydrogel is then

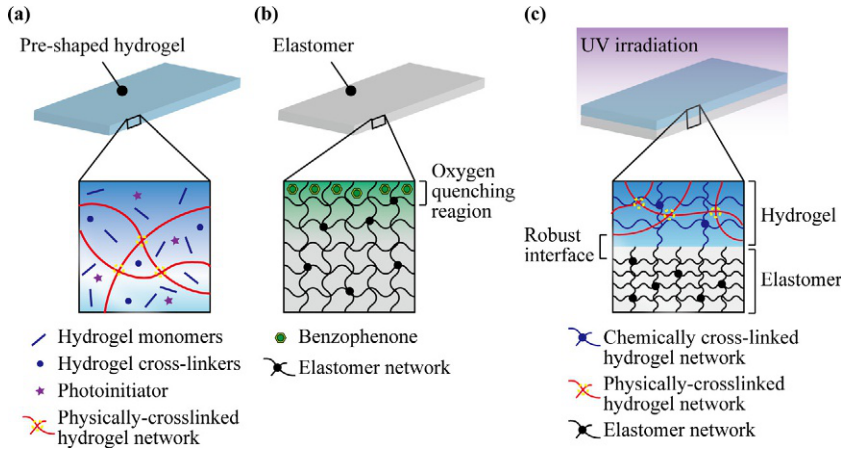

Fig. 21 (A) Hydrogel is first physically cross-linked. (B) The surface of a cured elastomer is treated with benzophenone. (C) The pre-shaped hydrogel and elastomer are assembled together followed by UV irradiation to chemically crosslink the other polymer network in the hydrogel.

cross-linked by UV irradiation and grafted on the surface of elastomer (Fig. 21C). Since the proposed method does not rely on specific types of polymers, it is expected that the integrated soft robots composed of elastomer and hydrogel can potentially transform their existing applications and enable new functions.

Another challenge for soft robot applications is that hydrogels are usually brittle. There are two main reasons: (i) Since hydrogels are swollen with solvent, the density of the polymer chain is low and the friction of the polymer chain is weak, (ii) Because of the non-uniformity of the mesh structure of the polymer network, the applied stress is concentrated in the weakest part. To overcome these problems, various types of polymer network design such as topological hydrogels (Okumura and Ito, 2001), nanocomposite hydrogels (Haraguchi and Takehisa, 2002), and double-network hydrogels(Zhao, 2014) have been developed. The topological hydrogel can adjust the inter-branch distance of the polymer chains by itself. Topological gels are polymer networks of polyrotaxane that are formed polyethylene oxide chains through cyclodextrin, a cyclic molecule. When the polymer chain is deformed under stress, the cyclodextrin moves in response to the deformation. As a result, the concentration of local stress can be prevented.

The strength of nanocomposite hydrogels is increased by minimizing the heterogeneity of the polymer network through the use of clay nanoparticles.

Nanocomposite hydrogels can be prepared by polymerization of polymers such as NIPAm with crosslinking agents in the presence of hectorite, which is clay particles of several tens of nanometers in size. 10–100 polymer chains are adsorbed on the surface of the clay particles by hydrogen bonding, which acts as a bridge and increases the strength of hydrogel.

The double-network hydrogel consists of a double polymer network with symmetrical properties, which are a brittle polymer network and a flexible polymer network, and achieves high strength by dissipating the applied stress. At the crack tip of a double-network hydrogel, the brittle network is first broken by stretching, and then the flexible network is broken by stretching. In order to fully stretch the flexible polymer chains at the crack tip, the brittle polymer network around the crack must be extensively broken before the flexible polymer chains can be fully stretched. This means that the brittle polymer network can efficiently absorb the elastic energy near the crack by viscous dissipation or large deformation for preventing crack growth. Various combinations of double-network hydrogel (Chen et al., 2015) including sodium alginate (Sun et al., 2012) and have been proposed and the double-network hydrogel actuator has also been proposed (Zheng et al., 2015).

Responsive speed to applied stimuli is an important factor in the application of stimuli-responsive hydrogels for soft robots. The typical response of stimuli-responsive hydrogel occurs in two steps: heat transfer or solvent diffusion into the hydrogel and the volume change by osmotic-pressure changes. Thus, the swelling/shrinking speed is also dependent on inversely proportional to the square volume of the hydrogel. The more response time of stimuli-responsive hydrogel is taken as the hydrogel larger. To improve the swelling/shrinking speed of the stimuli-responsive hydrogel, it is necessary to make the hydrogel smaller such as a thin fiber shape or sphere shape. In other words, it is effective to increase the surface-to-volume ratio to achieve fast response, and fast responsive hydrogel with porous structure has been reported (Jiang et al., 2015). In recent years, it is revealed that the response speed can be improved by devising the three-dimensional polymer networks through molecular design (Zhang et al., 2008). A typical example is the grafted hydrogel synthesized by Okano et al. (Kaneko et al., 1995). This grafted hydrogel has a graft structure in which multiple linear pNIPAm chains hang from the mesh polymer chains of the temperature-responsive pNIPAm hydrogel. The grafted linear pNIPAm chains have freely movable ends and they are therefore more mobile than cross-linked polymer chains. As the temperature is increased, the

hydrophobized graft chains quickly shrink due to dehydration. The contraction of the entire hydrogel is accelerated by the aggregation force of the formed hydrophobic liner chains. For another example, since the stimuli-responsive hydrogel expels the dehydrated solution when the volume is changed, to increase in the efficiency of solvent drainage during hydration by using amphiphilic polymers for rapid swelling/shrinking have also been reported(Yan et al., 2005).

6.2 Other functional hydrogels

Various hydrogels with novel functions such as self-growing (Matsuda et al., 2019), improving bio-adhesion (Nonoyama, 2020; Yuk et al., 2019) and conductivity (Chakraborty et al., 2019), and energy source (Schroeder et al., 2017) have also been reported in fields other than soft robot applications. Some of these functional hydrogels are briefly introduced. For self-growing hydrogels, force-induced polymer strand scission is the destructive trigger that initiates reconstruction. Rupture of a polymer chain by mechanical force typically generates mechanoradicals that can trigger chemical reactions and then polymerization was induced by the caused mechanoradicals for the reconstruction. Therefore, the hydrogels are substantially strengthened under repetitive loading through a structural destruction reconstruction process. In addition, conductive hydrogels were attractive materials for flexible electronics, which is also expected to use for components of soft robots. The conductive hydrogels divided into three categories: ion conducting gels, conducting polymer gels, and Supramolecular conducing gels. Ion conducting gels contain large amounts of metal ions, hydrogen ions, or ionic liquids, thus the hydrogels have conductivity. Conducting polymer gels usually possess highly π-conjugated polymeric chains. Some typical conducting polymers are polyacetylene (PA), polyaniline (PANI), polypyrrole (PPy), polythiophene (PTh), poly(phenylenevinylene) (PPV). Supramolecular conducing gels produced from supramolecular interactions that exhibit electrical conductivity. Supramolecular gels are bestowed with the magnificent property of responding to external stimuli like heat, light, ultrasound, mechanical shear owing to the non-covalent interactions that manufacture them.

By using such functional hydrogels, it is expected to construct systems that are integrated with biological and electronic devices. In the future, integrated multifunctional soft robots are expected through more development of other functional hydrogels.

7. Conclusion

In summary, we have introduced various hydrogels as materials that integrate multiscale functions. First, the nanoscale functions of hydrogels, especially their stimuli-responsive properties were explained. Since the stimuli-responsive hydrogel changes its volume in response to the external environment, it can simultaneously realize the sensing and actuator functions. These functions are very attractive for the realization of soft robots, and it is expected that stimuli-responsive hydrogels can be used to construct autonomous systems that respond to the external environment.

Next, the methods for fabricating various shapes of hydrogel were explained. Since hydrogels are obtained by cross-linking polymer networks, various shapes of hydrogels can be fabricated utilizing microfluidic devices, photolithography, and 3D printing. In addition, new systems could be constructed by devising stimuli-responsive hydrogel patterns and hydrogel shapes, as in the actuator application of spiral-shaped hydrogels. Therefore, it is desirable to develop a technology to realize more complex shapes in the future.

And then, we described the multi-scale function of hydrogels with functional materials. By encapsulating or grafting functional particles such as magnetic nanoparticles and platinum nanoparticles inside the hydrogel, hydrogels with magnetic responsiveness or catalytic functions can be realized. In addition to utilizing functions of materials, the integrated systems such as the rapid and remotely driving soft actuator composed of stimuli-responsive hydrogel and graphene by nIR irradiation were also achieved. For realizing soft chemical sensors, the combination of stimuli-responsive hydrogel and photonic colloidal crystal, which reflects visible-light wavelength through Bragg's diffraction, has been proposed. By using these systems, the intensity of the stimulus can be converted to visible color information. Living cells are also attractive materials for the driving force of soft robots or sensing elements, thus constructing and integrating the 3D tissue through hydrogels are a powerful tool to accomplish the bio-mimetic or bio-hybrid soft robots.

Finally, we presented two types of strategies for integrating micro-scale elements constructed with hydrogels: integrated with rigid body and hydrogel patterning integrated systems. By utilizing stimuli-responsive hydrogel as a driving source for rigid mechanisms, integrated systems that utilize the advantages of flexibility and rigidity, such as the skeletal muscle system of

a living body, can be realized. Moreover, by patterning various functional hydrogels, the advanced system such as motility control responding to the surrounding stimuli by integrating the shape transition function, the sensing function, and magnetic responsiveness.

In summary, we believe that the integration strategies of multi-scale elements based on hydrogel could open a new avenue for realizing advanced systems including soft robots, flexible devices, and biomimetics that take advantage of flexibility and biocompatibility, which cannot be achieved with conventional mechanical systems.

References

Banta S, Wheeldon IR, Blenner M: Protein engineering in the development of functional hydrogels, *Annu Rev Biomed Eng* 12:167, 2010.

Bassik N, Abebe BT, Laflin KE, Gracias DH: Photolithographically patterned smart hydrogel based bilayer actuators, *Polymer (Guildf)* 51:6093, 2010.

Bergeles C, Shamaei K, Abbott JJ, Nelson BJ: Single-camera focus-based localization of intraocular devices, *IEEE Trans Biomed Eng* 57:2064, 2010.

Buenger D, Topuz F, Groll J: Hydrogels in sensing applications, *Prog Polym Sci* 37:1678, 2012.

Ceylan H, Yasa IC, Yasa O, Tabak AF, Giltinan J, Sitti M: 3D-printed biodegradable microswimmer for theranostic cargo delivery and release, *ACS Nano* 13:3353, 2019.

Chakraborty P, Das S, Nandi AK: Conducting gels: a chronicle of technological advances, *Prog Polym Sci* 88:189, 2019.

Chen Q, Chen H, Zhu L, Zheng J: Fundamentals of double network hydrogels, *J Mater Chem B* 3:3654, 2015.

Cheng Y, Zheng F, Lu J, et al.: Bioinspired multicompartmental microfibers from microfluidics, *Adv Mater* 26:5184, 2014.

Cheng J, Jun Y, Qin J, Lee SH: Electrospinning versus microfluidic spinning of functional fibers for biomedical applications, *Biomaterials* 114:121, 2017.

Cui H, Zhao Q, Wang Y, Du X: Bioinspired actuators based on stimuli-responsive polymers, *Chem—An Asian J* 14:2369, 2019.

Cvetkovic C, Raman R, Chan V, et al.: Three-dimensionally printed biological machines powered by skeletal muscle, *Proc Natl Acad Sci U S A* 111:10125, 2014.

Du X, Cui H, Xu T, et al.: Reconfiguration, camouflage, and color-shifting for bioinspired adaptive hydrogel-based millirobots, *Adv Funct Mater* 30:1, 2020.

Fuhrer R, Athanassiou EK, Luechinger NA, Stark WJ: Crosslinking metal nanoparticles into the polymer backbone of hydrogels enables preparation of soft, magnetic field-driven actuators with muscle-like flexibility, *Small* 5:383, 2009.

Gačanin J, Synatschke CV, Weil T: Biomedical applications of DNA-based hydrogels, *Adv Funct Mater*.30, 2020. https://doi.org/10.1002/adfm.201906253.

Ge J, Yin Y: Responsive photonic crystals, *Angew Chemie—Int Ed* 50:1492, 2011.

Glotzer SC, Solomon MJ: Responsive photonic crystals, *Nat Mater* 6:557, 2007.

Haider H, Yang CH, Zheng WJ, et al.: Exceptionally tough and notch-insensitive magnetic hydrogels, *Soft Matter* 11:8253, 2015.

Haraguchi K, Takehisa T: Nanocomposite hydrogels: a unique organic–inorganic network structure with extraordinary mechanical, optical, and swelling/de-swelling properties, *Adv Mater* 14:1120, 2002.

Hayakawa M, Onoe H, Nagai KH, Takinoue M: Influence of asymmetry and driving forces on the propulsion of bubble-propelled catalytic micromotors, *Micromachines* 7, 2016. https://doi.org/10.3390/mi7120229.
Hayashi T, Takinoue M, Onoe H: DNA aptamer-linked structural-color hydrogel for repeatable biochemical sensing, In 20th international conference on solid-state sensors, actuators and microsystems. 2019, p 582.
Hennink WE, van Nostrum CF: Novel crosslinking methods to design hydrogels, *Adv Drug Deliv Rev* 64:223, 2012.
Hirata Y, Morimoto Y, Nam E, Takeuchi S: Portable biohybrid odorant sensors using cell-laden collagen micropillars, *Lab Chip* 19:1971, 2019.
Huang HW, Sakar MS, Petruska AJ, Pané S, Nelson BJ: Soft micromachines with programmable motility and morphology, *Nat Commun* 7:1, 2016.
Huang T, Huang H, Jin DD, et al.: Four-dimensional micro-building blocks, *Sci Adv*:1, 2020.
Ionov L: Biomimetic hydrogel-based actuating systems, *Adv Funct Mater* 23:4555, 2013.
Ionov L: Polymeric actuators, *Langmuir* 31:5015, 2015.
Jeon SJ, Hayward RC: Reconfigurable microscale frameworks from concatenated helices with controlled chirality, *Adv Mater* 29:1, 2017.
Jeon SJ, Hauser AW, Hayward RC: Shape-morphing materials from stimuli-responsive hydrogel hybrids, *Acc Chem Res* 50:161, 2017.
Jiang S, Liu F, Lerch A, Ionov L, Agarwal S: Unusual and superfast temperature-triggered actuators, *Adv Mater* 27:4865, 2015.
Jiang X, Zhao C, Fan X, et al.: A DNA-modified hydrogel for simultaneous purification, concentration and detection of targeted cfDNA in human serum, *RSC Adv* 9:3407, 2019.
Kahn JS, Hu Y, Willner I: Stimuli-responsive DNA-based hydrogels: from basic principles to applications, *Acc Chem Res* 50:680, 2017.
Kaneko Y, Sakai K, Kikuchi A, Yoshida R, Sakurai Y, Okano T: Influence of freely mobile grafted chain length on dynamic properties of comb-type grafted poly(N-isopropylacrylamide) hydrogels, *Macromolecules* 28:7717, 1995.
Kang E, Jeong GS, Choi YY, Lee KH, Khademhosseini A, Lee SH: Digitally tunable physicochemical coding of material composition and topography in continuous microfibres, *Nat Mater* 10:877, 2011.
Katuri J, Ma X, Stanton MM, Sánchez S: Designing micro- and nanoswimmers for specific applications, *Acc Chem Res* 50:2, 2017.
Kim J, Chung SE, Choi SE, Lee H, Kim J, Kwon S: Programming magnetic anisotropy in polymeric microactuators, *Nat Mater* 10:747, 2011.
Kirillova A, Maxson R, Stoychev G, Gomillion CT, Ionov L: 4D biofabrication using shape-morphing hydrogels, *Adv Mater* 29:1, 2017.
Kuo JC, Huang HW, Tung SW, Yang YJ: Autonomous planning and control of soft untethered grippers in unstructured environments, *Sensors Actuators A Phys* 211:121, 2014.
Lee KY, Mooney DJ: Alginate: properties and biomedical applications, *Prog Polym Sci* 37:106, 2012.
Lee Y, Song WJ, Sun JY: Hydrogel soft robotics, *Mater Today Phys* 15:100258, 2020.
Li Y, Huang G, Zhang X, et al.: Magnetic hydrogels and their potential biomedical applications, *Adv Funct Mater* 23:660, 2013.
Li H, Tan C, Li L: Review of 3D printable hydrogels and constructs, *Mater Des* 159:20, 2018.
Li M, Wang X, Dong B, Sitti M: In-air fast response and high speed jumping and rolling of a light-driven hydrogel actuator, *Nat Commun*:11, 2020a. https://doi.org/10.1038/s41467-020-17775-4.
Li J, Wu C, Chu PK, Gelinsky M: 3D printing of hydrogels: rational design strategies and emerging biomedical applications, *Mater Sci Eng R Reports* 140:100543, 2020b.
Lighthill J: Flagellar hydrodynamics, *SIAM Rev* 18:161, 1976.

Lin X, Xu B, Zhu H, Liu J, Solovev A, Mei Y: Catalytic/magnetic assemblies of rolled-up tubular nanomembrane-based micromotors, *Research* 2020:1, 2020.
Liska R, Schuster M, Inführ R, et al.: Photopolymers for rapid prototyping, *J Coat Technol Res* 4:505, 2007.
Liu J: Oligonucleotide-functionalized hydrogels as stimuli responsive materials and biosensors, *Soft Matter* 7:6757, 2011.
Liu X, Liu J, Lin S, Zhao X: Hydrogel machines, *Mater Today* 36:102, 2020.
Lv C, Sun XC, Xia H, et al.: Hydrogel actuators and sensors for biomedical soft robots: brief overview with impending challenges, *Sensors Actuators B Chem* 259:736, 2018.
Maeda K, Onoe H, Takinoue M, Takeuchi S: Controlled synthesis of 3D multicompartmental particles with centrifuge-based microdroplet formation from a multibarrelled capillary, *Adv Mater* 24:1340, 2012.
Magdanz V, Stoychev G, Ionov L, Sanchez S, Schmidt OG: Stimuli-responsive microjets with reconfigurable shape, *Angew Chemie* 126:2711, 2014.
Mano JF: Stimuli-responsive polymeric systems for biomedical applications, *Adv Eng Mater* 10:515, 2008.
Matsuda T, Kawakami R, Namba R, Nakajima T, Gong JP: Mechanoresponsive self-growing hydrogels inspired by muscle training, *Science* 363:504, 2019.
Matsunaga YT, Morimoto Y, Takeuchi S: Molding cell beads for rapid construction of macroscopic 3D tissue architecture, *Adv Mater* 23:90, 2011.
Momeni F, Hassani SMM, Liu NX, Ni J: A review on 4D printing material composites and their applications, *Mater Des* 122:42, 2017.
Mondschein RJ, Kanitkar A, Williams CB, Verbridge SS, Long TE: Polymer structure-property requirements for stereolithographic 3D printing of soft tissue engineering scaffolds, *Biomaterials* 140:170, 2017.
Morales D, Podolsky I, Mailen RW, Shay T, Dickey MD, Velev OD: Ionoprinted multi-responsive hydrogel actuators, *Micromachines*: 7, 2016. https://doi.org/10.3390/mi7060098.
Morimoto Y, Onoe H, Takeuchi S: Biohybrid robot powered by an antagonistic pair of skeletal muscle tissues, *Sci Robot* 3:1, 2018.
Morimoto Y, Onoe H, Takeuchi S: Biohybrid robot with skeletal muscle tissue covered with a collagen structure for moving in air, *APL Bioeng* 4, 2020, 026101.
Na JH, Evans AA, Bae J, et al.: Programming reversibly self-folding origami with micropatterned photo-crosslinkable polymer trilayers, *Adv Mater* 27:79, 2015.
Naficy S, Gately R, Gorkin R, Xin H, Spinks GM: 4D printing of reversible shape morphing hydrogel structures, *Macromol Mater Eng* 302:1, 2017.
Nakajima S, Kawano R, Onoe H: Stimuli-responsive hydrogel microfibers with controlled anisotropic shrinkage and cross-sectional geometries, *Soft Matter* 13:3710, 2017.
Nakayama D, Takeoka Y, Watanabe M, Kataoka K: Simple and precise preparation of a porous gel for a colorimetric glucose sensor by a templating technique, *Angew Chemie* 115:4329, 2003.
Nawroth JC, Lee H, Feinberg AW, et al.: A tissue-engineered jellyfish with biomimetic propulsion, *Nat Biotechnol* 30:792, 2012.
Nie M, Takeuchi S: Microfluidics based synthesis of coiled hydrogel microfibers with flexible shape and dimension control, *Sensors Actuators, B Chem* 246:358, 2017.
Nonoyama T: Robust hydrogel–bioceramics composite and its osteoconductive properties, *Polym J* 52:709, 2020.
Okumura Y, Ito K: The polyrotaxane gel: a topological gel by figure-of-eight cross-links, *Adv Mater* 13:485, 2001.
Ono A, Cao S, Togashi H, et al.: Specific interactions between silver(i) ions and cytosine–cytosine pairs in DNA duplexes, *Chem Commun*: 4825, 2008.

Onoe H, Okitsu T, Itou A, et al.: Metre-long cell-laden microfibres exhibit tissue morphologies and functions, *Nat Mater* 12:584, 2013.
Park S-J, Gazzola M, Park KS, et al.: Phototactic guidance of a tissue-engineered soft-robotic ray, *Science*:353, 2016.
Pawar SN, Edgar KJ: Alginate derivatization: a review of chemistry, properties and applications, *Biomaterials* 33:3279, 2012.
Peters C, Hoop M, Pané S, Nelson BJ, Hierold C: Degradable magnetic composites for minimally invasive interventions: device fabrication, targeted drug delivery, and cytotoxicity tests, *Adv Mater* 28:533, 2016.
Peyer KE, Zhang L, Nelson BJ: Bio-inspired magnetic swimming microrobots for biomedical applications, *Nanoscale* 5:1259, 2013.
Raman R, Cvetkovic C, Uzel SGM, et al.: Optogenetic skeletal muscle-powered adaptive biological machines, *Proc Natl Acad Sci U S A* 113:3497, 2016.
Raman R, Grant L, Seo Y, et al.: Damage, healing, and remodeling in optogenetic skeletal muscle bioactuators, *Adv Healthc Mater* 6:1, 2017.
Ramanujan RV, Lao LL: The mechanical behavior of smart magnet–hydrogel composites, *Smart Mater Struct* 15:952, 2006.
Richter A, Paschew G, Klatt S, Lienig J, Arndt K-F, Adler H-JP: Review on hydrogel-based ph sensors and microsensors, *Sensors* 8:561, 2008.
Ricotti L, Menciassi A: Bio-hybrid muscle cell-based actuators, *Biomed Microdevices* 14:987, 2012.
Ricotti L, Trimmer B, Feinberg AW, et al.: Biohybrid actuators for robotics: a review of devices actuated by living cells, *Sci Robot* 2:1, 2017.
Robinson JT, Tabakman SM, Liang Y, et al.: Ultrasmall reduced graphene oxide with high near-infrared absorbance for photothermal therapy, *J Am Chem Soc* 133:6825, 2011.
Saito H, Takeoka Y, Watanabe M: Simple and precision design of porous gel as a visible indicator for ionic species and concentration, *Chem Commun* 3:2126, 2003.
Schenck JF: Physical interactions of static magnetic fields with living tissues, *Prog Biophys Mol Biol* 87:185, 2005.
Schild HG: Poly(N-isopropylacrylamide): experiment, theory and application, *Prog Polym Sci* 17:163, 1992.
Schroeder TBH, Guha A, Lamoureux A, et al.: An electric-eel-inspired soft power source from stacked hydrogels, *Nature* 552:214, 2017.
Seo KD, Kwak BK, Sánchez S, Kim DS: Microfluidic-assisted fabrication of flexible and location traceable organo-motor, *IEEE Trans Nanobioscience* 14:298, 2015.
Shafranek RT, Millik SC, Smith PT, Lee CU, Boydston AJ, Nelson A: Stimuli-responsive materials in additive manufacturing, *Prog Polym Sci* 93:36, 2019.
Shao Y, Jia H, Cao T, Liu D: Supramolecular hydrogels based on DNA self-assembly, *Acc Chem Res* 50:659, 2017.
Shi X, Ostrovidov S, Zhao Y, et al.: Microfluidic spinning of cell-responsive grooved microfibers, *Adv Funct Mater* 25:2250, 2015.
Silverberg JL, Na JH, Evans AA, et al.: Origami structures with a critical transition to bistability arising from hidden degrees of freedom, *Nat Mater* 14:389, 2015.
Soto F, Wang J, Ahmed R, Demirci U: *Adv Sci* 7:1, 2020.
Sun JY, Zhao X, Illeperuma WRK, et al.: Highly stretchable and tough hydrogels, *Nature* 489:133, 2012.
Suzuki N, Iwase E, Onoe H: Microfluidically patterned dome-shaped photonic colloidal crystals exhibiting structural colors with low angle dependency, *Adv Opt Mater* 5:1, 2017.
Sydney Gladman A, Matsumoto EA, Nuzzo RG, Mahadevan L, Lewis JA: Biomimetic 4D printing, *Nat Mater* 15:413, 2016.
Takashima Y, Hatanaka S, Otsubo M, et al.: Expansion–contraction of photoresponsive artificial muscle regulated by host–guest interactions, *Nat Commun*: 3, 2012. https://doi.org/10.1038/ncomms2280.

Takeuchi N, Nakajima S, Yoshida K, Kawano R, Hori Y, Onoe H: Microfiber-shaped programmable materials with stimuli-responsive hydrogel, *Soft Robot*: 1, 2020.
Tian E, Wang J, Zheng Y, Song Y, Jiang L, Zhu D: Colorful humidity sensitive photonic crystal hydrogel, *J Mater Chem* 18:1116, 2008.
Tottori S, Takeuchi S: Formation of liquid rope coils in a coaxial microfluidic device, *RSC Adv* 5:33691, 2015.
Tsuchiya M, Kurashina Y, Onoe H: Eye-recognizable and repeatable biochemical flexible sensors using low angle-dependent photonic colloidal crystal hydrogel microbeads, *Sci Rep* 9:1, 2019.
Turco G, Donati I, Grassi M, Marchioli G, Lapasin R, Paoletti S: Mechanical spectroscopy and relaxometry on alginate hydrogels: a comparative analysis for structural characterization and network mesh size determination, *Biomacromolecules* 12:1272, 2011.
Uchida O: 4D printing of multi-hydrogels using direct ink writing in a supporting viscous liquid, *Micromachines* 10:433, 2019.
Vashist A, Kaushik A, Vashist A, et al.: Advances in carbon nanotubes - hydrogel hybrids in nanomedicine for therapeutics, *Adv Healthc Mater* 7:1, 2018.
Wang E, Desai MS, Lee SW: Light-controlled graphene-elastin composite hydrogel actuators, *Nano Lett* 13:2826, 2013.
Wang X, Qin XH, Hu C, et al.: 3D printed enzymatically biodegradable soft helical microswimmers, *Adv Funct Mater* 28:1, 2018.
Webber MJ, Appel EA, Meijer EW, Langer R: Supramolecular biomaterials, *Nat Mater* 15:13, 2015.
Wehner M, Truby RL, Fitzgerald DJ, et al.: An integrated design and fabrication strategy for entirely soft, autonomous robots, *Nature* 536:451, 2016.
Xing JF, Zheng ML, Duan XM: Two-photon polymerization microfabrication of hydrogels: an advanced 3D printing technology for tissue engineering and drug delivery, *Chem Soc Rev* 44:5031, 2015.
Xu B, Han X, Hu Y, et al.: A remotely controlled transformable soft robot based on engineered cardiac tissue construct, *Small* 15:1, 2019.
Yan H, Fujiwara H, Sasaki K, Tsujii K: *Angew Chemie—Int Ed* 44:1951, 2005.
Yasuda S, Hayakawa M, Onoe H, Takinoue M: Twisting microfluidics in a planetary centrifuge, *Soft Matter* 13:2141, 2017.
Ye G, Wang X: Glucose sensing through diffraction grating of hydrogel bearing phenylboronic acid groups, *Biosens Bioelectron* 26:772, 2010.
Ye BF, Zhao YJ, Cheng Y, et al.: Colorimetric photonic hydrogel aptasensor for the screening of heavy metal ions, *Nanoscale* 4:5998, 2012.
Yoon C, Xiao R, Park J, Cha J, Nguyen TD, Gracias DH: Functional stimuli responsive hydrogel devices by self-folding, *Smart Mater Struct* 23, 2014, 094008.
Yoshida K, Onoe H: Functionalized core-shell hydrogel microsprings by anisotropic gelation with bevel-tip capillary, *Sci Rep* 7:1, 2017.
Yoshida K, Onoe H: Soft spiral-shaped microswimmers for autonomous swimming control by detecting surrounding environments, *Adv Intell Syst* 2:2000095, 2020.
Yoshida S, Takinoue M, Iwase E, Onoe H: Dynamic transformation of self-assembled structures using anisotropic magnetized hydrogel microparticles, *J Appl Phys*:120, 2016. https://doi.org/10.1063/1.4961422.
Yoshida S, Takinoue M, Onoe H: Compartmentalized spherical collagen microparticles for anisotropic cell culture microenvironments, *Adv Healthc Mater*:6, 2017. https://doi.org/10.1002/adhm.201601463.
Yoshida K, Nakajima S, Kawano R, Onoe H: Spring-shaped stimuli-responsive hydrogel actuator with large deformation, *Sensors Actuators, B Chem* 272:361, 2018.
Yuk H, Zhao X: A new 3D printing strategy by harnessing deformation, instability, and fracture of viscoelastic inks, *Adv Mater*:30, 2018. https://doi.org/10.1002/adma.201704028.

Yuk H, Zhang T, Parada GA, Liu X, Zhao X: Skin-inspired hydrogel–elastomer hybrids with robust interfaces and functional microstructures, *Nat Commun* 7:1, 2016.
Yuk H, Varela CE, Nabzdyk CS, et al.: Dry double-sided tape for adhesion of wet tissues and devices, *Nature* 575:169, 2019.
Zhang XZ, Xu XD, Cheng SX, Zhuo RX: Strategies to improve the response rate of thermosensitive hydrogels, *Soft Matter* 4:385, 2008.
Zhang X, Pint CL, Lee MH, et al.: Optically- and thermally-responsive programmable materials based on carbon nanotube-hydrogel polymer composites, *Nano Lett* 11:3239, 2011.
Zhao X: Multi-scale multi-mechanism design of tough hydrogels: building dissipation into stretchy networks, *Soft Matter* 10:672, 2014.
Zhao Q, Dunlop JWC, Qiu X, et al.: An instant multi-responsive porous polymer actuator driven by solvent molecule sorption, *Nat Commun*:5, 2014. https://doi.org/10.1038/ncomms5293.
Zhao H, Chen Y, Shao L, et al.: Airflow-assisted 3D bioprinting of human heterogeneous microspheroidal organoids with microfluidic nozzle, *Small* 14:1, 2018.
Zheng WJ, An N, Yang JH, Zhou J, Chen YM: Half-metallic ferromagnetism and surface functionalization-induced metal–insulator transition in graphene-like two-dimensional Cr2c crystals, *ACS Appl Mater Interfaces* 7:1758, 2015.

CHAPTER SIX

Smart sensors for volatile organic compounds (VOCs) and their possible application as end of service life indicator (ESLI) for respirator cartridges

Filippo Pinelli[a,*] **and Marco Miceli**[b]

[a]Department of Chemistry, Materials and Chemical Engineering "Giulio Natta", Politecnico di Milano, Milan, Italy
[b]BLS Headquarters, Cormano, Milan, Italy
*Corresponding author: e-mail address: filippo.pinelli@polimi.it

Contents

1. Introduction 198
2. Smart sensors 200
   2.1 Smart materials 200
   2.2 Sensors applications 200
   2.3 Hydrogels 223
3. Conclusions 228
References 228

Abstract

In the last decade many different developments have taken place in the field of sensors driven by many new needs of the today world. In this context, gas sensors and volatile organic compounds sensors are for sure very interesting devices, thanks to the wide range of applications in which they can be employed. Smart, soft, highly sensitive systems are all examples of innovative typologies of instruments that can be fabricated working with proper formulated materials. In this work we are going to give an overview of the latest developed sensing materials that can be employed for volatile organic compound detection, focusing first of all on their synthesis and features and then going deeper in their engineering applications. All of the presented devices are analyzed from the perspective of their possible employment as end of service life indicator for respirator cartridges. This application, which represent a novelty in the field, would determine the possibility to monitor the service life of different personal protective equipment and would be a turning point for the workplace safety in various contexts.

Advances in Chemical Engineering, Volume 57
ISSN 0065-2377
https://doi.org/10.1016/bs.ache.2021.02.002

1. Introduction

Volatile organic compounds (VOCs) are organic chemicals characterized by a low-molecular-weight and by a high vapor pressure at room temperature (Li et al., 2020b). These peculiarities cause their so-called volatility: the evaporation, or sublimation, of a larger number of molecules that pass in gas phase in the surrounding air. VOCs are various and include many different chemicals with different features: because of this, in order to be consistent from case to case, the European Union has given a precise definition of VOC as "any organic compound having an initial boiling point less than or equal to 250 °C measured at a standard atmospheric pressure of 101.3 kP_a" (European Union, 1999).

VOCs are present in everyday life and play an important role in many natural and industrial processes: clear examples are ethanol, formaldehyde, isopropanol or acetone. Unfortunately, many of these compounds are dangerous to human health and associated with respiratory, allergic or immune responses and because of this great attention is given to them (Soni et al., 2018). As many other pollutants their effects are directly correlated with the extent and the intensity of the individual exposure and so the key point to prevent any harmful consequence is to be able to limit the exposure and protect users (Soni et al., 2018). A challenge of this kind is not trivial and, in any case and for any adopted solution, it is necessary to ensure that workers are exposed to chemical substances concentrations lower than the threshold limit value (TLV), the level to which an operator can be exposed day by day for a working life without harmful effects (Mills, 2016). In this context it is possible to point out two main strategies: on one side, in specific situations, it is possible to reduce VOCs emissions and be able to reach safe ambient conditions. By the other side, when this action cannot be realized, it is necessary to reduce the exposure of the single person to the harmful compound. This task is usually accomplish exploiting the PPE (personal protective equipment) that, if properly worn by the users, guarantees appropriate and complete protection (Decaens and Vermeersch, 2016). This second working strategy is clearly the one that requires greater attention: PPE technologies are widespread, find application in many industrial fields and they are applied in the protection from the most dangerous chemicals. It is clear how the ability to guarantee a complete and constant protection to the operators is the pivotal point of any PPE suppliers. Because of this in the last decades many advances have been obtained in the field, exploiting new materials, configuration and combination of technologies (Reddy et al., 2019).

In this context when masks or respirator cartridges are employed a key point, that is still an outstanding question, is to be able to know when it is time to replace them (Barro-Torres et al., 2012). Up to now every day in the majority of the working contexts, the replacement decision of the operators is based on some main factors like the general guidelines from cartridge suppliers on the PPE durability, the experience of the operator that work with that specific PPE or the smell of the user that is wearing the PPE (Mulvey et al., 2019). These factors are, unfortunately, weak guidance: they are strictly case and operator dependent, they do not take into account possible changes in the working environment and, for example, in the case the decision is based on the smell of the operator, they directly expose the workers to harmful compounds. It is therefore clear that in this way it is not possible to guarantee an appropriate protection to the operators. All these considerations, together with the need to constantly improve the safety of workers in the workplace, encouraged the ideas and thoughts on a way through which workers and operators can be able to monitor the service life of their PPE and be able to change them in time in order to be sure to be always well protected. A device with this functionality is usually called "End of service life indicator" (ESLI) (Favas, 2005) and it can be defined as follows:

> *An ESLI is a sensor device that warns the operator about the approaching expiration term of the service life of his PPE, so that a timely replacement of the equipment can take place.*

Commonly ESLI devices are intended to be designed in order to be integrated in their corresponding PPE in such a way that they can follow the adsorption profiles and the progression of gases on the filtering material and detect when the system is saturated. This is a pivotal point because it is the simpler way through which the ESLI device can track and monitor the life of the PPE exploiting its function (Checky et al., 2016). Unfortunately, although some of these devices are already available on the market, their diffusion is very limited and very few industries and companies use them. The reasons behind this can be many such as high costs, awkward technologies, lack of sensitivity or selectivity. Because of all these reasons, the development of proper ESLI technologies still remains an open challenge.

It is probably already clear to the reader that the core element in any ESLI device is the integrated sensor. In fact, the sensing ability of the device in detecting VOCs is pivotal in order to be able to understand the remaining service life of the equipment. In this context smart sensors represent for sure one of the most important technologies thanks to their versatility, tunability and easy integration in other primary equipment (Das and Roy, 2021). Obviously "smart sensor" is a broad topic, with multiple variables: in

Section 2 we broach the subject of smart sensing techniques focusing on main literature-reported technologies and their application as end of service life indicator.

2. Smart sensors

2.1 Smart materials

The technologies and the applied materials that support engineering applications have faced an important evolution in the last 20 years (Hruska, 2015). New smart materials have been developed and thoroughly studied, focusing on specific features that can be exploited in a wide range of applications. In the context of interest for this present work many materials such as metal-organic-frameworks, nanostructures or polymer of intrinsic microporosity can be employed and integrated as sensors devices for volatile organic compounds detection (Beluomini et al., 2019; Tung et al., 2020; Wang et al., 2020a). One of the most important properties for all of these systems is for sure the large specific surface area that guarantees high level of absorption and tunable behavior. Moreover, the presence of surface chemical functional groups can promote the adsorption of VOCs and enhance important sensing properties (Li et al., 2020b).

Every sensor obviously presents different working principle, anyway they commonly show a variation in their structural, electrical or optical properties subsequent to the interaction of the sensor with VOCs that permits to determine the presence of the gas (Favas, 2005). The integration of these sensors in respirator cartridges, their calibration and setting taking into account the working conditions of the whole system, allows to obtain an end of service life indicator for the cartridge that can improve the safety of users.

In Section 2.2 we are going to analyze different sensors solutions, focusing first of all on theoretical aspects of their structures and then going deeper in some of their possible specific applications for gas sensing and their potential employment as end of service life indicator.

2.2 Sensors applications

2.2.1 Polymer of intrinsic microporosity

One of the most recognized and useful material in the field of gas sensing is represented by polymers of intrinsic microporosity (PIM) (Carta et al., 2009). This unique class of structures is commonly classified as a porous organic polymer, containing a continuous network of interconnected intermolecular voids. The porosity of the structure is obtained by the inner macromolecular

chains that do not efficiently pack in the solid state and present a rigid non-linear feature. In order to guarantee permanent microporosity it is pivotal to avoid the rotation along the polymer chain (McKeown, 2020). This is realized through the use of fused ring structure; moreover, steric inhibition can be exploited to avoid changes of the conformation. Various synthesis methods are available, anyway because of the previous considerations, a conformationally locked monomer is needed and a polymerization reaction that determines a linkage with prohibited rotation have to be performed. Three main polymerization reactions can be realized. Briefly, the first typology of polymerization is represented by a double aromatic nucleophilic substitution mechanism that enable to obtain a dibenzodioxin linkage. The second possibility exploits the Troger's base formation, and finally it is possible to obtain this kind of polymer through the formation of amide linkages starting from monomeric units (Stanovsky et al., 2021).

These structures present important properties. First of all, a high solubility in common organic solvents can be noticed, this is probably determined by the rigid macromolecular structures that help to reduce the intermolecular cohesive interactions limiting the close contact between polymer chains. Moreover, these systems demonstrated to be thermally stable up to 450 °C and with also important strain resistance (Wang et al., 2020b). The microporosity is for sure the most important features of these polymers determining a high-free volume, high internal surface area and high affinity with gases.

All these properties made this material an ideal candidate for sensor fabrication to trace organic compound. A clear example of that is represented by the integration of this microporous material in a thin film transducer that produces changes in color upon exposure to a wide range of volatile organic compounds (Budd et al., 2004). This sensor was fabricated using a metalized (Ni metal) polyethylene terephthalate substrate, while the polymer microporous network was obtained by a bis catechol 5,5′,6,6′-tetrahydroxy-3,3,3′,3′-tetramethyl-1,1′-spirobisindane assembled using dibenzodioxane formation. The PIM formation occurred due to the number of spirocyclic linkages attached to each planar functional unit (Budd et al., 2004). A 4% wt solution of this polymer in chlorobenzene was prepared and cast onto the Ni-coated PET by spin-coating, to a dry thickness of 600 nm. Then a silver nanoparticle stack layer was spin coated onto the PIM layer using a solution 1:1 (w/w) of nanosilver metal suspension in methanol (40% wt). Finally, after this deposition, the system was heated at 150 °C for 1 h to sinter the silver nanoparticles (Christopher Thomas et al., 2011).

The working principle of the sensor is based on a reflective interference filter, realized by positioning the microporous material (500–600 nm thickness) between two reflective metallic layers (Checky et al., 2016; Rakow et al., 2010). Partial light reflection was provided by metallic mirror (10 nm thickness), while another portion of incident light was allowed to travel through the microporous layer. The light is reflected back through the stack by the permeable metallic mirror (200–300 nm thickness) and interferes optically with the light reflected off of the partial mirror. Adsorption of gases in microporous network, if the vapor concentration is up the minimum indication level (MIP), affects the light reflection properties of the system, determining a shift in the wavelength of reflected light. This mechanism, schematized in Fig. 1A, determines an optical output signal that can advise of gas presence and, if properly integrated, monitor the progressive gas adsorption in a respirator cartridge.

As it is shown in the Fig. 1B the system is highly responsive and respond at concentrations down to 50 ppb.

This technology is the first one that has been industrially implemented. As reported in literature (Checky et al., 2016), this optical sensor can be attached to the inside wall of an organic vapor resistor cartridge, next to the activated carbon of the filter, and be used as end of service life indicator for this specific device. When organic vapors move through the cartridge, they also pass through the permeable reflective layer and the PIM adsorb them. This is the cause of the color shift and it is possible to see the progression of organic vapors through the cartridge via the growth of the ESLI indicator bar. This mechanism is schematized in Fig. 2.

In this system the color change of the indicator does not represent an "end-state" reference color, but it monitors the progression of the gases adsorption on the filter and when any part of the indicator bar touches the marked end line it is time to change it. It is clear how the positioning of the sensor is not trivial, the sensing element (PIM) has to touch the active carbon so that it can follow its progressive saturation and be contacted by gases changing its reflectivity.

This kind of system has been tested with various organic vapors and in different conditions of humidity, temperatures and flow. Its performances, in each test realized, respected the NIOSH (National Institute of Safety and Health, USA) requirements, so that the end of cartridge life is indicated at or before 90% of the actual service life.

This device is one of the few systems of this kind already available on the market, and its efficacy have been widely demonstrated. Anyway, many

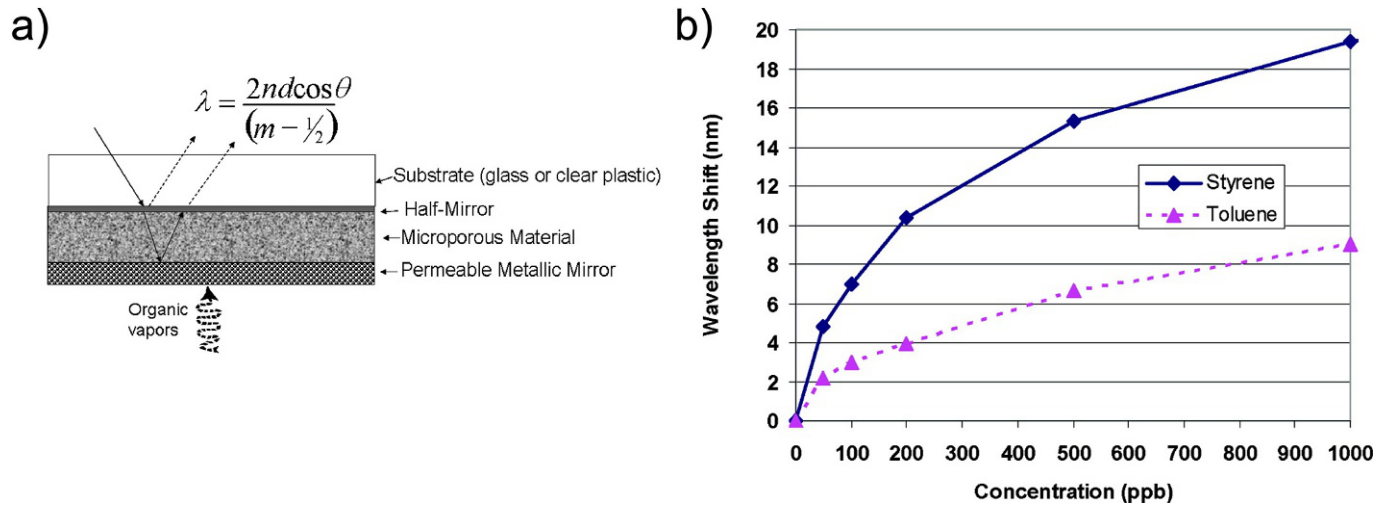

Fig. 1 (A) Schematization of the effect of gas absorption on the reflective properties of the system. (B) Responsivity of the system in presence of low concentration of styrene and toluene vapor. *Reproduced with modifications with permission of American Chemical Society: Rakow NA, et al: Visual indicator for trace organic volatiles,* Langmuir *26(6):3767–3770, 2010.*

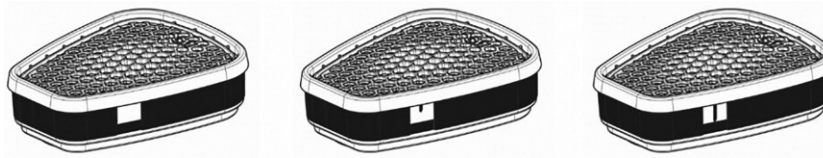

Fig. 2 Progression of the ESLI indicator bar in filter cartridge due to gases adsorption. *Reproduced by permission of Taylor and Francis: Checky M, et al: Evaluation of a passive optical based end of service life indicator (ESLI) for organic vapor respirator cartridges,* J Occup Environ Hyg *13(2):112–120, 2016.*

other technologies are available and can be developed to obtain a final system easily integrable in respirator cartridges. In Sections 2.2.2–2.2.4 we are going to analyze these upcoming strategies.

2.2.2 Metal organic frameworks (MOFs)

One of the most important family of upcoming materials in the field of gas absorption and sensing are the metal-organic frameworks (MOFs). They are a class of porous systems consisting of metal ions linked together by organic linkers with high internal surface areas up to 6000 m^2/g (Saeed et al., 2020). They are commonly identified as coordination networks containing potential voids. During its formation, the system starts extending, through repeating structures, in one dimension, but thanks to the cross-link between the chains the whole network can grow in two or three dimensions (Safaei et al., 2019). In literature various strategies for their synthesis are reported and they can be very different depending on the typology of MOFs realized (Cai et al., 2020). Here, for the sake of brevity, we are going to only give an overview of main employed fabrication technique. First of all, since the study of MOFs developed from the study of zeolite, they were initially produced in a similar way using hydrothermal or solvothermal techniques, with crystals slowly grown from a hot solution (Deng et al., 2021). In the years new techniques have been developed, employing microwave synthesis, ultrasound or electrochemistry. Moreover, great interest is today given to the solvent-free preparation of MOF films and composites, for example, employing the chemical vapor deposition (Wang and Astruc, 2020).

MOFs are very versatile materials, and they can be integrated with various engineering systems to exploit their properties, such as high absorption ability, employing them in gas sensing applications (Li et al., 2020a). A clearable example of that is represented by the use of metal organic

framework in the detection of volatile organic compounds (Khoshaman and Bahreyni, 2012). A sensitive nanoporous metal organic framework layer, obtained working with HKUST-1 MOFs (structural formula $Cu_3(BTC)_2(H_2O)$), was deposited, through a custom electro-spraying system, onto the surface of quartz resonator in order to realize a gravimetric sensor.

Quartz resonator is an electrical oscillator circuit based on mechanical resonance of a vibrating crystal to create an electrical output with a precise frequency (Alassi et al., 2017). In this specific case, the adsorption of the analyte gas on MOF induces a mass change that is detected by the system by a change in its output frequency. This kind of sensing guarantees high sensitivity, operability at room temperature, simple integration and low energy requirement. The deposited film demonstrated uniformity of mechanical and morphological properties, moreover the sensor performance evaluation at room temperature to different concentrations of acetone, THF and IPA confirmed the efficacy of this device, with a fall in its output frequency due to the adsorption of the organic vapor on the film. Fig. 3 represented the response of the electro-sprayed film to the aforementioned solvents, showing a pulse behavior of the system at varying gases concentration in the external environment.

Metal organic framework can be also integrated with other different structures. An example of that is represented by interdigitated electrodes (IDE) and the development of capacitive sensor based on them. Andrés and co-workers developed a sensor of this kind working with aluminum trimesate MOF (MIL-96(Al) MOF) thin film deposited via the Langmuir-Blodgett (LB) method onto Si/SiO_2 substrates incorporating interdigitated electrodes (Andrés et al., 2020). This device, schematized in Fig. 4, is able to adsorb on its surface gases of the external environment and produce a capacitive output signal through the electrodes, due to the variations of electric properties determined by the absorption of gases in the metal organic framework.

The best results have been obtained working for water vapor and methanol detection. The system showed high selectivity and fast response/recovery time. Furthermore, these sensors have been demonstrated to work at room temperature, be regenerable to several sensing cycles and stable for a considerable time span (at least 1 week). In Fig. 5 we have reported the output signals of these devices with capacitive response curve for MIL-96(Al) LB IDEs.

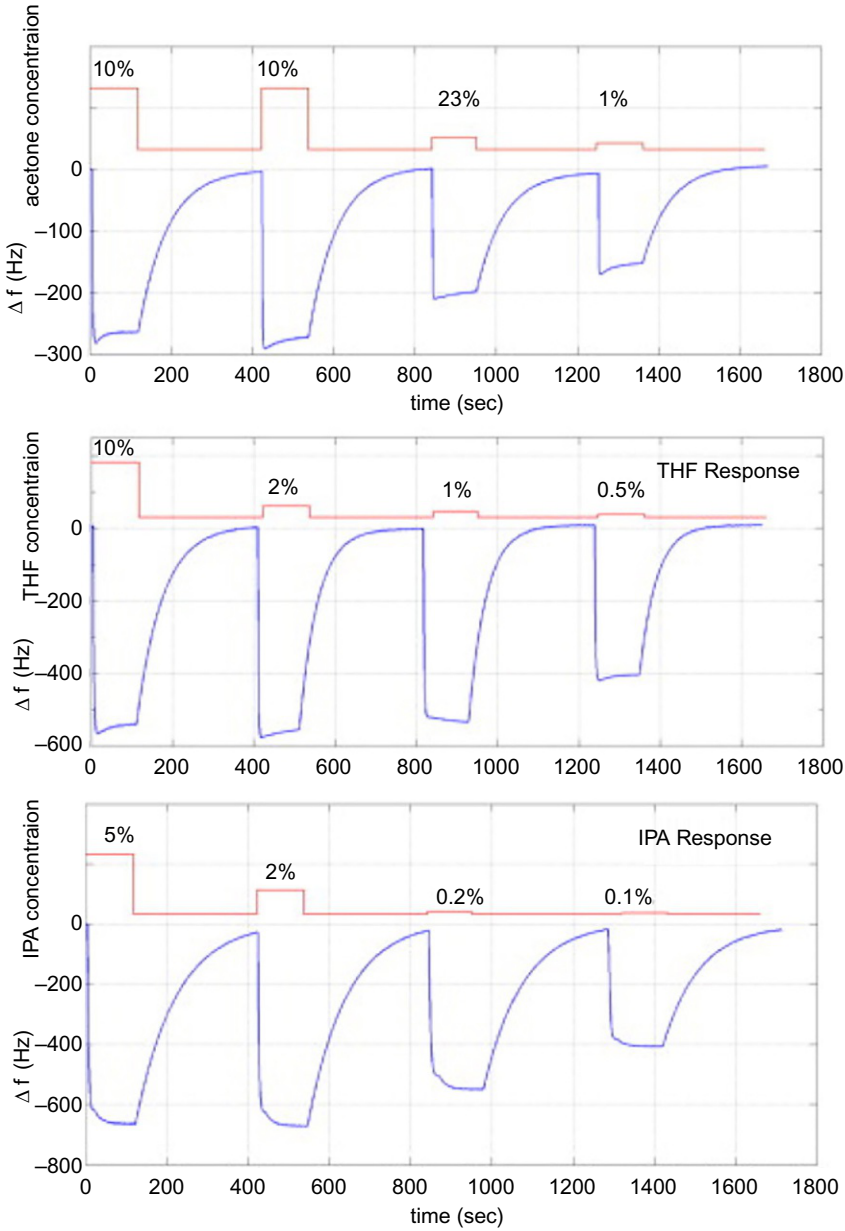

Fig. 3 Response of the electro-sprayed film to acetone, THF and IPA. *Reproduced by permission of Elsevier: Khoshaman AH, Bahreyni B: Application of metal organic framework crystals for sensing of volatile organic gases,* Sens Actuators B *162(1):114–119, 2012. https://doi.org/10.1016/j.snb.2011.12.046.*

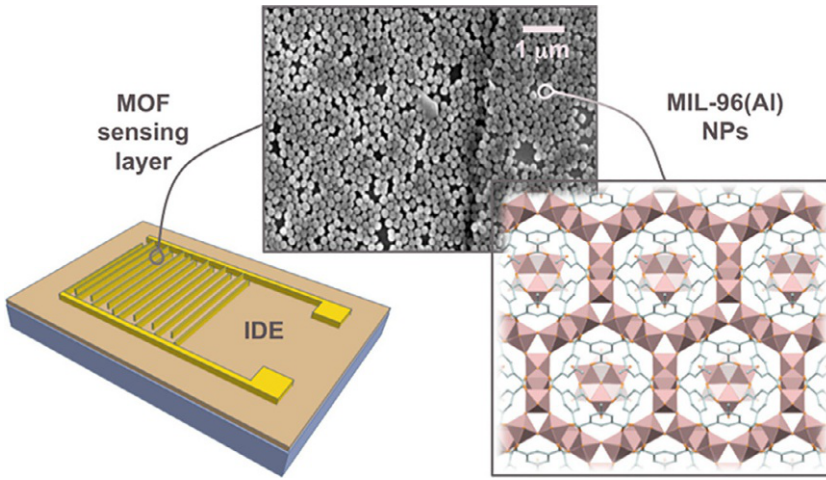

Fig. 4 Schematization showing MOF LB film characterization by SEM and its integration on interdigitated electrodes (IDE). *Reproduced by permission of American Chemical Society: Andrés MA, et al: Methanol and humidity capacitive sensors based on thin films of MOF nanoparticles,* ACS Appl Mater Interfaces *12(3):4155–4162, 2020.*

MOFs are a very important material thanks also to their versatility. In fact, one possible solution for many sensing applications consists in their conjugation with other constituents in order to obtain a final device with enhanced properties. This peculiarity is well evident working with MOFs/graphite or MOFs/graphene composites that have been widely explored in various fields, such as gas adsorption, but also catalysis, electrochemical energy conversion and energy storage (Sapsanis et al., 2015).

The synergistic effect of the constituents of the framework strongly improve the sensing ability of the system: for example, by one side graphene can act as a highly conductive sensing element, by the other side MOFs, thanks to their enormous surface area and subsequent adsorption ability, provide great sensitivity to the whole composite network. In literature various combination of this kind are reported: for example, a Cu-based MOF conjugated with either graphite oxide or aminated graphite oxide has been developed to detect low concentration of ammonia (Travlou et al., 2015). Similarly, another device employable in ammonia detection, has been designed exploiting the combination between polypyrrole-nanofiber-coated reduced graphene oxide composite and nanoscale benzene-1, 3,5-tricarboxylate (Cu BTC) MOFs (Yin et al., 2018). Another important strategy is represented by fabrication of graphene hybrid nanocomposite with selected MOFs for the detection of VOCs investigating the

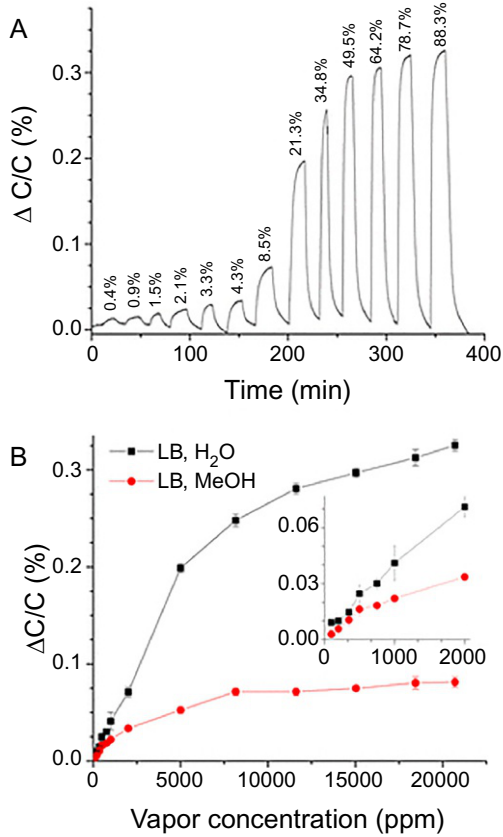

Fig. 5 (A) Capacitive response curve for water vapor for MIL-9(Al) LB IDEs. The peaks correspond to the measured relative humidity. (B) Normalized capacitive response of IDEs to water (black box) and methanol (red circles). *Reproduced by permission of American Chemical Society: Andrés MA, et al: Methanol and humidity capacitive sensors based on thin films of MOF nanoparticles,* ACS Appl Mater Interfaces *12(3):4155–4162, 2020.*

chemo-electrical responses of the framework after adsorption (Tung et al., 2020). The investigations on this device showed how the system working with copper-benzene-1,3,5-tricarboxylate (pG-Cu BTC) has very good sensing performance and present high sensitivity and selectivity especially respect to chloroform and methanol at 2.82–22.6 ppm level. Possible explanation for the specific selectivity to chloroform can be the affinity of chloroform molecules for hydrogen bonding to the Cu-BTC. Alongside, the high selectivity to methanol can be explained considering that the high polarity of methanol vapor can determine great interaction with the open metal sites in the apolar cages of the Cu-BTC MOF resulting in higher level

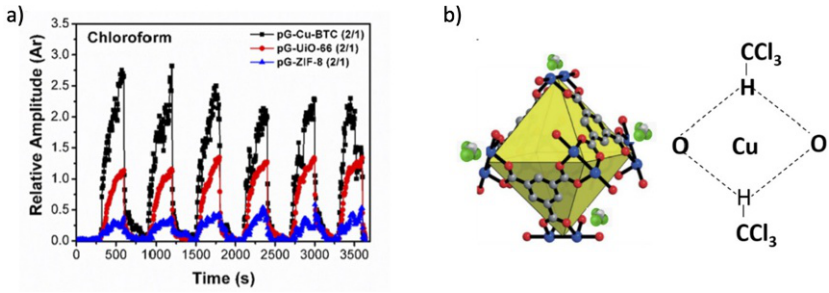

Fig. 6 (A) Sensing response of the presented system to chloroform, compared with other similar devices. (B) Representation of sensing mechanism of the pG-Cu BTC hybrid sensor toward chloroform vapor. *Reproduced with modifications by permission of Elsevier: Tung TT, et al: Graphene and metal organic frameworks (MOFs) hybridization for tunable chemoresistive sensors for detection of volatile organic compounds (VOCs) biomarkers,* Carbon *159:333–344, 2020. https://doi.org/10.1016/j.carbon.2019.12.010.*

of adsorption. In Fig. 6 the sensing response of the system to VOCs is reported (Fig. 6A), together with a representation of the sensing mechanism of the pG-Cu BTC hybrid sensor toward chloroform (Fig. 6B).

As the reader may have already understood metal organic frameworks are a very broad and under development topic, with many interesting characteristics for gas sensing applications. Various literature references are available and different fabrication strategies for versatile devices can be found especially for VOCs detection.

Up to now, no MOFs based sensor has been reported in literature as end of service life indicator for respirator cartridge. Anyway, we think that, thanks to the intrinsic high sensitivity of these devices their versatility and the possibility to obtain final systems of small dimensions, they can represent a future turning point for this application.

2.2.3 Optical fiber

Optical fibers are flexible, transparent fiber characterized by a diameter thicker than that of a human hair with the great ability to transmit lights. These devices are commonly made of silica or plastic and they find applications in various fields, like communications, electronics and sensors (Elosua et al., 2012; Joe et al., 2018). For the purpose of this work, we are going to focus on fiber-optic sensor and how proper formulated sensing materials can be integrated with optical fiber, exploiting the variation of the optical properties of the system as output signal. In fact, many advantages can be obtained working with this kind of devices, thanks to various properties such

as small size, no electrical power request or their immunity to external electrical field interference. Moreover, their formulation can be properly tuned for the intended application. Because of this, optical fiber-based sensors have been employed in the detection of volatile organic compounds and their applications as end of service life indicator have been discussed in literature (Joe et al., 2018).

An important work on the topic has been presented by Greenwald et al., that reported the development of an end of service life sensor based on optical measurement of a colored compound dispersed in a proper medium (Greenawald et al., 2015). In fact, a diffuse reflectance configuration can satisfy the size, applicability and cost requirement thanks to the great availability of required instrumentations such as small photodetectors, optical fibers and LED light sources. Various media can be employed for diffuse reflectance, including soil, paint, crystals and paper. Precisely, paper is an important substrate for real-time, low-cost sensors thanks to its lightweight, adaptability, porosity, large surface area and wicking ability. In this aforementioned paper, the authors worked with paper as substrate and pre-spotted its surface with a dilute monocyanocobinamide ($CN(H_2O)Cbi$) solution. Cobinamide (Cbi) is a cobalt-centered hydroxocobalamin analog that is used here as indicating system. This piece of functionalized paper was placed on the end of a bifurcated optical fiber and the reflectance spectrum of $CN(H_2O)Cbi$ was exploited in order to evaluate the presence of hydrogen cyanide gas. The chemical transformation from monocyanocobinamide ($CN(H_2O)$ Cbi) to dicyanocobinamide ($(CN)_2Cbi$) yields a color change from orange (peak absorbance at $\sim$510 nm) to violet (583 nm) that can be easily observed. This system has been demonstrated to be very sensitive and able to detect CN^- at concentrations as low as 0.25 nM cyanide in solution.

In Fig. 7 we have reported the response of the system to 1.0 and 5.0 ppm HCN.

The authors proposed a possible integration of this kind of sensor in order to develop an end of service life indicator to be used inside respirator cartridge. Their idea was to embed the sensor with direct contact to the carbon bed of the canister. Once HCN reaches a fixed point prior to breakthrough, the sensor provides a response due to the induced change in the cobinamide spectrum. The reaching of a defined value would determine the activation of an alarm in order to replace the cartridge. The small dimensions of the whole system make it feasible to integrate other sensing elements in the device.

The cobinamide has important features in the field of gas sensing even with other compounds such as ammonia and hydrogen sulfide. In fact the

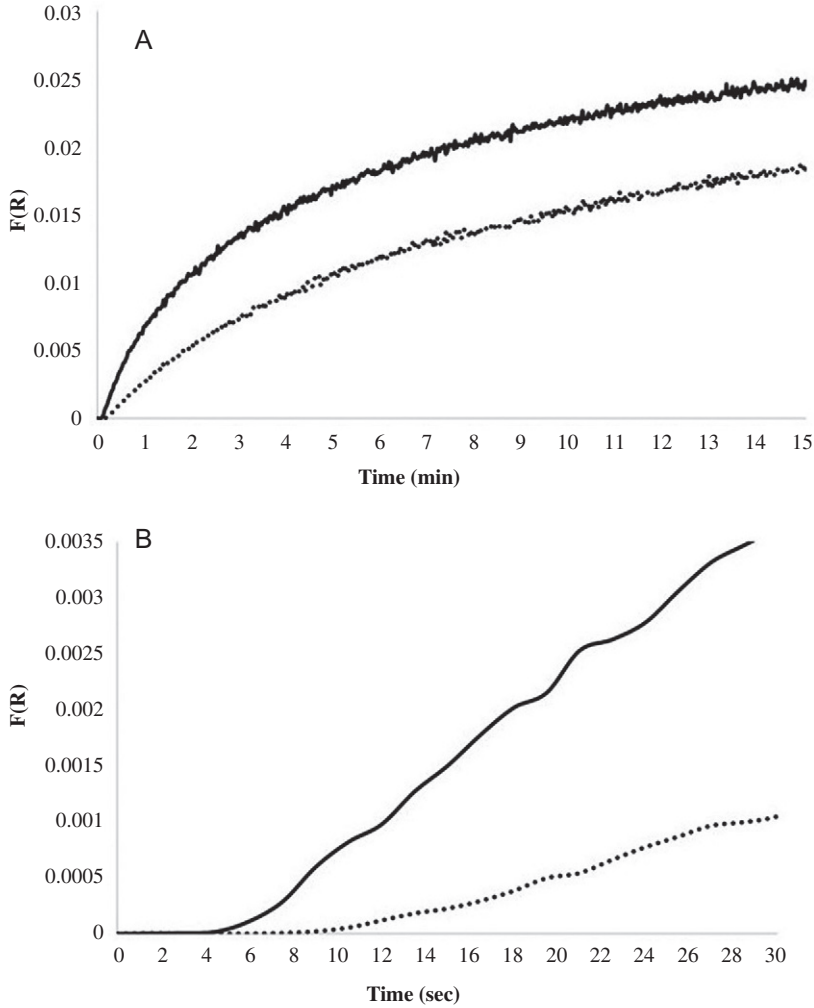

Fig. 7 (A) Profiles of the response of CN(H_2O)Cbi on glass fiber paper to 1.0 and 5.0 ppm HCN response at 583 nm (black line), 1.0 ppm HCN response at 583 nm (dotted line). (B) Expanded version of the same profiles in Fig. 7A. *Reproduced by permission of Elsevier: Greenawald LA, et al: Development of a cobinamide-based end-of-service-life indicator for detection of hydrogen cyanide gas,* Sens Actuators B *221:379–385, 2015. https://doi.org/10.1016/j.snb.2015.06.085.*

same authors proposed the development of a similar device based on functionalized paper placed over an optical fiber for the detection of hydrogen sulfide (Greenawald et al., 2016). The paper contains aquohydroxocobinamide (OH(H_2O)Cbi) and its reflectance spectrum was monitored

during exposure to hydrogen sulfide gas. H_2S is a reducing agent and it reacts with $(H_2O)_2$Cbi(III) to form a complex of Cbi(II) with SSH^{2-} determining a color change from red orange to a pale yellow and an increase in reflectance from 400 to 450 nm.

Thanks to small size, low cost and sensitivity this system can be used as an end of service life indicator in respirators with an integration similar to the one performed for the sensor used for the detection of hydrogen cyanide gas.

2.2.4 Micro- and nano-structures and composites systems

The field of micro- and nano-systems is a very broad and wide topic that is facing a great expansion in the last years (Nazemi et al., 2019). We have just talked about metal organic framework and how their large surface area guarantees important adsorption properties. Similarly, many micro- and nano-structures present this kind of peculiarity in term of available surface area and because of this they can be exploited for gas sensing applications.

In this section we are going to see various possible solutions working with this kind of devices: we focus first of all on their general features and then we go deeper in the analysis of their applications.

2.2.4.1 Nanorods

Nanorods are a very important nanoscale systems usually obtained by metals or semiconducting materials. Their aspect ratios (length divided by width) are commonly 3–5 and the characteristic dimension ranges from 1 to 100 nm (Meng et al., 2019).

Nanorods are produced by direct chemical synthesis: ligands are combined to act as shape control agents and they bond to different facets of the nanorod with variable strengths. This allow different faces of the system to grow with different rates and a final elongated object is obtained.

Various applications can be performed working with nanorods, exploiting optical properties, reflectivity of the systems and the influence of an applied electric field (Rao et al., 2019). Among them great attention is nowadays given to gas sensors based on nanorods and their application in volatile organic compounds detection.

In this context pristine and palladium (Pd) doped ZnO nanorods have been synthesized on a quartz crystal microbalance (QCM) in order to realize a volatile organic compound sensor working at room temperature (Öztürk et al., 2016). Briefly, quartz crystal microbalance is a device able to measure the mass variation per unit area by measuring the change in frequency of a

quart crystal resonator. This system, just presented in the section of metal organic framework, allows to determine the adsorbed quantity of gas on the material.

Pd doped and undoped ZnO nanorods were grown on ZnO thin film coated QCM transducers using electrochemical deposition working with a three-electrode system under constant potential at −0.9 V and at 80 °C. Then the obtained ZnO nanorods with different Pd dopant ions were annealed at 200 °C. This device is schematically reported in Fig. 8.

Various gas test has been realized on these systems and the obtained response curves have been compared. 0.5 mol% and 2.5 mol% Pd doped ZnO nanorods were exposed to multiple pulses of ethanol vapors with decreasing concentration in the range between 120 and 12 ppm at room temperature. The responses of the different sensors, due to the adsorbing mechanism of the analyte onto solid surfaces of the sensitive materials, were very close to each other and the frequency of each samples show a very rapid decrease due to the loading of mass. The sensors were recovered exploiting dry air. In Fig. 9 it is reported the behavior of this device when exposed to ethanol (Fig. 9A) and toluene (Fig. 9B) at room temperature.

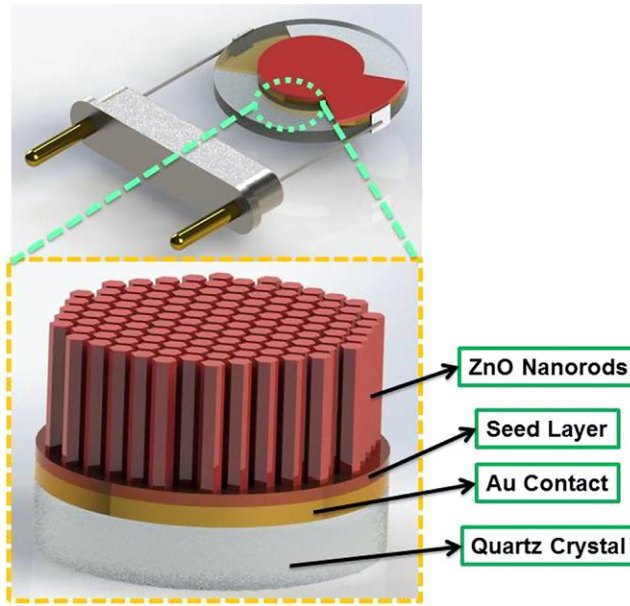

Fig. 8 Schematic representation of the integration of ZnO Nanorods on the QCM based mass sensitive sensor. *Reproduced by permission of Elsevier: Öztürk S, et al: Electrochemically growth of Pd doped ZnO nanorods on QCM for room temperature VOC sensors,* Sens Actuators B *222:280–289, 2016.*

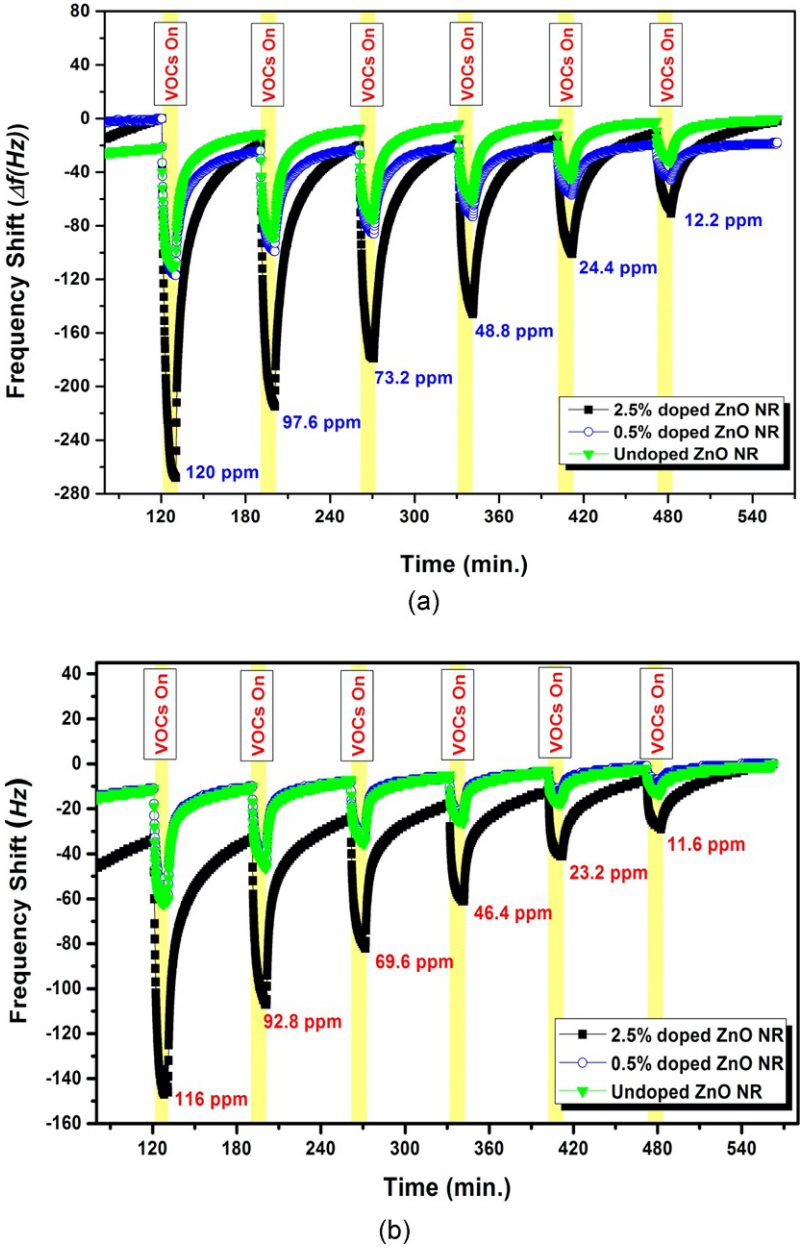

Fig. 9 Behavior of mass sensitive gas sensor when exposed to ethanol (A) and toluene (B) at room temperature. Pristine ZnO nanorods, 0.5 mol% and 2.5 mol% Pd doped nanorods over QCM (10 MHz) exposed to 10 min pulse of decreasing gas concentration are reported. *Reproduced by permission of Elsevier: Öztürk S, et al: Electrochemically growth of Pd doped ZnO nanorods on QCM for room temperature VOC sensors,* Sens Actuators B *222:280–289, 2016.*

Previous results make clear how these devices based on QCM and ZnO nanorods as transducers and sensitive materials respectively, can be successfully employed as sensors for volatile organic compounds. The small dimensions of the whole system, its sensibility and fast recovery give many possibilities for the integration of this device inside a respirator cartridge, for example, in the junction between the canister and the mask, in order to monitor its service life. One possible obstacle to this application is represented by costs or difficulties in the engineering of the device inside the cartridge.

Similarly, ZnO nanorods can be also applied in the sensing of NO_2 and NH_3. Ultrathin ZnO nanorods (~15 nm) are reported in literature, synthesized by a nanoseed-assisted wet chemical approach and then functionalized by Au nanoparticles by a photoreduction method (Wang et al., 2020a). This hybrid system showed visible-light-activity owing to the surface plasmon resonance (SPR) effects of Au nanoparticles. The sensor was selective in dark to NH_3 and to NO_2 under visible light ($\lambda = 532$ nm), moreover it showed high responsivity, short recovery time and excellent reversibility at room temperature. The schematization of this sensing process is represented in Fig. 10.

2.2.4.2 Tin oxide hollowspheres

Thanks to its properties of n-type semiconductor, SnO_2 has been widely studied for various applications such as catalyst support, electrodes development, electrochemical applications and even gas sensors. Many evidences have shown how the structural features of the materials strongly influences the performance of the SnO_2 based device (Das and Jayaraman, 2014). It is therefore clear that great attention is given to the proper formulation and shape of the material. Among the various nanostructures, hollow spheres have been reported as a very promising systems, thanks to their large surface area and less agglomeration (Zhang et al., 2009). In particular, SnO_2 hollowspheres can be employed as chemiresistive gas sensor for the detection of multiple VOCs selectively. Acharyya et al. synthetized this material through one step facile hydrothermal procedure, followed by high temperature heat treatment starting from chloride dihydrate (4 mmol), sodium citrate (2 mmol) and sodium hydroxide (10 mmol) in a 1:1 M solution of deionized water and ethanol, with the subsequent addition of polyethylene glycol (PEG-600) (Acharyya et al., 2020). Finally, the system was transferred to teflon-lined stainless-steel autoclave and kept at 180 °C for 12 h. The final product was recovered through filtration, washed with deionized water and dried. In order to investigate the electrical properties of the system,

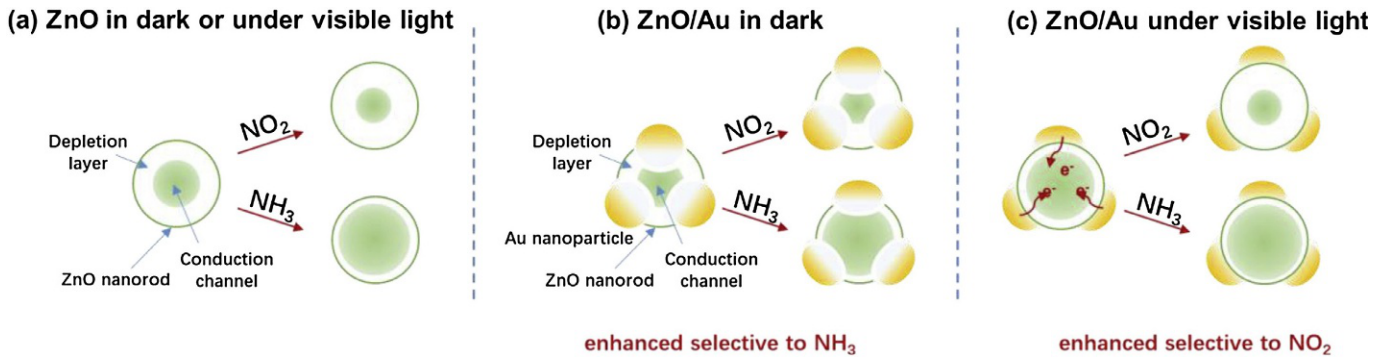

Fig. 10 Schematization of the surface plasmon characteristics of the ZnO nanorods in the different conditions for the sensing of NH_2 and NO_2. *Reproduced by permission of Elsevier: Wang J, et al: Room-temperature gas sensors based on ZnO nanorod/Au hybrids: visible-light-modulated dual selectivity to NO_2 and NH_3,* J Hazard Mater *381(July 2019):120919, 2020a.* https://doi.org/10.1016/j.jhazmat.2019.120919.

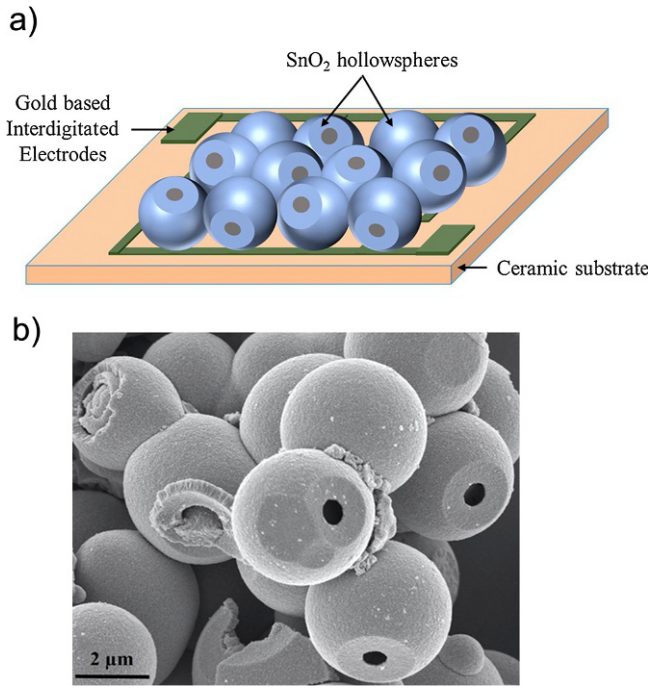

Fig. 11 (A) Schematic representation of the integration of the SnO_2 hollowspheres over the interdigitated electrodes. (B) FESEM image of the SnO_2 hollowspheres obtained with sodium citrate. *Reproduced with modifications by permission of Elsevier: Acharyya S, et al: Single resistive sensor for selective detection of multiple VOCs employing SnO_2 hollowspheres and machine learning algorithm: a proof of concept,* Sens Actuators B *321(June):128484, 2020. https://doi.org/10.1016/j.snb.2020.128484.*

the SnO_2 hollowspheres were drop-casted over interdigitated gold electrodes with a ceramic substrate. The schematic representation of the system together with a FESEM image of the structure is reported in Fig. 11.

Gas sensing measurement were carried out for this device using a cylindrical chamber inside which the desired concentration of VOCs in an air current was supplied. Analyses were realized with four different VOCs (formaldehyde, 2-propanol, toluene and methanol) at four different concentrations (25, 50, 100 and 200 ppm) in the temperature range 200–350 °C. When gases adsorb over the layer of hollowspheres a change in the resistance of the whole system can be detected and the results are reported in Fig. 12.

The system showed an excellent response with fast dynamics and recovery ability. Moreover, thanks to machine learning algorithms, it is possible to classify and identify different VOCs, obtaining good quantification and solving the issue of selectivity for the identification of different gases.

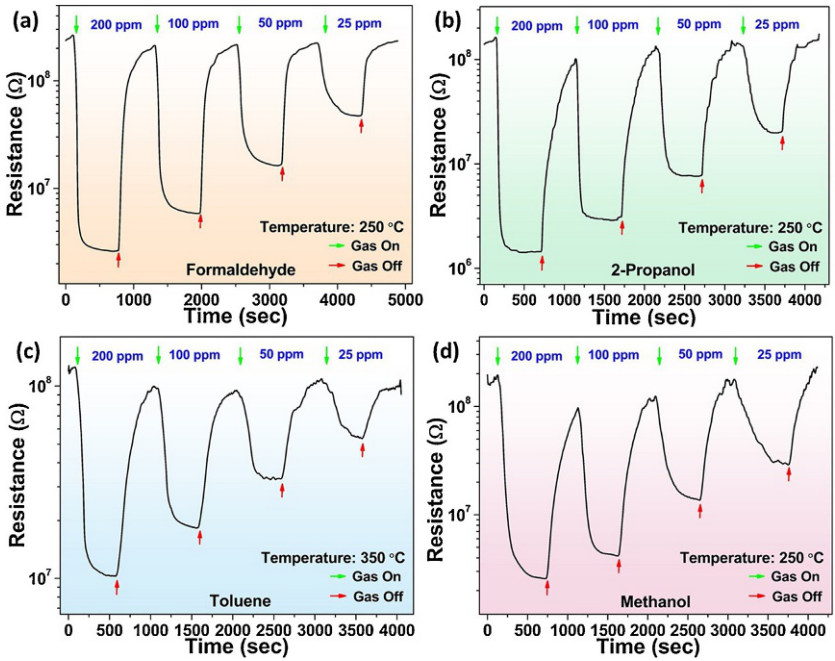

Fig. 12 Transient resistance plot for formaldehyde (A), 2-propanol (B), toluene (C) and methanol (D) with different input concentrations. Arrows pointing up: gas off, arrows pointing down gas on. *Reproduced with the permission of Elsevier: Acharyya S, et al: Single resistive sensor for selective detection of multiple VOCs employing SnO_2 hollow-spheres and machine learning algorithm: a proof of concept,* Sens Actuators B *321 (June):128484, 2020.* https://doi.org/10.1016/j.snb.2020.128484.

This system is for sure a great novelty in the field because, together with the possibility to monitor the quantity of adsorbed gases, it gives also the possibility to investigate, through the response of the system, which is the adsorbed gas guarantying the employability of this device in multiple fields even different from the application as end of service life indicators.

2.2.4.3 Nanocarbon composite sensor

One of the main chances related to the engineering is the possibility to study and combine different materials to exploit their properties, obtaining final devices with enhanced characteristics. This principle can be a very valuable strategy in the field of sensors, where there is the need to combine multiple features such as adsorption properties, sensitivity and responsivity.

In this context, an innovative device with these characteristics has been developed for the selective monitoring of nitrogen dioxide in air.

This system was realized combining the features of sensitivity and partial selectivity toward oxidizing agents of a molecular organic semiconductor, copper phthalocyanine, with the O_3 filtering capability of carbonaceous materials, located upstream the sensitive layer in the gas flux (Brunet et al., 2012). The possibility to detect NO_2 is achieved associating a mixture of carbon nanodiscs and nanocones, acting as ozone chemical filter, with the copper phthalocyanine as sensing element.

The resistive transduction of the material was investigated to analyze its response to the nitrogen oxide adsorption, examining if the ozone adsorption can influence this behavior. Moreover, the filtering ability of the system was studied observing the reduction of NO_x compounds in the stream. In Fig. 13 these behaviors are reported.

These results confirm the efficacy of these devices. The possibility to combine a sensing system with a filter can be a valuable strategy for the monitoring of the service life. Moreover, this sensor guarantees the possibility to achieve a selective NO_2 detection inside an environment where O_3 is present: this can be useful in various industrial contexts.

2.2.4.4 Carbon based systems

Activated carbon is a very valid and largely employed material in the field of filtration. Its features such as the presence of small, low-volume pores able to increase the surface area give important adsorption ability to this material that find large industrial application in the production of respirator cartridges. Alongside, active carbon-based systems can be employed in gas sensing devices as, for example, the carbon nanotubes (CNTs)-based sensors (Zaporotskova et al., 2016).

Carbon nanotubes belong to the family of fullerene structures and commonly two different types can be identified: single-walled carbon nanotubes (SWCNT's) and multiwalled carbon nanotubes (MWCNTs). A SWCNT is defined as a one-atom-thick layer of graphite rolled up into a seamless cylinder with a diameter in the range of nanometers and length on the order of 1–100 μm. By the other side, MWCNTs consist of nested single-wall carbon nanotubes bound together by van der Waals interactions in a tree ring-like structure. This kind of framework guarantees to these materials great mechanical resistance and thermal stability, moreover the electrical behavior of the system can be either metallic or semiconducting according to the formulation and affected by external conditions (Eatemadi et al., 2014).

When carbon nanotubes are exposed to certain gases, the change in the properties of their structures can be detected by various methods

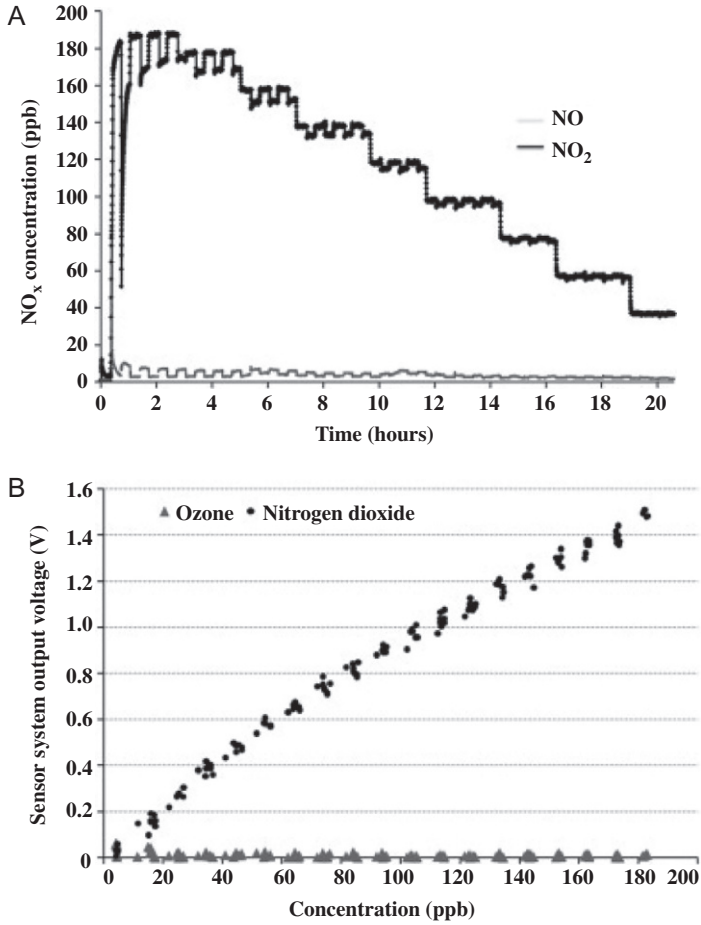

Fig. 13 (A) Filtering results obtained with carbon nanodiscs toward nitrogen dioxide. NO and NO_2 were given upstream and downstream the filter. During the experiments the gas concentrations remained constant. (B) Response curve of the sensor system toward ozone and nitrogen dioxide. *Reproduced with modification by permission of Elsevier: Brunet J, et al: An innovative gas sensor system designed from a sensitive organic semiconductor downstream a nanocarbonaceous chemical filter for the selective detection of NO_2 in an environmental context part I: development of a nanocarbon filter for the removal of ozone,* Sens Actuators B *173:659–667, 2012.* https://doi.org/10.1016/j.snb.2012.07.082.

investigating specific parameters: this can be a very important tool for gas sensing instruments. In particular for SWCNT there are four distinct sites for gas molecules to be absorbed onto: the external surface, the groove between two adjacent tubes, inside the pore of one single tube and in the

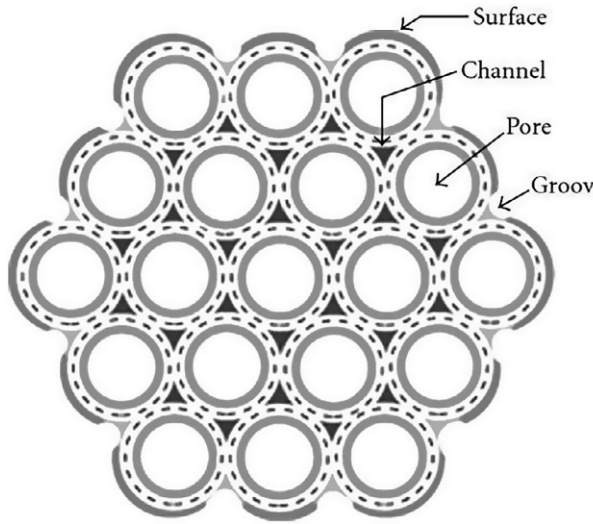

Fig. 14 Schematic representation of CNTs system and possible sites for gas adsorption in their structure. *Reproduced with modifications by permission of Hindawi: Wang Y, Yeow JTW: A review of carbon nanotubes-based gas sensors,* J Sens *2009:493904, 2009.*

interstitial channel between adjacent tubes (Wang and Yeow, 2009). This structure is schematically reported in Fig. 14: the gas adsorption in the sites is decided by the site availability and the binding energy of the gas molecules.

Commonly CNTs can be synthetized with different techniques such as arc-discharge technique, laser ablation technique or chemical vapor deposition. The fabricated CNTs have to be integrated to different gas sensor structures. One of the most common and functional devices through which CNTs properties can be investigated are the interdigitated electrodes. The material can be disposed over the substrate through various technique: CNTs can be simply casted over the electrodes, they can be printed through screen printing techniques or their fabrication can be achieved through dielectrophoresis (DEP) method. In particular DEP fabrication could establish a good electrical connection between the nanotubes and the electrodes and because of this it is many times preferred. Another important technique that determines enhanced sensing properties to the whole system, thanks to a better adhesion, is the direct growth of the CNT's mats on the substrate.

As aforementioned these systems present important gas adsorption properties, and the electronic properties of CNT's can be extremely sensitive to the exposed environment due to gas molecule adsorption: thermopower, resistance, density of state of the CNTs show significant changes after gas

exposure (Mao et al., 2014). Depending on CNTs formulation and its functionalization different behavior can be obtained in response to VOCs or different gases. An example of that is represented by the possibility to develop a composite thin film of polymethylmethacrylate (PMMA) with MWCNTs (Wang and Yeow, 2009). The exposure to different gases of this device at room temperature determines important changes in the resistance of the system that can be explained on the basis of volume expansion and polar interaction of the CNT surface with vapor molecules. These results are reported in Fig. 15.

The case just reported is an example of the possible synthesis and application of this kind of systems. The development of nano-devices and in particular the study on CNTs has created in the last decade huge potential in the development of smart sensors with enhanced properties in term of sensitivity, portability and low power requirement. Their versatility can lead to future applications of these kind of gas sensors in the field of service life monitoring for industrial devices.

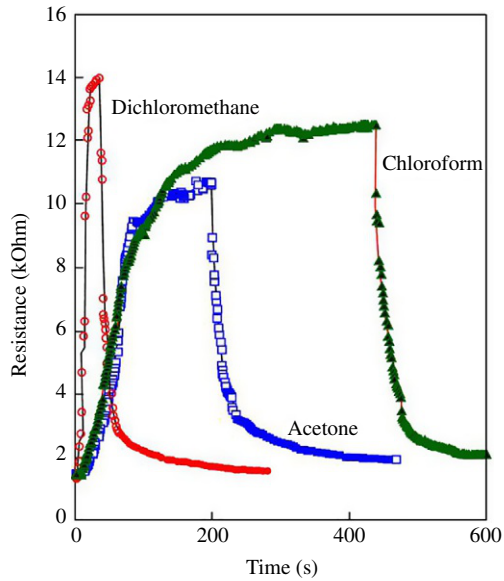

Fig. 15 Response of the CNT/PMMA composite to dichloromethane, chloroform and acetone vapors. *Reproduced by permission of Hindawi: Wang Y, Yeow JTW: A review of carbon nanotubes-based gas sensors,* J Sens *2009:493904, 2009.*

2.3 Hydrogels

Another upcoming technology in the field of sensing is represented by the hydrogels, which represent a wide family of innovative smart devices relevant for many different applications (Buenger et al., 2012; Pinelli et al., 2020). Hydrogels are colloidal structures of polymer chains with a three-dimensional network. Their main peculiarities are related to their hydrophilic and biocompatible nature thanks to their high-water content. Moreover, hydrogels matrix presents high porosity and flexibility and, most important, the ability to respond to external stimuli. Temperature variations, pH solution changes, light stimuli or the presence of specific molecules in the system can be sensed by the hydrogels and these stimuli induce in the framework an output signal such as a change of volume, size, shape, or a modification of the optical, electrical or mechanical properties of the gel (Ahmed, 2015).

In front of this wide variety of input and output signals that can be correlated with hydrogels sensing feature, it is clear how the tuning of the formulation of the system is pivotal in order to obtain a proper responsive device. The employment of certain polymers chains, specific system functionalization or the encapsulation in the matrix of enzymes, cells or bacteria are all examples of the tuning of the formulation to obtain specific behavior. Many possibilities can be exploited and because of this, many different sensing devices can be obtained, employable in many fields.

Hydrogels based sensor for gas detection can be usually divided in two big classes (Pinelli et al., 2020). First of all, they can be employed as passive protective element for a primary sensor or an electrode which is the real sensing element. In this application, which is for sure the less interesting, hydrogels are just a support element that can be employed to tune the sensitivity of the system and improve the performance. By the other side hydrogels can be modified through sensitive molecules or functionalized through the encapsulation of proper systems in order to obtain a final device with enhanced properties in term of gas sensing.

A clear example of that is represented by the work of Bai et al. (2011), in which they synthetize graphene oxide (GO)/conducting polymer composite hydrogels for ammonia gas detection. The system was realized through in situ polymerization of the precursor aromatic monomer in aqueous dispersions of graphene oxide sheets that were encapsulated inside the matrix thanks to the cross-linking formation of the polymeric network.

GO/polypyrrole, GO/poly(3,4-ethylenedioxythiophene) and GO/polyaniline were synthetized, and, in each case, the whole system was demonstrated to be able to conduct electricity thanks to its inner structure. By the other hand, thanks to its high surface area and the adsorption ability of the system, when the lyophilized hydrogel is exposed to an environment with ammonia gas, because of a dedoping process, the device faces an increase in its electric resistance that was detected through interdigitated electrodes. This behavior is guaranteed by the inner structure of the system, analyzed with SEM and TEM analyses as presented in Fig. 16.

The mechanism just presented is a very common strategy for the gas detection employing hydrogels: the exposure of the system to gases determine a doping or dedoping process and some of the characteristics of the system, such as the conductivity, are affected by this and investigated for sensors.

A similar strategy was employed for the development of a supramolecular hydrogel-based sensor (Zhi et al., 2020). Briefly, this system was synthetized from poly(vinyl alcohol) and carrageenan working with 1-vinyl-3-butylimidazolium and *N*,*N*′-methylenbis(acrylamide) and the gas sensing performance were evaluated in a sealed gas chamber at room temperature through the monitoring of the relative electric resistance variation via a multimeter. The system presented important sensing abilities, and it was demonstrated to be able to respond to target gases (e.g., NO_2, NH_3) in very low concentrations. This behavior can be explained considering the synergetic effect of three different supramolecular interactions: hydrogen bonding, molecular crystallization and electrostatic interactions. The first two contribute to the self-responsive ability of the system, instead the electrostatic interaction guarantees excellent conductivity and higher stability to the network. The profiles of the sensing ability of the system are reported in Fig. 17.

The systems just presented can be very useful devices in the field of sensors. Hydrogels can be formulated and functionalized with many different strategies obtaining different selective behaviors respect to different gases. The possibility to employ them as end of service life indicator is for sure related to the possibility to realize a hydrogel-based sensor with enhanced sensitivity and small dimensions, for example, working with a thin hydrogel film over interdigitated electrodes. None of this kind of devices is reported in literature for this specific application, but this research field of soft sensing is today facing an important expansion and it is going over more and more employments.

In Table 1 we have reported the main materials for gas detection we have described in this work with a focus on their possible applications.

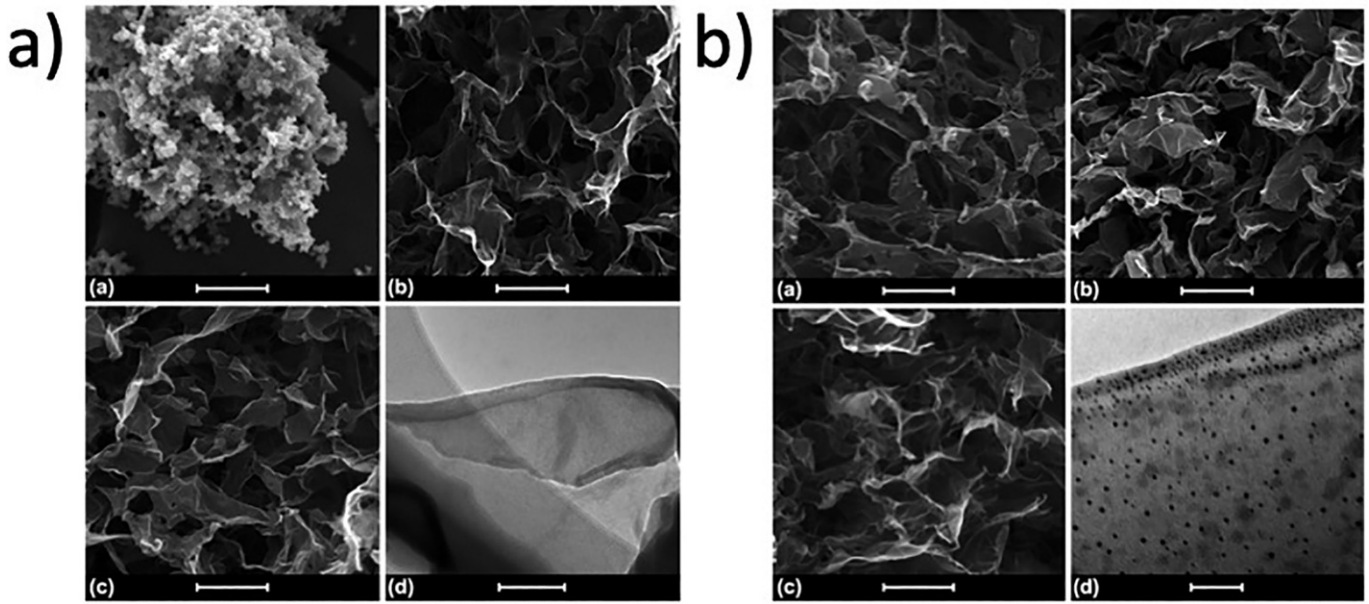

Fig. 16 (A) SEM image of (a) PPy particles prepared without GO, (b) of lyophilized GO solution, (c) of lyophilized GO/PPy composite hydrogel. (d) TEM image of GO/PPy composite sheets. (B) SEM images of lyophilized GO/poly(3,4-ethylenedioxythiophene) (a), GO/polyaniline (b) and GO/polypyrrole (c) composite hydrogels with also a TEM image of a GO/polypyrrole/Pt composite sheets. Scale bar (a–c) 10 μm (d) 50 nm. *Reproduced by permission of The Royal Society of Chemistry: Bai H, et al: Graphene oxide/conducting polymer composite hydrogels,* J Mater Chem *21(46):18653–18658, 2011.*

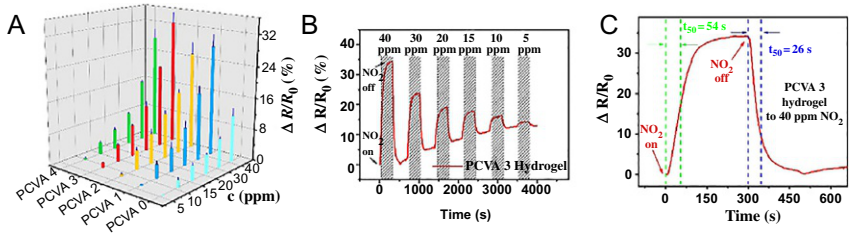

Fig. 17 PVCA gas sensor performance to NO_2: (A) response to NO_2 gas with a decrease in concentration from 40 to 5 ppm, (B) dynamic response of PVCA to NO_2 gas with a decrease in concentration from 40 to 5 ppm, (C) response time and recovery time profiles in the measurement of 40 ppm of NO_2. *Reproduced by permission of American Chemical Society: Zhi H, Gao J, Feng L: Hydrogel-based gas sensors for NO_2 and NH_3,* ACS Sens *5(3):772–780, 2020.*

Table 1 Summary list of the main materials that can be employed in volatile organic compounds detection with a focus on their features and possible sensing applications.

Materials	Features	Sensing application
Polymer of intrinsic microporosity	Porous organic polymer with a network of intermolecular voids. It is characterized by high free volume, high surface area and high affinity with gases	This material can be properly integrated with reflective metallic layers and the whole system exploits the reflective interference variations to investigate the progressive adsorption of gases on the material
Metal-organic-framework	Porous materials made of metal ions linked together by organic linkers. They possess high surface area (up to 6000 m^2/g) and exceptional adsorbent properties	Thanks to their surface area they can be integrated with other materials (e.g., graphene) or used as adsorbent medium in order to detect the presence of gases
Optical fiber	Flexible, transparent and thin fiber made of silica or plastic with the great ability to transmit light They do not require electrical power and they are immune to external electrical field	Optical fibers can be integrated with proper substrate and functionalized medium. The interactions with specific molecules guarantee changes in its optical properties

Table 1 Summary list of the main materials that can be employed in volatile organic compounds detection with a focus on their features and possible sensing applications.—cont'd

Materials	Features	Sensing application
Nanorods	Nanoscale systems obtained by metals or semiconducting materials with characteristic ratio of 3–5 and dimensions in the range of 1–100 nm They present important optical properties and reflectivity	Nanorods can be integrated with quartz crystal microbalance (QCM) and be exploited as sensitive material Similarly, they can be functionalized with Au NPs and then used as sensitive system exploiting the surface plasmon resonance of the Au NPs
Tin oxide hollowspheres	Nanostructures with characteristic shape characterized by large surface area and commonly made of semiconductive material (e.g., SnO_2)	SnO_2 hollowspheres can be employed as chemiresistive gas sensor. They can be disposed over interdigitated electrodes to investigate gas presence through electrical properties variations
Nanocarbon composites	Material obtained by the combination between carbonaceous systems and molecular organic semiconductor	This formulation combines important adsorbent properties with sensing abilities that can be investigated especially through electrical properties variation
Carbon nanotubes (CNT)	Tubes made of carbon, with diameters typically measured in nanometers They can be single or multi walled with a length on the order of 1–100 μm They present great mechanical and thermal stability and electrical behavior tunable depending on formulation and external conditions	Carbon nanotubes can adsorb gases in four different sites, and this ability is exploited to investigate gas presence depending on CNT properties variations (e.g., electrical properties)
Hydrogels (HG)	Colloidal structures made of polymer chains characterized by a three-dimensional network They present high porosity, flexibility and tunability	Hydrogels formulation can be easily tuned in order to obtain responsive final system The adsorption of gases over the HG surface determines doping or dedoping processes that result in variations of the properties of the system and its sensing ability

3. Conclusions

The development of gas sensing devices and sensitive systems has faced, in the last decade, an important expansion with a wide variety of different materials investigated and tested. The possibility of conjugating innovative technologies with highly sensitive structures gives many chances to various applications for the development of innovative smart highly sensitive sensors.

The applications of this kind of systems as end of service life indicator for respirator cartridge is for sure a field of great interest, especially due to the great importance that nowadays the security issues require in industry. The development of such a device would be a turning point for the production of respirator cartridge. In fact, by one side it would guarantee higher level of security for users wearing this kind of PPE and by other side it would enable, after proper certifications and evaluations, the possibility to use masks with respirator cartridges even in those applications in which today they can't be employed, for example, against odorless gases for which, because of the impossibility to detect the expiration of the PPE, it is today necessary the employment of breathing support devices (e.g., oxygen tank).

As the reader may understand, it is difficult, in face of the variety of available devices employable in the field, to give specific guidelines for the sensor developments for this intended application. For sure we can point out the need of a very responsive device, able to detect ppm or even ppb of gas in the environment. Moreover, small dimensions of the systems are required in order to enable their integration inside the PPE (e.g., respirator cartridge) and together with this, reasonable costs are mandatory in order to obtain a final device that could be economically competitive.

In this work we have given great attention to the sensing elements and their features in term of engineering fabrication. It is clear how, in real industrial applications, great consideration has to be given to proper integration of the sensor for the intended application, evaluating all the requirements and the specific needs of the considered case, together with the implementation of the instrumentation for the elaboration and transduction of the output signals.

References

Acharyya S, et al.: Single resistive sensor for selective detection of multiple VOCs employing SnO2 hollowspheres and machine learning algorithm: a proof of concept, *Sens Actuators B* 321(June), 2020, 128484. https://doi.org/10.1016/j.snb.2020.128484.

Ahmed EM: Hydrogels: introduction, preparation, characterization and applications: a review, *J Adv Res* 6(2):105–121, 2015.

Alassi A, Benammar M, Brett D: Quartz crystal microbalance electronic interfacing systems: a review, *Sensors* 17(12):1–41, 2017.

Andrés MA, et al.: Methanol and humidity capacitive sensors based on thin films of MOF nanoparticles, *ACS Appl Mater Interfaces* 12(3):4155–4162, 2020.

Bai H, et al.: Graphene oxide/conducting polymer composite hydrogels, *J Mater Chem* 21(46):18653–18658, 2011.

Barro-Torres S, Fernández-Caramés TM, Pérez-Iglesias HJ, Escudero CJ: Real-time personal protective equipment monitoring system, *Comput Commun* 36(1):42–50, 2012.

Beluomini MA, et al.: Electrochemical sensors based on molecularly imprinted polymer on nanostructured carbon materials: a review, *J Electroanal Chem* 840(April):343–366, 2019. https://doi.org/10.1016/j.jelechem.2019.04.005.

Brunet J, et al.: An innovative gas sensor system designed from a sensitive organic semiconductor downstream a nanocarbonaceous chemical filter for the selective detection of NO2 in an environmental context part I: development of a nanocarbon filter for the removal of ozone, *Sens Actuators B* 173:659–667, 2012. https://doi.org/10.1016/j.snb.2012.07.082.

Budd PM, et al.: Polymers of intrinsic microporosity (PIMs): robust, solution-processable, organic nanoporous materials, *Chem Commun* 4(2):230–231, 2004.

Buenger D, Topuz F, Groll J: Hydrogels in sensing applications, *Prog Polym Sci* 37(12):1678–1719, 2012. https://doi.org/10.1016/j.progpolymsci.2012.09.001.

Cai X, et al.: Nano-sized metal-organic frameworks: synthesis and applications, *Coord Chem Rev* 417:213366, 2020. http://www.sciencedirect.com/science/article/pii/S0010854520302393.

Carta M, Msayib KJ, McKeown NB: Novel polymers of intrinsic microporosity (PIMs) derived from 1,1-spiro-bis(1,2,3,4-tetrahydronaphthalene)-based monomers, *Tetrahedron Lett* 50(43):5954–5957, 2009. http://www.sciencedirect.com/science/article/pii/S0040403909015846.

Checky M, et al.: Evaluation of a passive optical based end of service life indicator (ESLI) for organic vapor respirator cartridges, *J Occup Environ Hyg* 13(2):112–120, 2016.

Christopher Thomas J, et al.: Optical sensor for diverse organic vapors at ppm concentration ranges, *Sensors* 11(3):3267–3280, 2011.

Das S, Jayaraman V: SnO2: a comprehensive review on structures and gas sensors, *Prog Mater Sci* 66:112–255, 2014. http://www.sciencedirect.com/science/article/pii/S0079642514000565.

Das M, Roy S: Polypyrrole and associated hybrid nanocomposites as chemiresistive gas sensors: a comprehensive review, *Mater Sci Semicond Process* 121(August 2020):105332, 2021. https://doi.org/10.1016/j.mssp.2020.105332.

Decaens J, Vermeersch O: 23—Wearable technologies for personal protective equipment: embedded textile monitoring sensors, power and data transmission, end-life indicators, In Koncar V, editor: *Smart textiles and their applications*, Oxford, 2016, Woodhead Publishing, pp 519–537. Woodhead publishing series in textiles. http://www.sciencedirect.com/science/article/pii/B9780081005743000230.

Deng Y, et al.: Metal-organic framework membranes: recent development in the synthesis strategies and their application in oil-water separation, *Chem Eng J* 405:127004, 2021. http://www.sciencedirect.com/science/article/pii/S1385894720331326.

Eatemadi A, et al.: Carbon nanotubes: properties, synthesis, purification, and medical applications, *Nanoscale Res Lett* 9(1):393, 2014. https://doi.org/10.1186/1556-276X-9-393.

Elosua C, et al.: Volatile organic compounds optical fiber sensor based on lossy mode resonances, *Sens Actuators B* 173:523–529, 2012. http://www.sciencedirect.com/science/article/pii/S0925400512007289.

European Union: *"The VOCs solvent emission directive": 1999/13/EC*, 1999.

Favas G: *End of service life indicator (ESLI) for respirator cartridges. Part 1: literature review*, Australia, 2005, Human Protection & Performance Division-Defence Science and Technology Organisation.

Greenawald LA, et al.: Development of a cobinamide-based end-of-service-life indicator for detection of hydrogen cyanide gas, *Sens Actuators B* 221:379–385, 2015. https://doi.org/10.1016/j.snb.2015.06.085.

Greenawald LA, Boss GR, Reeder A, Bell S: Development of a hydrogen sulfide end-of-service-life indicator for respirator cartridges using cobinamide, *Sens Actuators B* 230:658–666, 2016. https://doi.org/10.1016/j.snb.2016.02.129.

Hruska F: Trends in the sensor development, In Silhavy R, et al., editors: *Intelligent systems in cybernetics and automation theory*, Cham, 2015, Springer International Publishing, pp 45–55.

Joe HE, et al.: A review on optical fiber sensors for environmental monitoring, *Int J Precis Eng Manuf Green Technol* 5(1):173–191, 2018.

Khoshaman AH, Bahreyni B: Application of metal organic framework crystals for sensing of volatile organic gases, *Sens Actuators B* 162(1):114–119, 2012. https://doi.org/10.1016/j.snb.2011.12.046.

Li HY, Zhao SN, Zang SQ, Li J: Functional metal-organic frameworks as effective sensors of gases and volatile compounds, *Chem Soc Rev* 49(17):6364–6401, 2020a.

Li X, et al.: Adsorption materials for volatile organic compounds (VOCs) and the key factors for VOCs adsorption process: a review, *Sep Purif Technol* 235(October 2019):116213, 2020b. https://doi.org/10.1016/j.seppur.2019.116213.

Mao S, Lu G, Chen J: Nanocarbon-based gas sensors: progress and challenges, *J Mater Chem A* 2(16):5573–5579, 2014.

McKeown NB: Polymers of intrinsic microporosity (PIMs), *Polymer* 202:122736, 2020. http://www.sciencedirect.com/science/article/pii/S0032386120305668.

Meng L, et al.: Preparation and progress in application of gold nanorods, Ed. Laura Martinez Maestro, *J Nanomater* 2019:4925702, 2019. https://doi.org/10.1155/2019/4925702.

Mills D: Chapter 30—Health and safety, In Mills D, editor: *Pneumatic conveying design guide*, ed 3, 2016, Butterworth-Heinemann, pp 689–712. http://www.sciencedirect.com/science/article/pii/B9780081006498000305.

Mulvey D, et al.: Frequent and unexpected deviations from personal protective equipment guidelines increase contamination risks, *Am J Infect Control* 47(9):1146–1147, 2019. http://www.sciencedirect.com/science/article/pii/S0196655319301737.

Nazemi H, Joseph A, Park J, Emadi A: Advanced micro-and nano-gas sensor technology: a review, *Sensors* 19(6):1285, 2019.

Öztürk S, et al.: Electrochemically growth of Pd doped ZnO nanorods on QCM for room temperature VOC sensors, *Sens Actuators B* 222:280–289, 2016.

Pinelli F, Magagnin L, Rossi F: Progress in hydrogels for sensing applications: a review, *Mater Today Chem* 17:100317, 2020. https://doi.org/10.1016/j.mtchem.2020.100317.

Rakow NA, et al.: Visual indicator for trace organic volatiles, *Langmuir* 26(6):3767–3770, 2010.

Rao H, Xue X, Wang H, Xue Z: Gold nanorod etching-based multicolorimetric sensors: strategies and applications, *J Mater Chem C* 7(16):4610–4621, 2019. https://doi.org/10.1039/C9TC00757A.

Reddy SC, Valderrama AL, Kuhar DT: Improving the use of personal protective equipment: applying lessons learned, *Clin Infect Dis* 69(Suppl. 3):S165–S170, 2019. https://doi.org/10.1093/cid/ciz619.

Saeed T, et al.: Structure, nomenclature and viable synthesis of micro/nanoscale metal organic frameworks and their remarkable applications in adsorption of organic pollutants, *Microchem J* 159:105579, 2020. http://www.sciencedirect.com/science/article/pii/S0026265X20325601.

Safaei M, et al.: A review on metal-organic frameworks: synthesis and applications, *TrAC Trends Anal Chem* 118:401–425, 2019. http://www.sciencedirect.com/science/article/pii/S0165993619301840.

Sapsanis C, et al.: Insights on capacitive interdigitated electrodes coated with MOF thin films: humidity and VOCs sensing as a case study, *Sensors* 15(8):18153–18166, 2015.

Soni V, Singh P, Shree V, Goel V: Effects of VOCs on human health, In Sharma N, et al., editors: *Air pollution and control*, Singapore, 2018, Springer Singapore, pp 119–142. https://doi.org/10.1007/978-981-10-7185-0_8.

Stanovsky P, et al.: Upgrading of raw biogas using membranes based on the ultrapermeable polymer of intrinsic microporosity PIM-TMN-Trip, *J Membr Sci* 618:118694, 2021. http://www.sciencedirect.com/science/article/pii/S0376738820312709.

Travlou NA, Singh K, Rodríguez-Castellón E, Bandosz TJ: Cu-BTC MOF-graphene-based hybrid materials as low concentration ammonia sensors, *J Mater Chem A* 3(21): 11417–11429, 2015.

Tung TT, et al.: Graphene and metal organic frameworks (MOFs) hybridization for tunable chemoresistive sensors for detection of volatile organic compounds (VOCs) biomarkers, *Carbon* 159:333–344, 2020. https://doi.org/10.1016/j.carbon.2019.12.010.

Wang Q, Astruc D: State of the art and prospects in metal-organic framework (MOF)-based and MOF-derived nanocatalysis, *Chem Rev* 120(2):1438–1511, 2020.

Wang Y, Yeow JTW: A review of carbon nanotubes-based gas sensors, *J Sens* 2009, 2009, 493904.

Wang J, et al.: Room-temperature gas sensors based on ZnO nanorod/Au hybrids: visible-light-modulated dual selectivity to NO2 and NH3, *J Hazard Mater* 381(July 2019): 120919, 2020a. https://doi.org/10.1016/j.jhazmat.2019.120919.

Wang L, et al.: Polymer of intrinsic microporosity (PIM) films and membranes in electrochemical energy storage and conversion: a mini-review, *Electrochem Commun* 118:106798, 2020b. http://www.sciencedirect.com/science/article/pii/S1388248120301491.

Yin Y, et al.: Inducement of nanoscale Cu–BTC on nanocomposite of PPy–RGO and its performance in ammonia sensing, *Mater Res Bull* 99:152–160, 2018. http://www.sciencedirect.com/science/article/pii/S0025540817316215.

Zaporotskova IV, Boroznina NP, Parkhomenko YN, Kozhitov LV: Carbon nanotubes: sensor properties. A review, *Mod Electron Mater* 2(4):95–105, 2016. http://www.sciencedirect.com/science/article/pii/S2452177917300178.

Zhang J, et al.: NO2 sensing performance of SnO2 hollow-sphere sensor, *Sens Actuators B* 135(2):610–617, 2009.

Zhi H, Gao J, Feng L: Hydrogel-based gas sensors for NO2 and NH3, *ACS Sens* 5(3): 772–780, 2020.

This page intentionally left blank

CHAPTER SEVEN

Additive manufacturing of biomaterials

Miranda Torre[a], Sara M. Giannitelli[a], Emanuele Mauri[a], Marcella Trombetta[a], and Alberto Rainer[a,b,*]

[a]Department of Engineering, Università Campus Bio-Medico di Roma, Rome, Italy
[b]Institute of Nanotechnology (NANOTEC), National Research Council, Lecce, Italy
*Corresponding author: e-mail address: a.rainer@unicampus.it

Contents

1. Introduction 234
2. Tissue engineering 234
3. Drug delivery 235
4. 3D printing 236
   4.1 3D printable materials for TE scaffolds and DDSs 237
   4.2 3D printing technologies 243
5. Biomedical applications 247
   5.1 3D-printed scaffolds 248
   5.2 3D-printed DDS 252
6. Conclusions 254
References 255

Abstract

Additive Manufacturing (AM) encompasses a wide set of technologies characterized by freeform design, low production times and waste minimization. The possibility to manufacture personalized devices offered by AM is a promising feature in the clinical scenario, where the donor shortage for organ transplantation and the lack of fully effective systems for drug administration still represent a major issue.

The present work focuses on the processability of different biomaterials, from metals to hydrogels, via AM methodologies and on the basic principles of the most relevant techniques, including laser-based and extrusion-based fabrication processes. Current biomedical applications of these technologies, especially in the field of Tissue Engineering and Drug Delivery, will also be reviewed.

Advances in Chemical Engineering, Volume 57
ISSN 0065-2377
https://doi.org/10.1016/bs.ache.2021.03.003

1. Introduction

According to ASTM standards (ASTM F2792), Additive Manufacturing (AM) can be defined as "the process of joining materials to make objects from 3D model data, usually layer upon layer, as opposed to subtractive manufacturing methodologies". Subtractive processes, in fact, aim to remove material from a three-dimensional solid block leaving the desired shape, whereas additive processes build the final piece by the addition of material layers starting from a 3D computer model. The 3D model is then sliced into bidimensional (2D) layers which are transferred to the AM apparatus for the fabrication of the final object with an automated process (Giannitelli et al., 2015). Remarkable advances introduced by AM are represented by the design and development of complex-shaped products with a considerable reduction in manufacturing time and cost. This crucial aspect contributed to an optimization of the product development cycle in several settings (Srivatsan and Sudarshan, 2015).

Latest advancements in material synthesis and printing technologies brought to the development of multi-dimensional printing processes, enabling the fabrication of 3D objects with more sophisticated designs.

In the field of biomedicine, all of these advances introduced by AM have significantly improved the ability to produce three-dimensional objects with controlled structural and architectural properties in two major areas of applications, i.e., Tissue Engineering and Drug Delivery. The benefits imparted from a layer-by-layer fabrication, including the possibility to create multi-material and customizable devices, are extremely attractive in these fields.

The purpose of this work is to highlight the processability of biomaterials by means of Additive Manufacturing techniques for the fabrication of tissue engineering scaffolds and drug delivery systems.

2. Tissue engineering

Tissue Engineering (TE) is an interdisciplinary field that aims to develop biological substitutes able to restore, maintain or improve functions of healthy and unhealthy tissues by the application of principles and methods of both engineering and biological sciences (Langer and Vacanti, 1993).

TE approach is based on the fabrication of three-dimensional matrices, called scaffolds, used to host cells, providing mechanical support and biochemical cues for tissue formation (Mozetic et al., 2017). To enhance tissue growth, cells are supplied with growth factors, drugs, and nutrients and are

often cultured with the aid of dynamic systems such as bioreactors. The scaffold architecture is engineered to closely mimic the physiological tissue microenvironment, enabling the natural secretion of extracellular matrix components, as an evidence of a positive cellular grafting and response. Over the years, a multitude of biomaterials and designs have been investigated to find the optimal combination for a successful repair or regeneration of the target tissue. To achieve this goal, scaffolds must meet specific requirements, which include biocompatibility, suitable porosity, and biodegradability. Other important features concern specific mechanical properties for optimal short-term response of the scaffold without affecting the physiological functioning of tissues in the long-term. Generally, conventional fabrication techniques such as emulsion freeze-drying, electrospinning, solvent casting and particulate leaching, do not achieve a strict control on the internal scaffold microarchitecture or the obtainment of complex structures. In this regard, AM represents one of the most promising techniques, allowing the fabrication of 3D structures with customizable shape and tight control over the internal architecture. Free-shape design and controlled positioning of different biomaterials and multiple cell types are just an example of the attractive features of AM for scaffold fabrication. As an AM technique, 3D bioprinting represents an alternative to the classical tissue engineering strategies involving biodegradable scaffolds, onto which cells are seeded in a post-fabrication step. Bioprinting is based on the encapsulation of cells within a solution of hydrogel precursor (bioink) to be processed by means of an AM apparatus, resulting in a one-step process strategy to fabricate cell-laden constructs.

3. Drug delivery

Drug delivery encompasses any strategy intended to transport a pharmaceutical compound into the body. It is well known that the route and method of drug administration dramatically affect the kinetics of biodistribution and elimination and, consequently, the effectiveness of the therapy (Mauri et al., 2017; Webster, 2001). The concept of drug delivery has significantly evolved over the years from traditional immediate-release methods like oral ingestion or intravenous injection to targeted-release drug delivery strategies (Goole and Amighi, 2016). Since conventional methods can result in concentration peaks, the necessity to maintain the drug release at physiologically relevant concentrations for extended periods of time has emerged as a crucial aspect in the field, both to improve product efficacy and

to guarantee safety aspects for the patients. To avoid overdosing and to provide a controlled and sustained release of drugs by the modulation of their absorption and metabolization, many engineered drug delivery systems (DDSs) have been developed.

DDSs are based on the entrapment of a certain amount of therapeutic agent in carriers, e.g., polymeric matrices, nanoparticles, liposomes and micelles, to target a specific area within the body. The advantages introduced by these strategies, including the reduction of side effects and the maintenance of concentration values within the therapeutic ranges, have been extensively demonstrated (Kopeček, 2013; Sheikhpour et al., 2017).

Albeit conventional fabrication methods for DDSs (e.g., tableting, spray-drying, granulation and coating) are still the most widely adopted (Sastry et al., 2000), a growing interest in AM processes for pharmaceuticals has been witnessed, due to a compelling need for customized DDSs. So far, AM technologies have not yet found wide application, but they can enable the design of multiple-release dosage forms and the production of DDSs that are highly complex in microarchitecture and shape. Other benefits of AM are the ability to control the spatial distribution of the active pharmaceutical compound, the reduction of waste, and the possibility to prepare individualized forms by varying the dose strength (Prasad and Smyth, 2016).

4. 3D printing

According to ASTM standard terminology, 3D printing is a term often used synonymously with Additive Manufacturing; in particular associated with machines that are low end in price and/or overall capability (ASTM F2792). Nowadays, although many efforts have been made to clarify the terminology, the meaning of this term remains often ambiguous. In many papers (Chia and Wu, 2015; Moroni et al., 2018; Van Kampen et al., 2019), 3D printing is referred to a specific AM technology that makes use of powder particles and a binding material to produce the final piece (otherwise called powder bed printing); conversely, many others still identify this term with an assorted class of rapid prototyping techniques (Do et al., 2015; Donderwinkel et al., 2017).

It has been evidenced that the term 3D printing encompasses most of the total use in the recent literature when referring to a rapid prototyping technology (Chepelev et al., 2017).

In this work, the term will be related to any layer-by-layer fabrication process for the fabrication of three-dimensional objects from 3D model data.

Since the emphasis will be placed on biomedical applications of the latest AM technologies, a thorough evaluation of the specific AM variants goes beyond the final scope of the present paper.

4.1 3D printable materials for TE scaffolds and DDSs

In this section, an overview of the most important materials processed by means of AM technologies in the biomedical field will be provided (Table 1).

In the field of TE, research points at investigating the most suitable materials, both natural and synthetic, which could guarantee biocompatibility and optimal mechanical properties for the scaffold. The advantages of natural materials are due to their similarity to human extracellular matrix and their inherent biocompatibility. Conversely, the main advantage of synthetic materials is that they can be tailored with specific physical properties and that they are often endowed with controllable chemistry and defined mechanical properties. Despite that, synthetic materials often show poor biocompatibility, toxic degradation products and loss of mechanical properties during degradation (Gunatillake et al., 2003).

In the field of DDSs, the majority of 3D-printed systems to date is composed of polymeric materials designed to maximize the stabilization of drugs within the matrices and to control the degradation kinetics within the human body (Trenfield et al., 2019).

Materials for AM processes can be firstly classified into inorganic materials (metals, ceramics) and organic ones (thermoplastic polymers, hydrogels).

4.1.1 Inorganic materials

Metals commonly used to design AM scaffolds include stainless steel and titanium alloys such as nitinol or Ti6Al4V (Pei et al., 2017; Singh et al., 2020). Although these materials present desirable features such as high mechanical properties and stability and their use has been extensively validated for in vivo applications, they also present some limitations. Toxicity of metal ions and corrosion aspects are some of the drawbacks concerning the use of these metals in tissue engineering. Indeed, implantation of metal scaffolds can often result in the formation of a fibrotic capsule around the construct itself, thus inducing rejection responses from the organism.

Biodegradability issues have been overcome for those materials defined as "biodegradable metals" (BMs), i.e., metals expected to corrode gradually in vivo, with an appropriate host response elicited by the released corrosion products, and then dissolve completely (Zheng et al., 2014). Examples of

Table 1 Processability of biomaterials by means of additive manufacturing technologies.

		Technologies							
		Laser-dependent					Extrusion-based		
Biomaterials		**SLS/SLM**	**SLA**	**DLP**	**2PP**	**LIFT**	**FDM**	**DIW**	**FRESH**
Organic	PLA	Tan et al. (2005)					Arany et al. (2019), Gregor et al. (2017)		
	PCL	Bracci et al. (2013), Tsai et al. (2017)	Skoog et al. (2014)				Beck et al. (2017), Dong et al. (2017), Shor et al. (2017)		
	Gelatin					Riester et al. (2016)		Kolesky et al. (2016), Sears et al. (2015), Skardal et al. (2017)	Hinton et al. (2015)
	Collagen					Koch et al. (2012, 2018), Michael et al. (2013)		Sears et al. (2015)	Hinton et al. (2015), Lee et al. (2019)
	Hyaluronic acid					Koch et al. (2018), Sorkio et al. (2018)		Sears et al. (2015), Skardal et al. (2017)	

Agarose							Fan et al. (2016), Nadernezhad et al. (2016)	
Cellulose derivatives						Dumpa et al. (2020), Giri et al. (2020)	Contessi Negrini et al. (2018), Hodder et al. (2019), Li et al. (2017a), Rastin et al. (2020)	
Pluronic							Gioffredi et al. (2016), Gori et al. (2020)	
P(PF-co-EG)	Dean et al. (2012)	Dean et al. (2012)						
PLGA-PEG-PLGA							Serris et al. (2020)	
Polyvinylpyrrolidone							Khaled et al. (2018)	
Chitosan							Andriotis et al. (2020)	
Alginate				Mezel et al. (2010)			Gori et al. (2020), Hodder et al. (2019)	Hinton et al. (2015)
GelMA	Cui et al. (2020)		Ovsianikov et al. (2010, 2011)				Bertassoni et al. (2014), Rastin et al. (2020)	

Continued

Table 1 Processability of biomaterials by means of additive manufacturing technologies.—cont'd

Biomaterials		Technologies							
		Laser-dependent					Extrusion-based		
		SLS/SLM	SLA	DLP	2PP	LIFT	FDM	DIW	FRESH
	PEGDA		Goyanes et al. (2016)	Lu et al. (2006)	Kufelt et al. (2014), Xiao et al. (2013)			Skardal et al. (2017)	
	Fibrin/Fibrinogen					Gruene et al. (2011), Koch et al. (2018)		Kolesky et al. (2016), Skardal et al. (2017)	Hinton et al. (2015)
Inorganic	Titanium	Hsu and Ellington (2015), Singh et al. (2020), Pei et al. (2017)							
	Stainless steel	Singh et al. (2020)							
	BMs	Li et al. (2018)							
	Bioinert ceramics			Zhang et al. (2019)					
	Hydroxyapatite	Wiria et al. (2008)	Cui et al. (2020)	Zhang et al. (2019)			Shor et al. (2017)		
	Bioactive glasses			Xu et al. (2020)			Murphy et al. (2017)		

BMs are magnesium-based, iron-based, zinc-based and calcium-based alloys. Several studies have exploited BMs for 3D printed scaffolds (Chou et al., 2013; Zhuang et al., 2008); however, their potential use for implantable constructs is currently uncertain due to a limited set of data on their impact on cell viability and their biocompatibility in vivo (Tan and Tan, 2018).

Ceramic materials are often employed in orthopedic applications, because of their similarity to the mineral phase of natural bone. Porosity and high compressive strength of ceramics represent ideal features for substrates for bone tissue ingrowth. Bioinert ceramic scaffolds composed of alumina and/or zirconia displayed improved mechanical properties (tensile and compressive strength), interconnected microarchitectures, but no bioactivity. On the other hand, bioactive ceramic constructs composed of hydroxyapatite/tricalcium phosphate or calcium silicate showed superior biocompatibility (since the bone matrix itself is mainly composed of hydroxyapatite), improved cell adhesion, but low compressive strength (Du et al., 2018).

Bioactive glasses and glass-ceramics represent an intriguing class of materials featuring improved osteoconduction and osteostimulation, matched to adequate compressive strength and a high degree of biocompatibility (Hench, 2013; Wen et al., 2017).

4.1.2 Organic materials

Polymers, either synthetic or naturally derived, represent the predominant class of organic materials used for TE and DDS applications. Thermoplastic polymers can easily be processed via several AM technologies to produce 3D constructs with high porosity and surface area. Bioresorbable aliphatic polyesters such as polyglycolic acid (PGA), poly-lactic acid (PLA) and polycaprolactone (PCL) are typical examples of such polymers (Lam et al., 2009). Their use for biomedical purposes has been extensively validated, thanks to their inherent biodegradability and biocompatibility, along with minimum inflammatory response by biological tissues. Additionally, their mechanical properties are fully suitable for load-bearing applications, such as 3D constructs for orthopedic implants.

Hydrogels are appealing materials to be processed by means of 3D bioprinting technologies, since they retain large amounts of water within their structure, and this makes them a compelling environment for living cells. This feature arises from hydrophilic functional groups attached to the polymeric backbone. Besides, the presence of crosslinks among the network chains confers a strong resistance to dissolution. A major drawback of hydrogels is represented by their low mechanical strength which reduces their

application for load-bearing applications. According to the nature of the crosslinks, hydrogels are termed 'physical' when the connection is weak and reversible, or 'chemical' when the connection is established via strong covalent bonds and therefore irreversible. Physical strategies to induce reticulation of hydrogel chains include changes in temperature, pH, and ionic environment, whereas chemical induction is based on photopolymerization, enzymatic reactions, or the use of crosslinking agents.

The gelation process of many natural thermosensitive polymers generally occurs when the temperature is lowered: gelatin, collagen and agarose form gels at low temperatures whereas at high temperatures they adopt a random coil conformation in solution. Conversely, some other naturally derived hydrogels show inverse thermosensitive behavior: they are liquid below room temperature and gel at the so-called lower critical solution temperature (LCST) which is commonly higher. Methylcellulose and hydroxypropyl methylcellulose (HPMC) are classical examples of such polymers. Synthetic hydrogels able to thermally change their structure include, for example, poly(*N*-isopropylacrylamide) (pNIPAM), Pluronic, poly(propylene fumarate-*co*-ethylene glycol) and PLGA-PEG-PLGA copolymers (Leroux and Ruelgarie, 2004).

Chitosan, derived from the partial deacetylation of chitin, is one of the most investigated pH-dependent cationic polymers. Chitosan can dissolve in aqueous solvents at low pH (below 6.2) because of the protonation of its amino groups: basification of chitosan solutions above that pH level results in an immediate gelification of the polymeric chains.

A typical example of a hydrogel which crosslinks via ionic bonds is alginate, one of the most investigated materials in tissue engineering. Alginate gels are formed when divalent cations such as Ca^{2+}, Ba^{2+} or Sr^{2+} cooperatively interact with blocks of G monomers (α-L-guluronic acid) to form ionic bridges between different polymer chains. Mechanical properties and pore size of the ionically crosslinked gels can be easily handled by tuning the M (β-D-mannuronic acid) to G ratio of the polymer chain (Drury and Mooney, 2003).

Gelatin methacrylate (GelMA) is denatured collagen functionalized with photopolymerizable methacrylate (MA) groups, which enable the material to be covalently crosslinked by UV light. GelMA is widely investigated in the field of bioprinting, due to its abundancy, biocompatibility and easy-to-tune features, e.g., degree of methacrylation, rheological properties, mechanical behavior (Pepelanova et al., 2018).

Acrylation and methacrylation reactions are also applied to the functionalization of other hydrogel materials such as hyaluronic acid, carboxymethyl cellulose, poly(ethylene glycol) (PEG) in order to achieve a stable chemical crosslinking.

Finally, fibrin is an interesting case of enzyme-catalyzed crosslinked hydrogel, inspired by the natural polymerization process following vascular injury (Schneider-Barthold et al., 2016). In the coagulation cascade, thrombin cleaves two small amino acid sequences in the chain of the fibrin precursor, fibrinogen. As a consequence, polymerization sites within the molecule are exposed, leading to the formation of a 3D fibrin network. Further stabilization of this network is achieved by covalent crosslinking catalyzed by factor XIIIa (a transglutaminase). Fibrin-based hydrogels are widely applied in the clinics, nonetheless they often display mechanical instability and rapid degradation.

4.2 3D printing technologies

In this section, an overview of the most common AM technologies in the fields of interest is provided. Examples of these technologies are Selective Laser Sintering (SLS) or Melting (SLM), Stereolithography (SLA), and extrusion-based printing techniques such as Fused Deposition Modeling (FDM) and Direct Ink Writing (DIW), including the newest technologies of multi-material printing and Embedded 3D Printing (Fig. 1). All of these techniques have been extensively used for the manufacture of drug-eluting systems and tissue engineering scaffolds with geometrically intricate designs and a high level of structural complexity.

4.2.1 Laser-dependent technologies

Selective Laser Sintering (SLS) and Stereolithography (SLA) are techniques that use a light source as the manufacturing method to produce the final object (Lee et al., 2017).

SLS uses an infrared laser radiation to generate local heat onto a powder bed just beyond its melting point (to minimize the request of energy). The laser beam traces the shape of the first layer of the model to be built, fusing powder particles together by sintering. Once each layer is solidified, the z-axis of the AM apparatus moves and a new layer of powder is supplied using a mechanical roller. The powder that remains unaffected by the laser acts as a passive physical support for the model and remains in place until the model is complete (Almeida and Correia, 2016). Materials processed by SLS

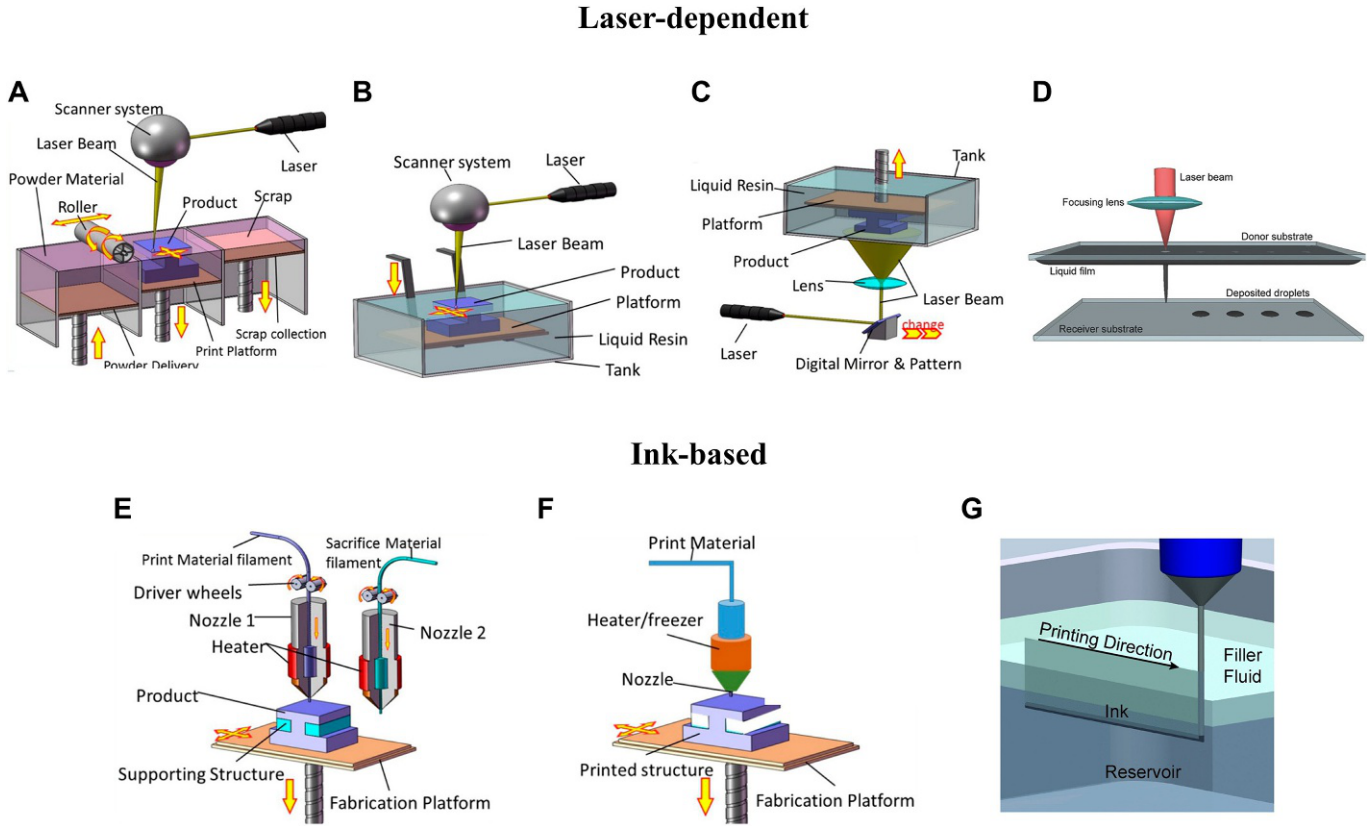

Fig. 1 Main AM technologies. Laser-dependent processes: (A) Selective Laser Sintering (SLS); (B) Stereolithography (SLA); (C) Digital Light Processing (DLP); (D) Laser-induced forward transfer (LIFT) and ink-based techniques: (E) Fused deposition modeling (FDM); (F) Direct Ink Writing (DIW); (G) Freeform reversible embedding (FRE). *Panels (A–C) and (E–F) Are adapted with permission from Xu Y, Wu X, Guo X, et al.: The boom in 3D-printed sensor technology, Sensors 17:1166, 2017, Panel (D) is adapted from Serra P, Piqué A: Laser-induced forward transfer: fundamentals and applications, Adv Mater Technol 4:1800099, 2019, Panel (G) is adapted from Muth JT, Vogt DM, Truby RL, et al.: Embedded 3D printing of strain sensors within highly stretchable elastomers, Adv Mater 26:6307–6312, 2014.*

can be either metals or polymers with 10–100 μm particle size (Kruth et al., 2003). The resolution achievable with this technique is slightly larger than the average particle size, meaning that the minimum pattern dimension is about 100 μm.

In the SLA process, the powder bed is replaced by a photosensitive resin bath. The liquid resin is hit by the light source, solidifying in the desired pattern. Once one layer is crosslinked by the local illumination, a new layer of resin is introduced, until the final construct is manufactured (Melchels et al., 2010). SLA machines can be distinguished depending on the solution adopted to transfer the desired pattern onto the resin. Projection-based systems use a digital micro-mirror device (DMD) to project the pattern, while vector-based systems perform a raster-scan of a micro-focused laser beam.

Two-photon polymerization (2PP) has the same working principle of SLA, but the light source is a micro-focused pulsed laser. In a 2-photon absorption transition, an atom or molecule is taken to an excited state by simultaneously absorbing two photons in a single quantum event. Due to the high non-linearity of the phenomenon, polymerization reaction takes place in a tiny focal volume.

Another attractive laser-assisted technique is Laser-Induced Forward Transfer (LIFT), which allows the formation of micropatterns of both solid and liquid materials.

In the case of solid materials, a donor substrate, consisting of a glass slide (transparent to the laser beam) precoated with the target material, is placed parallel to the acceptor substrate, where the pattern is going to be deposited, at a close distance to it. When the fast-pulse laser beam is focused on the target material, a small amount of it is transferred from the donor to the acceptor substrate. More in detail, the laser pulse is absorbed at the film-donor substrate interface, resulting in a local heating and in the generation of a melt front that propagates though the film until it reaches the free surface. When the material in the interface attains its boiling point, a vapor bubble is formed and the molten material is propelled toward the acceptor substrate (Serra and Piqué, 2019).

For the deposition of liquid inks (including, e.g., cell suspensions) needs to be deposited, the slide must be pre-coated with a laser-absorbing layer. In this case, the effect of the laser pulse results in the direct vaporization of a small fraction of the ink and, therefore, in the formation of a high-pressure vapor bubble that expands, transferring the ink to the acceptor substrate in a submicron droplet (Mota et al., 2020).

4.2.2 Extrusion-based technologies

Laser-based 3D printing technologies are very advantageous from a resolution point of view. However, the set of processable polymeric materials is mainly limited to rigid thermoplastics or photocurable resins.

Conversely, extrusion-based AM are compatible with several soft materials, including thermoplastic elastomers, silicones, hydrogels and so forth. Furthermore, most of these techniques are compatible with the simultaneous deposition of multiple materials, thus enabling the fabrication of functional graded materials that facilitate the transition from soft to rigid components avoiding stress enhancement at the interface of materials compliance mismatch.

In the FDM process, thermoplastic filaments are melted by heating and guided by an extruder to form the final 3D object. The material leaves the extruder in a liquid form and hardens immediately. The previously formed layer, which acts as a substrate for the next layer, must be maintained at a temperature just below the solidification point of the thermoplastic material to assure good interlayer adhesion. FDM is cost effective, user-friendly and it usually does not require post-processing steps (Zein et al., 2002).

Direct Ink Writing (DIW) technique relies on the tuning of the rheological properties of the extruded material to impart the optimal shear thinning behavior, offering the widest spectrum of printable materials that range from hydrogels to thermoset polymers to colloidal suspensions and fugitive organic inks (Lewis, 2006). On the other hand, a post-processing step is often required, since most of the printed inks demand for an additional crosslinking process like thermal curing, photopolymerization, or ionotropic crosslinking.

Multi-material DIW is an evolution of the traditional technique, that can be achieved by means of microfluidic printheads, core-shell devices or multiple switching syringes (Costantini et al., 2017, 2019). Microfluidics-assisted 3D printing enables the deposition of heterogeneous materials in a layer-by-layer fashion by swapping between two or more different inks when desired or by using mixing nozzles which produce a unique filament with combined properties from different materials. A single fiber of a construct fabricated by means of a core-shell device is made up of concentrically layered materials, imparting the whole structure a complexity which is not otherwise achievable.

Multiple syringes apparatus can enable both the simultaneous patterning of different inks or the patterning of different materials layer-by-layer, resulting in a multi-layered construct with vertical or horizontal rigid-to-soft gradients.

Embedded 3D printing (E3DP) is one of the most recent DIW technologies. This manufacturing approach pursues the direct patterning of inks within a soft polymeric matrix, which serves as a support, along predefined omnidirectional paths (Grosskopf et al., 2018). Both the ink and the matrix materials must have specific rheological features. As in every DIW technique, the ink must have a shear-thinning behavior with high yield stress. The same characteristics must be met by the matrix material, but the storage modulus and the yield stress values shall be an order of magnitude lower than those of the ink, to allow the needle to move freely throughout the bath, yet holding the printed structure in place. Thixotropic materials or solid-liquid suspensions (slurries) are suitable materials for the supporting bath.

A variant of the same technique, named FRE (Freeform Reversible Embedding) has been developed to demonstrate the possibility to print hydrophobic polymers with low viscosity and long cure times within a hydrophilic support bath (Hinton et al., 2016).

E3DP has been implemented in Tissue Engineering applications by Feinberg's group (Hinton et al., 2015; Lee et al., 2019), resulting in a newly emerged technique named FRESH (Freeform Reversible Embedding of Suspended Hydrogels), which is an improvement of the traditional printing in coagulation baths. In the printing process, the biocompatible polymeric matrix behaves as a Bingham fluid, opposing low mechanical resistance to the needle movements which impart high shear stresses to the matrix itself. Once the bioink is deposited within the bath, it is held in place thanks to the rigid-body behavior of the matrix at low shear stresses. At the end of the process, the matrix is allowed to melt (e.g., with higher cell-friendly temperatures) in a non-destructive manner and the final 3D structure is released.

5. Biomedical applications

Additive manufacturing represents an enabling technology for the fabrication of patient-specific implants (Haleem et al., 2020), the controlled delivery of therapeutics and the development in vitro models for drug screening and precision medicine (Mandrycky et al., 2016; Prendergast and Burdick, 2020). Printed constructs may be utilized directly following fabrication, or may undergo post-processing under static or dynamic culture conditions. While static culture methods involve standard culture procedures, dynamic culture systems imply external stimulation such as flow of media/nutrients through constructs, application of mechanical or electrical stimuli.

Advancements in microengineering and microfluidic technologies have contributed to the evolution of 3D printing with significant improvements in terms of heterogeneity of printed constructs, resolution, printing time, and automation of the printing process. For example, the application of microfluidics in the engineering of advanced extruders has enabled greater object heterogeneity, enhancing the speed of multi-material deposition via improved switching among different inks (Hardin et al., 2015; Zhang and Khademhosseini, 2017). These advancements may not only improve personalized 3D scaffolds for tissue engineering and regenerative medicine, but also offer better in vitro models of physiological systems, potentially helping to get new insights into tissue morphogenesis, pathogenesis, and drug-induced structural and functional remodeling.

5.1 3D-printed scaffolds

In the recent years, several healthy and diseased 3D tissue models have been developed by 3D printing, such as hepatic (Gori et al., 2020), kidney (Homan et al., 2016) and cardiac tissue 3D models (Zhang et al., 2016). Tumor models have been also engineered to investigate the efficacy of anti-cancer drugs targeting the progression of cancer cell proliferation and metastasis (King et al., 2014; Zhu et al., 2016). Although spheroids have for long represented the gold standard in this field, they do not fully recapitulate the heterogeneity of tumor microenvironments overlooking the effect of associated vasculature and neural network. In this sense, the use of bioprinting has introduced the possibility to print multiple cell types and growth factors/signaling molecules and to include vascularization into tumor models (Huang et al., 2014). As an example, cell bioprinting was successfully used to obtain an ovarian tumor model featuring a multicellular acini structure, through the dispensing of human ovarian cancer cells and human fibroblasts on a Matrigel substrate (Xu et al., 2011). Microextrusion of multiple cell types has also been performed to obtain multilayered pancreatic tumor (Sears et al., 2015) and breast cancer microenvironment (King et al., 2014). In addition to such studies, a tri-culture metastatic model has been recently developed using a stereolithography 3D printing technique for investigating the invasion of breast cancer cells into vascularized bone tissue (Cui et al., 2020). This simplified version of the "tumor-vessel-bone" metastatic niche was reproduced by incorporating various biocomponents and photocurable inks into a multifunctional 3D tissue matrix and resulted in a model of breast cancer cell metastasis (Fig. 2A).

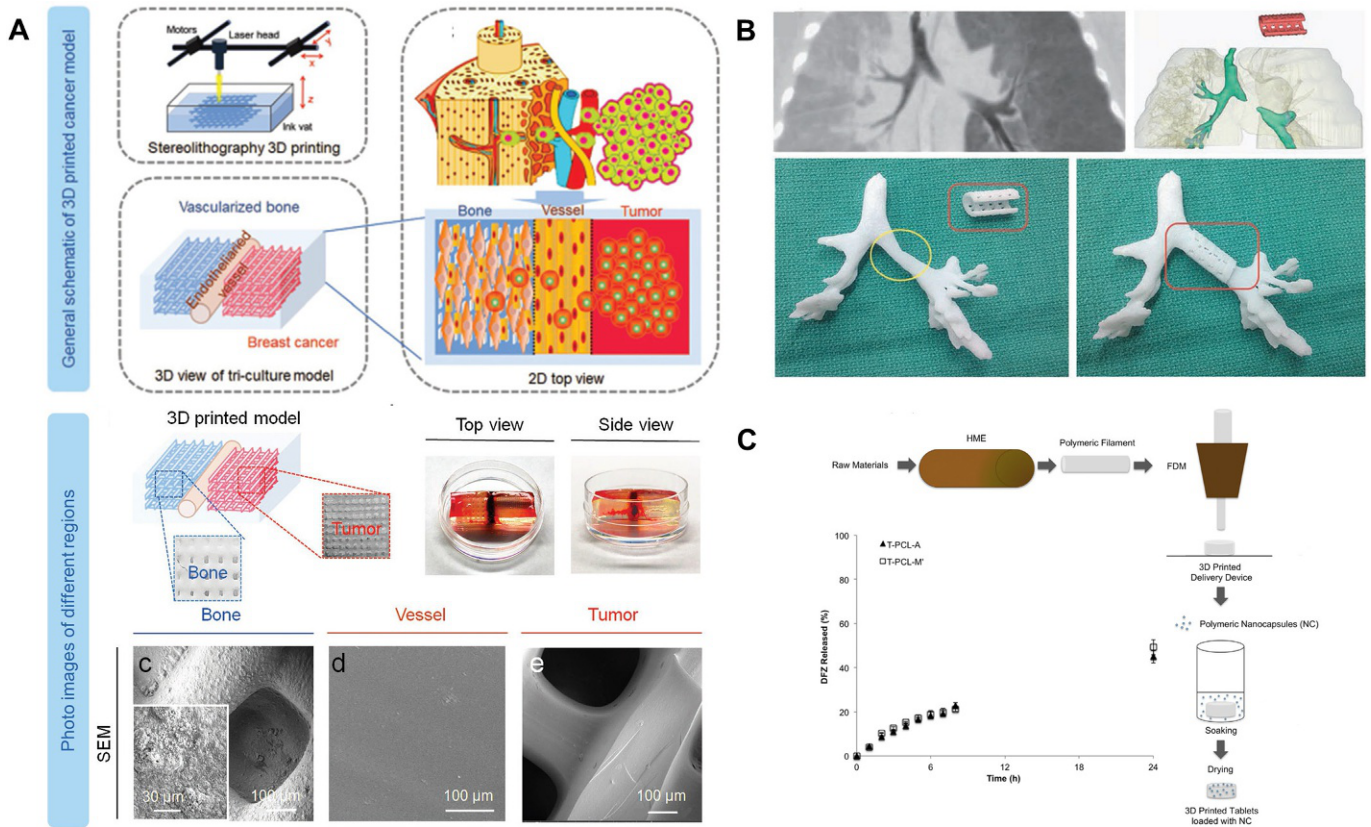

Fig. 2 (A) 3D printing of metastatic breast cancer in vitro model: schematic 3D view and photo/SEM images. (B) Patient-specific bioresorbable airway splint fabricated via SLS. (C) Schematic representation of an Additive Manufacturing process for the fabrication of drug-loaded tablets. *Panel (A) Adapted with permission from Cui H, Esworthy T, Zhou X, et al.: Engineering a novel 3D printed vascularized tissue model for investigating breast cancer metastasis to bone, Adv Healthc Mater 9:1900924, 2020. Panel (B) Adapted with permission Guzzi EA, Tibbitt MW: Additive manufacturing of precision biomaterials, Adv Mater 32:1901994, 2020. Panel (C) Adapted with permission from Beck RCR, Chaves PS, Goyanes A, et al.: 3D printed tablets loaded with polymeric nanocapsules: an innovative approach to produce customized drug delivery systems, Int J Pharm 528: 268–279, 2017.*

The integration of multiple tissue and organ types in multiorgan systems recapitulating human physiology is gaining far more attention for the achievement of truly predictive in vitro models with pathophysiological relevance. Bioprinting strategies can positively contribute to the advancements in this field by providing miniature 3D bioengineered components to be integrated within a single microfluidic device as a simplified model of an organism-on-a-chip for drug screening and toxicity studies. So far, the only available bioprinted body-on-a-chip multisystem integrated liver and cardiac tissue organoids bioprinted with customized tissue-specific bioinks into modular perfusable devices that were connected to a lung organoid at the air-liquid interface. The system was used to assess inter-organ responses to the administration of drugs and toxic agents (Skardal et al., 2017).

Additive manufacturing technologies can be also applied to create clinically viable tissue constructs mimicking the structural and functional integrity of native tissue to be replaced: from simpler architectures such as bone, skin, and cornea, through more organized tissues such as skeletal muscle, heart, and neural tissues to tissue interfaces such as the osteochondral segment and finally, to complete organs with vessels and functional internal structures. For example, conventional AM techniques have been used to produce patient-specific titanium truss cages for the repair of distal tibial disunion (Hsu and Ellington, 2015). PCL or PCL/tricalcium phosphate composites have been assembled via FDM and SLS and used in the clinics for bone restoration in dental and craniofacial applications (Youssef et al., 2017). In addition, patient-specific bioresorbable airway splints have been fabricated using SLS of PCL and clinically implanted for airway restoration (Fig. 2B) (Bracci et al., 2013).

Some of these 3D printed constructs have already been tested in clinical trials for functional tissue reconstruction and cosmetic augmentation (Mehrotra et al., 2019). Moreover, as bioprinting systems become more advanced, the potential for in situ biofabrication directly in the body is pushing in vivo applications closer to translation (Prendergast and Burdick, 2020). Some initial strategies focused on compact, handheld direct-write devices such as the bio-pen, have been successfully used for the treatment of chondral injuries (Di Bella et al., 2018; Duchi et al., 2017) and skin wounds (Hakimi et al., 2018). Other works have focused on modifying bioprinting systems commonly used in laboratory practices for clinical use such as the mobile skin bioprinting system developed for direct in situ treatment of extensive skin wounds (Albanna et al., 2019). Alternatively, other methods of in vivo biofabrication have incorporated versatile robotic arms as

the dispensing head of an inkjet bioprinter for in situ repair of skin defects with PEG diacrylate (PEGDA) hydrogel (Li et al., 2017b).

While much progress has been made with traditional printing systems, there are still many challenges to be solved for the fabrication of functional tissue constructs and in vitro models. The development of functional vasculature is one of the most critical challenges since the majority of bioprinting methods rely on a layer-by-layer approach, which faces great difficulties in the printing of complex hollow structures. A possible solution to address this problem is to incorporate sacrificial biomaterials within the bioink which give mechanical support during the 3D printing process and can be easily removed from the constructs in the post-processing steps, leaving channels or void spaces within the construct. To this aim, carbohydrate glass (Miller et al., 2012) and Pluronic F127 (Kolesky et al., 2014) have been successfully used as sacrificial materials to include perfused vascular network within 3D constructs. By this approach, thick vascularized tissues have been 3D printed using multiple bioinks loaded with mesenchymal stem cells, dermal fibroblasts for extracellular matrices, and vein endothelial cells for vasculature (Kolesky et al., 2016). However, the introduction of extra sacrificial materials resulted in increased complexity of the printing process, which either required rapid material exchanges at the bioprinting platform or the use of multiple nozzles laden with different inks. Furthermore, an ideal sacrificial material must be printable along with the non-sacrificial biomaterials and cellular components under the same conditions, and their dissolution mechanism must be cytocompatible. These conditions severely limit the range of applicable materials.

Another great challenge is the translation of these advances in regenerative medicine to the clinical arena (Jammalamadaka and Tappa, 2018). For this translation to occur, validation protocols and regulatory frameworks for 3D printed products must be standardized. For instance, successful regulatory pathways for 3D printed constructs have been developed by the Food and Drug Administration (FDA) with more than 100 3D printed medical devices cleared through the FDA 510(k) pathway and currently on the market, including patient-matched devices tailored to fit patient's anatomy ("Statement by FDA Commissioner Scott Gottlieb, M.D., on FDA ushering in new era of 3D printing of medical products; provides guidance to manufacturers of medical devices") (FDA, 2017). However, there are currently no FDA-approved or cleared biologic products made by additive manufacturing techniques in the United States (Ricles et al., 2018). Moreover, although some standards on quality control and standardization have been defined by

the International Organization for Standardization (ISO) and by the National Institute for Standards and Technology (NIST), a single set of parameters has yet to be uniformly adopted before AM technologies can effectively change the medical product landscape (Prendergast and Burdick, 2020).

5.2 3D-printed DDS

The design of drug delivery systems via 3D printing technologies relies on the flexibility to combine different components, such as polymers, additives and active molecules, and control their spatial distribution to create ad hoc products for the desired final application, which could range from oral drug delivery, to parenteral administration of the DDS or personalized medicine. Over the last years, researchers have highlighted the benefits of these formulates in terms of dosage form, production of complex geometries, reproducibility of scientific results, use of small amounts of therapeutic molecules compared to the standard administration routes, and reduction of waste (Prasad and Smyth, 2016). Furthermore, the printed structures can be characterized by tunable physico-chemical properties, such as permeability to specific solvents, porosity, hydrophilicity/lipophilicity balance, and grafting of chemical or biological functionalities, to address the controlled drug delivery criteria. One of the first examples of an industrial product obtained through the modulation of these parameters is Spritam®, a FDA-approved tablet of levetiracetam characterized by a high degree of degradation suitable to design a treatment of the epilepsy in children (Jamróz et al., 2017; Pravin and Sudhir, 2018).

Among the main configurations of great interest in the pharmaceutic field, 3D printed tablets have a prominent role. For example, in the last years, the group of Clive Roberts (Khaled et al., 2018) has manufactured tablets encapsulating paracetamol for oral delivery: they formulated a paste composed by the drug, excipients (polyvinylpyrrolidone and croscarmellose sodium) and water, and used a 3D extrusion-printing process to produce the DDS. In detail, they filled a syringe with the paste, and, at fixed printing parameters, the latter was extruded layer by layer until reaching the desired tablet dimension. This strategy ensured the optimization of the tablet density, geometry and porosity, and resulted in a high drug loading (80% w/w) reducing the loss of active principle detected in commercial formulates. In vitro studies demonstrated that about 90% of the paracetamol was released within the first 10 min promoting a rapid therapeutic effect in the biological compartments, and this trend was achieved thanks to the degradation kinetic

of the croscarmellose excipient, which absorbed water and swelled leading to the disintegration of the tablet. This 3D printing approach has defined new opportunities for the pharmaceutical industry due to the simple protocol used in the DDS design and the opportunity to avoid critical process conditions, such as high temperatures during the fabrication and the UV irradiation, commonly used in FDM and UV-curing based ink-jet methods (Okwuosa et al., 2016).

Moreover, Serris et al. (2020) have applied the same extrusion strategy to develop a PLGA-based hydrogel film for controlled drug delivery in brain cancer, with the challenge of delivering drugs using a smart release formulation to overcome the short half-life of the drug. They investigated three different configurations: single-layered, tri-layered, and core-in-shell films and tested their suitability using three drugs (paclitaxel, rapamycin, and lidocaine). In particular, the polymer film carrying paclitaxel and rapamycin were obtained using high-molecular-weight PLGA (H-PLGA), whereas the system delivering lidocaine was prepared using low-molecular-weight PLGA (L-PLGA). The multi-layered and the core-shell configurations were prepared by interchanging the two polymer mixtures. Exploiting the physical interactions between the drug and the polymer chains, and the different degradation rates of H-PLGA and L-PLGA via ester hydrolysis in aqueous environment, it was possible to tune the mechanism of drug release, ensuring a sustained profile over several days. The resulting 3D-printed films appeared as leading candidates for the local delivery of drugs in the brain to alleviate pain after peritoneal surgery.

FDM technology represents another alternative to customize the composition and properties of drug-eluting devices. As discussed in the literature (Goole and Amighi, 2016; Goyanes et al., 2016), this method is characterized by low cost, absence of organic solvents, feasibility of blending drugs with polymeric materials in a prior hot-melt extrusion step, design of multidrug systems and the opportunity to tune the release profiles of the active molecules through the shape and density of the printed system. Moreover, FDM can be integrated with other processes to produce innovative solid dosage forms: for example, Beck et al. (2017) have proposed the combination of the 3D printing with nanotechnologies (Fig. 2C). They soaked PCL filaments in drug-loaded nanocapsules to produce 3D printed tablets as a DDS; in particular, the FDM approach ensured the design of different tablet configurations, characterized by variation in porosity, density and specific surface area, resulting in the optimization of drug loading and drug release profiles. The originality of this work resides in the possibility

to convert nanomaterial suspensions into solid dosage forms to produce a novel device aimed at the personalized nanomedicine. Other polymers, such as PLA, cellulose derivatives, chitosan and cyclodextrins, are commonly used to create drug-loaded filaments to fabricate 3D tablets for gastrointestinal, wound and antimicrobial applications (Andriotis et al., 2020; Arany et al., 2019; Dumpa et al., 2020; Giri et al., 2020).

Instead, SLA was used by Goyanes et al. (2016) to obtain an anti-acne patch encapsulating salicylic acid. The fabrication process involved the use of a solution containing PEG and PEGDA photopolymerized by a photoinitiator after the addition of the anti-acne agent. The DDS showed higher resolution than specimens obtained through FDM technology.

Finally, DIW method can be used to produce aerogel structures with controlled 3D structures and inner pore architecture: Chi-Fung Li and co-workers produced cellulose nanocrystal aerogels and characterized their physico-chemical properties, highlighting the biocompatibility and biodegradability of the final system for different potential applications (Li et al., 2017a).

Thanks to the versatility, replicability and accuracy of the above-mentioned configurations, 3D-printed DDSs can be combined with mathematical modeling to predict both the drug release profiles and the effects on release kinetics due to changes in printing parameters. As a result, 3D printing techniques support the definition of an interdisciplinary approach in drug delivery scenario thanks to the opportunity to rationally combine the advantages of different strategies in a unique system, suitable to be innovative and pioneering in healthcare applications which still ask a successful therapy.

6. Conclusions

As extensively discussed, Additive Manufacturing offers several advantages in the field of biomedicine. A wide range of biomaterials with distinct features can be processed for the fabrication of 3D structures, including bioresorbable polymers, hydrogels, metal alloys and bioceramics. With the use of these materials and coupling complex designs with modern and highly developed techniques, a huge number of advanced in vitro models and drug delivery systems have been proposed over the last few years. Nonetheless, almost none of these systems has reached the clinical scenario, and still many issues remain unsolved and need to be overcome, especially for what concerns safety, efficacy and regulatory hurdles. The risk of rejection for

implantable devices, the speed of fabrication are typical examples, and economic aspects must also be considered. Despite that, AM technologies and related research in materials science are in continuous evolution, aspiring to the development of fully functional and vascularized organs and to establishment of regulatory-approved drug delivery systems.

References

Albanna M, Binder KW, Murphy SV, et al.: In situ bioprinting of autologous skin cells accelerates wound healing of extensive excisional full-thickness wounds, *Sci Rep* 9:1856, 2019.

Almeida HA, Correia MS: Sustainable impact evaluation of support structures in the production of extrusion-based parts, In *Environ footprints eco-design prod process*, 2016, Springer, pp 7–30.

Andriotis EG, Eleftheriadis GK, Karavasili C, et al.: Development of bio-active patches based on pectin for the treatment of ulcers and wounds using 3D-bioprinting technology, *Pharmaceutics* 12:56, 2020.

Arany P, Róka E, Mollet L, et al.: Fused deposition modeling 3D printing: test platforms for evaluating post-fabrication chemical modifications and in-vitro biological properties, *Pharmaceutics* 11:277, 2019.

Beck RCR, Chaves PS, Goyanes A, et al.: 3D printed tablets loaded with polymeric nanocapsules: an innovative approach to produce customized drug delivery systems, *Int J Pharm* 528:268–279, 2017.

Bertassoni LE, Cardoso JC, Manoharan V, et al.: Direct-write bioprinting of cell-laden methacrylated gelatin hydrogels, *Biofabrication* 6, 2014, 024105.

Bracci R, Maccaroni E, et al.: Bioresorbable airway splint created with a three-dimensional printer, *N Engl J Med* 368:2043–2045, 2013.

Chepelev L, Giannopoulos A, Tang A, et al.: Medical 3D printing: methods to standardize terminology and report trends, *3D Print Med* 3:1–9, 2017.

Chia HN, Wu BM: Recent advances in 3D printing of biomaterials, *J Biol Eng* 9:1–14, 2015.

Chou D, Wells D, Hong D, et al.: Novel processing of iron—manganese alloy-based biomaterials by inkjet 3-D printing, *Acta Biomater* 9:8593–8603, 2013.

Contessi Negrini N, Bonetti L, Contili L, et al.: 3D printing of methylcellulose-based hydrogels, *Bioprinting* 10:1–10, 2018.

Costantini M, Colosi C, Święszkowski W, et al.: Co-axial wet-spinning in 3D bioprinting: state of the art and future perspective of microfluidic integration, *Biofabrication* 11, 2019. 012001.

Costantini M, Testa S, Fornetti E, et al.: Engineering muscle networks in 3d gelatin methacryloyl hydrogels: influence of mechanical stiffness and geometrical confinement, *Front Bioeng Biotechnol* 5:1–8, 2017.

Cui H, Esworthy T, Zhou X, et al.: Engineering a novel 3D printed vascularized tissue model for investigating breast cancer metastasis to bone, *Adv Healthc Mater* 9:1900924, 2020.

Dean D, Wallace J, Siblani A, et al.: The calibration of continuous Digital Light Processing (cDLP) for the highly accurate additive manufacturing of tissue engineered bone scaffolds, *Innov Dev Virtual Phys Prototyp - Proc 5th Int Conf Adv Res Rapid Prototyp* 7:57–66, 2012.

Di Bella C, Duchi S, O'Connell CD, et al.: *In situ* handheld three-dimensional bioprinting for cartilage regeneration, *J Tissue Eng Regen Med* 12:611–621, 2018.

Do A, Khorsand B, Geary SM, et al.: 3D printing of scaffolds for tissue regeneration applications, *Adv Healthc Mater* 4:1742–1762, 2015.

Donderwinkel I, Van Hest JCM, Cameron NR: Bio-inks for 3D bioprinting: recent advances and future prospects, *Polym Chem* 8:4451–4471, 2017.
Dong L, Wang SJ, Zhao XR, et al.: 3D-printed poly (ϵ-caprolactone) scaffold integrated with cell-laden chitosan hydrogels for bone tissue engineering, *Sci Rep* 7:4–12, 2017.
Drury JL, Mooney DJ: Hydrogels for tissue engineering: scaffold design variables and applications, *Biomaterials* 24:4337–4351, 2003.
Du X, Fu S, Zhu Y: 3D printing of ceramic-based scaffolds for bone tissue engineering: an overview, *J Mater Chem B* 6:4397–4412, 2018.
Duchi S, Onofrillo C, O'Connell CD, et al.: Handheld co-axial bioprinting: application to in situ surgical cartilage repair, *Sci Rep* 7:5837, 2017.
Dumpa NR, Bandari S, Repka MA: Novel gastroretentive floating pulsatile drug delivery system produced via hot-melt extrusion and fused deposition modeling 3D printing, *Pharmaceutics* 12:52, 2020.
Fan R, Piou M, Darling E, et al.: Bio-printing cell-laden Matrigel-agarose constructs, *J Biomater Appl* 31:684–692, 2016.
FDA, Statement by FDA Commissioner Scott Gottlieb, M.D., on FDA ushering in new era of 3D printing of medical products; provides guidance to manufacturers of medical devices, 2017, FDA, (website): URL https://www.fda.gov/news-events/press-announcements/statement-fda-commissioner-scott-gottlieb-md-fda-ushering-new-era-3dprinting-medical-products, accessed 12.24.20.
Giannitelli SM, Mozetic P, Trombetta M, et al.: Combined additive manufacturing approaches in tissue engineering, *Acta Biomater* 24:1–11, 2015.
Gioffredi E, Boffito M, Calzone S, et al.: Pluronic F127 hydrogel characterization and biofabrication in cellularized constructs for tissue engineering applications, *Procedia CIRP* 49:125–132, 2016.
Giri BR, Song ES, Kwon J, et al.: Fabrication of intragastric floating, controlled release 3D printed theophylline tablets using hot-melt extrusion and fused deposition modeling, *Pharmaceutics* 12:77, 2020.
Goole J, Amighi K: 3D printing in pharmaceutics: a new tool for designing customized drug delivery systems, *Int J Pharm* 499:376–394, 2016.
Gori M, Giannitelli SM, Torre M, et al.: Biofabrication of hepatic constructs by 3D bioprinting of a cell-laden thermogel: an effective tool to assess drug-induced hepatotoxic response, *Adv Healthc Mater* 9, 2020, 2001163.
Goyanes A, Det-Amornrat U, Wang J, et al.: 3D scanning and 3D printing as innovative technologies for fabricating personalized topical drug delivery systems, *J Control Release* 234:41–48, 2016.
Gregor A, Filová E, Novák M, et al.: Designing of PLA scaffolds for bone tissue replacement fabricated by ordinary commercial 3D printer, *J Biol Eng* 11:1–21, 2017.
Grosskopf AK, Truby RL, Kim H, et al.: Viscoplastic matrix materials for embedded 3D printing, *ACS Appl Mater Interfaces* 10:23353–23361, 2018.
Gruene M, Pflaum M, Hess C, et al.: Laser printing of three-dimensional multicellular arrays for studies of cell-cell and cell-environment interactions, *Tissue Eng - Part C Methods* 17:973–982, 2011.
Gunatillake PA, Adhikari R, Gadegaard N: Biodegradable synthetic polymers for tissue engineering, *Eur Cell Mater* 5:1–16, 2003.
Hakimi N, Cheng R, Leng L, et al.: Handheld skin printer: *in situ* formation of planar biomaterials and tissues, *Lab Chip* 18:1440–1451, 2018.
Haleem A, Javaid M, Khan RH, et al.: 3D printing applications in bone tissue engineering, *J Clin Orthop Trauma* 11:S118–S124, 2020.
Hardin JO, Ober TJ, Valentine AD, et al.: Microfluidic printheads for multimaterial 3D printing of viscoelastic inks, *Adv Mater* 27:3279–3284, 2015.

Hench LL: Chronology of bioactive glass development and clinical applications, *New J Glas Ceram* 03:67–73, 2013.
Hinton TJ, Hudson A, Pusch K, et al.: 3D printing PDMS elastomer in a hydrophilic support bath via freeform reversible embedding, *ACS Biomater Sci Eng* 2:1781–1786, 2016.
Hinton TJ, Jallerat Q, Palchesko RN, et al.: Three-dimensional printing of complex biological structures by freeform reversible embedding of suspended hydrogels, *Sci Adv* 1, 2015, e1500758.
Hodder E, Duin S, Kilian D, et al.: Investigating the effect of sterilisation methods on the physical properties and cytocompatibility of methyl cellulose used in combination with alginate for 3D-bioplotting of chondrocytes, *J Mater Sci Mater Med* 30:1–21, 2019.
Homan KA, Kolesky DB, Skylar-Scott MA, et al.: Bioprinting of 3D convoluted renal proximal tubules on perfusable chips, *Sci Rep* 6:34845, 2016.
Hsu AR, Ellington JK: Patient-specific 3-dimensional printed titanium truss cage with tibiotalocalcaneal arthrodesis for salvage of persistent distal tibia nonunion, *Foot Ankle Spec* 8:483–489, 2015.
Huang TQ, Qu X, Liu J, et al.: 3D printing of biomimetic microstructures for cancer cell migration, *Biomed Microdevices* 16:127–132, 2014.
Jammalamadaka U, Tappa K: Recent advances in biomaterials for 3D printing and tissue engineering, *J Funct Biomater* 9:22, 2018.
Jamróz W, Kurek M, Łyszczarz E, et al.: Printing techniques: recent developments in pharmaceutical technology, *Acta Pol Pharm—Drug Res* 74:753–763, 2017.
Khaled SA, Alexander MR, Wildman RD, et al.: 3D extrusion printing of high drug loading immediate release paracetamol tablets, *Int J Pharm* 538:223–230, 2018.
King SM, Presnell SC, Nguyen DG: Abstract 2034: development of 3D bioprinted human breast cancer for *in vitro* drug screening, *Tumour Biol* 74:2034, 2014.
Koch L, Deiwick A, Schlie S, et al.: Skin tissue generation by laser cell printing, *Biotechnol Bioeng* 109:1855–1863, 2012.
Koch L, Deiwick A, Franke A, et al.: Laser bioprinting of human induced pluripotent stem cells—the effect of printing and biomaterials on cell survival, pluripotency, and differentiation, *Biofabrication* 10, 2018, 035005.
Kolesky DB, Homan KA, Skylar-Scott MA, et al.: Three-dimensional bioprinting of thick vascularized tissues, *Proc Natl Acad Sci U S A* 113:3179–3184, 2016.
Kolesky DB, Truby RL, Gladman AS, et al.: 3D bioprinting of vascularized, heterogeneous cell-laden tissue constructs, *Adv Mater* 26:3124–3130, 2014.
Kopeček J: Polymer-drug conjugates: origins, progress to date and future directions, *Adv Drug Deliv Rev* 65:49–59, 2013.
Kruth JP, Wang X, Laoui T, et al.: Assembly automation lasers and materials in selective laser sintering "Absorptance of powder materials suitable for laser sintering" lasers and materials in selective laser sintering, *Assem Autom* 2315:357–371, 2003.
Kufelt O, El-Tamer A, Sehring C, et al.: Hyaluronic acid based materials for scaffolding via two-photon polymerization, *Biomacromolecules* 15:650–659, 2014.
Lam CXF, Hutmacher DW, Schantz JT, et al.: Evaluation of polycaprolactone scaffold degradation for 6 months in vitro and in vivo, *J Biomed Mater Res A* 90:906–919, 2009.
Langer R, Vacanti JP: Tissue engineering, *Science* 260:920–926, 1993.
Lee A, Hudson AR, Shiwarski DJ, et al.: 3D bioprinting of collagen to rebuild components of the human heart, *Science* 365:482–487, 2019.
Lee H, Lim CHJ, Low MJ, et al.: Lasers in additive manufacturing: a review, *Int J Precis Eng Manuf—Green Technol* 4:307–322, 2017.
Leroux J, Ruel-garie E: In situ-forming hydrogels—review of temperature-sensitive systems, *Eur J Pharm Biopharm* 58:409–426, 2004.
Lewis JA: Direct ink writing of 3D functional materials, *Adv Funct Mater* 16:2193–2204, 2006.

Li VCF, Dunn CK, Zhang Z, et al.: Direct ink write (DIW) 3D printed cellulose nanocrystal aerogel structures, *Sci Rep* 7:1–8, 2017a.
Li X, Lian Q, Li D, et al.: Development of a robotic arm based hydrogel additive manufacturing system for in-situ printing, *Appl Sci* 7:73, 2017b.
Li Y, Jahr H, Lietaert K, et al.: Additively manufactured biodegradable porous iron, *Acta Biomater* 77:380–393, 2018.
Lu Y, Mapili G, Suhali G, et al.: A digital micro-mirror device-based system for the microfabrication of complex, spatially patterned tissue engineering scaffolds, *J Biomed Mater Res - Part A* 77:396–405, 2006.
Mandrycky C, Wang Z, Kim K, et al.: 3D bioprinting for engineering complex tissues, *Biotechnol Adv* 34:422–434, 2016.
Mauri E, Papa S, Masi M, et al.: Novel functionalization strategies to improve drug delivery from polymers, *Expert Opin Drug Deliv* 14:1305–1313, 2017.
Mehrotra S, Moses JC, Bandyopadhyay A, et al.: 3D printing/bioprinting based tailoring of *in Vitro* tissue models: recent advances and challenges, *ACS Appl Bio Mater* 2:1385–1405, 2019.
Melchels F, Feijen J, Grijpma DW: A review on stereolithography and its applications in biomedical engineering, *Biomaterials* 31:6121–6130, 2010.
Mezel C, Souquet A, Hallo L, et al.: Bioprinting by laser-induced forward transfer for tissue engineering applications: jet formation modeling, *Biofabrication* 2, 2010, 014103.
Michael S, Sorg H, Peck CT, et al.: Tissue engineered skin substitutes created by laser-assisted bioprinting form skin-like structures in the dorsal skin fold chamber in mice, *PLoS One* 8, 2013, e57741.
Miller JS, Stevens KR, Yang MT, et al.: Rapid casting of patterned vascular networks for perfusable engineered three-dimensional tissues, *Nat Mater* 11:768–774, 2012.
Moroni L, Burdick JA, Highley C, et al.: Biofabrication strategies for 3D in vitro models and regenerative medicine, *Nat Rev Mater* 3:21–37, 2018.
Mota C, Camarero-Espinosa S, Baker MB, et al.: Bioprinting: from tissue and organ development to in vitro models, *Chem Rev* 120:10547–10607, 2020.
Mozetic P, Giannitelli SM, Gori M, et al.: Engineering muscle cell alignment through 3D bioprinting, *J Biomed Mater Res Part A* 105:2582–2588, 2017.
Murphy C, Kolan K, Li W, et al.: 3D bioprinting of stem cells and polymer/bioactive glass composite scaffolds for bone tissue engineering, *Int J Bioprinting* 3:53–63, 2017.
Nadernezhad A, Khani N, Skvortsov GA, et al.: Multifunctional 3D printing of heterogeneous hydrogel structures, *Sci Rep* 6:1–12, 2016.
Okwuosa TC, Stefaniak D, Arafat B, et al.: A lower temperature FDM 3D printing for the manufacture of patient-specific immediate release tablets, *Pharm Res* 33:2704–2712, 2016.
Ovsianikov A, Deiwick A, Van Vlierberghe S, et al.: Laser fabrication of 3D gelatin scaffolds for the generation of bioartificial tissues, *Materials* 4:288–299, 2010.
Ovsianikov A, Deiwick A, Van Vlierberghe S, et al.: Laser fabrication of three-dimensional CAD scaffolds from photosensitive gelatin for applications in tissue engineering, *Biomacromolecules* 12:851–858, 2011.
Pei X, Zhang B, Fan Y, et al.: Bionic mechanical design of titanium bone tissue implants and 3D printing manufacture, *Mater Lett* 208:133–137, 2017.
Pepelanova I, Kruppa K, Scheper T, et al.: Gelatin-methacryloyl (GelMA) hydrogels with defined degree of functionalization as a versatile toolkit for 3D cell culture and extrusion bioprinting, *Bioengineering* 5:55, 2018.
Prasad LK, Smyth H: 3D printing technologies for drug delivery: a review, *Drug Dev Ind Pharm* 42:1019–1031, 2016.
Pravin S, Sudhir A: Integration of 3D printing with dosage forms: a new perspective for modern healthcare, *Biomed Pharmacother* 107:146–154, 2018.
Prendergast ME, Burdick JA: Recent advances in enabling technologies in 3D printing for precision medicine, *Adv Mater* 32, 2020, 1902516.

Rastin H, Ormsby RT, Atkins GJ, et al.: 3D Bioprinting of Methylcellulose/Gelatin-Methacryloyl (MC /GelMA) bioink with high shape integrity, *ACS Appl Bio Mater* 3:1815–1826, 2020.
Ricles LM, Coburn JC, Di Prima M, et al.: Regulating 3D-printed medical products, *Sci Transl Med* 10, 2018, eaan6521.
Riester D, Budde J, Gach C, et al.: High speed photography of laser induced forward transfer (LIFT) of single and double-layered transfer layers for single cell transfer, *J Laser Micro Nanoeng* 11:199–203, 2016.
Sastry SV, Nyshadham JR, Fix JA: Recent technological advances in oral drug delivery—a review, *Pharm Sci Technol Today* 3:138–145, 2000.
Schneider-Barthold C, Baganz S, Wilhelmi M, et al.: Hydrogels based on collagen and fibrin—frontiers and applications, *BioNanoMaterials* 17:3–12, 2016.
Sears R, Allen-Petersen B, Langer E: *Three-dimensional bioprinted pancreatic tumor model WO2016022830A1*, 2015.
Serra P, Piqué A: Laser-induced forward transfer: fundamentals and applications, *Adv Mater Technol* 4, 2019, 1800099.
Serris I, Serris P, Frey KM, et al.: Development of 3D-printed layered PLGA films for drug delivery and evaluation of drug release behaviors, *AAPS PharmSciTech* 21: 1–15, 2020.
Sheikhpour M, Barani L, Kasaeian A: Biomimetics in drug delivery systems: a critical review, *J Control Release* 253:97–109, 2017.
Shor L, Güçeri S, Wen X, et al.: Fabrication of three-dimensional polycaprolactone/hydroxyapatite tissue scaffolds and osteoblast-scaffold interactions in vitro, *Biomaterials* 28:5291–5297, 2017.
Singh S, Prakash C, Singh R: *3D printing in biomedical engineering*, 2020, Springer.
Skardal A, Murphy SV, Devarasetty M, et al.: Multi-tissue interactions in an integrated three-tissue organ-on-a-chip platform, *Sci Rep* 7:8837, 2017.
Skoog SA, Goering PL, Narayan RJ: Stereolithography in tissue engineering, *J Mater Sci Mater Med* 25:845–856, 2014.
Sorkio A, Koch L, Koivusalo L, et al.: Human stem cell based corneal tissue mimicking structures using laser-assisted 3D bioprinting and functional bioinks, *Biomaterials* 171: 57–71, 2018.
Srivatsan TS, Sudarshan TS: *Additive manufacturing innovations, advances, and applications*, 2015, CRC Press.
Tan X, Tan YJ: 3D printing of metallic cellular scaffolds for bone implants, In *3D 4D print biomed appl*, 2018, Wiley, pp 297–316.
Tan K, Chua C, Leong KF, et al.: Selective laser sintering of biocompatible polymers for applications in tissue engineering, *Biomed Mater Eng* 15:113–124, 2005.
Trenfield SJ, Awad A, Madla CM, et al.: Shaping the future: recent advances of 3D printing in drug delivery and healthcare, *Expert Opin Drug Deliv* 16:1081–1094, 2019.
Tsai KY, Lin HY, Chen YW, et al.: Laser sintered magnesium-calcium silicate/poly-ε-caprolactone scaffold for bone tissue engineering, *Materials* 10:1–14, 2017.
Van Kampen KA, Scheuring RG, Terpstra ML, et al.: Biofabrication: from additive manufacturing to bioprinting, In *Encyclopedia of tissue engineering and regenerative medicine*, 2019, Academic Press.
Webster AA: New Publication: Drug delivery: engineering principles for drug therapy, *J Pharm Technol* 17:304, 2001.
Wen Y, Xun S, Haoye M, et al.: 3D printed porous ceramic scaffolds for bone tissue engineering: a review, *Biomater Sci* 5:1690–1698, 2017.
Wiria FE, Chua CK, Leong KF, et al.: Improved biocomposite development of poly(vinyl alcohol) and hydroxyapatite for tissue engineering scaffold fabrication using selective laser sintering, *J Mater Sci Mater Med* 19:989–996, 2008.

Xiao Q, Ji Y, Xiao Z, et al.: Novel multifunctional NaYF4:Er3+,Yb3+/PEGDA hybrid microspheres: NIR-light-activated photopolymerization and drug delivery, *Chem Commun* 49:1527–1529, 2013.
Xu F, Celli J, Rizvi I, et al.: A three-dimensional in vitro ovarian cancer coculture model using a high-throughput cell patterning platform, *Biotechnol J* 6:204–212, 2011.
Xu F, Ren H, Zheng M, et al.: Development of biodegradable bioactive glass ceramics by DLP printed containing EPCs/BMSCs for bone tissue engineering of rabbit mandible defects, *J Mech Behav Biomed Mater* 103:103532, 2020.
Youssef A, Hollister SJ, Dalton PD: Additive manufacturing of polymer melts for implantable medical devices and scaffolds, *Biofabrication* 9, 2017, 012002.
Zein I, Hutmacher DW, Tan KC, et al.: Fused deposition modeling of novel scaffold architectures for tissue engineering applications, *Biomaterials* 23:1169–1185, 2002.
Zhang YS, Arneri A, Bersini S, et al.: Bioprinting 3D microfibrous scaffolds for engineering endothelialized myocardium and heart-on-a-chip, *Biomaterials* 110:45–59, 2016.
Zhang YS, Khademhosseini A: Advances in engineering hydrogels, *Science* 356, 2017, eaaf3627.
Zhang J, Huang D, Liu S, et al.: Zirconia toughened hydroxyapatite biocomposite formed by a DLP 3D printing process for potential bone tissue engineering, *Mater Sci Eng C* 105:110054, 2019.
Zheng YF, Gu XN, Witte F: Biodegradable metals, *Mater Sci Eng R Rep* 77:1–34, 2014.
Zhu W, Holmes B, Glazer RI, et al.: 3D printed nanocomposite matrix for the study of breast cancer bone metastasis, *Nanomed Nanotechnol Biol Med* 12:69–79, 2016.
Zhuang H, Han Y, Feng A: Preparation, mechanical properties and in vitro biodegradation of porous magnesium scaffolds, *Mater Sci Eng C* 28:1462–1466, 2008.

Conclusions

This book summarizes many different examples of functional machines and devices that can be designed using exclusively soft matter or combinations of hard and soft materials. It disclosed possible applications of these programmable materials, probably the most important advantage of soft materials usage. The examples discussed strongly support the potentialities of soft materials in overcoming the limitations of rigid microrobots in many different fields. They demonstrate that it is possible to achieve complex and dexterous actuation paths by simply introducing large deformable parts inside the device. Obviously, this requires using specific materials and fabrication technologies, which have been extensively treated in this book. In front of all these considerations, the most important idea suggested by this book is that the future of robotics will be realistically dominated by highly adaptable and smart soft devices. Soft materials have all the potentialities to fulfill these tasks, making them an essential choice for the robotic tools of tomorrow. The research field is still in a nascent stage, but it promises a large variety of applications as described in this book. We expect the next decade to see a further transfer of the scientific knowledge on soft robotics to many different fields of our everyday life.

This page intentionally left blank

Index

Note: Page numbers followed by "*f*" indicate figures and "*t*" indicate tables.

A

Active sensors, 125
Actuation strategy, soft microrobotics, 18, 20, 23
  advanced routes, 23–24
  chemical actuation, 20–21
  magnetic actuation, 21–23
N-Acylhomoserine lactones (AHLs), 144–145
Additive manufacturing (AM), 234
  biomaterials, 238–240*t*
  biomedical applications, 247–254, 249*f*
  drug delivery systems, 235–236
  3D printing, 236–237, 238–240*t*
    extrusion-based technologies, 246–247
    laser-dependent technologies, 243–245, 244*f*
    materials for TE scaffolds and DDSs, 237–243
  tissue engineering, 234–235
Agarose hydrogel microspring, fabrication process, 166–167, 167*f*
Alcohol detection, 140
Ammonia detection, 141
Anionic hydrogels, 128–129
Anisotropic swelling behavior, 171*f*
Aromatic VOCs, 106–107
Artificial bacterial flagella (ABFs), 5–6, 17, 22–23

B

Bacillus anthracis, 117
Bacteria
  N-acylhomoserine lactones, 144–145
  endospores, 117
  hydrogels, 144–145
Bifidobacterium pseudocatenulatum, 144–145
Biochemical sensing mechanism, hydrogels, 138–139
  enzyme-substrate interactions, 140–143
  living cells and bacteria, 144–145
  molecular interactions, 139–144
  stimuli-responsive, 177–178
Biodegradable drug-encapsulating microrobots, 17
Biodegradable metals (BMs), 237–241
Bio-hybrid actuator, robotics, 180–181, 180*f*, 183–184, 183*f*
Biohybrid soft microrobotics, 31–32
Bioinert ceramic scaffolds, 241
Biomedical applications
  additive manufacturing, 234, 247–254, 249*f*
  hydrogels sensors, 145–146
    cancer monitoring, 146
    cardiac rhythm monitoring, 146–148
    cell metabolite detection, 148–149
    tissue engineering, 149
    wound healing monitoring, 149–150
Biomimetic soft robots, 180–181, 180*f*
BioMOFs, 97–99, 98*f*, 113*f*
Biomolecules sensing, metal-organic frameworks, 109–118, 112–114*f*, 116*f*
Bioprinting, 16, 234–235, 250–251
Bio-receptor, 125–126
Bioresorbable aliphatic polyesters, 241
Biosensors, 125–126
  bacteria-based, 144–145
  DNA hydrogels, 143
  enzyme-based, 146, 148–149
  optical, 141
Bio-transducer, 125–126
Bragg's diffraction, 177–178
Brownian motion, magnetic nanoparticles, 174*f*, 175
Brunauer–Emmett–Teller (BET), 99

C

Calcium alginate hydrogel, 162–167, 162*f*
Cancer monitoring, 146
Carbon blacks (CB), 68
Carbon nanotube (CNT), 68
  hydrogel, 176–177

Carbon nanotube (CNT) (*Continued*)
multi-walled, 132, 219
sensing application, 219–222, 221–222*f*, 226–227*t*
single-walled, 176–177, 219
Carboxylate-based MOFs, 95
Cardiac muscles, 180–181
Cardiac rhythm, hydrogels sensors, 146–148
Cationic hydrogel, 128–129
Cell delivery, 16, 25–27
Cell fiber, fabrication process, 166–167, 167*f*
Cell metabolite detection, 148–149
Cellular apoptosis activity, metal-organic frameworks, 111–112, 112*f*
Centrifuge-based hydrogels, 163–164, 163*f*
Chemical actuation, soft microrobotics, 19*f*, 20–21
Chemical crosslinked hydrogels, 126–127, 168–173
Chemical sensors, 125–126
Chemiresistive gas sensor, 215–217
Chemotaxis, 31–32
Chitosan, 10, 20, 31, 242
Chlorinated volatile organic compounds (Cl-VOCs), 106–107
Chloroform, 207–209, 209*f*, 222*f*
Cobalt based MOF, 103
Cobinamide (Cbi), 210–212, 211*f*
Colorimetric sensing, 99–100
Compression sensor, hydrogels, 135, 136*f*
Conductive hydrogels, 189
Conductive polymers, 11–12
Conventional fabrication techniques, 234–236
Coordination polymers (CPs), 92–94
Coulomb's law, 5
Critical temperature, 128–129

D

DBP-PT, 101–102, 102*f*
De novo protein encapsulation, 115
Desalting method, 178–179
Dielectrophoresis (DEP) method, 221
Dipicolinic acid (DPA), 117
Direct ink writing (DIW) technique, 169–172, 171*f*, 244*f*, 246–247, 254
DNA hydrogels
biosensors, 143
soft microbotics, 13
structure and volume change, 160–161, 161*f*
Dopamine (3,4-dihydroxyphenylethylamine), 108–109
Double-network hydrogel, 188
Downscaling process, 5
Droplet–substrate interface, 74
Drug delivery systems (DDSs), 235–236
metal-organic frameworks, 110–112
soft microrobotics, 25
3D printing
biomedical applications, 252–254
materials, 237–243, 238–240*t*
Dual-network (DN) hydrogels, 130–132, 137, 147–148

E

Ecoflex, 60–62, 75–77
Elastic modulus, 61–62
Electrical sensors, 124
Electric double layer, 178–179, 178*f*
Electrochemically responsive soft materials, 8–9
Electrochemical sensors, 124
Electrodeposition, 13, 17–18
Electronic skins (e-skins), 46–47
inkjet-printed conductive gold electrodes for, 79–81, 80*f*
potentiometric, design of, 80*f*
sensors working-principle, 79
for thermo and mechano-sensation, 79
Electro-sprayed film, 205, 206*f*
Embedded 3D printing (E3DP), 247
End of service life indicator (ESLI), 199–200, 202, 204*f*
Enzyme-based biosensors, 146, 148–149
Enzyme-substrate interactions, hydrogels, 140–143
Escherichia coli, 144–145
Excited state intramolecular proton transfer (ESIPT), 104–105
Extrusion-based technologies, 9, 16, 238–240*t*, 246–247

F

Fabrication method
agarose hydrogel microspring, 166–167, 167*f*

cell fiber, 166–167, 167*f*
conventional fabrication techniques, 234–236
hydrogels, 161–173, 165*f*
layer-by-layer fabrication, 234
photolithographic, 169, 170*f*
Fiber-based gels, 126–127
Fibrin, 243
Fibronectin, biomimetic soft robots, 180–181, 180*f*
Finite element analysis (FEA), 75–77
Flatbed systems, 49
Flory-Rehner theory, 127–129
Fluorescence anisotropy (FA), 114–115
4D printing, 9
Freeform reversible embedding of suspended hydrogels (FRESH) technique, 247
Freeform reversible embedding (FRE) technique, 244*f*, 247
Fused deposition modeling (FDM), 244*f*, 246, 253–254

G

Gallium–indium (GaIn) nanoparticle inks, 73
Gas absorption
effect on reflective properties, 202, 203*f*
on reflective properties, 202, 203*f*
Gas adsorption, 202, 204*f*, 219–222, 221*f*
Gas sensor
hydrogels, 136–137
mass sensitive, ZnO nanorods, 213, 214*f*
volatile organic compounds, 200–222, 226–227*t*
carbon based systems, 219–222, 221–222*f*
hydrogels, 223–227, 225*f*
materials, 200
metal organic frameworks, 204–209, 207–208*f*, 226–227*t*
nanocarbon composite sensor, 218–219, 220*f*
nanorods, 212–215, 213*f*
optical fiber, 209–212, 226–227*t*
polymer of intrinsic microporosity, 200–204, 226–227*t*
tin oxide hollowspheres, 215–218, 217*f*
Gelatin methacrylate (GelMA), 242
Gelation process, 242
Glass fiber, CN(H_2O) Cbi on, 210, 211*f*
Glucose detection, 140
Glucose oxidase (GOX), 140–141
α-1,4-L-Glucuronic acid, 162, 162*f*
Gold nanoparticle (AuNPs) ink, 79–81, 81*t*
Gold nanorods, 144, 182–183
Graphene, 68, 176–177, 207–209
Green fluorescent protein (GFP), 95

H

Hard-soft hybrid microrobots, 28–30, 29–30*f*
Hazardous gases, MOF sensors, 105–106
Hydration, 127–128, 158–160
by amphiphilic polymers, 188–189
pNIPAm gel swell by, 158–160, 159*f*
Hydrogels (HG)., 126–129, 158 *See also specific hydrogels*
biochemical sensing mechanism, 138–139
enzyme-substrate interactions, 140–143
living cells and bacteria, 144–145
molecular interactions, 139–144
biomedical sensing applications, 145–146
cancer monitoring, 146
cardiac rhythm monitoring, 146–148
cell metabolite detection, 148–149
tissue engineering, 149
wound healing monitoring, 149–150
centrifuge-based, 163–164, 163*f*
chemical crosslinked, 126–127, 168–173
conductive, 189
fabrication method, 161–173, 165*f*
multi-scale function, 173
carbon nanotube, 176–177
graphene, 176–177
living cells, 180–181, 180*f*
magnetic nanoparticles, 174–175, 174*f*
photonic colloidal crystal, 177–179, 178*f*
Pt catalyst reaction, 175–176, 176*f*
nanocomposite, 187–188
nano-scale function
imparting functions to polymer chains, 160–161
stimuli responsiveness, 158–160
physical crosslinked, 126–127, 162–167, 162*f*, 186–187, 187*f*

Hydrogels (HG). (*Continued*)
physicochemical sensing mechanism, 129
compression sensor, 135, 136*f*
gas sensors, 136–137
hygrometers, 138
ionic strength sensors, 132–135
ions sensor, 132–135
pH sensing, 132–135
pressure and strain sensors, 135, 136*f*
temperature sensors, 130–132
self-growing, 189
sensing application, 223–227, 225*f*, 226–227*t*
soft microrobotics, 9–11
soft millirobots, 184–185, 184*f*
spiral-shaped, lope-coil effect, 164–166, 166*f*
swelling behavior, 126–129
3D bioprinting technologies, 241–242
volatile organic compounds, 223–227, 225*f*
Hydrogen peroxide, 19*f*, 20–21, 115, 141, 148–149, 175–176, 182–183
Hydrophobic interaction, 158–160, 159*f*
Hygrometers, 138

I

Inkjet-printable inks, 71–75, 73*t*, 74*f*
Inkjet-printable substrates, 62–64, 63*t*
Inkjet printing, 56–59
cartridge temperature, 58
continuous mode, 57–58, 57*f*
drop on demand (DOD) mode, 57–58, 57*f*
drop spacing, 59
piezoelectric DOD, 57*f*, 58
platen temperature, 59
print height, 59
resolution, 56–57
thermal inkjet printer, 57*f*, 58
waveform, 58, 59*f*
Inorganic materials, additive manufacturing, 237–241
Integrated soft robots
by bridging multiscale elements, 181–186
hydrogel patterning integrated systems, 184–186
with rigid body, 182–184, 182*f*
Intelligent polymerized crystalline colloidal arrays (IPCCAs), 130
Interdigitated electrodes (IDE), 205
International Organization for Standardization (ISO), 251–252
International Union of Pure and Applied Chemistry (IUPAC), 124–126
Inverse opal (IO), 133, 136–137
In-vivo microrobot guidance, 28
Ionic strength sensors, 132–135
Ions sensor, hydrogels, 132–135
IRONsperm, 17
Isoreticular MOFs (IRMOFs), 93–94

K

Kapton substrate, 79–81

L

Langmuir-Blodgett (LB) method, 205
Lanthanide luminescent MOFs, 96, 97*f*
Laser-dependent technologies, 238–240*t*, 243–245, 244*f*
Laser-induced forward transfer (LIFT), 244*f*, 245
Laser micromachining, 16–17
Layer-by-layer fabrication, 234
Ligand-based MOFs, 95
Light-controlled travelling-wave approach, 23–24
Light driven shape-changing polymers, 8–9
Light-responsive hydrogels, 129
Light-sensitive smart materials, 8–9
Lithography
photolithographic fabrication, 169, 170*f*
soft microrobotics, 16–17
stereolithography, 172–173, 173*f*, 243–245, 244*f*, 248, 254
two-photon, 14–15*f*, 15–16
Living cells, hydrogels, 144–145, 180–181
Localized actuation, 20
Long-range actuation, 20
Lope-coil effect, spiral-shaped hydrogels, 164–166, 166*f*
Lower critical solution temperature (LCST), 128–129, 158–160, 242
Low Reynolds number (Re), 4–6
Luminescent MOF (LMOFs), 96, 97*f*, 104–106, 114, 117

M

Magnetic actuation
  soft microrobotics, 21–23
  untethered soft millirobot, 184–185, 184*f*
Magnetic nanoparticles
  Brownian motion, 174*f*, 175
  hydrogel, 174–175, 174*f*
  soft microrobotics, 18
Magnetic resonance imaging (MRI), metal-organic frameworks, 97, 116–117
Magnetic sensors, 124
Magnetococcusmarinus, 31–32
β-1,4-D-Mannuronic acid, 162, 162*f*
Mass-sensitive sensors, 124, 213, 214*f*
Metal-organic frameworks (MOFs), 92–94
  applications, 93–94
  bioMOFs, 97–99, 98*f*, 113*f*
  biomolecules sensing, 109–118, 112–114*f*, 116*f*
  class of compounds, detection, 99–100, 100*t*
    hazardous gases, 105–106
    oxygen, 99–103, 100*t*, 101–103*f*
    small organic molecules, 108–109, 109*f*
    volatile organic compounds, 106–108, 107–108*f*
    water vapor, 103–105, 104–105*f*
  copper-benzene-1,3,5-tricarboxylate, 207–209
  intracellular sensing assays, 117–118
  lanthanide luminescent, 96, 97*f*
  mode of sensing, 96–97
  organic and inorganic synthesis, 94–96
  self-assembling synthesis, 92, 92*f*
  ssDNA detection based on, 113, 114*f*
  volatile organic compounds, 204–209, 207–208*f*, 226–227*t*
  ZIF-90 synthesis, 95–96, 96*f*
Methylviologen (MV), 101, 102*f*
Michaelis-Menten model, 139
Microdevices imaging, soft microrobotics, 26–27*f*, 28
Microfluidic device, 164, 165*f*, 170*f*, 180–181
Micromolding, 17–18
Microrobotics, 2–3, 28. *See also* Soft microrobotics
Microscale continuous optical printing (μCOP), 16
Micro stereolithography (μ-SLA), 15–16
Microsurgery applications, soft microrobotics, 27–28
MIL-96(Al) LB IDEs, 205, 208*f*
Mode of sensing, metal-organic frameworks, 96–97
Moisture-stable LMOF, 107–108
Multi-dimensional printing process, 234
Multi-flow micro-fluidic device, 170*f*
Multi-material direct ink writing (DIW) technique, 246
Multi-walled carbon nanotubes (MWCNTs), 132, 219
MXenes, 135

N

Nanocarbon composite sensor
  application, 218–219, 220*f*, 226–227*t*
  volatile organic compounds, 218–219, 220*f*
Nanocomposite hydrogels, 187–188
Nanocrystal-MOFs (NMOFs), 114
Nanorods, 212–215, 213*f*
  gold, 144, 182–183
  with polyelectrolyte hinges, 28–30
  sensing application, 226–227*t*
  ZnO nanorods
    QCM based mass sensitive sensor, 213, 213*f*
    quartz crystal microbalance, 215
    surface plasmon characteristics, 215, 216*f*
National Institute for Standards and Technology (NIST), 251–252
National Institute of Safety and Health (NIOSH), 202
Natural templating, soft microrobotics, 17
Near-infrared light (nIR), 176–177
Newton's law, 65–67
NIR-emiting lanthanides, 96
Nitroaromatic compounds (NACs), 106–107
No-core fiber sensors (NCFS), 133

O

Ohnesorge number (Oh), 72
Oligonucleotides, metal-organic frameworks, 112–113, 115

One-dimensional (1D) MOFs, 92–94
Optical fiber, volatile organic compounds, 209–212, 226–227*t*
Optical sensors, 124
Organic ligands, 92, 95, 99–100
Organic materials, additive manufacturing, 241–243
Origami hydrogel, 169, 170*f*
Oxygen, MOF sensors, 99–103, 100*t*, 101–103*f*

P

PAAm hydrogel, 130–132, 131*f*
Passive sensors, 125
Personal protective equipment (PPE), 198–199
Photocurable hydrogel, 169, 170*f*
Photoinduced electron transfer (PET), 113
Photolithographic fabrication, 169, 170*f*
Photonic colloidal crystal hydrogels, 177–179, 178*f*
Photonic crystals (PCs), 130
pH sensing, hydrogels, 132–135
Physical crosslinked hydrogels, 126–127, 162–167, 162*f*, 186–187, 187*f*
Physical sensors, 125–126
Physicochemical sensing mechanism, hydrogels, 129
  compression sensor, 135, 136*f*
  gas sensors, 136–137
  hygrometers, 138
  ionic strength sensors, 132–135
  ions sensor, 132–135
  pH sensing, 132–135
  pressure and strain sensors, 135, 136*f*
  temperature sensors, 130–132
Plasmonic microgels, PAAm hydrogel, 130–132, 131*f*
Plastic deformation, 61–62
Polychlorinated dibenzo-*p*-dioxins (PCDDs), 108
Poly(dimethylsiloxane) (PDMS), 60–62, 69–70
Polyester, 53–54
Poly(3,4-ethylenedioxythiophene): poly(styrenesulfonate) (PEDOT: PSS), 73
Poly(ethylene glycol) diacrylate (PEGDA), 10
Polyethylene naphthalate (PEN), 62–63
Poly (ethylene terephthalate) (PET), 60, 62–63
Polymer binders, 70
Polymer network, 158
  cross-linking, 161, 168–169, 168*f*
  functional materials in, 173
  polyrotaxane, 187
  with symmetrical properties, 188
  three-dimensional, through molecular design, 188–189
Polymer of intrinsic microporosity (PIM), 200–204, 226–227*t*
Polymersomes, 12
Poly(*N*-isopropylacrylamide) (PNIPAM), 130–132, 158–160, 159*f*, 168–173, 176–177
Polypeptides, 176, 180–181
Polypyrrole (PPy), 11–12
Polyrotaxane, polymer network, 187
Polyvinyl alcohol (PVA) hydrogel, 130–132
Porous nano-MOFs, 110
Post synthetic modification (PSM) approach, 94
Powder bed printing, 236
Pressure sensors, hydrogels, 135, 136*f*
Printing stroke, 51
Propulsion, 18, 20, 23
  chemical actuation, 20–21
  magnetic actuation, 21–23
  melting and photosynthetic, 23–24
  self-powered, 20–21
Propulsion matrix, 5–6
Pt catalyst reaction, hydrogels, 175–176, 176*f*
Pyridine-based MOFs, 95

Q

QCM based mass sensitive sensor, 213, 213*f*
Quantum dots (QDs), 134–135, 141
Quartz crystal microbalance (QCM), 134, 143, 212–213
Quartz resonator, 205

R

Radiation sensitive sensors, 124
Radical polymerization, 168–169, 168*f*
Radio imaging techniques, 28

Ratiometric fluorescence sensor, 134–135
Redox reactivity, 101, 101*f*
Reflective interference filter, 202, 203*f*
Regenerative medicine, 251–252
Rhodamine-B isothiocyanate (RhB), 101–102, 102*f*
Robotics
  bio-hybrid actuator, 180–181, 180*f*, 183–184, 183*f*
  at microscale, 4–6
  soft (*see* Soft robotics)

S

Scaffolds, 234–235
  bioinert ceramic, 241
  metal-organic frameworks, 114–115
  3D printing, 237–243, 238–240*t*, 248–252
Screen-printable inks, 64–71, 66–67*f*
  fillers, 68
  polymer binders, 70
  solvents/additives, 70
Screen-printable substrates, 60–62, 61*t*, 61*f*
Screen printing, 47–56, 53*f*
  hand system, 50–51
  key performance indicators (KPI), 52, 52*f*
  printer components, 48*f*, 49–50
  printing stroke, 51
  screen mesh, 53–54, 53*f*
  semi or fully automated system, 50–51
  snap-off distance, 50–51, 55–56
  stencil printing, 51
Selective laser sintering (SLS), 243–245, 244*f*
Self-assembly
  materials for soft microrobotics, 12, 18
  metal-organic frameworks, 92, 92*f*
Self-electrophoresis mechanism, 20–21
Self-folding microrobot, 25
Self-growing hydrogels, 189
Self-propelled micromotors, 20–21
SEM
  macrophage interaction with robot and 3D printed zwitterionic microrobot, 7*f*
  metastatic breast cancer, 3D printing, 249*f*
  MOF LB film characterization, 205, 207*f*
  plasmonic microgels, AuNPs, 130–132, 131*f*
  PPy particles, 224, 225*f*
Sensors. *See also specific sensors*
  active*vs.* passive, 125
  classification, 124
Shape-morphing devices, 24
Short-range actuation, 20, 24
Silver nano-dendrites (AgND), 65–67
Silver nanofibers (AgNWs), 130–132
Silver nanoparticles (AgNPs), 72
Single crystal X-ray diffraction analysis, 94
Single-molecule magnet (SMM) behavior, 103
Single-walled carbon nanotube (SWCNT), 176–177, 219
Site-direct immobilization techniques, 143
Skeletal muscle tissues, 183–184, 183*f*
Skinning/crusting effect, 74
Small organic molecules, MOF sensors, 108–109, 109*f*
Smart sensors, volatile organic compounds (VOCs), 200–222
  hydrogels, 223–227, 225*f*
  materials, 200
  metal organic frameworks, 204–209, 207–208*f*, 226–227*t*
  micro- and nano-systems, 212, 226–227*t*
    carbon based systems, 219–222, 221–222*f*
    nanocarbon composite sensor, 218–219, 220*f*
    nanorods, 212–215, 213*f*
    tin oxide hollowspheres, 215–218, 217*f*
  optical fiber, 209–212, 226–227*t*
  polymer of intrinsic microporosity, 200–204, 226–227*t*
Soft actuators, 75
Soft earthworm robot, stretchable screen printed nanocomposite sensors for feedback–loop control of, 75–78, 78*f*
Soft materials, 2, 6–8
Soft microrobotics, 2–3
  actuation strategy, 18, 20, 23
    advanced routes, 23–24
    chemical actuation, 20–21
    magnetic actuation, 21–23
  advantages, 25
  applications, 25–28
  biohybrid, 31–32

Soft microrobotics (*Continued*)
cell delivery, 25–27
conductive polymers, 11–12
drug delivery, 25
electrodeposition, 17–18
manufacturing techniques, 13, 14–15*f*, 17–18
laser micromachining, 16–17
lithography, 16–17
natural templating, 17
3D printing, 15–16
materials for, 6–13
microdevices imaging and guidance, 26–27*f*, 28
micromolding, 17–18
microsurgery applications, 27–28
self-assembled materials, 12
stimuli-responsive smart materials, 8–9
synthetic and natural hydrogels, 9–11
Soft millirobot, multi-motion of, 184–185, 184*f*
Soft-porous MOFs, 94. *See also* Metal-organic frameworks (MOFs)
Soft robotics, 2–3. *See also* Soft microrobotics
applications, 187
biomimetic, 180–181, 180*f*
inkjet printing, 56–59, 57*f*, 59*f*
conductive gold electrodes for e-skin, 79–81, 80*f*
inks, 71–75, 73*t*, 74*f*
substrates, 62–64, 63*t*
integrated (*see* Integrated soft robots)
printed devices for, 75–81
screen printing, 47–56, 48*f*, 52–53*f*
inks, 64–71, 66–67*f*
stretchable screen printed nanocomposite sensors for feedback–loop control, 75–78, 78*f*
substrates, 60–62, 61*t*, 61*f*
spiral-shaped hydrogels, 164–166
Soft spiral-shaped microswimmers, 185–186, 185*f*
Spermbots, 32
Sperm-like actuation, 22–23
Spin-coating, 201
Spiral-shaped hydrogels, lope-coil effect, 164–166, 166*f*
Spritam®, 252
ssDNA detection, 113, 114*f*
Stencil printing, 51
Stereolithography (SLA), 172–173, 173*f*, 243–245, 244*f*, 248, 254
Stimuli-responsive hydrogel, 158. *See also* Hydrogels (HG)
features, 185–186
nano-scale function, 158–160
patterned and stripe patterned, 169, 170*f*
problems of, 186–189
propulsion mechanism, 182–183, 182*f*
swelling/shrinking speed, 188–189
3D printing to 4D printing, 169, 170*f*
Stomatocytes, 12
Strain sensors, hydrogels, 135, 136*f*
Stretchable electronics, 46–49, 64
Sub-building units (SBUs), 95
Supramolecular conductive PANI/PSS–UPy hydrogels, 147*f*
Surface-enhanced Raman spectroscopy (SERS), 141, 142*f*
Surface plasmon resonance (SPR), 133, 143, 215, 216*f*
Surface tension, of inkjet-printable inks, 73–74
Surface wettability, 61–62
Swelling behavior, 126–129, 133
Syringe-based printing, 16

T

Temperature sensitive materials, soft microrobotics, 8–9
Temperature sensors, hydrogels, 130–132
Tetraphenylethene (TPE) derivative, 106–107
Thermal-responsive hydrogel, 158–160, 182–183
Thermometric sensors, 124
Thermoplastic polymers, 241
Thermoplastic polyurethane (TPU), 60–62, 69–70
3D bioprinting, 234–235
3D printing, 169–172, 236–237
biomedical applications, 248–252, 249*f*

extrusion-based technologies, 238–240*t*, 246–247
laser-dependent technologies, 238–240*t*, 243–245, 244*f*
materials for TE scaffolds and DDSs, 237–243, 238–240*t*
inorganic materials, 237–241
organic materials, 241–243
metastatic breast cancer, 248, 249*f*
soft microrobotics, 15–16
stimuli-responsive smart materials, 9
zwitterionic microrobot, 7*f*, 13
Tin oxide hollowspheres, 215–218, 217*f*, 226–227*t*
Tissue engineering (TE)
additive manufacturing, 234–235
embedded 3D printing, 247
hydrogels sensors, 149
3D printing
biomedical applications, 248–252
materials, 237–243, 238–240*t*
Topological hydrogel, 187
Toxic gases, 105–106
TPU. *See* Thermoplastic polyurethane (TPU)
Triphenylene-2,6,10-tricarboxylate (TTCA), 101, 102*f*
Triphosphaazatriangulene, 104, 105*f*
Troger's base formation, 200–201
T-sensors, 132
Two-dimensional MOFs, 92–94
Two-photon lithography (2PL), 14–15*f*, 15–16
Two-photon polymerization (TPP/2PP), 172–173, 173*f*, 245

U

Ultrasound sonication, 71
Ultrathin ZnO nanorods, 215
Untethered soft millirobot, 184–185, 184*f*
Upper critical solution temperature (UCST), 128–129
Urea detection, 141

V

Vaporization method, photonic colloidal crystals, 178–179, 178*f*
Viologen-functionalized MOFs, 101
Viscosity, of inkjet-printable inks, 73, 73*t*
Volatile organic compounds (VOCs), sensors applications, 198–222, 226–227*t*
carbon based systems, 219–222, 221–222*f*
hydrogels, 223–227, 225*f*
materials, 200
metal organic frameworks, 106–108, 107–108*f*, 204–209, 207–208*f*, 226–227*t*
nanocarbon composite sensor, 218–219, 220*f*
nanorods, 212–215, 213*f*
optical fiber, 209–212, 226–227*t*
polymer of intrinsic microporosity, 200–204, 226–227*t*
tin oxide hollowspheres, 215–218, 217*f*

W

Water vapor, MOF sensors, 103–105, 104–105*f*
Wound healing, 149–150

X

X-ray crystallography, 94

Y

Young's equation, 63–64

Z

ZIF-90 synthesis, 95–96, 96*f*, 115
Zinc-imidazolate frameworks (ZIFs), 95–96, 115
ZnO nanorods
quartz crystal microbalance, 213, 213*f*, 215
surface plasmon characteristics, 215, 216*f*

This page intentionally left blank

Serial Editor
Davide Moscatelli
Politecnico di Milano, Italy

ELSEVIER

ACADEMIC PRESS
An imprint of Elsevier
elsevier.com/books-and-journals

ISBN 978-0-12-820646-1